

**DESIGN AND DEVELOPMENT OF COMPACT  
MICROWAVE LOWPASS FILTERS WITH HIGHER  
ORDER HARMONICS SUPPRESSION FOR  
WIRELESS COMMUNICATION SYSTEMS**

*A THESIS*

*Submitted by*

**REKHA T K**

*for the award of the degree*

*of*

**DOCTOR OF PHILOSOPHY**



**DIVISION OF ELECTRONICS ENGINEERING  
SCHOOL OF ENGINEERING  
COCHIN UNIVERSITY OF SCIENCE AND TECHNOLOGY, KOCHI**

**APRIL 2019**

*Dedicated to the Almighty*

## **THESIS CERTIFICATE**

This is to certify that the thesis entitled **DESIGN AND DEVELOPMENT OF COMPACT MICROWAVE LOWPASS FILTERS WITH HIGHER ORDER HARMONICS SUPPRESSION FOR WIRELESS COMMUNICATION SYSTEMS** submitted by **Rekha T K** to the Cochin University of Science and Technology, Kochi for the award of the degree of Doctor of Philosophy is a bonafide record of research work carried out by her under my supervision and guidance at the Division of Electronics Engineering, School of Engineering, Cochin University of Science and Technology. The contents of this thesis, in full or in parts, have not been submitted to any other University or Institute for the award of any degree or diploma.

I further certify that the corrections and modifications suggested by the audience during the pre-synopsis seminar and recommended by the Doctoral Committee of Ms. Rekha T K have been incorporated in the thesis.

Kochi-682 022  
Date: 05.04.2019

**Prof. (Dr.) Abdulla P**  
Research Guide  
Div. of Electronics Engineering  
School of Engineering  
Cochin University of Science and Technology

## **DECLARATION**

I hereby declare that the work presented in the thesis entitled **DESIGN AND DEVELOPMENT OF COMPACT MICROWAVE LOWPASS FILTERS WITH HIGHER ORDER HARMONICS SUPPRESSION FOR WIRELESS COMMUNICATION SYSTEMS** is based on the original research work carried out by me under the supervision and guidance of Dr. Abdulla P, Professor, for the award of degree of Doctor of Philosophy with Cochin University of Science and Technology. I further declare that the contents of this thesis in full or in parts have not been submitted to any other University or Institute for the award of any degree or diploma.

Kochi-682 022

Date: 05.04.2019

**Rekha T K**

Division of Electronics Engineering

## **ACKNOWLEDGEMENT**

Foremost, I would like to express my sincere gratitude to my research supervisor, Dr. Abdulla P, Professor, Division of Electronics, School of Engineering, Cochin University of Science and Technology, for his continuous support, motivation and enthusiasm towards my research work. He was very particular that his students should build up confidence and self reliance along with the achievement of the doctoral degree. His guidance and inspiration were the vital factors behind the completion of the work within the allotted time limit of three years.

My heartfelt thanks to Dr. Jibu Kumar M G, Doctoral Committee member, for his commendable suggestions and directives for my research work. My sincere thanks also to Dr. P Mohanan, Dr. C K Aanandan, and Dr. K Vasudevan for their valuable suggestions and encouragement. I am extremely thankful to the University Grants Commission for giving me the chance to attend the Ph D program under Faculty Development Scheme.

My deep gratitude goes to the NSS Management for their valuable support in completing all the formalities during the various stages of the PhD program. I am greatly indebted to Prof. R Prasanna Kumar, Education Secretary, Sri. C B Sivasankaran Nair, Superintendent and Smt. Sathy P, former Senior Grade Clerk for their valuable support and guidance. My heartfelt gratitude to Dr. E B Sureshkumar, the former principal of NSS College Rajakumari, who supported me a lot in the final stages of my research work. The earlier incumbents also helped me generously in availing FDP of UGC. The teaching and non-teaching staffs of my parent institution were very considerate to me for fulfilling my studies. I am thankful to each one of them. I would like to specifically mention my intimate colleague Dr. Reji A P, for her timely help during my FDP period.

I would also like to express my heartfelt thanks to Dr. Raphika P M and Dr. Jasmine P M for their valuable technical assistance during various stages of my research work. Dr. Jasmine P M has offered moral support to me during the entire tenure of my research period with her inspiring and motivating words. I will always cherish the period spent with my dear friend, Ms Anu A R. She was very cooperative and helpful to me during my work. My sincere thanks to fellow research scholars, Ms. Ami Iqbal, Mr. Sam Kollannore U, Ms. Nizamol T A, Ms. Sheeba Varghese, Ms. Libimol V A, Ms. Anju Mathews and Mr. M Ameen for their valuable support in my studies. My dear friends, Dr. Veena M S and Ms Sindhu Rani have helped me a lot in finalizing the research papers. My sincere thanks to both of them. I am also very much thankful to Mr. Biju C R, Mr. Anil Kumar A T, Mr. Shahul Hameed P A, Ms. Linimol V T and Dr. Radhakrishnan for their timely help in various technical issues. I also thank all the staff members of Section A for the warm and invaluable help. My special thanks to Ms. Azra Baker for her valuable guidance in fulfilling the administrative formalities from time to time.

The inspiration and prayers of my parents helped me a lot in many situations during my research period. My deepest gratitude goes to my husband, K Muraleekrishnan for his love and support throughout my life. I am really proud of my husband for his encouragement, care and patience. My daughters, Aparna and Amrita offered whole hearted cooperation when I was busy with my research work.

Above all there is that supreme power whose blessings paved the way towards my goal.

**Rekha T K**

## ABSTRACT

**KEYWORDS:** Defected ground structure; lowpass filter; patch resonators; sharp roll-off; wide stopband.

Microwave filters play a major role in today's wireless communication networks. The thesis is based on different planar techniques for the design of compact microstrip lowpass filters. Three approaches are introduced for this. Cascading multiple patch resonators to design miniaturized lowpass filters with good selectivity and wide stopband is presented in the first section. Triangular and polygonal shaped patch resonators, interdigital structures embedded between high-low impedance resonators along with coupled inductive stub resonators, folded stepped impedance and modified hexagonal shaped resonators are used here to design filters. In the second method, defected ground structures are used to realize compact lowpass filters with high harmonic rejection. A lowpass filter designed to achieve compact size, sharp roll-off rate and wide stopband using defected ground and defected microstrip structures is presented in the third section. In the second and third methods, the characteristics of the basic filters are improved while retaining the compact size. The LC equivalent circuit of the filters is developed and compared successfully with EM simulated and measurement results. The material used to design and realise the above said lowpass filters is the low cost, easily available FR4 substrate with permittivity 4.4 and thickness 0.8 mm.

# TABLE OF CONTENTS

	<b>Page</b>
ACKNOWLEDGEMENT -----	i
ABSTRACT -----	iii
LIST OF TABLES -----	ix
LIST OF FIGURES -----	x
ABBREVIATIONS -----	xvi
NOTATION -----	xviii
<b>CHAPTER 1 INTRODUCTION -----</b>	<b>1</b>
1.1 The Electromagnetic Spectrum -----	1
1.2 Microwave Filters -----	3
1.3 Methodology -----	5
1.3.1 Electromagnetic Simulation Software -----	5
1.3.2 Fabrication Process and Measurement -----	7
1.4 Motivation and Objective -----	8
1.5 Thesis Organization -----	10
<b>CHAPTER 2 BASIC FILTER THEORY AND REVIEW OF LITERATURE -----</b>	<b>13</b>
2.1 Prototype of a Lowpass Filter -----	13
2.2 Types of Lowpass Filters -----	16
2.2.1 Butterworth Lowpass Filter -----	16
2.2.2 Chebyshev Lowpass Filter -----	17
2.2.3 Elliptic Function Filter -----	18
2.3 The S-parameters of a Practical Lowpass Filter -----	19
2.3.1 Cutoff Frequency, $f_c$ -----	20
2.3.2 Roll-off Rate, $\zeta$ -----	21
2.3.3 Relative Stopband Bandwidth -----	21
2.3.4 Normalized Circuit Size -----	22
2.3.5 Sharpness Factor -----	22
2.4 Basic Microstrip Structure -----	23
2.4.1 Discontinuities in the Microstrip -----	25
2.4.2 Coupled Lines -----	26
2.5 Microstrip Resonators -----	27
2.6 Conventional Design Methods of Microstrip Lowpass Filter -----	28



2.6.1	Filter Design Using Stepped Impedance Resonator -----	29
2.6.2	Filter Design Using Open Stub Resonator -----	31
2.7	Defected Ground Structures -----	32
2.8	Defected Microstrip Structures -----	35
2.9	Review of Literature -----	35

**CHAPTER 3      COMPACT LOWPASS FILTER DESIGN USING  
PATCH RESONATORS AND OPEN  
STUBS/SUPPRESSING CELLS ----- 49**

3.1	Introduction -----	49
3.2	Lowpass Filter Using Patch Resonators and Open Stubs (Filter-I) -	53
3.2.1	Resonator-1 Design and Analysis -----	54
3.2.2	Resonator-2 Design -----	59
3.2.3	Cascaded Symmetrical Structure of Resonator-1 and Resonator-2 ---	64
3.2.4	Cascaded Structure with Open Stubs -----	65
3.2.5	Equivalent Circuit of Filter-I -----	67
3.2.6	Analysis of Coupling Capacitor, $C_c$ -----	69
3.2.7	Efforts for Improving Impedance Matching in the Passband -----	70
3.2.8	Structure of the Proposed Filter-I -----	73
3.2.9	Field Distribution in the Proposed Filter -----	75
3.2.10	Fabrication and Measurement Results -----	76
3.2.11	Performance Comparison of Filter-I -----	78
3.3	Lowpass Filter Design with High Harmonic Suppression (Filter-II) --	79
3.3.1	Suppressor Unit -----	80
3.3.2	The Proposed Filter Design -----	81
3.3.3	Fabrication and Measurement Results -----	82
3.3.4	Performance Evaluation of Filter-II -----	85
3.4	Chapter Summary -----	85

**CHAPTER 4      COMPACT MICROSTRIP LOWPASS FILTERS  
WITH SHARP ROLL-OFF AND ULTRA-WIDE  
STOPBAND----- 88**

4.1	Introduction -----	88
4.2	Compact Microstrip Lowpass Filter with Ultra-wide Stopband (Filter-1) -----	92
4.2.1	Primary Stepped Impedance (SI) Lowpass Filter Design -----	93
4.2.2	Comparison of Frequency Response Characteristics of Primary SI Lowpass Filter with Basic Lowpass Filter -----	95

4.2.3	Basic Lowpass Filter - Equivalent Circuit -----	96
4.2.4	Parametric Analysis -----	98
4.2.5	Design of Improved Basic lowpass filter -----	100
4.2.6	Design of Coupled Inductive Stub Resonator -----	101
4.2.7	The Lowpass Filter Design-----	103
4.2.8	EM Field Distribution Along the Proposed Filter -----	104
4.2.9	Measured and Simulated Results -----	105
4.2.10	Performance Comparison of Filter-1 -----	108
4.3	Compact Lowpass Filter with Sharp Roll-off Using Folded Stepped Impedance Resonator (Filter-2) -----	109
4.3.1	Design Procedure of Mirrored Modified Hexagonal Shaped Resonator -----	109
4.3.2	Design of Folded Stepped Impedance Resonator -----	112
4.3.3	Parametric Analysis of FSIR -----	113
4.3.4	Design of Lowpass Filter (Filter-2) -----	114
4.3.5	Fabrication and Measurement Results -----	116
4.3.6	Performance Comparison of Filter-2 -----	117
4.4	High Selectivity and Ultra-Wide Stopband Microstrip Lowpass Filter (Filter-3) -----	118
4.4.1	Design of Filter-3 -----	119
4.4.2	Analysis of Resonator-1 -----	119
4.4.3	Analysis of Resonator-2 -----	122
4.4.4	Cascaded Arrangement of Resonator-1 and Resonator-2 -----	124
4.4.5	Final Layout of Filter-3 -----	125
4.4.6	Equivalent Circuit of Filter-3 -----	126
4.4.7	Measured and Simulated Results -----	127
4.4.8	Performance Comparison of Filter-3 -----	130
4.5	Chapter Summary -----	131

**CHAPTER 5      COMPACT MICROSTRIP LOWPASS FILTERS  
                         USING DEFECTED GROUND STRUCTURES -----133**

5.1	Introduction -----	133
5.2	Improved Frequency Response of Microstrip Lowpass Filter Using Defected Ground Structures (Filter-I) -----	136
5.2.1	Basic Microstrip Lowpass Filter Design -----	136
5.2.2	Characteristics of H-Shaped DGS-----	142
5.2.3	Compact Stepped Impedance Filter with Wide Stopband (Filter-1) --	145

5.2.4	Improved Lowpass Filter Design (Filter-2)-----	148
5.2.5	Field Distribution of Filter-2-----	150
5.2.6	Simulation and Measurement Results of Filter-2 -----	150
5.2.7	Performance Comparison of Filter-I-----	153
5.3	Compact Multilayer Microstrip Lowpass Filter with Wide Stopband (Filter-II) -----	154
5.3.1	The Design of Main Resonator -----	154
5.3.2	The Characteristics of Modified Dumbbell DGS -----	159
5.3.3	The Filter-II Structure -----	161
5.3.4	Filter Analysis and Discussion -----	163
5.3.5	The Equivalent Circuit of Filter-II -----	165
5.3.6	Fabrication and Results -----	167
5.3.7	Performance Comparison of Filter-II-----	169
5.4	Chapter Summary -----	170
<b>CHAPTER 6</b>	<b>COMPACT, SHARP ROLL-OFF LOWPASS FILTER WITH WIDE STOPBAND USING DEFECTED STRUCTURES-----</b>	<b>173</b>
6.1	Introduction -----	173
6.2	Design of the Proposed DGS -----	176
6.2.1	Comparison of the Basic DGS with the Modified DGS -----	176
6.2.2	LC Equivalent Circuit of the Modified DGS -----	179
6.2.3	Phase Characteristics of Modified DGS and SWF -----	180
6.2.4	Parametric Analysis of Modified DGS-----	182
6.3	The Lowpass filter Design Using Modified DGS -----	184
6.3.1	Characteristics of Symmetrical UIS -----	185
6.3.2	Equivalent Circuit of the Proposed Filter -----	187
6.3.3	Comparison Between Filters with Basic DGS and Modified DGS- 189	
6.3.4	Experimental Results -----	189
6.4	The Spurline Resonator-----	191
6.5	Improved Lowpass Filter Using DGS-DMS Technique-----	193
6.5.1	Experimental Results -----	194
6.5.2	Performance Evaluation -----	196
6.6	Chapter Summary -----	196

<b>CHAPTER 7</b>	<b>CONCLUSION AND FUTURE SCOPE OF THE WORK -----</b>	<b>198</b>
7.1	Summary of the Work and Conclusion-----	198
7.2	Scope of Future Developments in the Work -----	202
<b>REFERENCES</b> -----		<b>204</b>
<b>LIST OF PUBLICATIONS</b> -----		<b>217</b>
<b>CURRICULUM VITAE</b>		

## LIST OF TABLES

<b>Table</b>	<b>Title</b>	<b>Page</b>
3.1	Comparison of the frequency response characteristics of the proposed Filter-I with other works from the literature -----	79
3.2	Comparing the characteristics of the proposed work with other related works -----	85
3.3	Comparing the performance characteristics of the proposed lowpass filters using cascaded multiple patch resonators -----	86
4.1	Comparison between proposed work and related works from the literature -----	108
4.2	Comparison of the proposed filter with other related works -----	118
4.3	The physical dimensions of the proposed lowpass filter layout -----	125
4.4	The comparison of the Filter-3 with other works from the literature -----	131
4.5	Comparing the performance characteristics of the proposed filters -----	131
5.1	Performance comparison of the proposed work with related works -----	153
5.2	Comparison between the proposed Filter-II and similar works in the literature -----	170
5.3	Comparing the performance characteristics of the proposed filters-----	171
6.1	Comparing the characteristics of basic DGS and the modified DGS -----	179
6.2	Comparing the performance characteristics of the proposed work with other related works -----	196

## LIST OF FIGURES

Figure	Title	Page No
1.1	Electromagnetic spectrum -----	2
1.2	The photograph of MITS Auto lab -----	7
2.1	Lowpass prototype filter with degree $n$ -----	14
2.2	Butterworth lowpass filter response -----	17
2.3	Chebyshev lowpass filter response -----	18
2.4	Elliptic function response -----	19
2.5	Transmission and reflection characteristics of a microstrip lowpass filter -----	20
2.6	The general structure of the microstrip -----	23
2.7	The thickness versus cutoff frequency of FR4 substrate -----	25
2.8	The cross sectional view of coupled microstrip lines -----	26
2.9	Quasi TEM modes of the coupled microstrip lines (a) For even mode (b) For odd mode -----	26
2.10	$\lambda_g/4$ line resonator -----	27
2.11	$\lambda_g/2$ line resonator -----	28
2.12	Patch resonator (a) Circular (b) Triangular -----	28
2.13	The layout of 3 pole SIR lowpass filter -----	30
2.14	The S-parameters of 3 pole SIR filter -----	30
2.15	The layout of a 3 pole lowpass filter using open stub -----	31
2.16	The frequency response characteristics of a 3 pole lowpass filter using open stub -----	31
2.17	Different geometries of DGS used in the literature -----	34
3.1	Resonator-1 of Filter-I (a) Structure (b) LC equivalent circuit -----	55
3.2	Resonator-1 loaded on the main high impedance transmission line (a) Structure (b) LC equivalent circuit (c) EM and LC circuit simulation result -----	57
3.3	The frequency response characteristics of Resonator-1 (a) for different values of $l_1$ (b) For various values of $b$ -----	58
3.4	(a) Symmetrical structure of Resonator-1 (b) The simulated S-Parameters -----	59
3.5	The layout of Resonator-2 -----	60
3.6	(a) Structure of two units of Resonator-2 (b) LC equivalent circuit of the right angle bended microstrip line -----	61

3.7	(a) LC equivalent circuit of two units of Resonator-2 (b) Frequency response characteristics of LC circuit and EM simulation -----	62
3.8	(a) Symmetrical structure of two units of Resonator-2 (b) Simulated frequency response characteristics -----	64
3.9	(a) Combined symmetrical structure of Resonator-1 and Resonator-2 (b) Simulated S-Parameters -----	65
3.10	Structure of open stub -----	65
3.11	Layout of the cascaded symmetrical Resonator-1, Resonator-2 and open stubs -----	67
3.12	LC equivalent circuit of cascaded symmetrical Resonator-1, Resonator-2 and open stubs-----	68
3.13	Frequency response characteristics of EM and LC circuit simulation -----	69
3.14	Microstrip gap between the resonators -----	70
3.15	Simulated S-Parameters of the cascaded structure of symmetrical Resonator-1, Resonator-2 and open stubs -----	71
3.16	Simulated frequency response characteristics of the lowpass filter for various values of $l_2$ (a) Reflection characteristics (b) Transmission characteristics -----	72
3.17	Simulated frequency response of the filter for inductive stub structure of Resonator-2 as stair shaped and single step for length $l_2 = 6.7$ mm -----	73
3.18	Structure of the proposed lowpass filter -----	74
3.19	Simulated frequency response characteristics of the proposed filter -----	74
3.20	Electromagnetic field distribution of proposed filter (a) At frequency 1 GHz (b) At frequency 7.5 GHz -----	76
3.21	(a) Prototype of the Filter-I (b) Measured and simulated frequency response characteristics -----	77
3.22	Measured and simulated group delay characteristics of the Filter-I -----	78
3.23	(a) The configuration of the suppressing unit (b) Its frequency response characteristics -----	80
3.24	Layout of Filter-II -----	82
3.25	Simulated frequency response characteristics -----	82
3.26	The proto type of the Filter-II -----	83
3.27	The measured and simulated results of Filter-II -----	83
3.28	The measured group delay of the Filter-II -----	84

3.29	The measured group delay of the Filter-II in the 77% of the passband -----	84
4.1	Layout of the primary SI lowpass filter -----	93
4.2	The frequency response characteristics of the primary SI lowpass filter -----	94
4.3	The structural layout of the basic lowpass filter -----	95
4.4	The frequency response characteristics of the basic lowpass filter -----	95
4.5	The comparison of frequency response characteristics of the primary SI filter and the basic lowpass filter -----	96
4.6	LC equivalent circuit of the basic lowpass filter -----	97
4.7	The transmission characteristics of the basic lowpass filter for different values of $C_i$ -----	99
4.8	The variation in transmission zero values for increasing values of $C_i$ -----	99
4.9	Transmission characteristics of the basic lowpass filter for various values of $l_d$ -----	100
4.10	Geometry of the improved basic lowpass filter -----	100
4.11	The frequency response characteristics of the improved basic lowpass filter -----	101
4.12	Layout of the coupled inductive stub resonator -----	102
4.13	Comparison of the frequency response characteristics of the single stub and coupled stub resonator -----	103
4.14	The structure of the proposed lowpass filter (Filter-1)-----	103
4.15	Simulated frequency response characteristics of Filter-1 -----	104
4.16	The field distribution of Filter-1 (a) In the passband frequency of 1 GHz (b) In the stopband frequency of 4.1 GHz -----	105
4.17	(a) The prototype of the proposed lowpass filter (b) Simulated and measured results -----	106
4.18	The measured group delay of the proposed lowpass filter -----	107
4.19	The measured VSWR of the proposed lowpass filter -----	108
4.20	Step by step design process of MMHSR and its simulation result (a) A 3-pole lowpass filter (b) A high impedance stub loaded with tapered structure (c) Modified hexagonal shaped resonator (d) Mirrored modified hexagonal shaped resonator (e) Transmission characteristics of Fig.4.20a,b,c,d -----	110
4.21	Structure of folded stepped impedance resonator -----	112



4.22	Frequency response characteristics of the folded stepped impedance resonator -----	113
4.23	Transmission characteristics of FSIR (a) For various values of horizontal stub length, $L_7$ (b) Different values of rectangular patch width, $L_9$ -----	114
4.24	Structural geometry of the proposed lowpass filter -----	115
4.25	The simulated characteristics of the Filter-2 -----	115
4.26	The fabricated lowpass filter (a) Photograph (b) Measured and simulated results -----	117
4.27	(a) The structure of Resonator-1 (b) The frequency response -----	120
4.28	The LC equivalent circuit of Resonator-1 -----	121
4.29	(a) Layout of Resonator-2 (b) Frequency response -----	122
4.30	LC equivalent circuit of Resonator-2 -----	123
4.31	(a) Cascaded structure of Resonator-1 and Resonator-2 (b) Frequency response -----	124
4.32	Layout of the proposed Filter-3 -----	125
4.33	(a) The LC equivalent circuit of Filter-3 (b) Frequency response of EM and LC circuit simulation -----	126
4.34	(a) The fabricated prototype of Filter-3 (b) Comparison between the measured and simulated results -----	128
4.35	The measured group delay of Filter-3 -----	129
4.36	The measured group delay of Filter-3 for 63 % of the passband -----	129
4.37	The measured VSWR of Filter-3 -----	130
5.1	The primary resonator (a) Structure (b) LC equivalent circuit (c) Frequency response characteristics -----	139
5.2	a) Layout of the basic lowpass filter (b) Simulated frequency response -----	140
5.3	One pole H-shaped DGS lowpass filter (a) Schematic diagram (b) Transmission response of EM and LC circuit simulation (c) LC equivalent circuit (d) Current distribution at resonant frequency -----	144
5.4	Frequency response of H-shaped DGS (a) For various values of $a$ (b) For various values of $c$ -----	145
5.5	Layout of the proposed Filter-1 (a) Top view (b) Bottom view -----	146
5.6	(a) LC equivalent circuit of Filter-1 (b) Frequency response of measured, EM and LC circuit simulation of Filter-1 -----	148

5.7	The structure of Filter-2 (a) Top view (b) Bottom view -----	149
5.8	EM field distribution of Filter-2 (a) In the passband frequency of 1 GHz. (b) In the stopband frequency of 11 GHz-----	150
5.9	a) Top and bottom view of the Filter-2 (b) Measured and simulated frequency response -----	151
5.10	The measured group delay of Filter-2 -----	152
5.11	The measured VSWR of Filter-2 -----	152
5.12	The T-shaped resonator (a) LC equivalent circuit (b) Layout (c) The comparison of EM and LC circuit simulation -----	155
5.13	$S_{21}$ characteristics of the filter for different values of $A_2$ -----	157
5.14	Modified T-shaped structure. (a) Layout (b) Frequency response characteristics -----	158
5.15	One pole lowpass filter with modified dumbbell DGS (a) Structure (b) Frequency response characteristics -----	159
5.16	One pole lowpass filter with modified dumbbell DGS (a) Surface current at resonant frequency (b) Electric field at resonant frequency (c) LC equivalent circuit (d) Comparison between EM simulation and circuit simulation -----	160
5.17	3 D view of the Filter-II -----	162
5.18	Layout of the proposed filter (a) Top view (b) Bottom view -----	163
5.19	Simulated S-parameters of the Filter-II (a) Filter with OS only (b) Filter with OS and SSRs (c) Filter with OS, SSRs and SCs (d) The proposed Filter-II -----	165
5.20	The LC equivalent circuit of Filter-II -----	166
5.21	The EM and LC circuit simulation result of Filter-II -----	166
5.22	The proposed Filter-II (a) Top view (b) Bottom view (c) Measured and simulated results -----	168
5.23	Measured and simulated group delay -----	169
5.24	The measured VSWR of Filter-II -----	169
6.1	a) Layout of one pole basic DGS filter (b) Structure of the proposed one pole modified DGS filter (c) Comparison of frequency response characteristics -----	177
6.2	a) The LC equivalent circuit of one pole filter with modified DGS (b) Comparison between EM and LC circuit simulation results -----	180
6.3	Phase characteristics of microstrip line with modified DGS, microstrip line with basic DGS and the microstrip line without DGS -----	181

6.4	Slow wave factor of modified DGS -----	182
6.5	The frequency response characteristics of modified DGS based filter for different values of $a'$ , $g$ and $l_f$ -----	184
6.6	Layout of the proposed filter (a) Top view (b) Bottom view -----	185
6.7	The equivalent circuit of the top surface of the proposed structure -----	186
6.8	a) LC equivalent circuit of the proposed filter (b) EM and LC circuit simulation comparison -----	188
6.9	Comparing the frequency response characteristics of filter with basic DGS and modified DGS -----	189
6.10	a) Measured and simulated results of the proposed filter (b) Top and bottom prototype -----	190
6.11	Measured results of the proposed filter -----	191
6.12	Configuration of spurline resonator -----	192
6.13	a) LC equivalent circuit of the spurline filter (b) Comparing EM and LC circuit simulation -----	193
6.14	Geometry of the DGS-DMS lowpass filter (a) Top view (b) Bottom view -----	194
6.15	Proto type of the DGS-DMS lowpass filter -----	195
6.16	Frequency response characteristics of DGS-DMS lowpass filter -----	195
6.17	Measured passband group delay -----	195

## ABBREVIATIONS

BCMRC	Beeline Compact Microstrip Resonant Cell
CMRC	Compact Microstrip Resonant Cell
CSDGS	Cross Shaped Defected Ground Structure
CSRR	Complementary Split Ring Resonators
DBS	Dual Band Stub
DGS	Defected Ground Structure
DMS	Defected Microstrip Structure
EBG	Electromagnetic Band Gap
EM	Electromagnetic
FR4	Fire Resistant Grade 4
FSIR	Folded Stepped Impedance Resonator
GSM	Global System for Mobile
HF	High Frequency
HFSS	High Frequency Structure Simulator
HTS	High Temperature Superconducting
IPD	Integrated Passive Device
MMHSR	Mirrored Modified Hexagonal Shaped Resonator
MMIC	Monolithic Microwave Integrated Circuit
MOM	Method of Moments
NCS	Normalized Circuit Size
OCSR	Open Complementary Split Ring Resonator
PBG	Photonic Band Gap
PCB	Printed Circuit Board
PCS	Personal Communications Service
RF	Radio Frequency

RFID	Radio Frequency Identification
RL-PB	Return Loss-Passband
RSB	Relative Stopband Bandwidth
SCMRC	Spiral Compact Microstrip Resonant Cell
SI	Stepped Impedance
SIS	Stepped Impedance Stub
SMA	Sub Miniature version A
SRR	Split Ring Resonator
SWF	Slow Wave Factor
TCMRC	Tapered Compact Microstrip Resonant Cell
TEM	Transverse Electromagnetic
TSV	Through Silicon Via
TZ	Transmission Zero
UHF	Ultra High Frequency
UIS	Uniform Impedance Stub
UMTS	Universal Mobile Telecommunications System
VHF	Very High Frequency
VSWR	Voltage Standing Wave Ratio
WLAN	Wireless Local Area Network

## NOTATION

### English Symbols

$c$	Free space velocity of electromagnetic waves
$f_c$	Cutoff frequency of the filter
$f_0$	Resonant frequency of the filter
$f_s$	Stopband frequency of the filter
$g_0$	Source resistance
$h$	Thickness of substrate
$L_I$	Insertion loss
$L_R$	Return loss
$n$	Order of the filter
$S_{11}/S_{22}$	Reflection coefficient scattering parameter
$S_{12}/S_{21}$	Transmission coefficient scattering parameter
$S/N$	Signal to noise ratio
$t$	Thickness of the conducting strip
$v_p$	Phase velocity
$w$	Width of the conducting strip
$Y_e$	Even mode input admittance
$Y_o$	Odd mode input admittance
$Z_{0C}$	Characteristic impedance of a microstrip line
$Z_0$	Source impedance

## Greek Symbols

$\xi$	Roll-off rate or selectivity of the filter
$\tau_p$	Phase delay
$\tau_d$	Group delay
$\beta$	Propagation constant
$\theta$	Electrical length of microstrip line
$\tan \delta$	Loss tangent of substrate
$\alpha_{max}$	Attenuation point at the frequency $f_s$
$\alpha_{min}$	3 dB attenuation point
$\lambda_0$	Free space wavelength
$\lambda_g$	Guided wavelength at the 3 dB cutoff frequency of the filter
$\epsilon_r$	Relative permittivity or dielectric constant of substrate
$\epsilon_{re}$	Effective permittivity of substrate

# CHAPTER 1

## INTRODUCTION

### 1.1 THE ELECTROMAGNETIC SPECTRUM

The electromagnetic spectrum is the distribution of all relevant frequencies of electromagnetic radiation. It covers frequency components ranging from 1 Hertz to above  $10^{25}$  Hertz. These frequencies are divided into separate frequency bands and are addressed by different names. Earlier, the known part of Electromagnetic spectrum was only the visible light. The ancient Greeks identified the travel of light as straight lines and analyzed the light properties such as reflection and refraction. William Herschel discovered infrared radiation in 1800, which falls next to visible light. He observed that maximum temperature is developed by the frequency component beyond red. In the next year, 1801, Johann Rittar worked on the other end of the spectrum and named the new part of the spectrum as ultra violet radiation. In 1845, Michael Faraday first linked electromagnetic radiation to electromagnetism and he noticed that the light polarization is analogues to magnetic field. In 1860's James Clerk Maxwell realized that the electromagnetic waves travel at the speed of light and he subsequently developed four partial differential equations for electromagnetic field. In 1886, Heinrich Hertz attempted to prove the theoretical equations of Maxwell and tried to generate radio waves. He found that the radio waves travel at the speed of light and possess the properties of reflection and refraction. He generated the microwaves and measured its properties and this paved the way for the invention of wireless communication such as wireless telegraphy and radio. During an experiment in 1895, Wilhelm Rontgen noticed an emission of new radiations and he



named these as X-rays. He found that these rays were able to travel through biological substances and get reflected by any denser matter, and thus it can be used for medical analysis of human body. The end portion of electromagnetic spectrum was occupied with gamma rays. In the year 1900, the French physicist, Paul Ulrich Villard, during the experimentation on the radio activity of radium, noticed a new type of radiation. As per his theory, these radiations are similar to alpha and beta particles, but can penetrate more powerfully. In 1903, Ernest Rutherford named these radiations as gamma rays. Afterwards, in 1910 William Henry Bragg established that these rays also come under electromagnetic radiation and are not particles as believed earlier. Fig. 1.1 shows the electromagnetic spectrum.

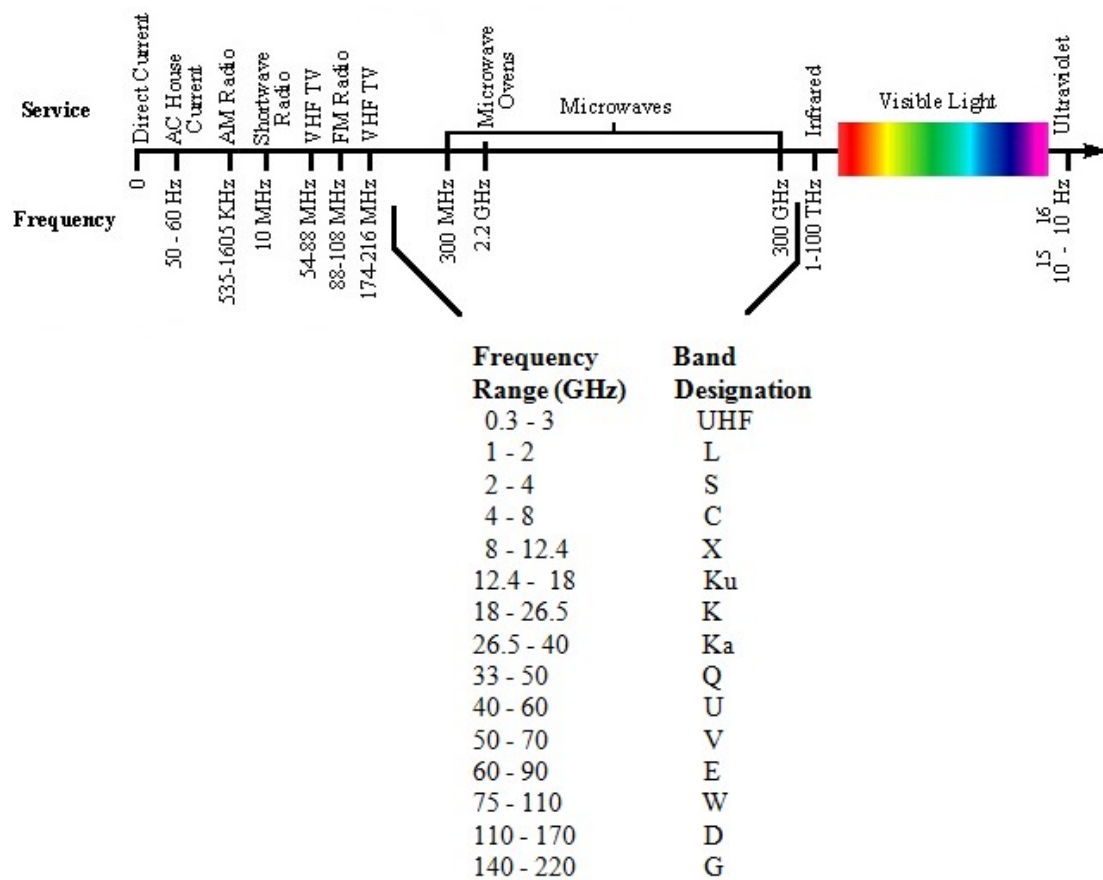


Fig. 1.1 Electromagnetic spectrum

The thesis is concentrated on radio frequency/microwave spectrum. The microwaves are radio waves with frequency ranging from 300 MHz to 300 GHz. In terms of wavelength the spectrum extends from one meter to one millimeter. The microwave technology has been used in a wide range of applications. Conventionally it has been used in telecommunication areas and also in sensing and imaging applications. The areas of applications are categorized as but not limited to radar, defence, security, food processing, point to point communication, satellite, cellular technology etc. All these applications operate in the frequency range from 300 MHz to 300 GHz and these frequencies are divided into different frequency bands, shown in Fig. 1.1.

## **1.2 MICROWAVE FILTERS**

The electromagnetic spectrum is very limited and it is necessary to be shared for different applications. Thus the concept of filtering is very important in the RF/microwave frequency applications. The important function of the filter is to separate different frequency components and to differentiate the wanted signal from unwanted ones. Also they are used to restrict the radio frequency (RF) signals within the assigned spectral limits. Depending on the specifications, RF filters designed using distributed element circuits can be realized using waveguide, microstrip, coaxial line etc. Day to day applications of radio frequencies include the wireless communications, which uses microwave filters meeting requirements such as:

- High performance
- Low cost
- Lighter weight
- Compact size

Most RF/microwave filters are formed using one or more than one coupled resonators. Planar transmission lines, for example, stripline, microstrip, coplanar waveguide etc are used to make good resonators and thereby filters. The resonating frequency of the resonator determines the frequency response characteristics of that particular filter.

Different microstrip components often considered in filter design include lumped inductors and capacitors, quasi lumped elements and resonators. Resonators are any type of structure, which contains at least one oscillating electromagnetic field. The resonators are distributed elements and may be termed as quarter wavelength resonators or half wavelength resonators, since they are  $\lambda_g/4$  long or  $\lambda_g/2$  long, where  $\lambda_g$  is the guided wavelength at the fundamental resonant frequency. The choice of components depends on the type of filters, the adopted fabrication techniques, acceptable losses, power handling capability and the operating frequency.

The microstrip resonator is the common choice for the development of RF and microwave circuits. The important advantages of microstrip resonator are its small size, easy processing using photolithography and adaptability with active components. Compared to other resonators, the important disadvantage of microstrip resonator is the increased value of insertion loss.

Nowadays filters find applications not only in the field of communication, but also in different types of electrical equipments. Based on the frequency response, filters are mainly classified as lowpass filter, highpass filter, bandpass filter and band reject filter. The thesis is concentrated in the design and development of compact microstrip lowpass filters with good in-band and out-of- band frequency response characteristics.

### **1.3 METHODOLOGY**

The methodology used for simulation studies and the experimental results of the fabricated prototype are very critical for achieving the desired filter characteristics. The parametric analyses of proposed filters designed at a particular cutoff frequency are carried out using full wave electromagnetic (EM) simulation software's IE3D and Ansys HFSS. The final optimized structure is fabricated using photolithography and by using Printed Circuit Board (PCB) proto typing machine "MITS Auto Lab". The measurements are taken using Vector Network Analyzer.

Microwave filters have to be fabricated in low cost, easily available, thermally stable substrates. The substrate used for the prototype fabrication in our work is FR4 of thickness 0.8 mm. By precision design methods, high performance compact filters can be fabricated using this FR4 material.

Due to high power handling capability, patch resonators are commonly used for the design of microstrip lowpass filters. Another important advantage of using the patch resonator is the lower conductor loss as compared to the microstrip filter using line resonators. Based on the application of filters, the patches may have different shapes. Some typical shapes are triangular, circular, ring, rectangular etc.

#### **1.3.1 Electromagnetic Simulation Software**

The software simulations of different lowpass filter structures are performed using EM simulation software's IE3D and Ansys High Frequency Structure Simulator (HFSS).

IE3D, a full wave EM simulator, based on Method of Moments (MOM), is used for analyzing the characteristics of the filter such as S-parameter, group delay, voltage standing wave ratio (VSWR) etc. It is also used for the design of antenna, radio frequency identification (RFID), monolithic microwave integrated circuits (MMICs), IC interconnects, microwave and millimeter wave circuits etc. IE3D solves Maxwell's equations in integral form using green functions. It is used to analyze the surface current and electric field distribution of the simulated structure for better understanding the behavior of the filter in the passband and stopband characteristics and to prove the rationality of the equivalent circuit. MODUA is used as the circuit simulator of IE3D. The user can define lumped element parameters such as R, L, C, open circuit, short circuit and interconnections on MODUA for the EM and LC circuit simulation. All LC equivalent circuits designed in the thesis are carried out using the MODUA of IE3D.

Ansys HFSS is the globally accepted EM simulation software, which uses full wave Finite Element Method to compute the behavior of high frequency components. HFSS is used to extract the parameters such as S, Y and Z and to visualize the 3D EM fields and also used to analyze the group delay, VSWR etc of the microstrip structures. The effect of various filter parameters can be effectively studied using the optimization tool available with HFSS. Among the different boundary schemes of HFSS, the radiation boundary and perfect electric conductor boundary is commonly used in the proposed work. The scalar and vector representation of E, H and J values demonstrate the behavior of the filters in the passband and stopband characteristics.

### 1.3.2 Fabrication Process and Measurement

Photolithography is the process of transferring the geometrical structures from photolithographic sheet to the photo resistive substrate surface using ultra violet light energy.

MITS Auto Lab is a standard equipped camera monitoring system with auto tool change machine. Using MITS Auto Lab, we can fabricate single sided, double sided, multilayer and high density printed circuit boards easily. This PCB prototyping machine is used for precision cutting and fine finish of the PCB prototype, which gives accurate results compared to the structure fabricated using photolithography. It produces high quality PCBs without using any chemical raw material. The machine is capable of milling up to a minimum width of 0.1 mm which ensures a high degree of accuracy for the fabricated structure. The photograph of MITS Auto lab is shown in Fig. 1.2.

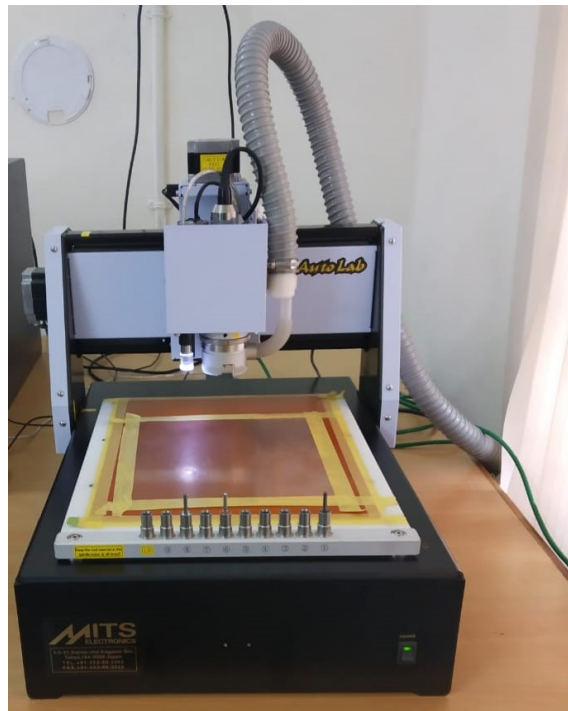


Fig. 1.2 The Photograph of MITS Auto Lab

Our microwave lab is equipped with the Rohde & Schwarz ZVL 13 and Rohde & Schwarz ZVB 20 Vector Network Analyzers, which are used for the measurement of filter characteristics. These instruments form a complete solution for the characterization of passive or active networks over 9 KHz to 13.6 GHz frequency range and 10 MHz to 20 GHz range respectively. The RF signal is fed to the proposed fabricated filter from the analyzer S-parameter test set through cables and SubMiniature version A (SMA) connectors. At high frequencies, the cables and connectors tend to be lossy. So before taking measurements, the instrument should be calibrated for two ports in open, short and through conditions suitably. The two ports of the filter are connected to the Network Analyzer for measuring the S-parameters such as the transmission characteristics ( $S_{21}$ ) and reflection characteristics ( $S_{11}$ ) and also for measuring the group delay and VSWR of the proposed structure.

#### **1.4 MOTIVATION AND OBJECTIVE**

Microwave filters play a significant role in various equipments used in our day to day life. Applications are different, ranging from common entertainment systems to sophisticated communication networks used in satellite television, military, radar systems etc. In the communication field, cellular radio is widely accepted and popular nowadays than the conventional wired telephony. RF and microwave filters are very commonly used in these systems to filter out the unwanted frequencies, while permitting wanted signals without any attenuation. Cellular communication needs filters with specific performance characteristics in base stations as well as mobile handsets. Thus the recent development and huge expansion of communication systems demanded various novel filter techniques featuring miniaturized, high

performance, light weight and low cost designs. Filters have the important property of frequency selective transmission, and are able to transmit energy in the passband and attenuate energy in the stopband.

High frequency harmonics are generated at different stages of digital switching circuits and can cause severe interference with other devices and systems. It is necessary to block all unwanted frequency components and permit only the required band of signals. Lowpass filters with high performance and compact size and capable of suppressing higher order harmonics are in great demand nowadays. It finds wide applications in modern wireless communication systems.

In microwave filter design, the lumped element realization is not often used because the wavelength is very short beyond the range of these circuit elements. Thus various distributed circuit element realizations are commonly used because one or more dimensions of elements are comparable with the signal wavelength.

Cost of the raw material is equally important along with high performance while designing filters for commercial applications. Thus FR4 substrate is a suitable choice for its low cost, easy availability and light weight. Using this substrate, a lowpass filter with good selectivity and wide stopband is realized.

The main objective of this research work is the design and development of such high performance microstrip lowpass filters, which are fabricated in FR4 substrate of thickness 0.8 mm. Different techniques are adopted for the design like cascading planar resonators, embedding interdigital structures between rectangular patches, using folded stepped impedance resonators and introducing defected structures. The



improvement in the performance characteristics of the basic lowpass filter using defected ground structures is studied in detail. The basic defected ground structure, modified by introducing interdigital slots between the square head slots to improve the roll-off rate and to reduce the circuit size of the filter is also analyzed. The LC equivalent circuits of the proposed filters are developed and compared with EM and measured results. The EM field distribution is used to study the rationality of the equivalent circuit and the characteristics of the filter in the passband and stopband.

## **1.5 THESIS ORGANIZATION**

The entire work is described in seven chapters.

Chapter 1 discusses the introduction of electromagnetic waves and characteristics of microwave filters. The methodology and motivation of the present work and thesis organization are also presented in this chapter.

Chapter 2 presents a detailed analysis of the earlier works to understand the different design techniques adopted to develop a high performance planar lowpass filter. The review of various high performance lowpass filter design methods using variety of resonators, defected ground resonator structures and defected microstrip structures are also discussed. The chapter summarizes different types of lowpass filters and the critical parameters which play a major role in the performance analysis.

Chapter 3 deals with a compact microstrip lowpass filter designed using cascaded patch resonators and open stubs/suppressing cells. The LC equivalent circuit of the filter is developed. The circuit simulation results are compared with the EM simulation results. A novel technique adopted to improve the impedance matching in

the passband is also presented. An extended work for improving the order of harmonic suppression using diamond shaped patch resonators as suppressing cells with reduced circuit size is also described.

Chapter 4 analyzes three high performance lowpass filters. An effort made to improve the roll-off rate and stopband bandwidth without sacrificing the compactness of the structure is described. In the first filter, Filter-1, an interdigital structure is embedded between microstrip stepped Hi-Lo impedance resonators, and symmetrical series connected coupled inductive stubs with rectangular patch capacitors are utilized to achieve filter characteristics such as high selectivity, wide stopband bandwidth and small physical size. In the second microstrip filter design, Filter-2, the roll-off rate is further improved using folded stepped impedance resonators. Here, wide stopband is achieved using modified hexagonal shaped resonators and cascading this structure with folded stepped impedance resonators, a filter with sharp roll-off rate of 151 dB/GHz and wide stopband up to 10.12 GHz is achieved. This work is extended so as to achieve wide stopband along with high selectivity and named as Filter-3.

Chapter 5 deals with two high performance lowpass filters designed and developed using defected ground structures to extend the stopband bandwidth. In the first filter, the frequency response characteristics of a basic microstrip lowpass filter, designed using stepped impedance resonators and uniform impedance stubs, is improved using H-shaped defected ground structures. Due to defects etched in the ground plane of the basic lowpass filter, the harmonic suppression is improved from 5<sup>th</sup> to 10<sup>th</sup> order with compact size and good impedance matching. In the second filter design, improved roll-off rate is achieved using stair shaped resonators and wide stopband bandwidth is

obtained using defected ground structures, open stub and suppressing cells. Here the characteristics of each resonator are analyzed to achieve sharp roll-off and wide stopband from the filter. These filters are used for L-band applications.

In chapter 6, a defected ground structure based filter is modified to achieve an improvement in roll-off rate and reduction in circuit size. Wide stopband bandwidth of the filter is achieved by placing mirrored open stubs in the 50  $\Omega$  microstrip line and a spurline resonator which acts as defected microstrip structure in the top microstrip line. The filter is very compact and it is designed for use in L-band applications.

Chapter 7 concludes the work and important achievements of the proposed filters are mentioned. Different lowpass filter design methods using FR4 substrate are analyzed and a conclusion is made that the proposed filters are having improved characteristics better than most of those which have been built so far using the same material. The scope of future developments is also discussed here.

## CHAPTER 2

### BASIC FILTER THEORY AND REVIEW OF LITERATURE

The basic lowpass filter theory behind the work is discussed in this chapter. The classification of different lowpass filters is also covered. The basic concept of microstrip line, its design equations, and the general principles behind the conventional methods of lowpass filter design are outlined. A detailed analysis of the earlier works in the relevant fields to understand the different design techniques adopted in the development of a high performance lowpass filter is also conducted.

#### 2.1 PROTOTYPE OF A LOWPASS FILTER

Generally a lowpass filter is defined as a filter, where the element values are normalized to achieve the condition that the source resistance becomes unity, denoted as  $g_0 = 1$ , and the cutoff angular frequency as unity denoted as  $\Omega_c = 1$  (rad/s) (Mattaei *et al.*, 1980). Filter synthesis methods for realizing the transfer functions were first initiated by the network synthesis method described in Darlington (1939), Saal and Ulbrich (1958), Weinberg (1962), Papoulis (1962) and Cauer (1958). Later the rational transfer functions for the prototype filters were developed using Temes and Mitra (1973); Rhodes (1976). An ideal lowpass filter eliminates all frequencies above cutoff frequency while permitting all frequencies below the specified value without any change and thus the frequency response appears in a rectangular function. But the transition region of the practical filters does not behave as that of a theoretical ideal filter. Fig. 2.1 demonstrates the generalized form of an  $n$ -pole lowpass prototype filter for realizing the Butterworth and Chebyshev response.

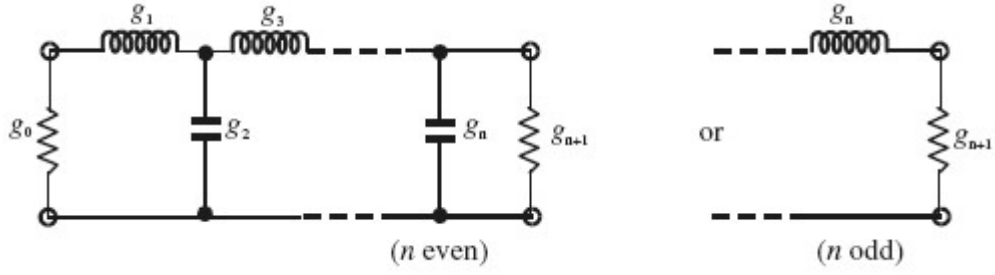


Fig. 2.1 Lowpass prototype filter with degree  $n$

From Fig. 2.1, it is noted that,  $n$  = number of reactive elements,  $g_i$  for  $i = 1$  to  $n$  represent the inductance of series inductor or the capacitance of parallel capacitor.  $g_0$  = source resistance or source conductance,  $g_{n+1}$  = load resistance or load conductance,  $g$  values represent the inductance in henries, capacitance in farads, resistance in ohms and conductance in mhos.

The transfer function of two port filter network is the mathematical expression of  $S_{21}$ . The magnitude squared transfer function of a passive network of lossless nature is represented as,

$$|S_{21}(j\Omega)|^2 = \frac{1}{1 + \varepsilon^2 F_n^2(\Omega)} \quad (2.1)$$

where,  $\varepsilon$  is the ripple constant and  $F_n(\Omega)$  represent the characteristic function. The radian frequency variable is denoted as  $\Omega$  with the cutoff frequency as  $\Omega = \Omega_c = 1$  rad/s.

Two important parameters of the filter are the insertion loss and the return loss. The insertion loss,  $L_I$  between the two ports  $m$  and  $n$  is defined as,

$$L_I = -20 \log_{10} |S_{mn}| \text{ dB} \quad m, n=1, 2 (m \neq n) \quad (2.2)$$

Based on the transfer function of Equation (2.1), the insertion loss of the filter can be computed as follows,

$$L_I(\Omega) = 10 \log_{10} \frac{1}{|S_{21}(j\Omega)|^2} \text{ dB} \quad (2.3)$$

The return loss of the filter is calculated using the formula,

$$L_R = -20 \log_{10} |S_{nn}| \text{ dB} \quad n=1, 2 \quad (2.4)$$

For a lossless two port network,  $|S_{11}|^2 + |S_{21}|^2 = 1$ , the return loss can be found using the Equation (2.5) as,

$$L_R(\Omega) = 10 \log_{10} (1 - |S_{21}(j\Omega)|^2) \text{ dB} \quad (2.5)$$

The voltage standing wave ratio, VSWR can be used instead of return loss and it is defined as,

$$\text{VSWR} = \frac{1 + |S_{11}|}{1 - |S_{11}|} \quad (2.6)$$

When the load is perfectly matched, all the transmitted power from the source is delivered to the load and the value of VSWR is 1.

When a signal is propagated through a frequency selective network, for example a filter circuit, some delay occurs in the output signal as compared to the input signal. The two important parameters that have an important role in characterizing filter performance related to this delay are the phase delay and the group delay.

The phase delay is defined as,

$$\tau_p(\omega) = \frac{\phi_{21}}{\omega} \text{ s} \quad (2.7)$$

where  $\phi_{21}$  is represented in radians and the angular frequency,  $\omega$  is represented in radians per second.

Another important term, group delay is the rate of change of transmission signal phase angle with respect to the corresponding frequency. The angle is represented in radians and the frequency in radians per unit time. For microwave frequencies, ie. in the GHz range, the unit of group delay is in nanoseconds.

$$\tau_d(\omega) = -\frac{d\phi_{21}}{d\omega} \text{ nanoseconds} \quad (2.8)$$

Flat and consistent group delay is important in many lowpass filter applications. For an ideal lowpass filter, the group delay should be constant throughout the passband region.

## 2.2 TYPES OF LOWPASS FILTERS

The practical response of lowpass filters are listed below.

### 2.2.1 Butterworth Lowpass Filter

The amplitude squared transfer function of Butterworth filters have insertion loss  $L_I$  = 3 dB at the cutoff frequency  $\Omega_c = 1$  given by,

$$|S_{21}(j\Omega)|^2 = \frac{1}{1 + \Omega^{2n}} \quad (2.9)$$

where the order of the filter is represented by  $n$ , which corresponds to the total number of reactive elements in the lowpass prototype filter. This type of filter response is also called maximally flat because its transfer function has the maximum  $(2n-1)$  number of zero derivatives at  $\Omega = 0$ . Thus the maximally flat approximation of lowpass filter in the passband is best at  $\Omega = 0$ , and the response deteriorates when  $\Omega$  approaches the cutoff frequency  $\Omega_c$  and its response characteristics is shown in Fig.

2.2. Thus the Butterworth filter is also known as maximally flat filter.

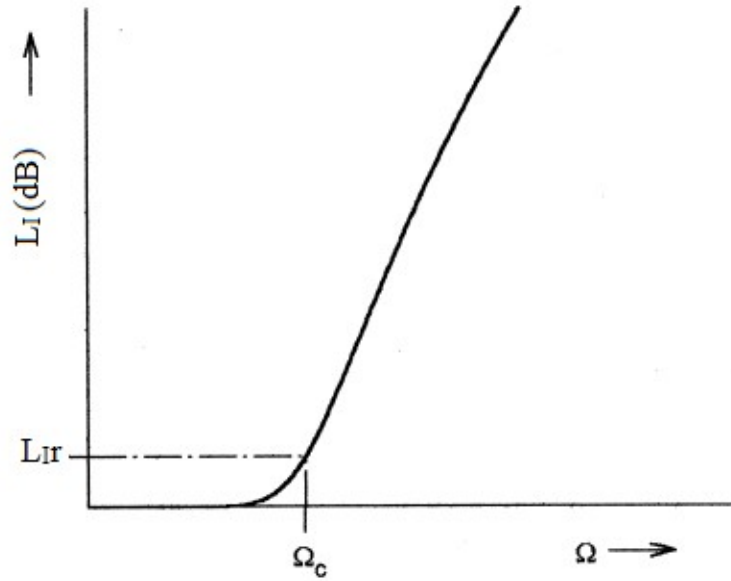


Fig. 2.2 Butterworth lowpass filter response

### 2.2.2 Chebyshev Lowpass Filter

The Chebyshev response has equal ripples in the passband and maximally flat response in the stopband. The response characteristics of the Chebyshev lowpass filter is shown in Fig. 2.3. Chebyshev filter has sharper transition band as compared to the Butterworth filter. The amplitude squared transfer function of the Chebyshev filter has its transfer function represented as

$$|S_{21}(j\Omega)|^2 = \frac{1}{1 + \varepsilon^2 T_n^2(\Omega)} \quad (2.10)$$

where  $\varepsilon$  is the ripple constant related with the specified passband ripple  $L_{Ir}$  in dB given by,

$$\varepsilon = \sqrt{10^{\frac{L_{Ir}}{10}} - 1} \quad (2.11)$$



The Chebyshev function is represented as  $T_n(\Omega)$  of order  $n$  and is defined as,

$$T_n(\Omega) = \begin{cases} \cos(n \cos^{-1}\Omega) & \text{for } |\Omega| \leq 1 \\ \cosh(n \cosh^{-1}\Omega) & \text{for } |\Omega| \geq 1 \end{cases} \quad (2.12)$$

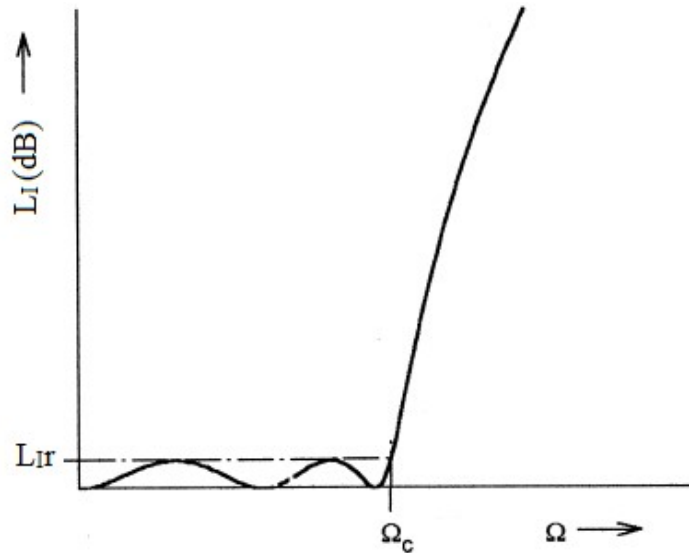


Fig. 2.3 Chebyshev lowpass filter response

### 2.2.3 Elliptic Function Filter

The Butterworth and Chebyshev filter responses have monotonically increasing attenuation in the stopband. In some applications, it is necessary to specify minimum stopband attenuation and in this case, the cutoff rate of the filter can be improved. These type of filters are called Elliptic function filters. Thus the Elliptic function filter has sharper cutoff rate as compared to the Butterworth and Chebyshev type filters. But this type of filter has equal ripples in both passband and stopband response characteristics. The frequency response characteristics of Elliptic function filters are shown in Fig. 2.4.

The transfer function of Elliptic function response is represented as,

$$|S_{21}(j\Omega)|^2 = \frac{1}{1 + \varepsilon^2 R_n^2(\xi, \Omega/\Omega_0)} \quad (2.13)$$

where the elliptic rational function of  $n^{\text{th}}$  order is represented as  $R_n$ ,  $\Omega_0$  is the cutoff frequency of the filter,  $\xi$  is the selectivity factor of the filter,  $\varepsilon$  is the passband ripple factor. The passband ripple is represented by the ripple factor and the combination of selectivity factor and ripple factor specifies the ripples present in the stopband.

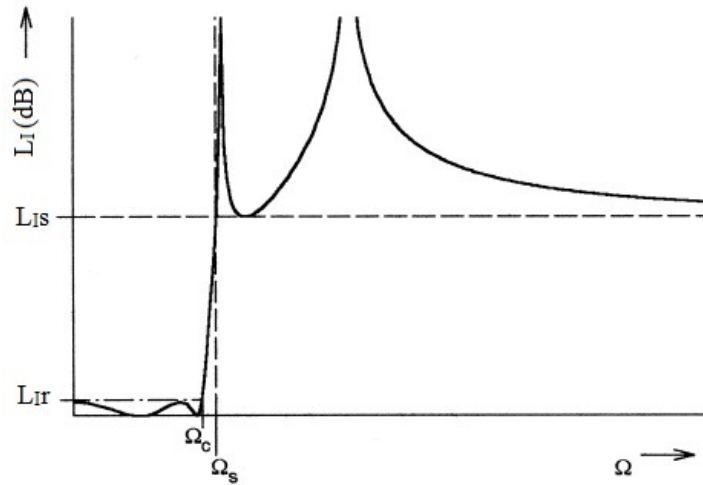


Fig. 2.4 Elliptic function response

### 2.3 THE S-PARAMETERS OF A PRACTICAL LOWPASS FILTER

The scattering parameters (S-parameters) of a two port filter network are directly measurable at RF/microwave frequency and the transmission coefficients ( $S_{12}$  and  $S_{21}$ ) and reflection coefficients ( $S_{11}$  and  $S_{22}$ ) of lowpass filter can be expressed directly in terms of its S-parameter characteristics. The S-parameter ( $S_{11}$  or  $S_{21}$ ) are generally complex term and conveniently expressed in terms of amplitude and phase.

Their amplitudes are often given in decibels and defined as,

$$20\log_{10} |S_{mn}| \text{ dB, where } m, n = 1,2 \quad (2.14)$$

The transmission and reflection characteristic of a microstrip lowpass filter is shown in Fig. 2.5.

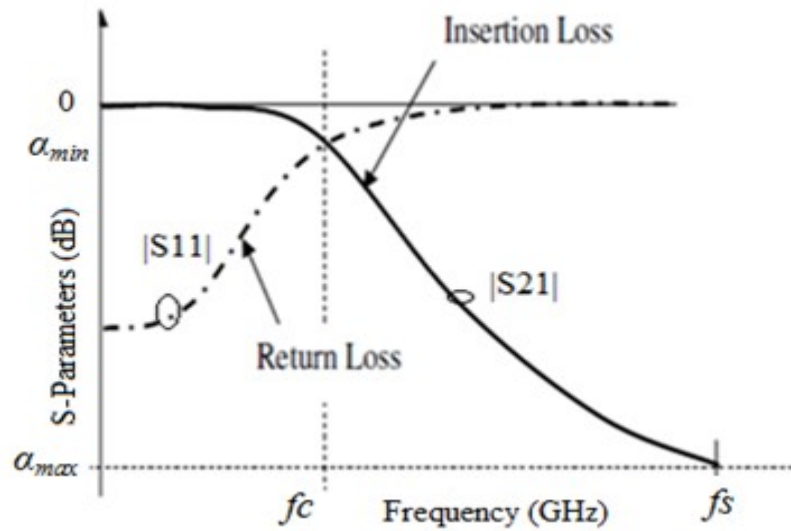


Fig. 2.5 Transmission and reflection characteristics of a microstrip lowpass filter

The important terms related to the lowpass filter are:

### 2.3.1 Cutoff Frequency, $f_c$

The cutoff frequency is one of the important characteristics of the filtering devices and it is the point where the filter attenuates the signal. The cutoff frequency of a lowpass filter is the border in the system's frequency response where the energy flowing through the system starts decreasing. It is the frequency at which the ratio of output/input has magnitude of 0.707 or in decibels, it is the -3dB point or the 3 dB down point.

### 2.3.2 Roll-off Rate, $\xi$

The roll-off rate of the filter is defined as the steepness of the transmission function with respect to the frequency. The roll-off rate is applied to the insertion loss of the network and it is the transition from passband to the stopband.

The roll-off rate,  $\xi$  is calculated using the formula,

$$\xi = \frac{\alpha_{\max} - \alpha_{\min}}{f_s - f_c} \quad (2.15)$$

where  $f_s$  is the stopband frequency,  $f_c$  is the 3 dB cutoff frequency,  $\alpha_{\max}$  is the attenuation point at the frequency  $f_s$  and  $\alpha_{\min}$  is the 3 dB attenuation point.

### 2.3.3 Relative Stopband Bandwidth

The most important function of the lowpass filter is the suppression of the unwanted harmonics. For this, the stopband bandwidth of the lowpass filter should be wide enough. The relative stopband bandwidth (RSB) is defined as the ratio of stopband bandwidth to the stopband centre frequency and it is relative with respect to the stopband suppression level of the filter.

$$\text{RSB} = \frac{\text{stopband bandwidth}}{\text{stopband centre frequency}} \quad (2.16)$$

The high value of RSB and high suppression level are important parameters for the design of lowpass filter which can suppress the highest order harmonics. It is also expressed in terms of percentage.

### 2.3.4 Normalized Circuit Size

A lowpass filter with smaller circuit size is one of the stringent requirements for wireless communication applications. The normalized circuit size (NCS) of the filter is defined as the ratio between the physical size of the filter and the guided wavelength of the filter.

The NCS is calculated as follows,

$$\text{NCS} = \frac{\text{physical size (length x width)}}{\lambda_g^2} \quad (2.17)$$

where  $\lambda_g$  is the guided wavelength at the 3 dB cutoff frequency and its value is calculated using the expression,

$$\lambda_g = \frac{\lambda_0}{\sqrt{\epsilon_{re}}} = \frac{c}{f\sqrt{\epsilon_{re}}} \quad (2.18)$$

where  $c$  is the velocity of light in vacuum and  $\epsilon_{re}$  is the relative permittivity of the substrate.

### 2.3.5 Sharpness Factor

The sharpness factor of a lowpass filter is defined as,

$$\text{sharpness factor} = \frac{f_0}{f_c} \quad (2.19)$$

where  $f_0$  is the resonant frequency and  $f_c$  is the 3 dB cutoff frequency. For an ideal lowpass filter, the value of sharpness factor is unity. But for practical lowpass filters, the value will be always greater than one. The lower value of sharpness factor indicates the sharper transition from passband to stopband and thus the selectivity of the filter is high.

## 2.4 BASIC MICROSTRIP STRUCTURE

The basic structure of a microstrip is depicted in Fig. 2.6. A conducting microstrip line of width,  $w$  having its thickness  $t$  is placed on the top of the dielectric substrate. The dielectric substrate has its relative dielectric constant  $\epsilon_r$ , and thickness  $h$  is used as shown in the Figure. The bottom plane of the substrate is the conducting ground plane.

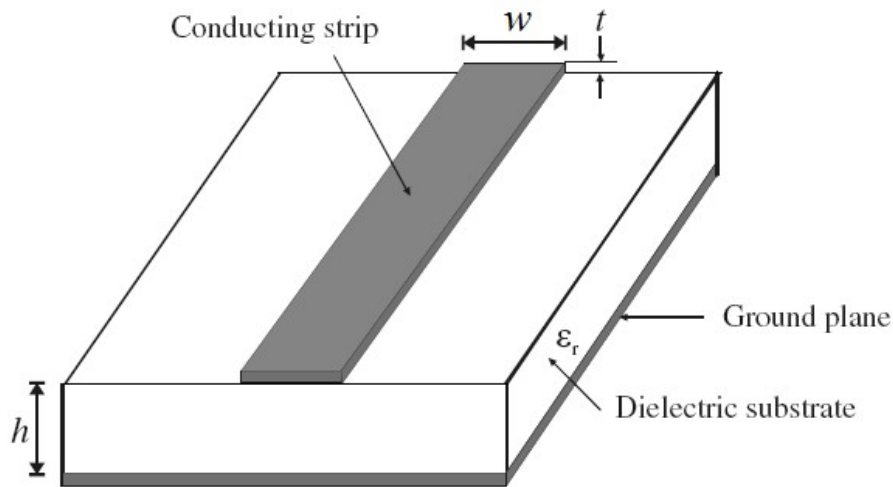


Fig. 2.6 The General Structure of the Microstrip

The fields in the microstrip does not support pure TEM wave due to its inhomogeneous nature (because the fields in microstrip extend within air above the microstrip and dielectric below). Thus due to the presence of the two guided media in the microstrip, (air and the dielectric substrate), quasi-TEM approximation is commonly used, and its wave propagation velocity depends not only on the properties of the material such as permeability and the permittivity, but also on its physical dimensions (Hong and Lancaster, 2001). The transmission characteristics of the microstrip mainly depend on two important parameters namely, effective dielectric constant,  $\epsilon_{re}$  and the characteristic impedance,  $Z_{0C}$ . The effective dielectric constant depends on the relative permittivity of the substrate, width,  $w$  of the microstrip line

and the thickness of the dielectric substrate. The characteristic impedance of the microstrip line depends not only on the line width  $w$  and thickness  $h$ , but also on the effective dielectric constant of the microstrip. The closed form expressions for the calculation of  $\epsilon_{re}$  and  $Z_{0C}$  are in Equations (2.20) - (2.24) (Hong and Lancaster, 2001).

For  $w/h \leq 1$ ,

$$\epsilon_{re} = \frac{\epsilon_r + 1}{2} + \frac{\epsilon_r - 1}{2} \left\{ \left( 1 + 12 \frac{h}{w} \right)^{-0.5} + 0.04 \left( 1 - \frac{w}{h} \right)^2 \right\} \quad (2.20)$$

$$Z_{0C} = \frac{\eta}{2\pi\sqrt{\epsilon_{re}}} \ln \left( \frac{8h}{w} + 0.25 \frac{w}{h} \right) \quad (2.21)$$

where  $\eta$  is the free space wave impedance and its value is  $120\pi$ .

For  $w/h \geq 1$ ,

$$\epsilon_{re} = \frac{\epsilon_r + 1}{2} + \frac{\epsilon_r - 1}{2} \left( 1 + 12 \frac{h}{w} \right)^{-0.5} \quad (2.22)$$

$$Z_{0C} = \frac{\eta}{\sqrt{\epsilon_{re}}} \left\{ \frac{w}{h} + 1.393 + 0.677 \ln \left( \frac{w}{h} + 1.444 \right) \right\}^{-1} \quad (2.23)$$

The guided wavelength,  $\lambda_g$  of quasi TEM mode of the microstrip is given by,

$$\lambda_g = \frac{\lambda_0}{\sqrt{\epsilon_{re}}} \quad (2.24)$$

where  $\lambda_0$  is the free space wavelength at the 3 dB cutoff frequency.

The substrate thickness,  $h$  has an important role in defining the performance characteristics of the filter. The cutoff frequency versus the thickness of the FR4 substrate is shown in Fig. 2.7. As the value of  $h$  decreases, the cutoff frequency also reduces and thus compactness of the filter is achieved. Thus we can conclude that by reducing the thickness of the substrate, the size miniaturization of the filter can be achieved.

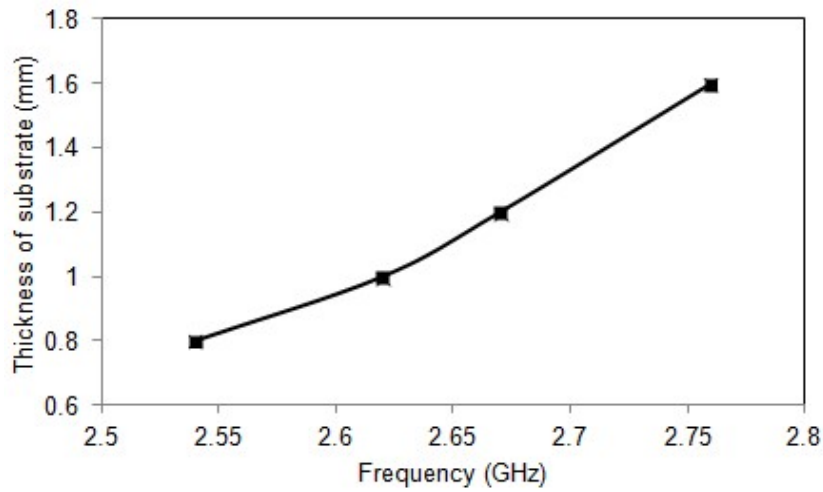


Fig. 2.7 The thickness versus cutoff frequency of FR4 substrate

#### 2.4.1 Discontinuities in the Microstrip

Microstrip discontinuities are commonly found in the structural layout of the practical filters which include step discontinuity, bend, gaps between microstrips and open ended discontinuity. The effect of discontinuity in microstrip lines are accurately modelled and can be considered in the filter designs with electromagnetic simulations. The closed form expressions for the equivalent circuit models of the discontinuities are useful in several circuit analysis. For microstrip discontinuities, numerous closed-form expressions are available in the open literature. The bend and gap discontinuity useful for equivalent circuit analysis is discussed in detail in the coming chapter.



### 2.4.2 Coupled Lines

Coupled lines are commonly used for the implementation of microstrip filters. Fig. 2.8 shows the cross sectional view of a pair of coupled microstrip lines, each having width  $w$ , and arranged in parallel configuration and separated by spacing,  $s$ .  $\epsilon_r$  is the dielectric permittivity of the substrate and  $h$  is the thickness of the substrate.

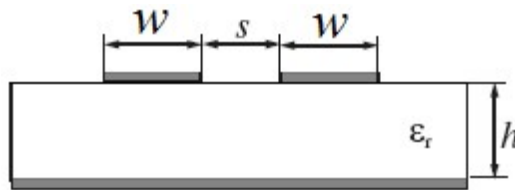


Fig. 2.8 The cross sectional view of coupled microstrip lines

The coupled line structure shown in Fig. 2.9 supports two quasi TEM modes, which are termed as even mode and the odd mode. In these two modes, the fields are distributed differently above and below the microstrip line.

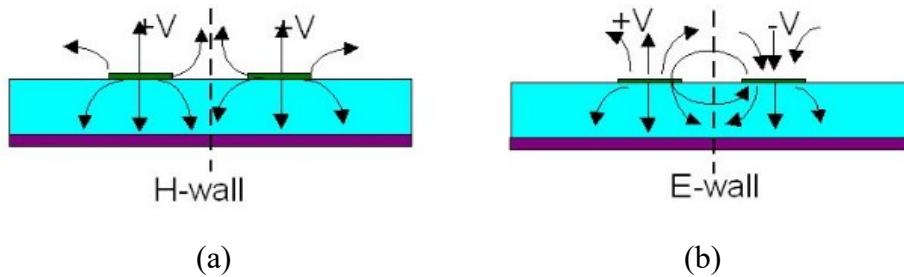


Fig. 2.9 Quasi TEM modes of the coupled microstrip lines (a) For even mode  
(b) For odd mode

As shown in the Fig. 2.9(a), for even mode of excitation, both coupled microstrip lines have same potentials, for example say positive values, which results a magnetic wall at the symmetric plane. Thus, in the even mode of excitation, no current flows between the two strip conductors. When odd mode is excited, both coupled microstrip lines have opposite potentials, which result in an electric wall at the symmetry plane

as shown in the Fig. 2.9(b). Generally, these two quasi TEM modes will be excited at the same time and will propagate with different phase velocity. Thus the coupled microstrip lines are characterized by the effective dielectric constant as well as characteristic impedance of these even and odd modes.

## 2.5 MICROSTRIP RESONATORS

Microstrip resonators are widely used in applications of filters, oscillators, tuned amplifiers etc. A resonator is a structure, which contains at least one oscillating EM field. The microstrip resonators used for the filter designs are classified as lumped element or quasi lumped element resonators and distributed line resonators and patch resonators. The lumped element or quasi-lumped element resonators, which are formed by lumped or quasi-lumped inductors and capacitors will resonate at  $\omega_0 = 1/\sqrt{LC}$ .

The distributed line resonators are also termed as quarter wavelength resonators or half wavelength resonators because they are  $\lambda_g/4$  or  $\lambda_g/2$  long, where  $\lambda_g$  is the guided wavelength at the cutoff frequency. In the  $\lambda_g/4$  resonator, the total length of the stub is 1/4 of the guided wavelength and in the  $\lambda_g/2$  resonator, the length of the stub is 1/2 of the guided wavelength. The  $\lambda_g/4$  line resonator is used as a shunt series resonator as shown in Fig. 2.10(a) and  $\lambda_g/4$  line resonator may be used as shunt parallel resonance as shown in Fig. 2.10(b).

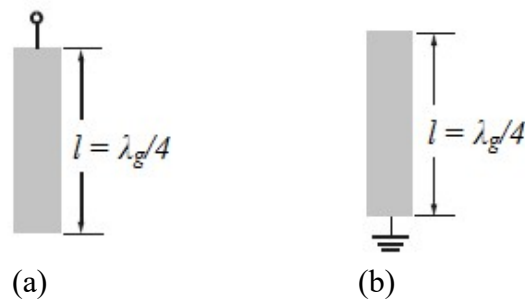


Fig. 2.10  $\lambda_g/4$  line resonator

Fig. 2.11 shows the distributed line resonator used as half wavelength resonator. The quarter wavelength and half wavelength line resonators can be used in different configurations for the implementation of various filter designs (Hong and Lancaster, 1996).

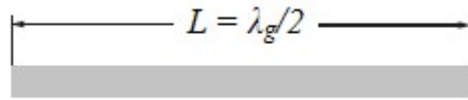


Fig. 2.11  $\lambda_g/2$  line resonator

Patch resonators are of great interest nowadays for designing planar filters. Due to its high power handling capability and lower conductor loss, it is widely used than microstrip type line resonators (Monsour *et al.* 1996; Hong and Lancaster, 2000). Based on the applications, patches are designed in different shapes such as triangular, circular etc. Some typical patch shapes are shown in Fig. 2.12.

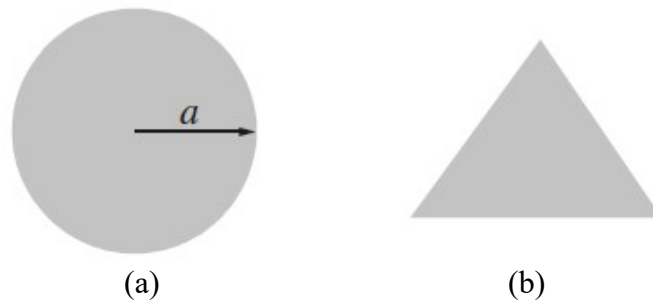


Fig. 2.12 Patch resonator (a) Circular (b) Triangular

## 2.6 CONVENTIONAL DESIGN METHODS OF MICROSTRIP LOWPASS FILTER

The conventional microstrip lowpass filter design methods are the stepped impedance LC ladder type resonator and open circuited stub resonator.

### 2.6.1 Filter Design Using Stepped Impedance Resonator

The general structural layout of a three pole stepped impedance microstrip lowpass filter is shown in Fig. 2.13. The structure consists of cascaded high impedance and low impedance lines arranged alternatively. The physical length of the high and low impedance lines should be very much shorter than its associated guided wavelength to act as semi lumped elements. The characteristic impedance of the high and low impedance lines are represented as  $Z_L$  and  $Z_C$  respectively and are calculated using the Equation (2.21) and (2.23). If the value of  $Z_L > Z_0$ , the high impedance line is better approximated to series inductance and if  $Z_C < Z_0$ , the low impedance transmission line behaves as the shunt capacitance, where  $Z_0$  is the source impedance and its value is  $50 \Omega$ . The physical length of high impedance line is represented as  $l_L$  and the low impedance rectangular line is  $l_C$ . The  $l_L$  and  $l_C$  are calculated using the Equations (2.25)-(2.26),

$$l_L = \frac{\lambda_{gL}}{2\pi} \sin^{-1} \left( \frac{\omega_c L_1}{Z_L} \right) \quad (2.25)$$

$$l_C = \frac{\lambda_{gc}}{2\pi} \sin^{-1} (\omega_c C_1 Z_c) \quad (2.26)$$

where  $\lambda_{gL}$  and  $\lambda_{gc}$  are the corresponding guided wavelength at the cutoff frequency and are calculated using the Equation (2.24) and  $\omega_c$  is the angular cutoff frequency. The high impedance line is approximated to the inductance  $L_1$  and the low impedance line is represented as capacitance  $C_1$ . The values of the layout are  $l_L = 9.81$  mm,  $l_C = 7.11$  mm,  $w_L = 0.2$  mm and  $w_C = 4.0$  mm. The filter is fabricated using the substrate of relative permittivity 10.8 and thickness 1.27 mm. The frequency response characteristics of the three pole lowpass filter is shown in Fig. 2.14. From the

transition characteristics, it is seen that the transition from passband to stopband is very wide and thus the roll-off rate of the stepped impedance resonator (SIR) filter is very low.

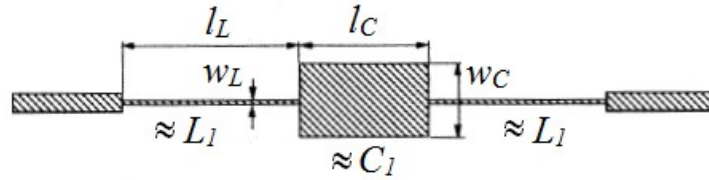


Fig. 2.13 The layout of 3 pole SIR lowpass filter

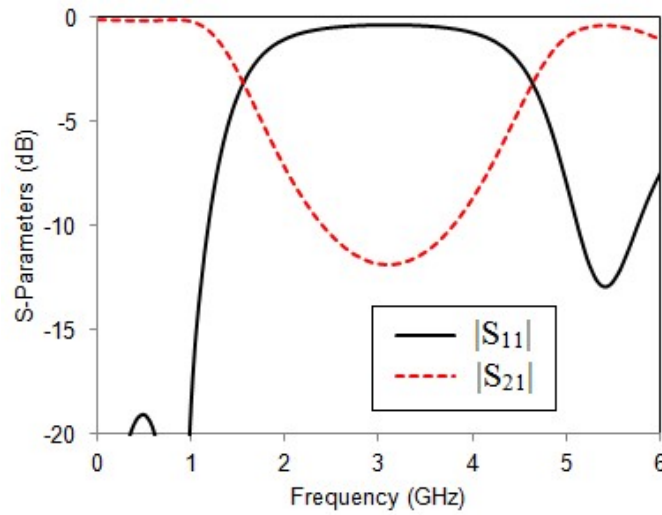


Fig. 2.14 The S-parameters of 3 pole SIR filter

Thus the SIR type filter consists of transmission lines of different characteristic impedance alternatively arranged. The resonance characteristic of the SIR is changed by varying the values of  $Z_L$  and  $Z_C$  as shown in Equation (2.27).

$$R_{SIR} = \frac{Z_C}{Z_L} \tag{2.27}$$

Lower value of  $R_{SIR}$  represents the increased stopband bandwidth of the lowpass filter.

### 2.6.2 Filter Design Using Open Stub Resonator

Another method of microstrip realization of lowpass filter design is by using shunt capacitor as the open circuited stub, which is placed between the high impedance transmission lines. The structural layout of a 3 pole lowpass filter using open stub resonator is shown in Fig. 2.15. The physical length of the open circuited stub should be less than  $\lambda_g/4$ , where  $\lambda_g$  is the guided wavelength, so as to short out transmission and cause an attenuation pole, which will increase the stopband bandwidth of the filter.

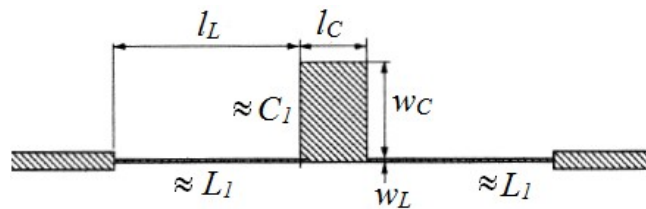


Fig. 2.15 The layout of a 3 pole lowpass filter using open stub

The structure is fabricated using the same substrate as in SIR filter design. The frequency response characteristics of the filter is shown in Fig. 2.16. As seen in the Figure, wider stopband bandwidth with a transmission zero at 5.8 GHz is achieved in this type of filter as compared to the SIR filter.

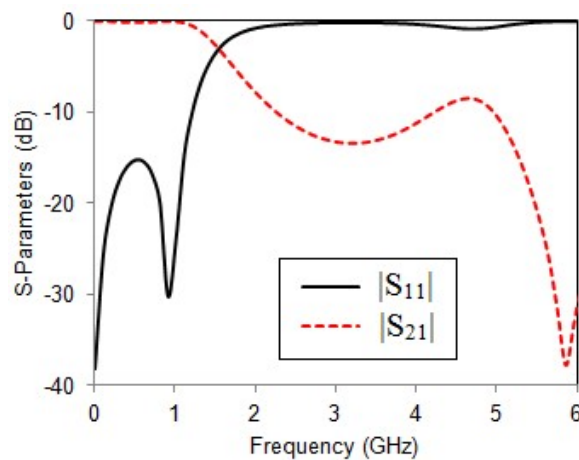


Fig. 2.16 The frequency response characteristics of a 3 pole lowpass filter using open stub

From the frequency response characteristics shown in Fig. 2.14 and Fig. 2.16, the designed filters have gradual transition from passband to stopband and hence the selectivity of the filters is very low. The stopband bandwidth of the filters is narrow and thus it is able to suppress only the first or second order harmonics. To achieve sharp cutoff frequency, higher number of reactive elements are to be incorporated, which will naturally increase the physical size of the filter.

## **2.7 DEFECTED GROUND STRUCTURES**

The concept of defected ground structures (DGSs) is a new area of research, and its evolution originated primarily from the studies of photonic band gap (PBG) structures. The PBG structures are used for EM applications and are referred as electromagnetic band gap (EBG) structures. They are periodic in nature, which prevent EM wave to propagate through them for a certain band of frequencies called stopband and allows to pass through a range of frequencies called passband. For microstrip structures, its ground plane is a suitable choice to implement EBG structures. But it was very difficult to use PBG based structures in microwave and millimeter frequency range because of the complexity of modelling and extraction of equivalent circuit and its parameters.

In 1999, a new etched lattice is proposed by Park *et al.* (1999) and named it as "PBG unit structure". They simplified the geometry of PBG and used a single cell of dumbbell shaped defect etched from the ground plane to achieve stopband in C- band and X- band. Further Kim *et al.* (2000), used the same structure and named it as defected ground structure. Thus the DGS is regarded as the simplified variant of printed EBG structure on the ground plane.

As the name implies, the defected ground structure is the single defect or the periodic number of defects etched from the ground plane of the microstrip substrate (printed circuit board (PCB)) to achieve a feature of stopping the electromagnetic wave propagation through the substrate over a certain band of frequencies. The important property of DGS slots is its resonant behavior and this characteristic depends on the size and shape of the DGS slots. The etched DGS slot under a microstrip line disturbs the current distribution occurring in the ground plane and this disturbance changes the equivalent line parameters such as line capacitance and inductance over the defected region.

DGS geometries reported in the literature include some simple shaped structures such as rectangular dumbbell head (Kim *et al.*, 2000), circular dumbbell head (Abdul-Rahman *et al.*, 2004), spiral shaped (Kim *et al.*, 2002), "U" shaped and "V" shaped (Woo *et al.*, 2006), dumbbell "H" shaped (Mandal and Sanyal, 2006), cross shaped (Chen *et al.*, 2006), double equilateral "U" (Ting *et al.*, 2006), concentric ring shaped (Guha *et al.*, 2006) etc. Different complex structures such as the split ring resonator (SRR) (Hou, 2008; Burokur *et al.*, 2005), complementary split ring resonator (Mandal *et al.*, 2006), fractal shaped (Liu, 2003) are also examined. The DGS slots are used to implement filters to suppress the unwanted harmonics, to improve the transition from passband to stopband, to achieve compactness in microwave circuits and other RF applications. Some of the simple and complex DGS shapes are shown in the Fig. 2.17. Different geometrical shapes of DGS slots have been explored by different authors to improve the performance of the filter in the passband and in the stopband and to achieve compactness and ease of design.



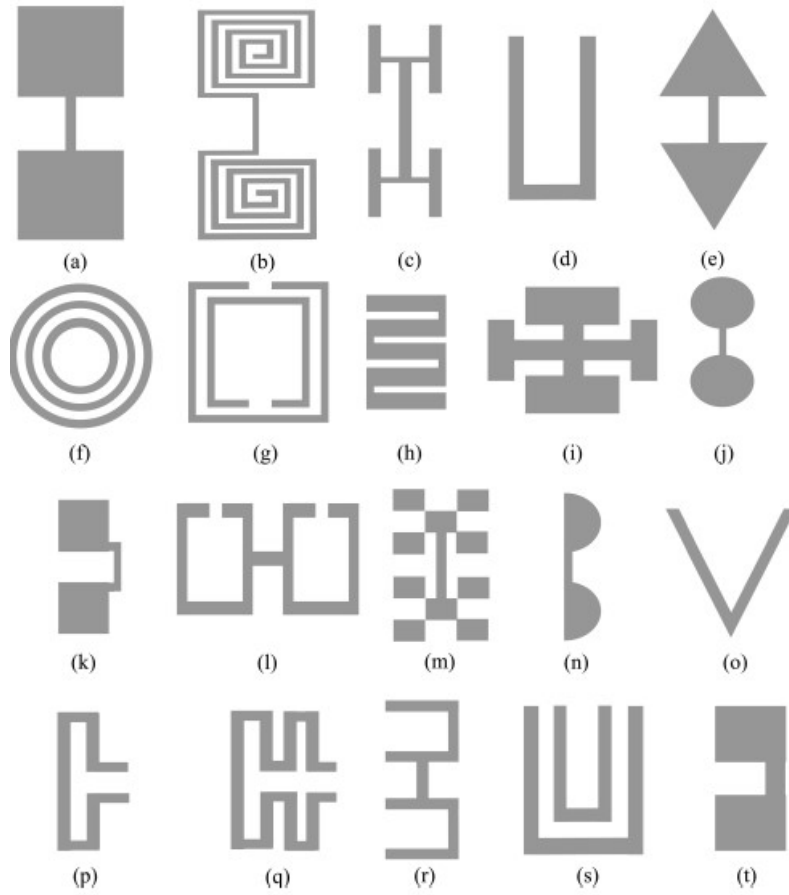


Fig 2.17 Different geometries of DGS used in the literature: (a) dumbbell shaped (b) spiral shaped (c) H shaped dumbbell (d) U shaped (e) dumbbell arrow head (f) concentric ring (g) split ring resonators (h) interdigital structures (i) cross shaped structures (j) dumbbell circular head (k) square head with U-slot (l) dumbbell-open loop (m) fractal shaped (n) half circle dumbbell (o) V shaped (p) L shaped (q) meander (r) U shaped head dumbbell (s) double equilateral U-shaped (t) square head slot with narrow slot gap.

Lowpass filter designed using DGS has many attractive features which include,

1. Simple structure
2. Wide stopband bandwidth with high suppression level than the conventional structure
3. Low insertion loss
4. Lowpass filters can be realized and implemented using smaller element values.

## **2.8 DEFECTED MICROSTRIP STRUCTURES**

Slots etched on the microstrip line called defected microstrip structures (DMSs) make a defect in the circuit, which are utilized to design filters, amplifiers, dividers etc. These defects in microstrip line create resonance characteristics. Thus similar to DGS, DMS also has stopband filter characteristics in a specific range of frequencies. These stopband characteristics depend on the size and shape of the slot in the microstrip line. DMS based structures are more immune to cross talk as well as ground plane interferences.

## **2.9 REVIEW OF LITERATURE**

Lowpass filters are the most important part of an RF/microwave systems to separate different frequencies and to suppress the unwanted high frequency harmonics. The emerging applications of modern wireless communication systems continue to challenge RF/microwave filters with stringent requirements such as small size, low insertion loss, sharp roll-off rate, wide stopband and low cost. The conventional microstrip lowpass filter design using stepped impedance L-C ladder filters and open stub filters are widely used in many radio frequency applications (Hong & Lancaster, 2001). However, these type of filters suffer from low value of roll-off rate and poor spurious frequency suppression in the stopband. Different methods used to overcome this problem and for the design of high performance planar lowpass filters are the one using a variety of resonators, and the design with DGS and the filter using DGS and DMS.

Due to the advantages of easy fabrication and smaller size, microstrip hairpin resonators have drawn much attention during the end of twentieth century in the design of lowpass filters. The first stepped impedance hairpin resonator used for

lowpass filter design is presented by Hsieh and Chang (2001). But the stopband bandwidth of the filter is limited and thus it was unable to suppress the harmonics. The stopband bandwidth is increased by using cascaded hairpin resonators, which results in increased physical size of the filter (Hsieh and Chang, 2003). By replacing the rectangular low impedance stub of hairpin resonator by radial stub, wide stopband planar lowpass filter is designed with compact size in Wei *et al.* (2011). A compact, wide stopband lowpass filter designed using a coupled line hairpin unit, two open circuited stubs and spiral shaped slot is introduced in Wei *et al.* (2012). However, the transition from passband to stopband is gradual and stopband suppression level of the filter is only 10 dB. The roll-off rate of the filter is improved by placing shunt open circuited stubs connected at the feed points of a coupled hairpin shaped resonator as presented by Velidi and Sanyal (2011). The passband and stopband bandwidth achieved in this filter is very low with low return loss in the passband. A compact lowpass filter is designed by combining meander line, coupled rectangular shaped patch and open circuited stubs to obtain wide stopband bandwidth is introduced in Chen *et al.* (2015). In all these filters different techniques have been used to improve the roll-off rate of the filter by maintaining compact size, but still the achieved roll-off rate of the filter was low. The roll-off rate of the filter is improved using modified hairpin resonator with long straight slots is designed in Abdipour *et al.* (2017). Here the rectangular patches of the conventional hairpin resonator are folded inside its free area for achieving smaller physical size and improved frequency response.

Spurious passband suppression is achieved in microstrip line filters by using split ring resonators (SRRs) as reported in García-García *et al.* (2004). SRRs are etched from the upper substrate side, which is in close proximity to the microstrip line conductor

strip, a strong magnetic coupling occurs between the line and etched ring, at the SRRs resonant frequency. This inhibits signal propagation and allows the rejection of undesired passband frequency.

Open complementary split ring resonators (OCSRRs) are the dual counter parts of the open split ring resonators, which are first proposed in coplanar waveguide technology by Velez *et al.* (2009) for miniaturizing the size of the microwave components. In Aznar *et al.* (2009), the authors demonstrated that the OCSRRs are electrically small particles which are used to design microstrip lowpass filters with sharp transition from passband to stopband. Here the cascaded arrangement of several OCSRR stages in a microstrip line is used to improve the out of band rejection and thereby increasing the stopband bandwidth. But the physical size of the filter is very large. A compact lowpass filter designed using OCSRR and open circuited stub is presented in Karthikeyan and Kshetrimayum (2011). This filter design offers more deep and wide rejection bandwidth with good selectivity than the cascaded stages of OCSRR existed at that time.

A cascaded lowpass filter designed using a microstrip line section and an interdigital capacitor is introduced by Tu and Chang (2005). The interdigital capacitor provides large capacitance value and thus finite attenuation pole is located near the passband and achieves good roll-off rate. Due to cascaded structure, the physical size of the filter is large. A compact lowpass filter with good selectivity and wide stopband bandwidth is designed by introducing an interdigital structure between symmetric rectangular shaped capacitors as presented by Li and Li (2008). Two cascaded asymmetric stepped impedance hairpin units are designed to generate compact, sharpened skirt and wide

stopband lowpass filter is demonstrated by Li *et al.* (2010); Yasuzumi *et al.* (2010). Here an interdigital structure is introduced between two low impedance sections of the hairpin unit to obtain two flexibly adjusted transmission zeros and thus larger zero separation is obtained without changing the stepped impedance unit. To achieve compactness in the lowpass filter design and to obtain good roll-off rate, symmetrically loaded radial shaped patches and coupled capacitors in interdigital arrangement along with meandered main high impedance transmission line are introduced by Wang *et al.* (2010). A wide stopband up to 7<sup>th</sup> harmonic suppression is achieved in this design. A compact lowpass filter with wide stopband and elliptic function response is achieved by designing a modified semi-circular shaped patch resonator in series with a semi-circle stepped impedance resonator is presented by Hayati *et al.* (2012). Here, the selectivity of the filter is improved by loading interdigital structures between the semi-circle patch. The roll-off rate and stopband bandwidth of the filter, improved using symmetrical cascaded modified hairpin resonator and U-shaped resonator is reported by Karimi *et al.* (2014). Here the high frequency harmonic rejection is achieved by modifying the centre hairpin resonator with a quasi interdigital structure and thereby wide stopband bandwidth is obtained.

One dimensional (1-D) compact microstrip resonant cell (CMRC) proposed by Xue *et al.* (2000), exhibiting remarkable slow wave and band stop performance, has inspired the researchers to reduce the size of the filters. However, its narrow stopband and low roll-off rate limited its application in practical circuits. The CMRC structures utilized for low frequency applications should be very compact to achieve reduced circuit size. To reduce the size of planar circuits, spiral CMRC (SCMRC) and asymmetric CMRC structures are developed by Xue *et al.* (2003). Here the width of

CMRC is increased which enhances the line inductance and capacitance values and leads to stronger slow-wave effect. A new SCMRC that has stronger slow wave effect is reported by Yum *et al.* (2003). By incorporating dual-band stub (DBS) with the SCMRC structures, unwanted high frequency harmonics are eliminated to achieve wide stopband bandwidth. Open stub SCMRC resonators are utilized to design a microstrip lowpass filter of compact size, low insertion loss in the passband and 20 dB stopband up to 6.5 GHz is presented by Gu and Sun (2005). A wide stopband bandwidth of 118 % at 20 dB suppression level is achieved using cascaded in-line arrangement of beeline CMRC (BCMRC) structures, which exhibits remarkable slow-wave characteristics as presented by Zhang *et al.* (2006). But the filter suffers from low roll-off rate and low value of return loss in the passband and large circuit size. An improved CMRC is implemented by adding two unsymmetrical T-shaped patches of different size to the original CMRC structure, leading to the generation of four additional transmission zeros and thus achieved wide stopband bandwidth as presented by Deng *et al.* (2007). However, these filters are designed by cascading uniform CMRCs in series, suffer from poor impedance matching in the passband and insufficient stopband suppression. These two disadvantages are overcome by developing a lowpass filter using tapered periodical CMRC topology introduced by Li *et al.* (2009). Replacing uniform CMRCs with non uniform tapered CMRC topology, the filter achieves very good performance characteristics of simple structure, good impedance matching, good return loss and suppression of up to tenth harmonics. Hayati and Lotfi (2010a) described a slit-loaded tapered CMRC to design an elliptic function microstrip lowpass filter with sharp selectivity. Compared with conventional tapered CMRC, the slit-loaded tapered CMRC has reduced size,

improved skirt performance due to low value of transition band and flat response in the passband. However, this filter is not suitable for extended passband applications. A front coupled tapered CMRC (TCMRC) used to design compact lowpass filter is presented by Hayati and Lotfi (2010b). Here instead of two tapered structures connected back to back with high impedance line, a high impedance and tapered cell with front coupling is used for stopband improvement. The non-uniform increments of inductance and capacitance make the structure a slow-wave transmission line and leads to the generation of multipoint resonance and this results in a wide stopband bandwidth.

Cascading multiple patch resonators are used to design a lowpass filter with sharp transition characteristics and wide stopband. A patch resonator that features strong slow-wave effects, compact size with sharp roll-off and a wide stopband with high suppression level is proposed by Li *et al.* (2009). It is seen that increasing the inductance value results in sharper roll-off and lower cutoff frequency and wide stopband is achieved by cascading the resonant patches. A miniaturized lowpass filter with sharp roll-off is obtained by symmetrical arrangement of triangular shaped patch and high and low impedance resonators as reported by Wang *et al.* (2010). By properly combining the resonators, the rejection of spurious harmonics occur and a wide stopband bandwidth is achieved. The filter achieves attractive features such as sharp selectivity from passband to stopband, compact size but its passband return loss is low and stopband suppression level is only 15 dB. A compact microstrip lowpass filter capable of suppressing up to sixteenth order harmonics at 15 dB rejection level is introduced by Wang *et al.* (2012). The circuit size of the filter is reduced by using meander transmission line. Here cascaded triangular and radial shaped patch

resonators are used to obtain multiple transmission zeros and thereby achieving wide stopband bandwidth with high rejection level. Cascading patch resonators of triangular shaped and polygonal shaped structures are used by Cui *et al.* (2012), to design a compact and ultra wide band rejection lowpass filter. The filter is able to suppress up to 14<sup>th</sup> order harmonics and compact size is achieved using meander transmission line. But both these filters suffer from low roll-off rate. Hayati *et al.* (2013), introduced a lowpass filter with sharp selectivity and ultra wide stopband characteristics using high impedance meandered transmission line loaded by triangular and polygonal shaped patches. The meandered transmission lines are used to reduce the circuit size and to improve the transition band from passband to stopband. A microstrip lowpass filter that exhibits a quasi-elliptical response with high value of out of band rejection for application in RFID receiver circuits is presented by Mirzaee and Virdee (2013). Here, two resonators with high-low impedance segments are used and these resonators are connected to each other with four inductive transmission paths. By cascading the resonators, the filter achieves high passband return loss and wide stopband up to 20 GHz. Compact planar lowpass filters designed using stepped impedance patch resonators are presented by Raphika *et al.* (2014); Raphika *et al.* (2016). The filters are developed using low cost FR4 substrate of 1.6 mm thickness. The sharp roll-off rate, low insertion loss and wide stopband made the filter suitable for various high frequency applications. Abdipour *et al.* (2015); Hayati *et al.* (2018) designed a microstrip lowpass filter using asymmetric high and low impedance patches and radial stubs to achieve high relative stopband bandwidth. However, due to cascaded arrangement of high and low impedance stubs, the physical size of the filter is large.



Radial stub exhibits better performance characteristics than low impedance rectangular stub and thus this structure is used as an alternative to a conventional straight stub (Giannini *et al.*, 1984; Sorrentino and Roselli, 1992). Compared to stepped impedance lowpass filters, the radial stub filters have better roll-off rate, wide stopband bandwidth, and compact size. To extend the stopband with high suppression level Ma and Yeo (2010); Ma *et al.* (2012), introduced compact stepped impedance hairpin resonators loaded with radial stubs. A planar lowpass filter designed using a coupled line transformer connected with a radial stub, termed as transformed radial stubs is reported by Ma *et al.* (2011), to achieve good roll-off and wide stopband characteristics with compact size. However, the roll-off rate of these filters is low. To increase the same and stopband bandwidth of radial resonator, two folded open stubs are added to the basic radial resonator by Hayati *et al.* (2014). By adding two open stubs, multiple transmission zeros are generated, which increases the sharpness and stopband bandwidth of the filter.

Fractal structures are used to improve the passband as well as stopband characteristics of microstrip lowpass filters. The Hi-Lo planar lowpass filters using Koch fractal geometry is used to enhance the passband performance characteristics of the microstrip lowpass filter. The improvement in passband performance is due to the gradual changes of the steps of fractal shaped microstrip line and thus the current discontinuity effect is negligible (Chen *et al.*, 2007). A semi-fractal technique is applied to hairpin microstrip resonator to enhance the selectivity of the planar lowpass filter as presented by Karimi *et al.* (2013). However, the designed lowpass filter structure is very complicated.

Stepped impedance hexangular shaped resonators are used to design lowpass filter with wide stopband (Hayati *et al.*, 2015; Sheikhi *et al.*, 2017a). Here both structures are added with symmetrical arrangement of open stubs to increase the attenuation level in the stopband. However, the roll-off rate of these filters is low.

Lowpass filters designed using T shaped resonators to obtain wide stopband bandwidth with low insertion loss are presented by Sheikhi *et al.* (2017b); Shama *et al.* (2018). Although wide stopband is achieved in this type of resonators, the major shortcoming observed in these filters is low selectivity.

Lowpass filters designed using stepped impedance resonators and open circuited stubs are presented by Wang *et al.* (2010); Shaman *et al.* (2015). To reduce the physical size of the filter, the straight high impedance transmission line is replaced by the semicircular transmission line in Wang *et al.* (2010). Lowpass filter designed for wide passband performance is reported in Shaman *et al.* (2015). Here the width of the inductive lines are chosen to be very thin ( $w = 0.05$  mm) to obtain high characteristic impedance. As we know, the inductive lines with shorter length and higher characteristic impedance gives better approximation to lumped elements and thus the stopband performance of the filter is improved. However, the narrow inductive lines are very difficult to fabricate and the filter is used to suppress only up to 3<sup>rd</sup> order harmonic passband.

Mousavi *et al.* (2016) designed a microstrip lowpass filter with high performance characteristics using modified T-shaped resonators. The important feature of these resonators is that the transmission zero location can be changed easily by using transfer function.

Cascaded square shaped open loop resonators are used to design highly compact microstrip lowpass filter as presented by Hammed *et al.* (2018). However, the roll-off rate as well as stopband bandwidth of the designed filter are very low.

Modern wireless communication systems demand compact, portable components and hence researchers are working towards the advanced development of RF front end circuits. Different approaches are used to design compact microwave filters to improve the performance of communication systems. PBG research, proposed by Yablonovitch (1987), was used in the optical region but its properties are scalable and it is applicable to wide frequency ranges. PBG structures are periodic in nature, used for certain frequency band rejection and are widely used in the microwave and millimeter wave applications (Ellis and Rebeiz, 1996; Radisic *et al.*, 1998; Kesler *et al.*, 1996). However, the equivalent circuit extraction in PBG based structures are difficult and fabrication is also complicated. So these structures are not commonly used for the design of microwave circuits. To alleviate these difficulties Park *et al.* (1999), designed the first defected ground structure, and developed a filter with microstrip line on top of the substrate and single dumbbell shaped defect etched on the ground metallic plane, and derived the equivalent circuit also. Thus DGS is the single or periodic number of defects etched from the ground metallic plane of the planar circuits. Kim *et al.* (2000), proved that the cutoff frequency of the proposed DGS depends on the effective inductance of unit DGS lattice etched from the ground metallic plane. A lowpass filter designed using microstrip defected ground structure is presented by Ahn *et al.* (2001). The author reported here that the etched defect in the ground plane disturbs the current distribution and changes the transmission line characteristics such as line capacitance and inductance. The equivalent circuit of the

DGS unit is derived using field analysis method and by employing the extracted parameters, the band gap effect of the DGS section is explained. Abdel-Rahman *et al.* (2004), examined the effect of geometrical shape of DGS slot for the performance of high and low impedance planar lowpass filter. The author noted that the geometrical shape has great influence on the characteristics of lowpass filter and compared the rectangle, square, dumbbell and arrow headed slots of equal area. Better sharpness and improved stopband response is achieved by using the arrow headed slot. A detailed review about DGS is covered by Kumar and Machavaram (2013).

Fractal shaped DGS was introduced by Liu *et al.* (2003), to design a compact lowpass filter with better selectivity and band gap than the conventional dumbbell DGS. The dimension of a conventional 11<sup>th</sup> order lowpass filter is reduced by 22.43 % using fractal shaped DGS as presented by Kufa and Raida (2013).

Baena *et al.*, 2005 explained that by properly coupling SRRs to the microstrip line, planar structures with effective negative constituent parameters can be obtained. The characteristics of a maximally flat conventional lowpass filter is improved by incorporating them with CSRRs as presented by Abid and Zhirun (2007). By etching five identical CSRR rings underneath the conventional structure, improved roll-off rate and compactness are achieved for the filter.

A microstrip line with spiral DGS slot proposed by Kim *et al.* (2002) provides compact structure with steep transition characteristics. But its narrow stopband characteristics restrict its use in lowpass filter design, and thus not useful for passband harmonics suppression. A compact H headed dumbbell DGS proposed by

Mandal and Sanyal (2006a), has sharp roll-off and wide stopband characteristics. The proposed filter has 26.3% reduction in length and is more compact than the DGS based lowpass filters developed so far. Mandal and Sanyal (2006b), proposed complementary split ring resonators (CSRR) to design and develop lowpass filter for the first time. This designed filter has the advantages of sharp roll-off and low insertion loss in the passband.

The new cross shaped DGS (CSDGS) was proposed by Chen *et al.* (2006), to develop a lowpass filter, which has not only sharp transition characteristics but also wide stopband bandwidth. The sharper transition band is achieved using only one unit of CSDGS structure and multiple transmission zeros are generated to suppress the higher order harmonics. High harmonic rejection with wide stopband obtained using two types of resonators such as dumbbell DGS and stepped impedance type shunt stub is reported by Park *et al.* (2007). But both the filters suffer from low roll-off rate.

The interdigital DGS slot is introduced by Balalem *et al.* (2007), to develop a quasi elliptic function lowpass filter. Here the slot resonant frequency is controlled by changing the interdigital slot fingers. The selectivity of the designed filter is very low.

A compact C-shaped DGS lowpass filter is introduced by Boutejdar *et al.* (2008), to develop a filter with wide stopband and low passband insertion loss. Here C-shaped open loop resonators are used to design a compact lowpass filter and wide stopband performance of the filter is achieved using cascaded C-shaped open loop resonators.

A planar lowpass filter designed using quasi yagi DGS and open stubs to obtain wide stopband with high suppression level and sharp selectivity is presented by Boutejdar (2014). The main attraction of this structure is that the stopband is controlled by the precision tuning of the dimensions of yagi arms. However, the stopband of the filter extends only till 11 GHz and thus only up to 5<sup>th</sup> order harmonic suppression is achieved.

Belbachir *et al.* (2016) introduced a lowpass filter with very good filtering characteristics for microwave mixer applications. The developed filter is a dual plane structure consisting of radial resonators and coupled C shaped DGS (C-CDGS) and derived the LC equivalent circuit of C-CDGS. However, the stopband return loss of this filter is high.

A lowpass filter designed using folded patches and high impedance lines on the top plane and a hybrid combination of slot and stepped impedance resonators on the bottom plane is reported by Jiang and Xu (2017). Due to the generation of multiple transmission zeros, a wide stopband bandwidth is achieved using this filter. However, the roll-off rate of the filter is very low and the structure is very complex and thus difficult to fabricate.

An M-shaped slot etched from the microstrip line to achieve bandstop characteristics is presented by La *et al.* (2011). Due to the narrow stopband characteristics of DMS based filters, it is not used to suppress even the first order harmonics and thus not suitable to design lowpass filter. But, defected microstrip resonators can be used with DGS structures to widen the stopband bandwidth of the lowpass filter.

Boutejdar *et al.* (2015), developed a wide stopband lowpass filter with DGS and DMS. The stopband behavior of DGS and DMS are utilized to suppress the unwanted harmonics. But the stopband of the filter is from 1.3 GHz to 8.3 GHz and thus suppression up to only 7<sup>th</sup> order harmonics is possible.

A sharp roll-off lowpass filter designed using dual plane structure with open stubs, DMS and DGS resonators is introduced by Zhang and Li (2016). The designed structure achieves good passband characteristics, but the stopband return loss of the filter is very high and its value approaches more than 10 dB in a certain range of frequencies.

A new approach of filter design is by adopting highly conductive graphene films in place of conventional copper films to achieve good performance (Zhou *et al.*, 2018). Advanced techniques like integrated passive device (IPD) (Hsiao *et al.*, 2015), through silicon via (TSV) (Yin *et al.*, 2019), etc are being used nowadays to achieve compactness. But the structure fabrication is complicated and expensive.

## CHAPTER 3

### COMPACT LOWPASS FILTER DESIGN USING PATCH RESONATORS AND OPEN STUBS/SUPPRESSING CELLS

#### 3.1 INTRODUCTION

This century witnessed expeditious development in wireless communication systems. Cellular telephony, HF/VHF/UHF radio communication systems, radar etc play a major role in common man's day to day life. Compact, low cost, light weight and high performance lowpass filter is one of the essential components in such systems. In a typical RF communication system, local oscillator and mixer are followed by a lowpass filter, to remove the unwanted harmonics or spurious signals. Lowpass filters with low insertion loss, high roll-off rate and wide stopband bandwidth at high suppression level are necessary for achieving the linearity of RF front-end circuits and to reduce the signal to noise (S/N) ratio in high frequency communication applications. One example of such a system is a millimetre wave receiver, which needs to convert an incoming RF signal from the antenna to an L-band signal for base-band signal processing. Here a high performance lowpass filter is needed to suppress the mixed frequencies and to eliminate the leakages from the front-end circuits and local oscillator (Chu *et al.*, 1985).

The basic component in the design of microstrip lowpass filter is the resonator. Nowadays microstrip patch resonators are getting more consideration in the design of lowpass filters due to its inherent power handling capability and lower conductor losses. Usually patch resonator filters have larger size, but this may not be a problem when the filters are operating at high frequencies. By cascading the simple patch



resonators, multiple transmission zeros are generated at high frequencies, which naturally increases the stopband bandwidth of the filter. To increase the selectivity, and thereby the efficiency in the spectrum utilization, the generation of finite frequency transmission zeros are highly demanded for modern wireless communication applications.

Lowpass filter design using conventional structures such as stepped impedance resonators and open stubs suffer from gradual roll-off and narrow stopband bandwidth, which results in the suppression of only the first or second order harmonics (Hong and Lancaster, 2001). To increase the roll-off rate and to obtain wide stopband bandwidth, more sections are to be added and that will naturally increase the overall physical size of the filter. A lowpass filter using stepped impedance and open stubs are proposed by Wang *et al.* (2010) and as compared to the conventional structure, semicircular stepped impedance resonators (SIRs) are used here to achieve compactness.

Dual plane technique is commonly used nowadays to design high performance lowpass filters. Defected structures such as defected ground and defected microstrip structures are used widely to design lowpass filter with wide stopband and high suppression level. Designing cascaded interdigital slots on the ground plane of a stepped impedance structure, multiple transmission zeros are generated to obtain wide stopband and sharp roll-off (Liu *et al.*, 2015). Complimentary split ring resonator shaped structure with two C-shaped resonators are used as defected ground structures (DGSs) and a composite resonator on the top surface of the substrate is used to design sharp roll-off lowpass filter with low insertion loss as presented by Xiao *et al.*, 2015. Only up to 2nd order

harmonics suppression is possible using this complex structure. A compact lowpass filter designed using hexagonal shaped resonator with symmetric open stubs is presented by Kumar and Parihar, 2016. To extend the stopband bandwidth, high frequency multiple transmission zeros are generated by introducing three semi circular slots on the ground plane. However, the structure complexity is high.

A stepped impedance hairpin unit with interdigital structure, and modified symmetrical hairpin type resonator are introduced by Li *et al.* (2010); Abdipour *et al.* (2017) to obtain compact lowpass filter with good in band and out of band characteristics. But the stopband bandwidth achieved in both filters is low.

Lowpass filters designed using cascaded multiple patch resonators are presented by Raphika *et al.* (2014); Raphika *et al.* (2016). The filters have many advantages such as compact size and sharp roll off, while the return loss in the passband is low and it is able to suppress only the lower order harmonics.

In this chapter, two planar lowpass filters, Filter-I and Filter-II, of compact size, high harmonics rejection, good roll-off rate and impedance matching have been designed using cascaded patch resonators and open stubs/suppressing cells on the high impedance main transmission line. Here, the cutoff frequency and transmission zero frequency are controlled easily by changing the length and width of the resonators. The purpose of designing and cascading patch resonators on high impedance transmission line is to generate a flat passband lowpass filter with good selectivity and a wide stopband bandwidth. Flat passband of the filter is obtained by introducing close poles in the passband. Good selectivity is achieved by the filter structures

having infinite attenuation at finite frequency and the occurrence of first transmission zero very close to the cutoff frequency of the filter. First step in the design of the proposed lowpass filter, Filter-I, is the development of Resonator-1, which generates deep transmission zero. Then the design is further extended to the development of Resonator-2 and by cascading the symmetrical arrangement of one unit Resonator-1 and two units of Resonator-2, wide stopband with sharp roll-off rate is achieved. To further extend the stopband so as to achieve high harmonic suppression, open stubs are introduced in the structure. To improve the impedance matching in the passband of the filter, a novel high impedance stub arrangement is used, thereby the proposed filter satisfies wide stopband with high return loss and low insertion loss in the passband while retaining the compact size. The filter is cost effective because it is fabricated using FR4 glass epoxy substrate. From the proposed design it was found that there is only optimum number of elements used to maximize filter stopband and minimize passband losses. The cutoff frequency of Filter-I is 2.44 GHz and the stopband with better than 22 dB rejection level is extended from 2.84 GHz to 16 GHz. The relative stopband bandwidth of the filter at 22 dB suppression level is calculated using Equation (2.16) and its value is 139.5 %. The roll-off rate of the structure is 67.27 dB/GHz at 40 dB suppression level. The normalized circuit size of the Filter-I is  $0.038 \lambda_g^2$ , where  $\lambda_g$  is the guided wavelength at the cutoff frequency.

To extend the stopband bandwidth and thereby to suppress the higher order harmonics and to improve the roll-off rate of the filter with reduced circuit size of Filter-I, Filter-II is designed. The symmetrical open stub of Filter-I is replaced by the suppressing cells. Here, four high-low impedance resonators are utilized to generate transmission zeros at high frequencies and to obtain high suppression level. The 3 dB

cutoff frequency of Filter-II is 2.57 GHz. At 40 dB attenuation point, the corresponding frequency is 2.97 GHz and thus the achieved filter roll-off rate is 92.5 dB/GHz. Within the passband, the insertion loss is very low and its value is within 0.4 dB up to 1.65 GHz. The measured stopband is from 2.78 GHz to 20 GHz at 18 dB rejection level. The RSB of Filter-II is 151.2 %. The normalized circuit size of the filter is  $0.0339 \lambda g^2$ .

Measured results of the developed lowpass filters are in good agreement with the simulation results, thereby proving the validity of the proposed approach. All simulations are carried out using the full wave EM simulation software, IE3D.

### **3.2 LOWPASS FILTER USING PATCH RESONATORS AND OPEN STUBS (FILTER-I)**

The proposed filter consists of two symmetrical stepped impedance patch resonators of different shaped patches and the cascaded arrangement of these resonators on the high impedance main transmission line create multiple transmission zeros at their resonant frequencies. Two open stubs are placed at both ends of the main transmission line to increase the stopband bandwidth of the filter. The passband insertion loss and return loss are improved by introducing a novel stair shaped high impedance stub arrangement instead of single step arrangement in Resonator-2. The designed filter has good in-band and out-of-band frequency response characteristics and is able to reject up to 6<sup>th</sup> order harmonics at the suppression level of 22 dB. The filter structure is very simple and easy to fabricate and its physical size is 17.4 mm x 10 mm. The proposed Filter-I is useful for wireless LAN, L-band and Bluetooth networking applications.

### 3.2.1 Resonator-1 Design and Analysis

The first step in the design of Filter-I is the Resonator-1. Fig. 3.1(a) shows the geometry of Resonator-1 and 3.1(b) represents its LC equivalent circuit model. Resonator-1 is designed using a high impedance straight stub connected in series with a low impedance polygonal patch and these two form a quarter guided wavelength resonator and thus act as semi-lumped elements. The length and width of high impedance stub is represented as  $l_1$  and  $w$  and the patch as  $a$  and  $b$ . The optimized dimensions of Resonator-1 are  $l_1 = 0.3$  mm,  $w = 0.2$  mm,  $a = 4.4$  mm,  $b = 6.0$  mm, and  $\theta = 45^\circ$ . The high impedance stub acts as an inductor,  $L_{R1}$  and the low impedance patch, as a capacitor,  $C_{R1}$  in the equivalent lumped model. The characteristic impedance of high impedance stub and low impedance patch is calculated using Equations (2.21) and (2.23) for an FR4 substrate with relative dielectric constant,  $\epsilon_r$  as 4.4, thickness,  $h$  of 0.8 mm and dielectric loss tangent of 0.02. The straight stub has a characteristic impedance,  $Z_{LR1}$  of 120.5  $\Omega$  with electrical length  $\theta_{L1}$  and that of the polygonal patch,  $Z_{CR1}$  of 18.74  $\Omega$ , with electrical length  $\theta_{C1}$ , thereby satisfying the design considerations as,  $Z_{CR1} < Z_0 < Z_{LR1}$ , where  $Z_0$  represents the characteristic impedance of 50  $\Omega$  microstrip feed line. The effective dielectric constant of the microstrip line of width  $w$  and height  $h$  and the corresponding guided wavelength  $\lambda_{gL}$  are calculated at the cutoff frequency,  $f_{c1}$  of 2.53 GHz using Equations (2.20) and (2.23). The equivalent inductance  $L_{R1}$  can be calculated using the Equation (3.1),

$$L_{R1} = \frac{Z_{LR1} \sqrt{\epsilon_{re}}}{c} l_1 \quad (3.1)$$

where  $c$  is the velocity of light in vacuum.

The guided wavelength,  $\lambda_{gc}$  corresponding to the width of polygonal patch  $b$  is 61.23 mm at frequency,  $f_{c1}$ . The value of capacitance for the dimension  $a$  is computed using the relation (3.2) as

$$C_{R1} = \frac{a}{f_{c1} \lambda_{gc} Z_{CR1}} \quad (3.2)$$

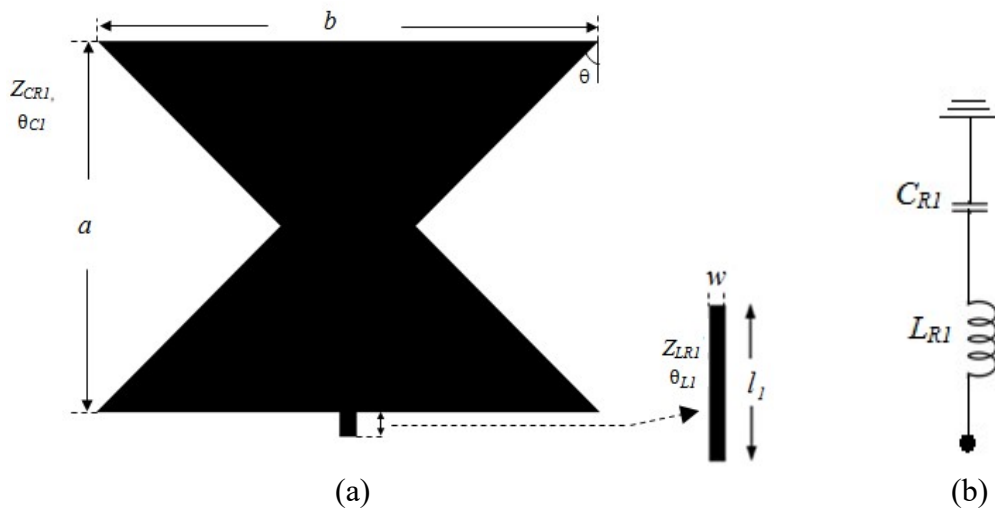


Fig. 3.1 Resonator-1 of Filter-I (a) Structure (b) LC equivalent circuit

To understand the microstrip implementation of the filter structure, EM simulation software IE3D is used. The series  $LC$  resonator of Fig. 3.1 is loaded to the main transmission line,  $TL_1$  having the calculated characteristic impedance value of  $120.5 \Omega$  is shown in Fig. 3.2(a). To understand the design principle of the filter, the equivalent LC model is extracted using quasi-lumped element technique as shown in Fig. 3.2(b). As seen in the equivalent circuit,  $L_H$  is the inductance of the main high impedance transmission line  $TL_1$ .  $L_{R1}$  and  $C_{R1}$  represent the inductance and capacitance of the high impedance rectangular stub modelled by  $TL_2$  and polygonal shaped patch of dimension  $a \times b$ . There is only negligible coupling capacitance occurs between the polygonal shaped

patch and the high impedance main transmission line and thus it is not considered in the analysis of the circuit. The dimensions of the proposed filter are  $TL_1 = 7.9$ ,  $TL_2 = 0.3$ ,  $l_1 = 0.3$ ,  $w = 0.2$ ,  $a = 4.4$ ,  $b = 6.0$ , (all in mm). The calculated values of  $L$  and  $C$  are as follows,  $L_H = 5.06$  nH,  $L_{R1} = 0.2079$  nH and  $C_{R1} = 1.515$  pF.

The EM and LC circuit simulation of the Resonator-1 are compared in Fig. 3.2(c). The EM simulated 3 dB cutoff frequency of the Resonator-1 is at 2.53 GHz. Resonator-1 creates a transmission zero, located at about 6.18 GHz with attenuation level near 48.13 dB. Due to small value of resonance inductance  $L_{R1}$  of Resonator-1, transmission zero appears in the higher frequency region, which results a wide stopband bandwidth. A very low insertion loss in the passband is achieved by Resonator-1, but its transmission characteristics show gradual transition from the passband to stopband. Using the equivalent circuit, the two port network parameters such as ABCD and S-parameters are calculated and the effective elements of the Resonator-1 structure are analyzed.

The ABCD parameters of the two port network is expressed in Equation (3.3),

$$\begin{bmatrix} A & B \\ C & D \end{bmatrix} = \begin{bmatrix} \frac{Z_{R1} + j\omega L_H}{Z_{R1}} & \frac{2j\omega L_H Z_{R1} + j^2 \omega^2 L_H^2}{Z_{R1}} \\ \frac{1}{Z_{R1}} & \frac{Z_{R1} + j\omega L_H}{Z_{R1}} \end{bmatrix} \quad (3.3)$$

where  $Z_{R1}$  is represented in Equation (3.4) as,

$$Z_{R1} = \frac{1 - \omega^2 L_{R1} C_{R1}}{j\omega C_{R1}} \quad (3.4)$$

Based on the ABCD parameters, the  $S_{11}$  and  $S_{21}$  parameters of the Resonator-1 are as follows (Hong and Lancaster, 2001),

$$S_{11} = \frac{A + B/Z_0 - CZ_0 - D}{A + B/Z_0 + CZ_0 + D} \quad S_{21} = \frac{2}{A + B/Z_0 + CZ_0 + D} \quad (3.5)$$

Substituting the values of ABCD parameters in Equation (3.5) and simplifying, the finite frequency transmission zero depends on the relation (3.6).

$$f_0 = \frac{1}{2\pi\sqrt{L_{R1}C_{R1}}} \quad (3.6)$$

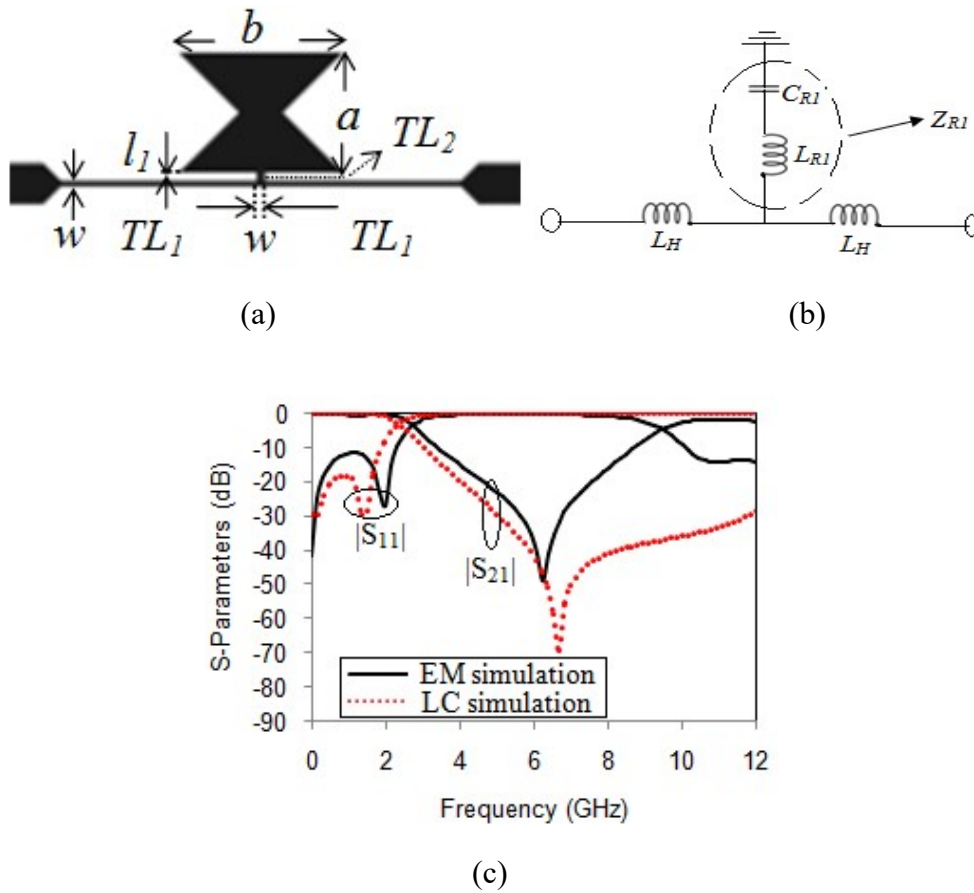


Fig. 3.2 Resonator-1 loaded on the main high impedance transmission line  
 (a) Structure (b) LC equivalent circuit (c) EM and LC circuit simulation result



From the Fig. 3.2, it is clear that the lumped element values of  $L_{RI}$  and  $C_{RI}$  depend on the corresponding microstrip implementation of the series resonant element. The effect of frequency response of the Resonator-1 is studied by changing the parameters of the series resonant element. Fig. 3.3(a) and Fig. 3.3(b) show the frequency response characteristics of the filter for different values of  $l_1$  and  $b$ . As values of  $l_1$  and  $b$  increase, the inductance and capacitance of the filter increase and the cutoff frequency and the resonant frequency of the filter decrease. Also it is noted that the increase in value of  $l_1$  does not make any change in the value of passband return loss, but increase in the value of  $b$  improves the passband return loss of the filter. The stopband bandwidth of the filter is also increased by increasing value of  $b$ . Thus by changing the length and width of the high impedance rectangular stub ( $TL_2$ ) and the low impedance open-ended line, the cutoff frequency and resonant frequency are easily tuned.

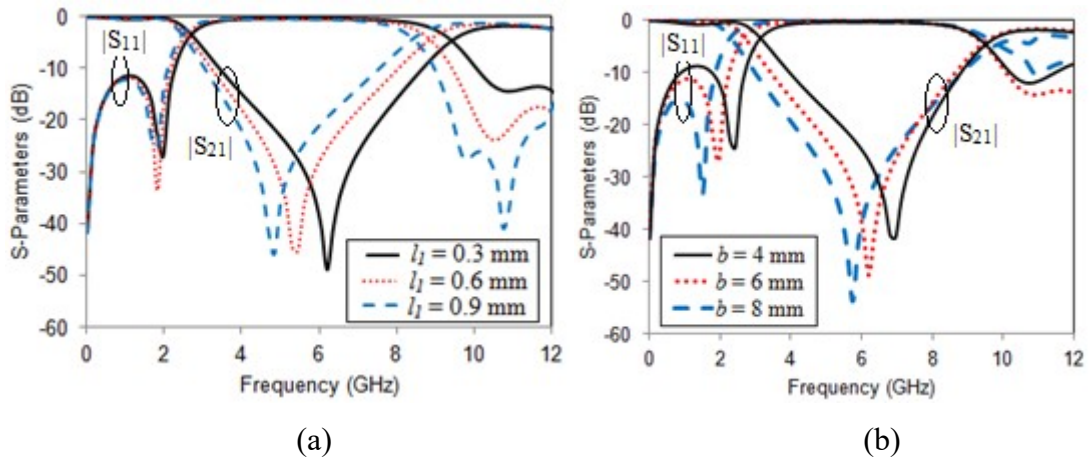


Fig. 3.3 The frequency response characteristics of Resonator-1 (a) For different values of  $l_1$  (b) For various values of  $b$

The stopband bandwidth of Resonator-1 is improved by loading the structure symmetrically on the main high impedance transmission line as shown in Fig. 3.4. In the symmetrical Resonator-1 structure, the transmission zero shifts towards the higher frequency due to the decrease in the value of inductance. Here, two series LC

resonators are in shunt with the main high impedance transmission line and thus the total effective inductance value decreases and the effective capacitance value increases. The transmission zero,  $TZ_1$  appears at frequency 7.6 GHz as shown in Fig. 3.4(b). Here, the stopband bandwidth of the filter is improved due to the increase in the value of effective capacitance. The in-band filter characteristics is also improved by the lower value of insertion loss ( $< 0.4$  dB) and higher value of return loss ( $> 20$  dB).

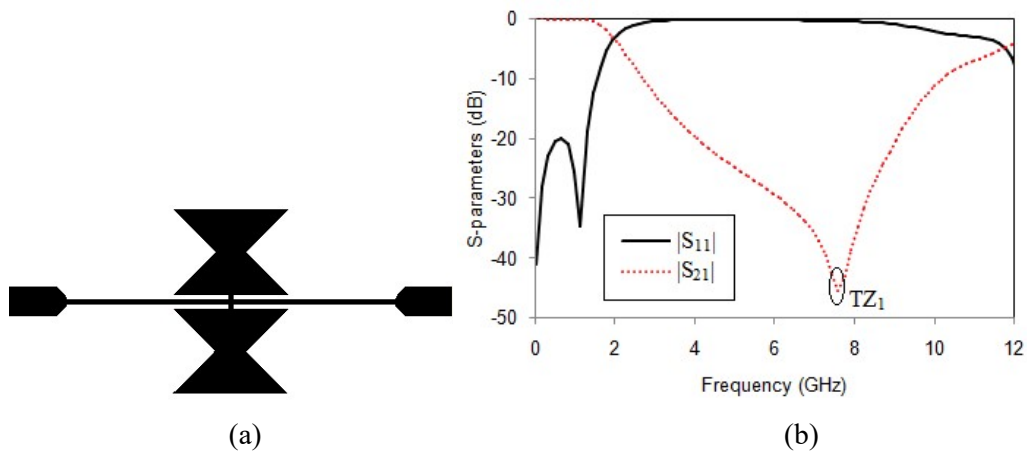


Fig. 3.4 (a) Symmetrical structure of Resonator-1 (b) The simulated S-Parameters

### 3.2.2 Resonator-2 Design

The next step in the development of the proposed Filter-I is the design of Resonator-2. Resonator-2 is a single stepped stub of characteristic impedance  $Z_{LR2}$  of  $120.5 \Omega$  having electrical length,  $\theta_{L2}$  connected in series with a triangular patch of characteristic impedance  $Z_{CR2}$  as  $39.76 \Omega$ . The structural layout of Resonator-2 is shown in Fig. 3.5. The dimensions of the layout are  $l_2 = 5.3$  mm,  $w = 0.2$  mm,  $a = 4.4$  mm and  $d = 2.2$  mm. The LC resonator is connected to the main transmission line having an impedance of  $120.5 \Omega$ . One unit of Resonator-2 will create only one transmission zero at 3.74 GHz with attenuation level near 30.909 dB. The 3 dB cutoff frequency,  $f_{c2}$  of Resonator-2 is at 2.67 GHz.

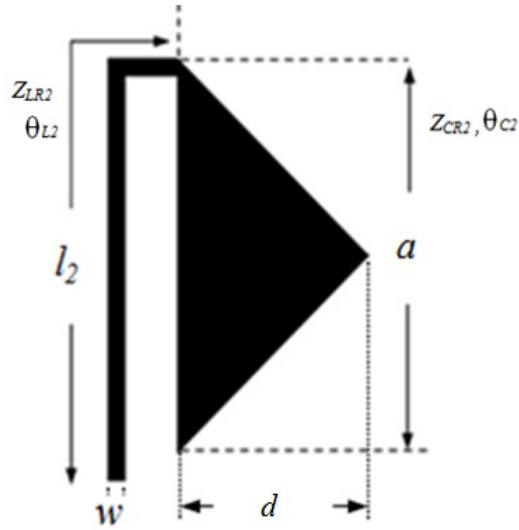
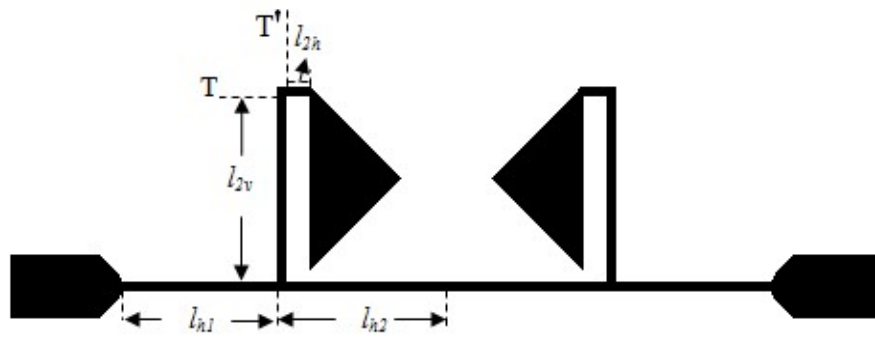


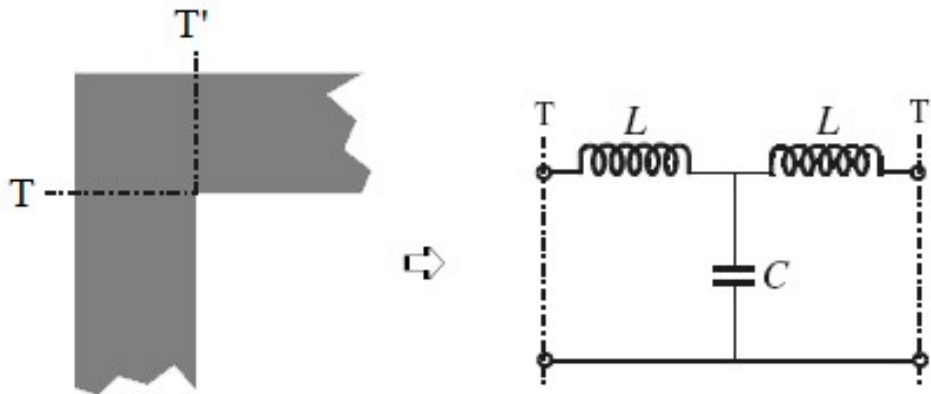
Fig. 3.5 The layout of Resonator-2

The selectivity of the filter can be improved by connecting one more unit of Resonator-2 to the opposite side of Resonator-1. Its configuration is shown in Fig. 3.6(a). The right-angle bend T-T' of the single stepped stub can be modelled by an equivalent T-network, which is shown in Fig. 3.6(b).

For the analysis of LC equivalent circuit, the single stepped stub  $l_2$  of Resonator-2 is divided as  $l_{2v}$ , T-T' and  $l_{2h}$ . The vertical length of high impedance stub  $l_2$  is represented as  $l_{2v}$ , the square shaped T-T' is the right-angle bend and the horizontal length of the stub is represented as  $l_{2h}$ . The single stepped stub of Resonator-2 is placed at a distance  $l_{h1}$  from the end of high impedance main transmission line and  $l_{h2}$  is the distance from the centre of high impedance main transmission line to the single stepped stub. The optimized dimensions of Fig. 3.6(a) are  $l_{2v} = 4.5$  mm,  $l_{2h} = 0.4$  mm, T-T' is 0.2 mm x 0.2 mm,  $l_{h1} = 3.8$  mm and  $l_{h2} = 4.1$  mm.



(a)



(b)

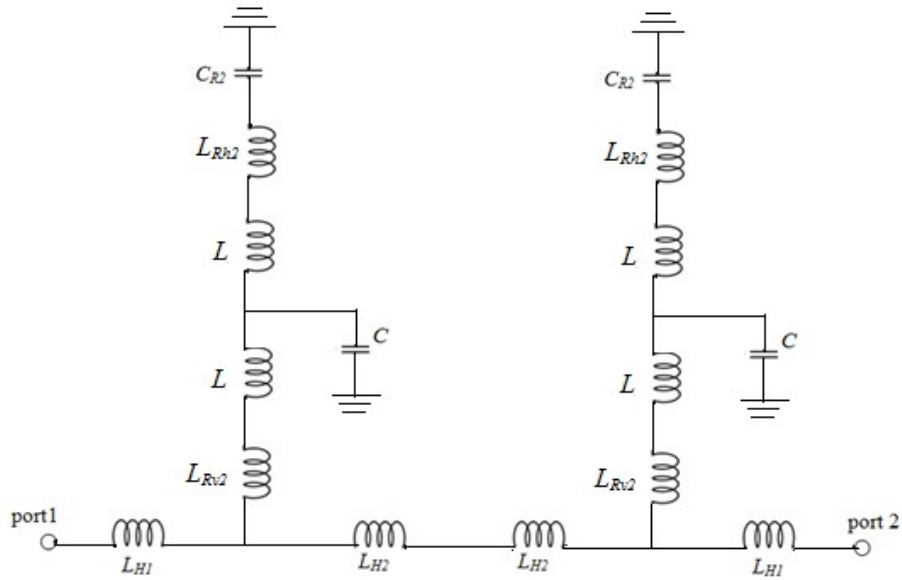
Fig. 3.6 (a) Structure of two units of Resonator-2 (b) LC equivalent circuit of the right angle bended microstrip line

The right-angle bend of the microstrip line is modelled as equivalent T network shown in Fig. 3.6(b), which is the parallel combination of  $L$  and  $C$  circuit. The  $L$  and  $C$  values are calculated using the following closed form expressions (Gupta *et al.* 1996).

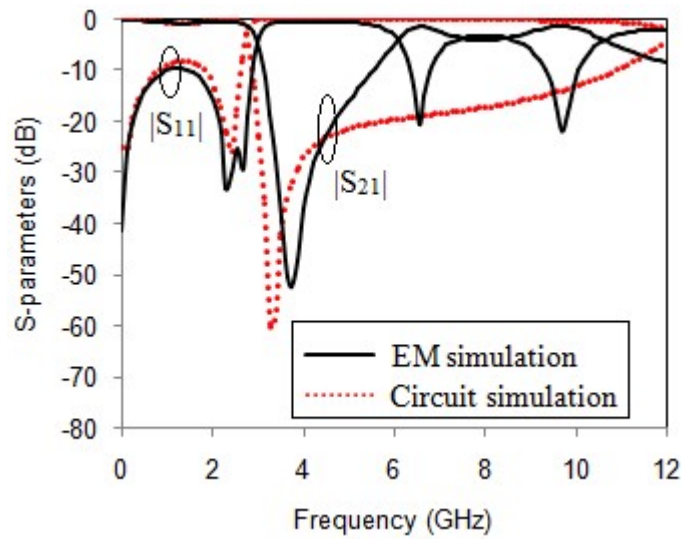
$$\frac{C}{w} (\text{pF/m}) = \frac{(14\epsilon_r + 12.5)w/h - (1.83\epsilon_r - 2.25)}{\sqrt{w/h}} + \frac{0.02\epsilon_r}{w/h} \quad (3.7)$$

$$\frac{L}{h} (\text{nH/m}) = 100 \{ 4\sqrt{w/h} - 4.21 \} \quad (3.8)$$

Here, the width of the microstrip line  $w$  is 0.2 mm,  $h = 0.8$  mm and  $\epsilon_r = 4.4$ . The values of  $C$  and  $L$  calculated using the above equations are  $C = 0.005159$  pF and  $L = 0.176$  nH.



(a)



(b)

Fig. 3.7 (a) LC equivalent circuit of two units of Resonator-2 (b) Frequency response characteristics of LC circuit and EM simulation

The LC equivalent circuit of two units of Resonator-2 and its simulated frequency response characteristics are shown in Fig. 3.7(a) and (b) respectively.  $L_{H1}$  and  $L_{H2}$  represent the corresponding equivalent inductance of main high impedance transmission line of length  $l_{h1}$ ,  $l_{h2}$  respectively and  $L_{Rv2}$  and  $L_{Rh2}$  represent the equivalent inductance of single stepped stub of length  $l_{2v}$  and  $l_{2h}$  respectively.  $C_{R2}$  represents the capacitance between the microstrip triangular patch and the ground plane and the value is calculated using the Equation (3.2) at the cutoff frequency  $f_{c2}$ . The calculated  $L$  and  $C$  values of the equivalent lumped elements of the proposed Resonator-2 are  $L_{H1} = 2.6346$  nH,  $L_{H2} = 2.8426$  nH,  $L_{Rv2} = 3.1199$  nH,  $L = 0.176$  nH,  $L_{Rh2} = 0.4159$  nH,  $C_{R2} = 0.68319$  pF and  $C = 0.005159$  pF. The  $LC$  circuit simulation result is in good approximation with the EM simulation result, which is shown in Fig. 3.7(b).

Fig. 3.8(a) shows symmetrical arrangement of two units of Resonator-2 placed at the centre of main high impedance transmission line and its simulated characteristics is shown in Fig. 3.8(b). The filter exhibits two transmission zeros,  $TZ_2$  and  $TZ_3$ , which are placed at about 3.68 GHz and 4.05 GHz with attenuation level 53.57 dB and 61.93 dB respectively. These transmission zeros are generated by the resonance of the high impedance single stepped stub loaded by triangular shaped patches and its resonant frequency depends on the structural parameters of symmetrically loaded Resonator-2. As the number of transmission zeros increases, the stopband bandwidth of the filter is also improved with high suppression level. Here, the transmission zero  $TZ_2$  occurs very close to the cutoff frequency and thus the sharpness of the filter is improved. The passband return loss of the filter is also improved, with low insertion loss in the passband.

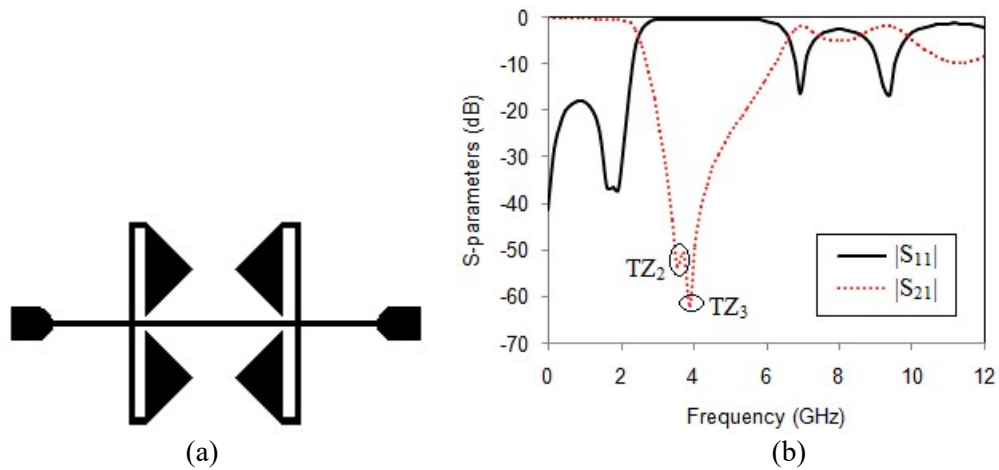


Fig. 3.8 (a) Symmetrical structure of two units of Resonator-2 (b) Simulated frequency response characteristics

### 3.2.3 Cascaded Symmetrical Structure of Resonator-1 and Resonator-2

The performance characteristics of the filter is greatly improved by suitably cascading the symmetrical structure of Resonator-1 and two units of Resonator-2 on the main high impedance transmission line. Fig. 3.9 shows the structural layout and frequency response characteristics of the filter with symmetrical arrangement of one unit of Resonator-1 and two units of Resonator-2.

The cascaded arrangement of these two resonators results in better rejection of spurious passband, and thus the stopband performance of the filter is greatly enhanced. It is observed from Fig. 3.9(b) that the steepness of transition from passband to stopband is improved and thus the transition band is reduced resulting in an improved roll-off rate of the filter. The stopband is from 2.86 GHz to 8.55 GHz with the attenuation level of 20 dB and thus achieving better stopband performance. However, the passband return loss value is very low and it is nearly 7 dB only.

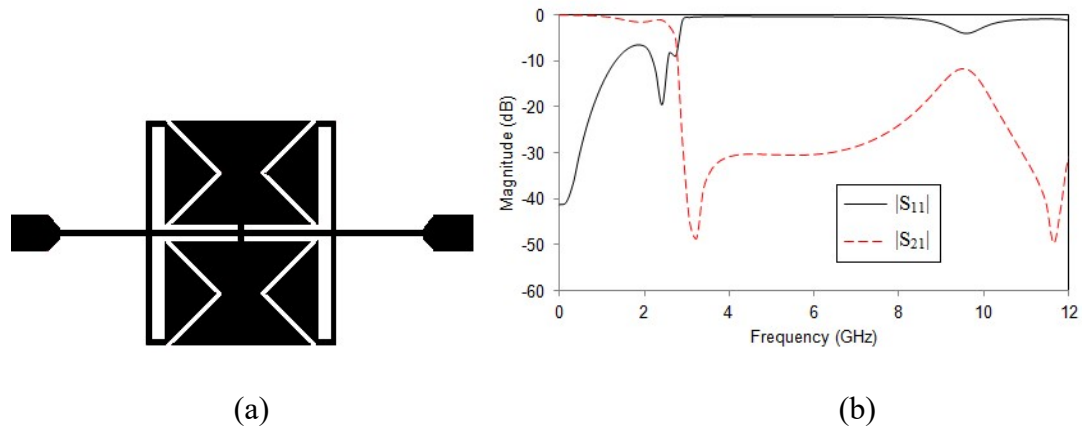


Fig. 3.9 (a) Combined symmetrical structure of Resonator-1 and Resonator-2  
 (b) Simulated S-Parameters

### 3.2.4 Cascaded Structure with Open Stubs

In the practical applications of wireless communication systems, a lowpass filter with wide stopband bandwidth at high rejection level is necessary for higher order harmonics suppression. The bandwidth of the cascaded filter can be greatly enhanced by connecting open circuited stubs on both sides of the resonators. The open circuited stub produces a transmission zero when the physical length of the stub is less than the quarter guided wavelength. The cascaded filter with open stub at both ends of the high impedance main transmission line, exhibits wide stopband characteristics.

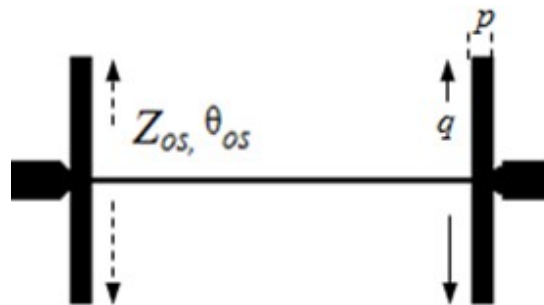


Fig. 3.10 Structure of open stub



Fig. 3.10 shows the symmetrical structure of the open stubs where  $Z_{os}$  and  $\theta_{os}$  represent the characteristic impedance and electrical length respectively. The length and width of open circuited stub are  $p$  and  $q$  respectively. The calculated value of  $Z_{os}$  is  $12.14 \Omega$ . For the straight stub, the equivalent capacitance is derived using Hong and Lancaster, (2001) and the relation is given in Equation (3.9) as,

$$C_{os} = \frac{\tan(\theta_{os})}{2\pi f_{c3} Z_{os}} \quad (3.9)$$

where  $f_{c3}$  is the simulated 3 dB cutoff frequency of the filter. Each open stub acts as shunt capacitor to the ground plane. At high frequencies, the capacitive reactance decreases, and the open circuited stub acts as a short circuit to the ground. This short out transmission and causes attenuation peak in the stopband, which suppresses the higher order harmonics and thus extends the stopband. The optimized values of  $p$  and  $q$  are 0.8 mm and 10 mm respectively.

Fig. 3.11 shows the cascaded structure of symmetrical Resonator-1, Resonator-2 and open circuited stubs. Resonator-1 is placed between two units of Resonator-2 and these three units are symmetrically loaded on the centre of a main high impedance transmission line, together with two open circuited stubs, which are connected at both ends of the main high impedance transmission line.

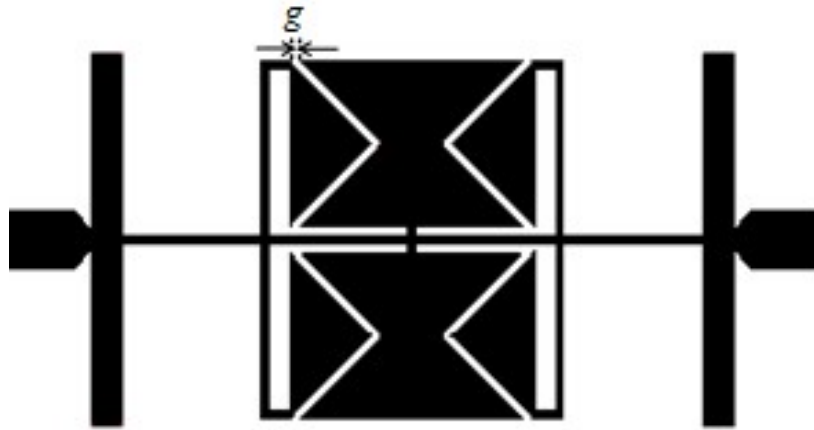


Fig. 3.11 Layout of the cascaded symmetrical Resonator-1, Resonator-2 and open stubs

### 3.2.5 Equivalent Circuit of Filter-I

Fig. 3.12 shows the LC equivalent circuit of the cascaded symmetrical Resonator-1, Resonator-2 and open circuited stubs.  $L_{R1}$  represents the equivalent inductance of high impedance straight stub of Resonator-1 and  $C_{R1}$  is the capacitance between the microstrip polygonal shaped patch and the ground plane.  $C_{R2}$  represents the capacitance between microstrip triangular shaped patch and the ground plane and  $C_{OS}$  is the capacitance of the open circuited stub and the ground metallic plane. The capacitance  $C_c$  is formed by the capacitive coupling between the polygonal and triangular shaped patches and its value depends up on the gap  $g$  between the resonators. The detailed analysis of the coupling capacitor  $C_c$  is shown below. The optimized value of the spacing  $g$  between the polygonal and triangular shaped patches is 0.3 mm. At high frequency values, the inductance of main high impedance line block transmission by having infinite series reactance, whereas the capacitance of open circuited stub shorts out transmission by having infinite shunt susceptance. The calculated values of the lumped elements of the proposed lowpass filter design are  $L_{H1} = 2.6346$  nH,  $L_{H2} = 2.8426$  nH,  $L_{R1} = 0.2079$  nH,  $L_{Rv2} = 3.1199$  nH,  $L = 0.176$  nH,  $L_{Rh2} = 0.4159$  nH,

$C_{R1} = 1.515$  pF,  $C_{R2} = 0.68319$  pF,  $C = 0.005159$  pF,  $C_{OS} = 0.4343$  pF and  $C_c = 0.03837$  pF. Fig. 3.13 shows the LC and EM simulation results of the cascaded structure, which are in good approximation with each other. As seen in the Figure, enhanced stopband performance is achieved under the combined effect of two types of resonators and open stubs. The 3 dB cutoff frequency of the filter is 2.64 GHz.

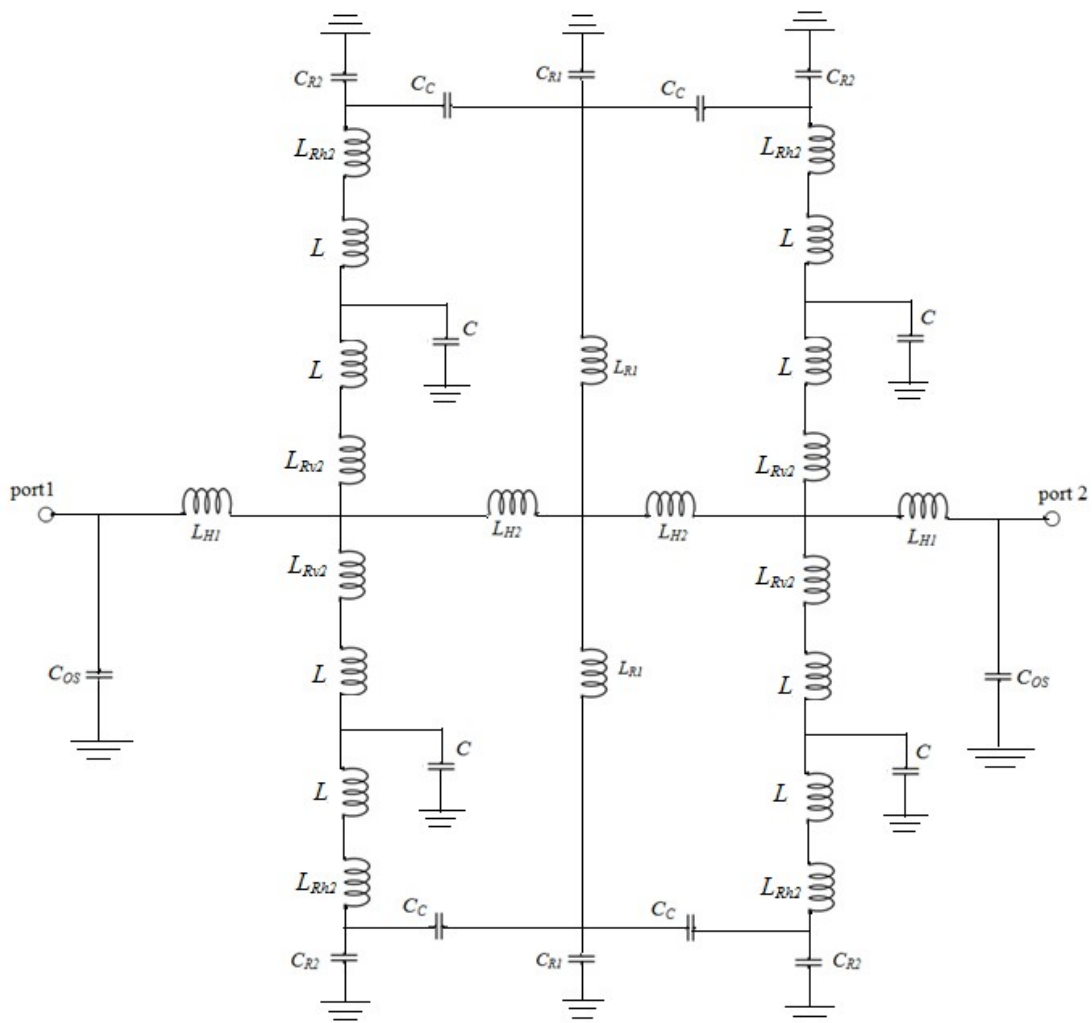


Fig. 3.12 LC equivalent circuit of cascaded symmetrical Resonator-1, Resonator-2 and open stubs

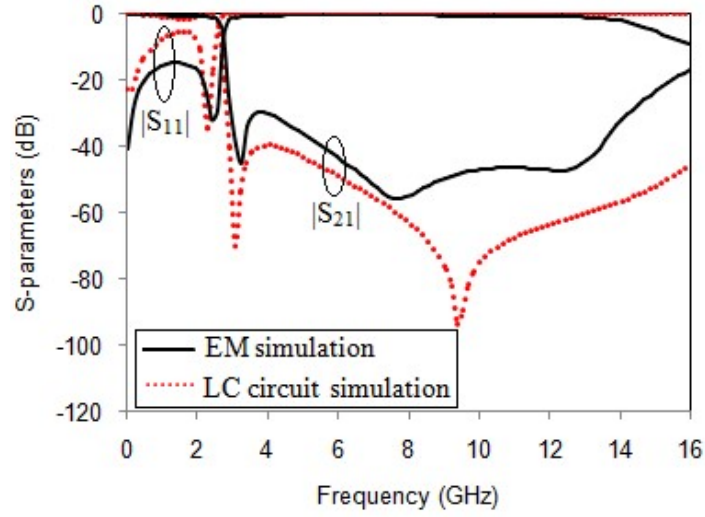


Fig. 3.13 Frequency response characteristics of EM and LC circuit simulation

### 3.2.6 Analysis of Coupling Capacitor, $C_c$

The microstrip gap  $g$  between the polygonal and triangular shaped resonator and its corresponding equivalent circuit are shown in Fig. 3.14.  $C_c$  represents the coupling capacitance between the two resonators and  $C_l$  is the parasitic capacitance. The values of  $C_c$  and  $C_l$  are calculated using the Equations (3.10)-(3.17) (Hong and Lancaster, 2001) as follows.

$$C_c = 0.5C_o - 0.25C_e \quad (3.10)$$

$$C_l = 0.5C_e \quad (3.11)$$

where the variables  $C_e$  and  $C_o$  are calculated as follows.

$$\frac{C_o}{W} (\text{pF/m}) = \left( \frac{\epsilon_r}{9.6} \right)^{0.8} \left( \frac{g}{W} \right)^{m_o} \exp(K_o) \quad (3.12)$$

$$\frac{C_e}{W} (\text{pF/m}) = 12 \left( \frac{\epsilon_r}{9.6} \right)^{0.9} \left( \frac{g}{W} \right)^{m_e} \exp(K_e) \quad (3.13)$$

The variables  $m_o$ ,  $k_o$ ,  $m_e$  and  $k_e$  are calculated using equations,

$$m_o = \frac{W}{h} [0.619 \log(W/h) - 0.3853] \quad (3.14)$$

$$k_o = 4.26 - 1.453 \log(W/h) \quad (3.15)$$

$$m_e = 0.8675 \quad (3.16)$$

$$k_e = 2.043 (W/h)^{0.12} \quad (3.17)$$

The substrate used in the design is FR4 with  $\epsilon_r = 4.4$ ,  $h = 0.8$  mm and  $W$  is the width of the line and its value is 2.2 mm. The calculated values of  $m_o$ ,  $k_o$ ,  $m_e$  and  $k_e$  are  $m_o = -0.31228$ ,  $k_o = 3.622$ ,  $m_e = 0.8675$  and  $k_e = 2.3066$ . The calculated values of  $C_o$  and  $C_e$  are,  $C_o = 0.082143$  pF and  $C_e = 0.0105$  pF. The values of  $C_c$  and  $C_l$  are  $C_c = 0.03837$  pF and  $C_l = 0.00525$  pF. The value of  $C_l$  is very small and thus neglected in the circuit analysis.

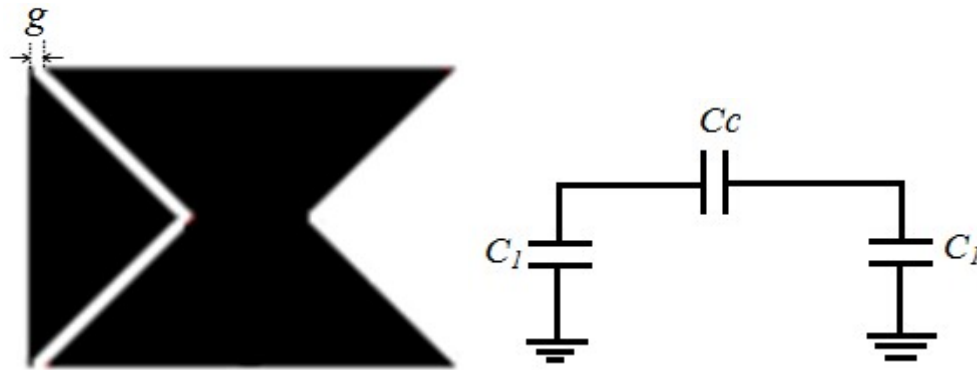


Fig. 3.14 Microstrip gap between the resonators

### 3.2.7 Efforts for Improving Impedance Matching in the Passband

An ideal lowpass filter should have low values of insertion loss and high return loss values in the passband. The EM simulation result of the cascaded symmetrical structure of Resonator-1, Resonator-2 and open stubs is shown in Fig. 3.15.

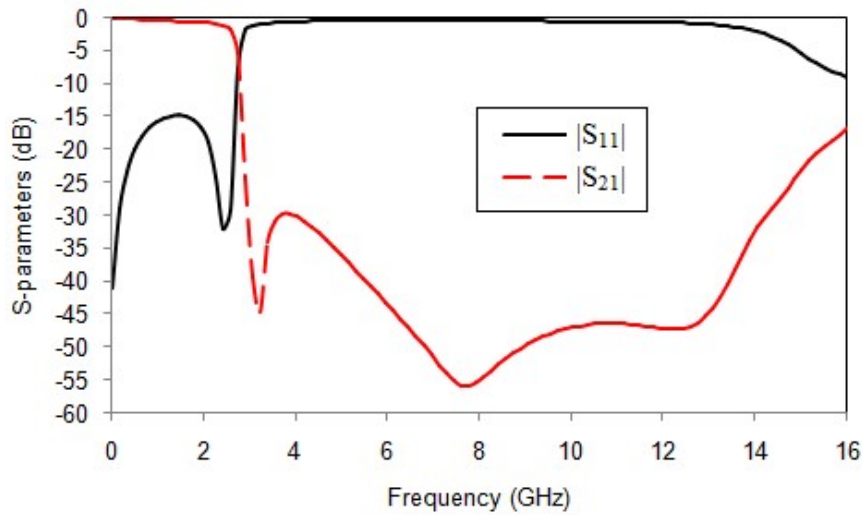
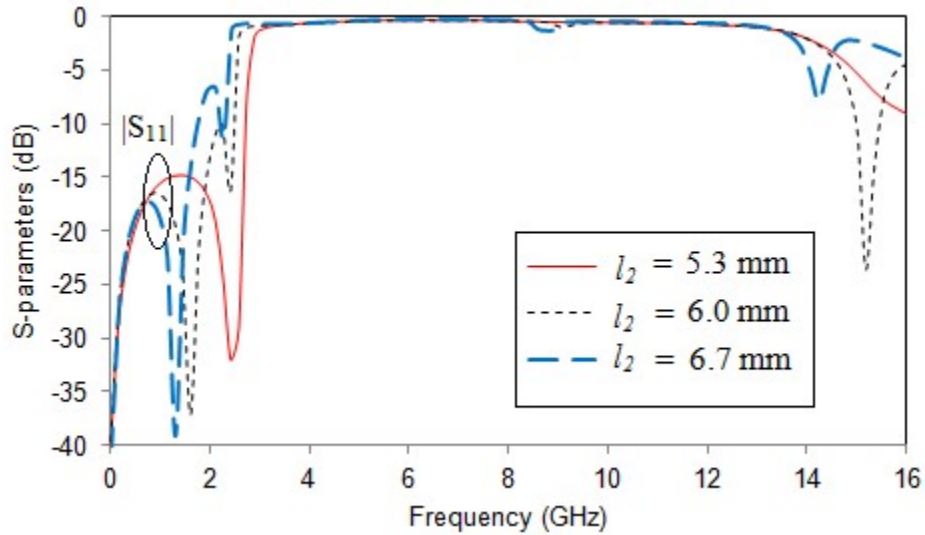


Fig. 3.15 Simulated S-parameters of the cascaded structure of symmetrical Resonator-1, Resonator-2 and open stubs

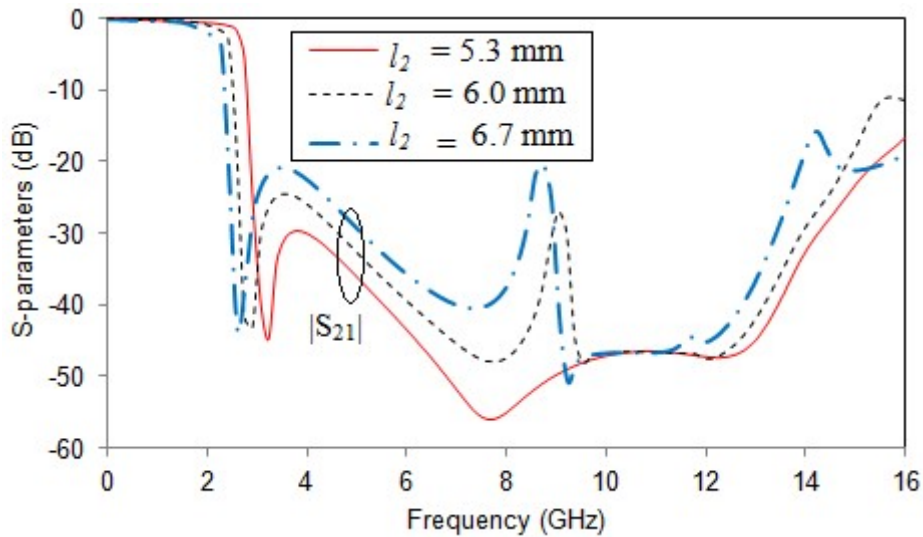
The insertion loss in the passband of the filter is less than 0.62 dB from DC to 1.7 GHz and the return loss is only 14.8 dB. By increasing the length of high impedance single stepped stub of Resonator-2 ( $l_2$ ), (only the length of  $l_2$  in horizontal direction is increased) the characteristics of the filter is changed. Fig. 3.16 shows the reflection and transmission characteristics of the filter for different values of stub length  $l_2$ .

From the Fig. 3.16(a), we can observe that as the length of high impedance single stepped stub of Resonator-2 increases, the return loss improves only in the lower frequencies of the passband, but deteriorates at increasing passband frequency values. At the same time, from the transmission characteristics of Fig. 3.16(b), transmission poles occur at nearly 9 GHz and due to these spurious signals arise in the stopband, the rejection level of the filter decreases. Also, it is seen that by increasing the length of high impedance stub of Resonator-2, the cutoff frequency as well as the first resonating frequency of the filter move towards the lower frequency end and thus its value decreases.

Thus, to improve the passband characteristics of the filter and at the same time to make the structure more compact, a novel high impedance stub arrangement is introduced here. The single stepped high impedance stub of Resonator-2 is modified in the form of stair shaped high impedance stub, with five steps of increasing step size.



(a)



(b)

Fig. 3.16 Simulated frequency response characteristics of the lowpass filter for various values of  $l_2$  (a) Reflection characteristics (b) Transmission characteristics

Fig. 3.17 shows the comparison between the high impedance stub of Resonator-2 connected as single step and stair shaped of length  $l_2$  as 6.7 mm, between main high impedance transmission line and triangular shaped patch. For single stepped resonator structure, the filter suffers from poor impedance matching in the passband and spurious harmonics arising in the stopband. These two drawbacks of the filter are eliminated by using the stair shaped high impedance stub. Thus, by the introduction of stair shaped high impedance stub, the impedance matching as well as stopband attenuation level of the filter is improved to a great extent.

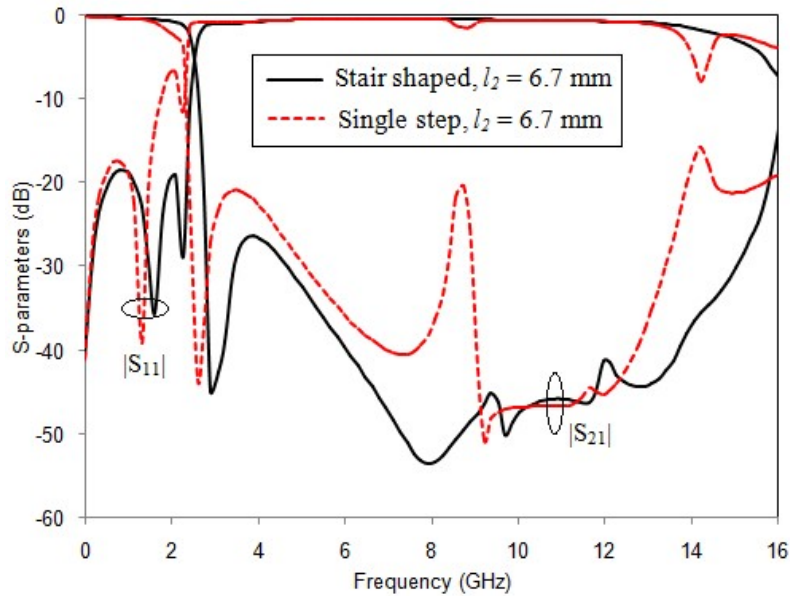


Fig. 3.17 Simulated frequency response of the filter for inductive stub structure of Resonator-2 as stair shaped and single step for length  $l_2 = 6.7$  mm

### 3.2.8 Structure of the Proposed Filter-I

The passband return loss values have been improved from 14.8 dB to 18.5 dB and thereby the values of insertion loss in the passband decrease from 0.62 dB to 0.5 dB. Due to increase in the inductance value of Resonator-2, the 3 dB cutoff frequency of the Filter-I decreases and its value in the proposed design is 2.44 GHz. Fig. 3.18



shows the final structure of the Filter-I, where the single stepped high impedance inductive stub of Resonator-2 is modified as stair shaped of increasing step size and Fig. 3.19 shows the simulated frequency response characteristics of the final filter.

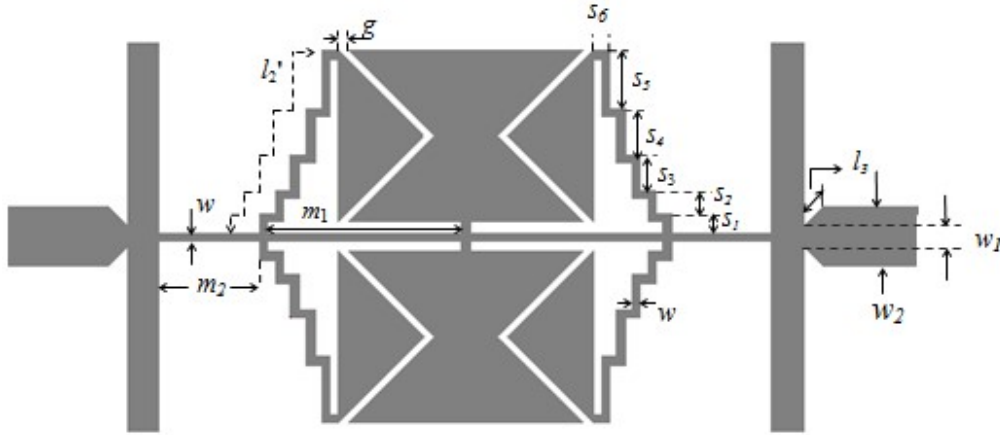


Fig. 3.18 Structure of the proposed lowpass filter

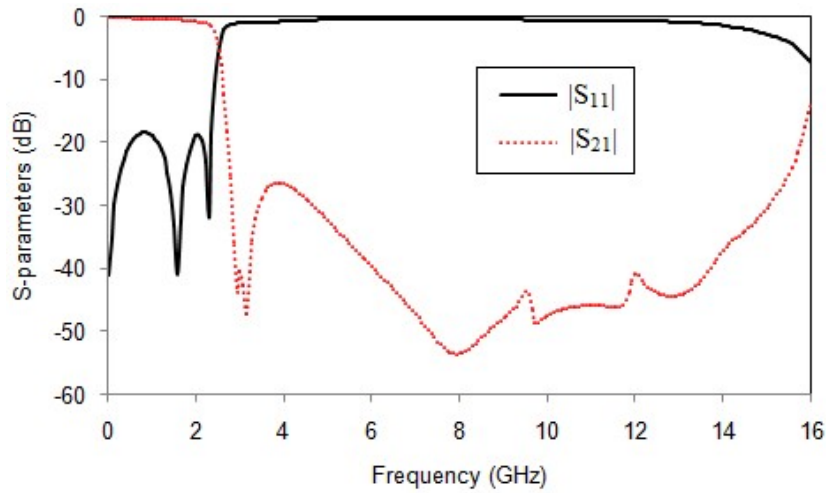


Fig. 3.19 Simulated frequency response characteristics of the proposed filter

Based on these analyses, a microstrip lowpass filter is designed and its structure is fabricated. Two microstrip lines at both sides of the filter with width  $w_2$  are utilized to match the impedance at the input and output (I/O) ports to  $50 \Omega$ . Two tapered lines of width  $w_1$  and length  $l_3$  are inserted between the open stub and  $50 \Omega$  I/O port gives marginal improvement in the insertion loss. The optimized parameters of the structure

are as follows:  $m_1 = 5.0$ ,  $m_2 = 2.6$ ,  $w = 0.2$ ,  $w_1 = 0.5$ ,  $w_2 = 1.5$ ,  $s_1 = 0.5$ ,  $s_2 = 0.6$ ,  $s_3 = 0.9$ ,  $s_4 = 1.2$ ,  $s_5 = 1.5$ ,  $s_6 = 0.4$ ,  $l_3 = 0.5$  and  $g = 0.3$  (all in millimeters). The total length of stair shaped stub is,  $l_2' = 5*s_6 + s_1 + s_2 + s_3 + s_4 + s_5$ .

The phase velocity of a lossless structure can be expressed as in Equation (3.18) as,

$$v_p = \frac{1}{\sqrt{LC}} \quad (3.18)$$

Increasing the length of the high impedance stub by introducing stair shaped design enhances the effective inductance and the small value of the coupling gap,  $g$  between the resonators improves the effective capacitance of the filter. By cascading the resonators, equivalent inductance and capacitance value increases, which corresponds to decrease in the phase velocity, and thus a slow wave effect is achieved. A wide stopband bandwidth up to 16 GHz (at 22 dB suppression level) is obtained, due to multiple transmission zeros contributed by two types of patch resonators together with two open circuited stubs. The 3 dB cutoff frequency of the proposed filter is 2.44 GHz, with low insertion loss and good impedance matching in the passband.

### 3.2.9 Field Distribution in the Proposed Filter

The current distribution of the proposed filter in the passband and stopband is analyzed to study the filter characteristics as described in Fig. 3.20. At 1 GHz, it is seen from the Fig. 3.20(a) that most of the energy is coupled from input port to output port through the narrow high impedance line and only negligible energy travels through the series resonators, which proves its passband characteristics and the transmitted power from input port to output port through the high impedance main transmission line shows its inductive nature. At frequency 7.5 GHz, the transmitted power from the source is either

reflected back or passed through the open stub and practically no transmitted energy appears in the output port. This not only proves its stopband characteristics but also the capacitive behavior of the open stub as shown in Fig. 3.20(b).

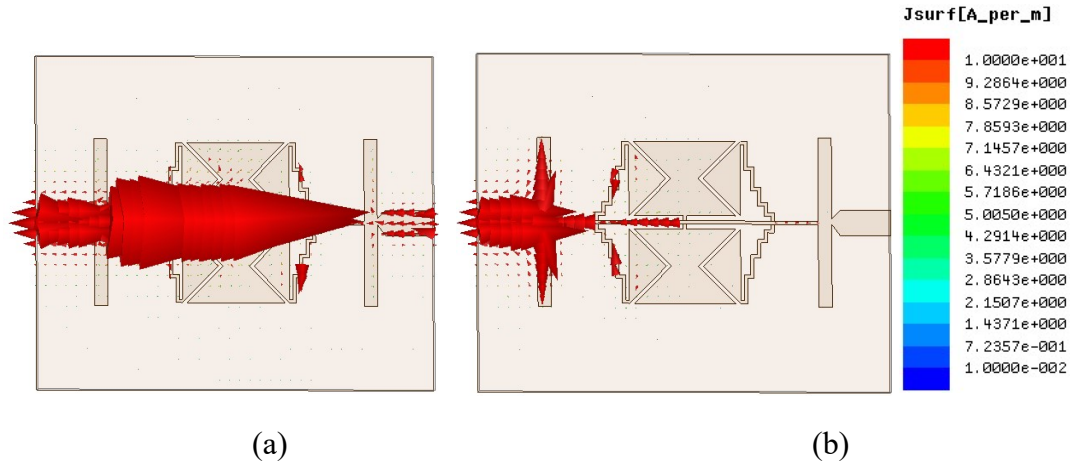
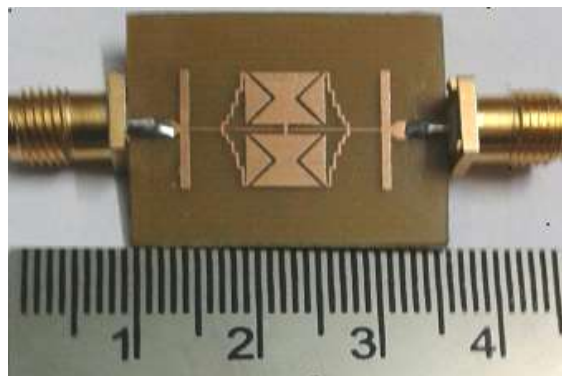


Fig. 3.20 Electromagnetic field distribution of proposed filter (a) At frequency 1 GHz (b) At frequency 7.5 GHz

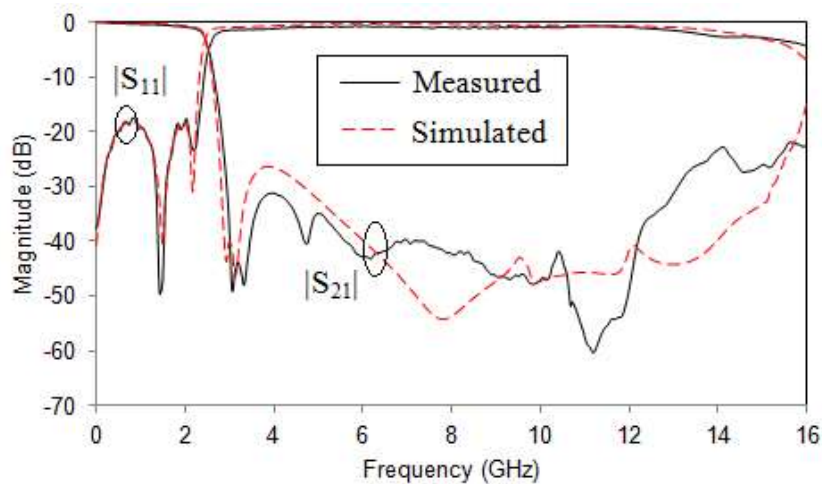
### 3.2.10 Fabrication and Measurement Results

The Filter-I is fabricated on an FR4 substrate with relative permittivity 4.4, dielectric loss tangent 0.02 and thickness of 0.8 mm. The prototype of the fabricated filter structure along with SMA connectors is shown in Fig. 3.21(a). The fabricated structure is measured using R & S ZVB 20 Vector Network Analyzer. The measurement results are in good agreement with the simulated results as illustrated in Fig. 3.21(b). The measured results show that the 3 dB cutoff frequency is 2.44 GHz. The minimum return loss is better than 17.74 dB over the entire passband and the suppression level better than 22 dB from 2.85 GHz to 16 GHz. The suppression level of 31 dB is achieved from 2.94 GHz to 13.04 GHz. Thus wide stopband suppression is obtained in 77% of overall stopband bandwidth. The insertion loss in the passband is less than 0.67 dB from DC to 1.7 GHz. The higher value of insertion loss in the

passband of the filter is due to the inherent dielectric losses of FR4 substrate at microwave frequencies. The return loss in the stopband is very close to 0 dB and nearly 4.3 dB at the end of the stopband. The selectivity or roll-off rate of the structure is calculated using Equation (2.15), is 67.27 dB/GHz at 40 dB suppression level. The physical size of the filter is only 17.4 mm x 10 mm, which corresponds to a normalized circuit size of  $0.257\lambda_g \times 0.148\lambda_g$ , where  $\lambda_g$  is the guided wavelength at the cutoff frequency. The relative stopband bandwidth of the proposed filter is 139.5%.



(a)



(b)

Fig. 3.21 (a) Prototype of the Filter-I (b) Measured and simulated frequency response characteristics

The measured and simulated group delay shown in Fig. 3.22 shows good approximation. The group delay is almost flat in the passband with the peak to peak variation of 0.4 ns. There is a significant increase in group delay characteristics, when the frequency approaches the cutoff frequency of the filter.

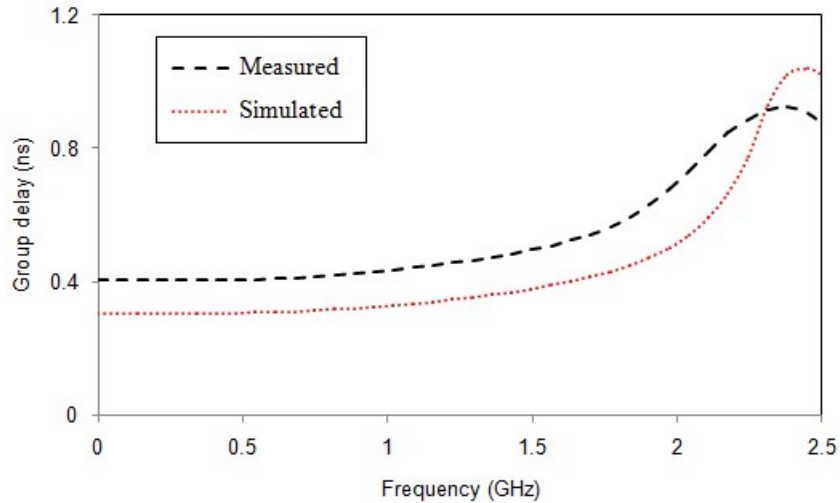


Fig. 3.22 Measured and simulated group delay characteristics of the Filter-I

### 3.2.11 Performance Comparison of Filter-I

Table 3.1 shows the performance comparison of the Filter-I with other published works. From the table, it is clear that the proposed filter is having high passband performance with wide stopband bandwidth and thus able to suppress the higher order harmonics of up to 6<sup>th</sup> order. The Filter-I is compared to other filters fabricated using FR4 substrate and low loss tangent substrates and the characteristics such as return loss-passband (RL-PB), cutoff frequency ( $f_c$ ), stopband and order of harmonic suppression are indicated in the table. The designed structure has wide as well as deep stopband with good passband characteristics such as low insertion loss and high return loss of 17.74 dB.

Table 3.1 Comparison of the frequency response characteristics of the proposed Filter-I with other works from the literature

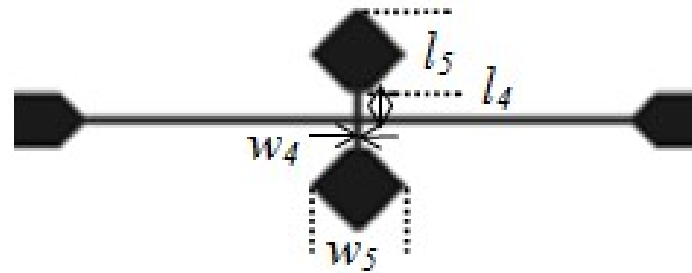
Ref.	RL-PB (dB)	$f_c$ (GHz)	Stopband (GHz @ dB)	Harmonics suppression	Substrate/dielectric loss tangent
Liu <i>et al.</i> (2015)	15	3.11	(3.24 to 10.7 @25)	3 <sup>th</sup> order	RT duroid/ 0.0009
Cao <i>et al.</i> (2012)	10	3.17	(3.4 to 10 @ 25)	3 <sup>rd</sup> order	PTFE/0.0027
Hayati <i>et al.</i> (2014)	20	4.24	(4.37 to 19 @ 20)	4 <sup>nd</sup> order	RT duroid/ 0.0009
Raphika <i>et al.</i> (2014)	20	5.55	(5.88 to 11.8 @15)	2 <sup>nd</sup> order	FR4/0.02
Raphika <i>et al.</i> (2016)	17	2.28	(2.49 to 11 @ 23)	4 <sup>th</sup> order	FR4/0.02
Filter-I	17.74	2.44	(2.94 to 13.04 @ 31) (2.85 to 16 @ 22)	6 <sup>th</sup> order	FR4/0.02

### 3.3 LOWPASS FILTER DESIGN WITH HIGH HARMONIC SUPPRESSION (FILTER-II)

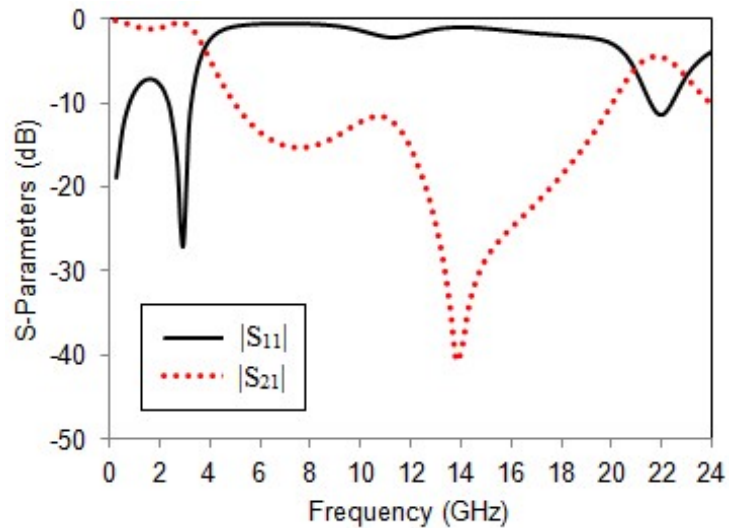
To improve the characteristics of Filter-I, Filter-II is designed by replacing the open circuited stubs with suppressing cells. The proposed lowpass filter, Filter-II is designed to generate flat passband characteristics with good selectivity and wide stopband bandwidth. Here, Filter-II is designed to improve the roll-off rate of Filter-I with reduced physical size and to obtain higher order of harmonic suppression. The dimensions of Resonator-1 and Resonator-2 used for Filter-II design are same as that used in the design of Filter-I. The open circuited stub of Filter-I is replaced by the symmetrical high-low impedance resonators which function as suppressing cells to generate attenuation poles at high frequencies.

### 3.3.1 Suppressor Unit

To extend the stopband bandwidth of the proposed filter, mirrored symmetrical arrangement of suppressing cell is used. Filter-II is designed by replacing the open stubs in Filter-I by diamond shaped resonators. The rectangular high impedance stub is loaded on a diamond shaped low impedance patch and used as the suppressing unit. The suppressing units generate transmission zero at high frequencies, which suppress the transmission peaks and widen the stopband bandwidth of the filter. The structure and frequency response characteristics of the proposed unit are shown in Fig. 3.23.



(a)



(b)

Fig. 3.23 (a) The configuration of the suppressing unit (b) Its frequency response characteristics

The dimensions of the suppressor unit are  $l_4 = 0.65$  mm,  $l_5 = 2.2$  mm,  $w_4 = 0.2$  mm,  $w_5 = 2.6$  mm. The proposed Filter-II is designed and developed using FR4 substrate having its dielectric constant 4.4, thickness of 0.8 mm and loss tangent 0.02. All EM simulations are carried out using full wave simulation software IE3D.

### 3.3.2 The Proposed Filter Design

The individual series resonators such as one unit of Resonator-1 and two units of Resonator-2 are connected in shunt with the high impedance main transmission line and by cascading these symmetrical resonators with mirrored suppressing cells, a wide stopband lowpass filter is designed with sharp transition skirt and low insertion loss in the passband. The layout of Filter-II and its simulated S-parameters are shown in Fig. 3.24. The dimensions of Filter-II are  $w_2 = 1.5$ ,  $a = 1.05$ ,  $b = 0.75$ ,  $m_1 = 4.95$ ,  $g = 0.3$  and  $w = 0.2$  (all in mm). The optimized filter is having 14.6 mm x 9.6 mm physical size. The simulated 3 dB cutoff frequency is 2.455 GHz. The designed filter has wide rejection band at 19 dB suppression level from 2.675 GHz to 24 GHz. The skirt selectivity of the structure is 98.66 dB/GHz (the frequency at 3 dB is 2.455 GHz and frequency at 40 dB is 2.83 GHz). The simulated results of Fig. 3.25 shows that the designed Filter-II can suppress up to 9<sup>th</sup> order harmonics.



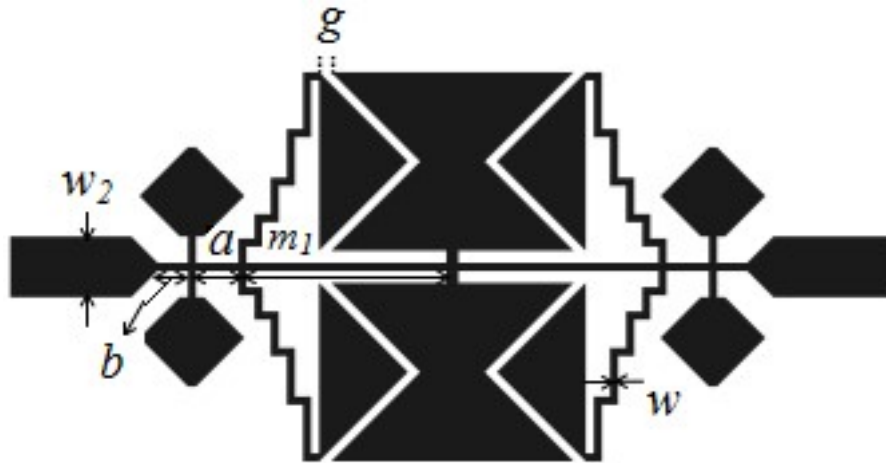


Fig. 3.24 Layout of Filter-II

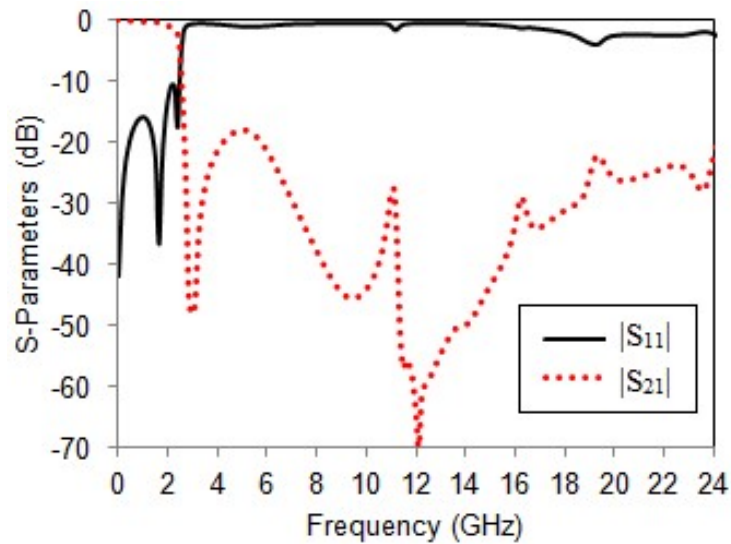


Fig. 3.25 Simulated frequency response characteristics

### 3.3.3 Fabrication and Measurement Results

The proposed filter is printed on FR4 substrate and its measurements are taken using R & S ZVB 20 Vector Network Analyzer available in our laboratory. The photograph of the fabricated filter is shown in Fig. 3.26. The frequency response characteristics of the measured and simulated results, which are compared in Fig. 3.27. It is observed from Figure that both the results are in very good agreement with each other. The 3

dB cutoff frequency of the measured filter is 2.57 GHz. At 40 dB attenuation point, the corresponding frequency is 2.97 GHz and achieved filter selectivity is 92.5 dB/GHz. Within the passband, the insertion loss is very low and its value is within 0.4 dB till 1.65 GHz. The return loss of the constructed structure is better than 14 dB in the low frequencies of the passband. The measured stopband is from 2.78 GHz to 20 GHz at 18 dB rejection level. The RSB is calculated using Equation (2.16) and its value is 1.512.

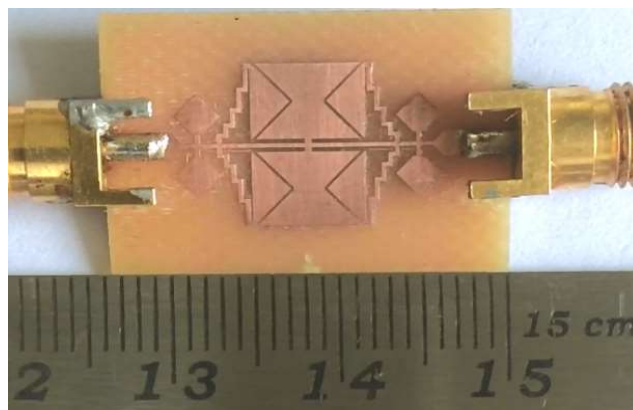


Fig. 3.26 The proto type of the Filter-II

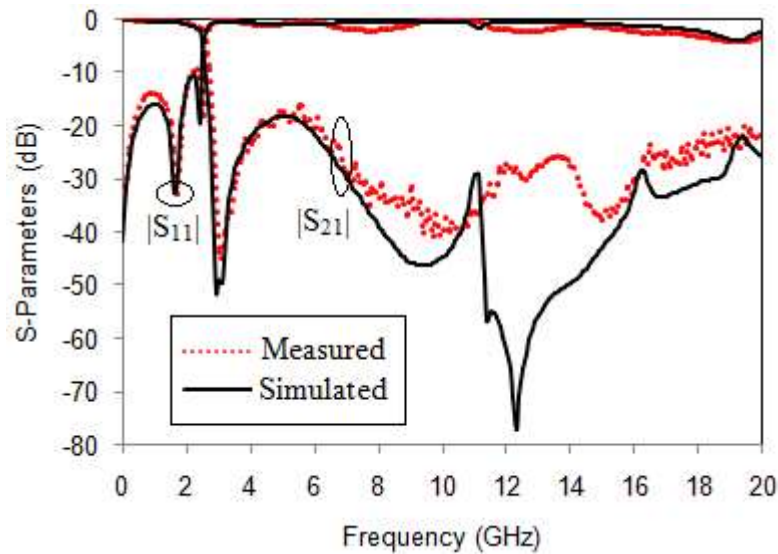


Fig. 3.27 The measured and simulated results of Filter-II

The group delay (envelope delay) of the proposed Filter-II in the passband frequency is shown in Fig. 3.28. As shown in the Figure, the group delay is almost flat in 77 % of the passband and it increases on approaching the cutoff frequency. Flat group delay indicates that all the transmitted energy is received at the destination without any distortion. Fig. 3.29 shows the passband group delay of the filter till 2 GHz frequency and it is seen that the group delay is almost flat in the considered frequency range.

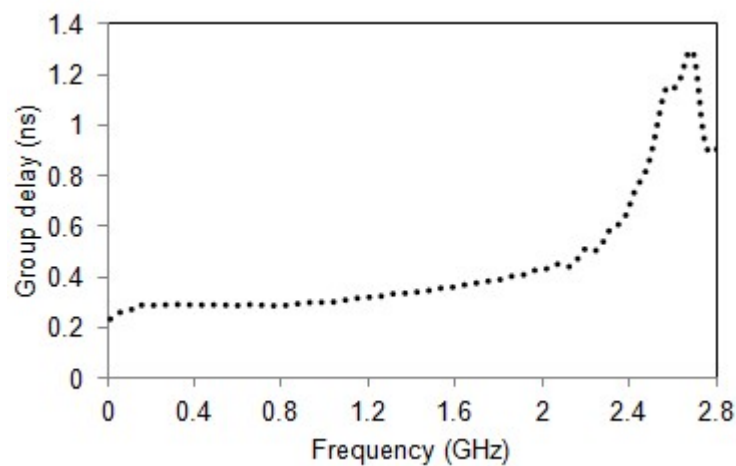


Fig. 3.28 The measured group delay of the Filter-II

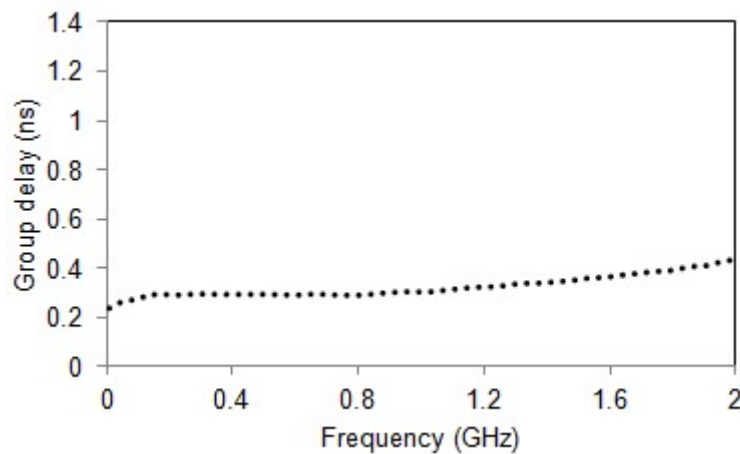


Fig. 3.29 The measured group delay of the Filter-II in the 77% of the passband

### 3.3.4 Performance Evaluation of Filter-II

Table 3.2 summarizes some published works with the proposed one. The main features of the designed filter are compact size, good passband and wide stopband bandwidth. Compared with other works, the proposed filter offers high relative stopband bandwidth and thus able to suppress up to 7<sup>th</sup> order harmonics.

Table 3.2 Comparing the characteristics of the proposed work with other related works

Ref	$f_c$ (GHz)	SB up to (GHz)	RSB (%), Rej. (dB)	Harmonic suppression	Physical size (mm)
Li <i>et al.</i> (2010)	1.0	5.5	119.7, 20	5 <sup>th</sup> order	22.4 x 24.05
Xiao <i>et al.</i> (2015)	3.37	9.2	90.6, 20	2 <sup>nd</sup> order	9.3 x 8.6
Abdipour <i>et al.</i> (2017)	1.69	10	145, 20	6 <sup>th</sup> order	13.8 x 8.6
Filter-I	2.44	16	139.5, 22	6 <sup>th</sup> order	17.4 x 10
Filter-II	2.57	20	151.2, 18	7 <sup>th</sup> order	14.6 x 9.6

### 3.4 CHAPTER SUMMARY

This chapter presents the design and development of two microstrip lowpass filters, Filter-I and Filter-II. By cascading multiple patch resonators of different shapes, multiple transmission zeros are generated at high frequencies, which widen the stopband bandwidth and the suppression of higher order harmonics is achieved. Both filters are having compact physical size and are suitable for use in wireless LAN, L-band and Bluetooth networking applications. The performance characteristics of both the designed filters are compared in Table 3.3.

Table 3.3 Comparing the performance characteristics of the proposed lowpass filters using cascaded multiple patch resonators

Filter Type	$f_c$ (GHz)	$\xi$ (dB/GHz)	Size (mm <sup>2</sup> )	NCS ( $\lambda_g^2$ )	RSB (%)	IL-PB (dB)	Harmonic suppression
Filter-I	2.44	67.27	17.4x10	0.038	139.5	0.6	6 <sup>th</sup> order
Filter-II	2.57	92.5	14.6x9.6	0.0339	151.2	0.4	7 <sup>th</sup> order

A detailed analysis of a microstrip lowpass filter, symmetrically loaded with multiple patch resonators and open stubs is presented in Filter-I. The LC equivalent circuit of the filter is developed and compared to the EM simulation result and found that both the results are similar. The measured cutoff frequency of the filter is 2.44 GHz. The passband insertion loss of the filter is very low and its value is 0.6 dB. The physical size of the filter is 17.4 mm x 10 mm. The filter achieves high RSB of 139.5 % referred to the suppression level of 22 dB and thus able to suppress more than 6<sup>th</sup> order harmonics along with good selectivity and impedance matching.

A compact microstrip lowpass filter with very good in-band and out-of-band performance is designed using multiple patch resonators and suppressing cells is introduced in Filter-II. The cutoff frequency of Filter-II is 2.57 GHz with small physical size of 14.6 mm x 9.6 mm. The designed filter has very low insertion loss of 0.4 dB with high RSB of 151.2% and able to reject up to 7<sup>th</sup> order harmonics. The filter has advantages of low cost, high harmonic rejection and good selectivity and thus can be used for various wireless communication applications.

To further improve the in-band and out-of band performance characteristics of the filter, different new approaches in lowpass filter design such as using interdigital structures, folded stepped impedance resonators etc are proposed in chapter 4.

## CHAPTER 4

# COMPACT MICROSTRIP LOWPASS FILTERS WITH SHARP ROLL-OFF AND ULTRA-WIDE STOPBAND

### 4.1 INTRODUCTION

High performance compact filter structures are used in emerging applications of modern wireless communication. Lowpass filters are key components in modern microwave communication systems to suppress the unwanted harmonics which are generated by nonlinear devices. The passband to stopband transition rate and the stopband bandwidth are important parameters of lowpass filter design. Sharp roll-off is achieved by the generation of an attenuation pole very near to the cutoff frequency and wide stopband is due to the formation of multiple transmission zeros in the stopband region.

Different methods are used in the literature to design a compact lowpass filter having advantages like sharp roll-off and high harmonics rejection. Numerous high performance lowpass filters fabricated using some generic structures called defected ground structures (DGSs), which have wide stopband bandwidth and slow wave effect are reported by Zhang and Li (2016); Yang *et al.* (2012). Wang and Hsu (2018), proposed slotted ground plane resonators as band rejection components to obtain wide stopband. A wide stopband lowpass filter designed using defected ground structure technique for wireless communication system is presented by Vala *et al.* (2017). However, the steepness of transition from passband to stopband of these filters is very low. A lowpass filter with sharp roll-off and wide stopband designed using hexagonal shaped resonator and semicircular slots is introduced by Kumar and Parihar, (2016). However, the passband insertion loss of the filter is high. Sen *et al.*

(2018) presented a lowpass filter with good performance characteristics by incorporating defected structures in the modified rectangular shaped split ring resonators. But the physical size of the structure is high and has the ability to suppress only up to 2<sup>nd</sup> order harmonics.

A compact size lowpass filter with a wide stopband characteristic achieved using modified stepped impedance hairpin unit and meandered open stub is introduced by Xu and Duan (2017). However, the designed filter suffers from low roll-off rate and stopband bandwidth. Zhang *et al.* (2015) proposed a compact, highly selective lowpass filter using folded coupled rhombic stubs. A compact planar lowpass filter developed by introducing interdigital structures within rectangular shaped coupled capacitors is presented by Li and Li (2008). But only quasi elliptic frequency response and stopband up to 9.35 GHz are achieved using this structure. Cascaded patch resonators of triangular and funnel shaped patches utilized to obtain sharp roll-off characteristics are proposed by Raphika *et al.* (2014). However, the filter is used to suppress only up to 2<sup>nd</sup> order harmonics.

A microstrip lowpass filter designed using coupled hairpin shaped resonator is presented by Velidi and Sanyal (2011). To achieve wide stopband up to 4.5 GHz, open stubs are placed in the feed points of the resonator. The cutoff frequency of the filter is 0.5 GHz only and therefore its passband region is very narrow. Wei *et al.* (2012) developed a lowpass filter of compact size using coupled hairpin shaped structure, one spiral shaped slot in the microstrip line and a pair of open stubs. Here the filter is used to achieve wide stopband bandwidth up to 20 GHz, but the stopband suppression level is only 10 dB.



A deep stopband lowpass filter using open complementary type split ring resonator and open circuited stubs is introduced by Karthikeyan and Kshetrimayum (2011). Even though the stopband suppression level of the filter is high, the stopband bandwidth achieved is only up to 6 GHz with low roll-off rate and large physical size of the fabricated prototype. A lowpass filter with semi-circle and semi-ellipse patch resonators loaded by rhomboid and delta-stub structures used for obtaining wide stop bandwidth up to 19 GHz at 20 dB suppression level is reported by Hayati *et al.* (2010c). But the structure is rather complex with large circuit size and sharpness of the filter is relatively low. To reduce the circuit size of the filter, a patch resonator that features strong slow wave effects is described by Li *et al.* (2009). This filter achieves wide stopband with high suppression level, but the roll-off rate of the filter is low.

A stepped impedance radial stub hairpin resonator developed to achieve wide stopband rejection is proposed by Wei *et al.* (2011). However, only 10 dB rejection level is achieved here for spurious frequency suppression from 2 to 12 GHz. A cascaded microstrip lowpass filter with triangular and polygonal patch resonators with meandered transmission line is introduced by Cui *et al.* (2012). The filter is able to suppress high value of harmonics, but the passband region of the filter is low. A cascaded semicircle ended stub resonator and modified radial patch is used to design a compact microstrip lowpass filter (Hayati *et al.*, 2012b). But the filter suffers from low roll-off rate and stopband bandwidth is extended only from 1.8 GHz to 13.93 GHz.

Validi and Sanyal (2010) presented a lowpass filter designed using parallel coupled structures, which is shorted at the centre. The filter is used to suppress up to  $5f_c$ . However, the physical size of the filter is large and it occupies 3.6 mm x 85.65 mm.

Cascaded polygonal shaped patches loaded by corrugated and straight stubs are used to design lowpass filter with wide stopband up to 13.4 GHz in Raphika *et al.* (2015). But the structure fabrication complexity is high due to the presence of corrugations and the filter suffered from low selectivity.

The above mentioned filter offers good stop bandwidth at the cost of moderate roll-off rate. So it is attempted to design a filter having improvement in both the characteristics. Efforts to improve the selectivity along with wide stopband and compact size are being greatly explored.

In this chapter, three lowpass filters, Filter-1, Filter-2 and Filter-3 are designed and developed, which have sharp roll-off rate together with a wide stopband bandwidth.

Filter-1 is developed using symmetric dual stepped high-low impedance resonators placed on the high impedance transmission line. An interdigital structure embedded between the symmetric dual stepped high-low impedance resonators provides improved roll-off rate together with the generation of finite attenuation poles at high frequency. Stopband of the Filter-1 is widened by introducing series connected coupled inductive stubs and the rectangular patch capacitors. The achieved roll-off rate of Filter-1 is 79.5 dB/GHz and the measured RSB is 131.2% at 18 dB suppression level.

Filter-2 has been designed and developed using symmetric folded stepped impedance resonator (FSIR) and a mirrored modified hexagonal shaped resonator (MMHSR). The FSIRs symmetrically connected on both ends of the high impedance main transmission line together with MMHSR are used to obtain a lowpass filter with sharp roll-off and

wide stopband characteristics. The stopband bandwidth at 20 dB suppression level is from 2.1 GHz to 10.12 GHz and the passband to stopband transition slope is 151 dB/GHz. The RSB of Filter-2 is 131.2% at 20 dB suppression level.

The RSB of Filter-2 is improved in Filter-3 by placing a pair of open stubs at the end of high impedance transmission line and its value is 162.15 % at 20 dB rejection level and thus able to suppress more than 10<sup>th</sup> order harmonics. The roll-off rate of Filter-3 is 148.59 dB/GHz. The measured insertion loss is less than 0.2 dB in the entire passband and the return loss is better than 12.5 dB. All the three filters are fabricated using low cost FR4 substrate of  $\epsilon_r = 4.4$ , thickness  $h$  of 0.8 mm and dielectric loss tangent 0.02. All simulations are carried out using Electromagnetic simulation software IE3D.

#### **4.2 COMPACT MICROSTRIP LOWPASS FILTER WITH ULTRA-WIDE STOPBAND (FILTER-1)**

A basic microstrip lowpass filter is designed using symmetric dual Hi-Lo impedance resonators with interdigital structure embedded between the low impedance rectangular patches. The interdigital structures generate one additional transmission zero, which is very near to the cutoff frequency and thus the selectivity of the filter is improved. To extend the stopband bandwidth and to maintain compact physical size, symmetrically paired capacitors are introduced between high impedance stubs of the basic microstrip lowpass filter and cascaded arrangement of coupled inductive stubs with rectangular patches. The physical dimension of these resonators is only quarter guided wavelength long and thus act as semi-lumped elements. The proposed filter is designed, simulated and fabricated using the same raw material as mentioned above.

#### 4.2.1 Primary Stepped Impedance (SI) Lowpass Filter Design

Fig. 4.1 shows the symmetrical arrangement of dual stepped impedance resonators connected to the main high impedance transmission line, which is connected to the input-output port of  $w = 1.5$  mm. To avoid sharp discontinuity effect, a tapered microstrip structure of length  $l_0$  is introduced between the I/O ports and main high impedance transmission line. The stepped impedance resonator consists of a shorted stub connected in series with a rectangular patch. These stepped impedance resonators are very much shorter than its associated guided wavelength and behave as semi lumped elements. The characteristic impedance of the stub is represented as  $Z_{01}$  and its value calculated using Equation (2.21) is  $120.5 \Omega$ . The value of  $Z_{01}$  is much greater than the source impedance value of  $Z_0 (50 \Omega)$  and thus the stub acts as lumped element inductor. The characteristic impedance of the rectangular patch is represented as  $Z_{02}$  and its value is  $35.47 \Omega$ . This low impedance open circuited line behaves as lumped capacitor because its value is less than the source impedance value. These series LC resonant branches are connected in shunt with the main high impedance transmission line to short out transmission at corresponding resonant frequencies.

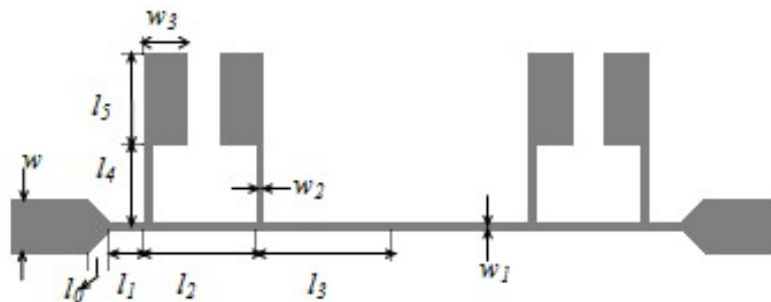


Fig. 4.1 Layout of the primary SI lowpass filter

The frequency response characteristics of the primary SI lowpass filter shown in Fig. 4.2 has one finite frequency transmission zero,  $TZ_1$ . The transmission zero frequency depends on the dimension of the series resonant branch of high/low impedance lines. The  $TZ_1$  occurs at frequency 5.85 GHz at 55.96 dB suppression level. The cutoff frequency of the primary SI lowpass filter is 4.52 GHz and the transmission zero  $TZ_1$  occurs at 5.85 GHz. Thus the roll-off rate of the filter is very low.

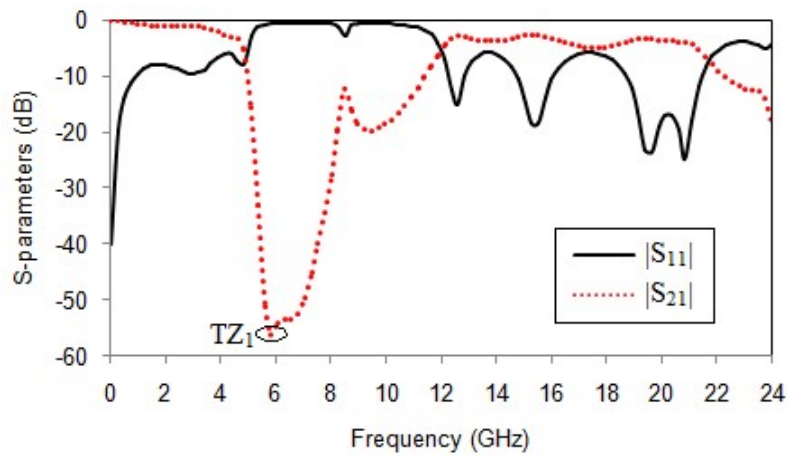


Fig. 4.2 The frequency response characteristics of the primary SI lowpass filter

To obtain sharp cutoff frequency, it is desirable to use lowpass filter structures, which gives infinite attenuation at finite frequency values (Hong and Lancaster, 2001). Thus to improve the roll-off rate of the filter, the primary SI lowpass filter is modified as basic microstrip lowpass filter with interdigital structures embedded between the dual rectangular patches. The structure of the basic microstrip lowpass filter is shown in Fig. 4.3. The interdigital structure of length  $l_d$  and width  $w_d$  is introduced between the symmetric dual rectangular patches and the addition of interdigital structure does not increase the overall physical size of the primary SI filter. The frequency response characteristics of the basic lowpass filter is depicted in Fig. 4.4.

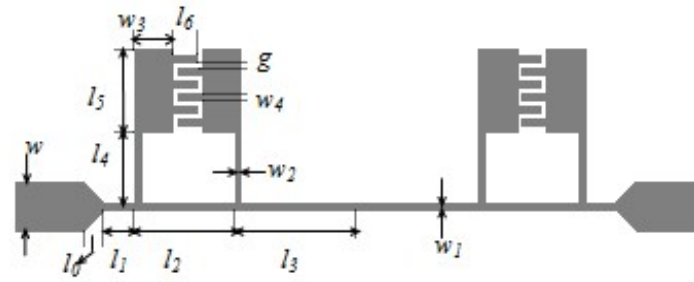


Fig. 4.3 The structural layout of the basic lowpass filter

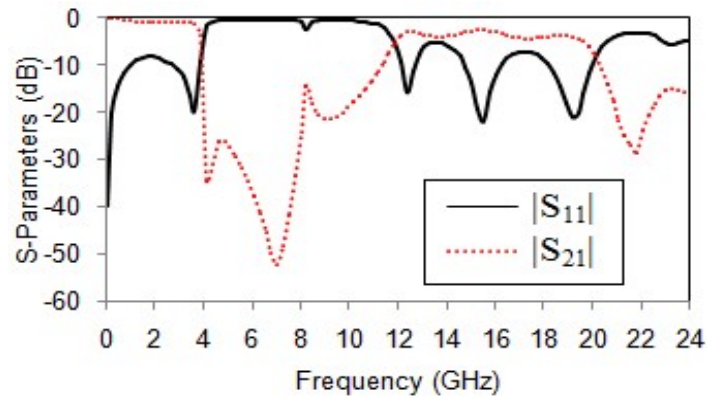


Fig. 4.4 The frequency response characteristics of the basic lowpass filter

#### 4.2.2 Comparison of Frequency Response Characteristics of Primary SI Lowpass Filter with Basic Lowpass Filter

The comparison of frequency response of the primary SI filter and the basic lowpass filter is shown in Fig. 4.5. The cutoff frequency of the basic lowpass filter is 3.86 GHz. As shown in Figure, the basic lowpass filter generates two transmission zeros  $TZ_2$  and  $TZ_1'$  at frequencies 4.1 GHz and 7.02 GHz respectively. With the introduction of interdigital structure, the transmission zero  $TZ_1$  of primary SI filter is shifted towards the higher frequency end and is represented as  $TZ_1'$ . One additional transmission zero,  $TZ_2$  is also generated very near to the cutoff frequency and thus the roll-off rate of the basic lowpass filter increases. On adding interdigital structure between the symmetric dual rectangular patches, a strong electrical coupling occurs between the resonators and this enhances the total energy in the circuit and thus the roll-off rate of the filter increases. Thus the interdigital structure provides higher

capacitance, and it depends on the number of fingers of width  $w_4$ , length  $l_6$  and spacing  $g$  between the fingers. The stopband bandwidth of the basic lowpass filter also increases due to the generation of two transmission zeros  $TZ_2$  and  $TZ_1'$ , one near to the cutoff frequency and the other towards the higher frequency end, and its value is from 4.0 GHz to 8.1 GHz at 20 dB suppression level. The element values of the basic microstrip lowpass filter are  $l_0 = 0.65$ ,  $l_1 = 1.0$ ,  $l_2 = 3.3$ ,  $l_3 = 4.1$ ,  $l_4 = 2.3$ ,  $l_5 = 2.6$ ,  $l_6 = 0.8$ ,  $w_1 = w_2 = 0.2$ ,  $w_3 = 1.25$ ,  $w_4 = 0.2$ ,  $w = 1.5$  and  $g = 0.2$  (all dimensions in mm).

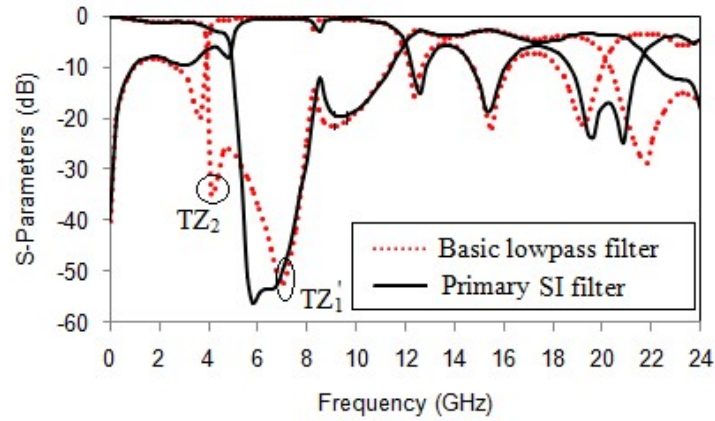


Fig. 4.5 The comparison of frequency response characteristics of the primary SI filter and the basic lowpass filter

#### 4.2.3 Basic Lowpass Filter - Equivalent Circuit

The equivalent circuit of basic lowpass filter by assuming it as a lossless circuit is depicted in Fig. 4.6. Here,  $Y_{01}$  and  $Y_{02}$  represent the characteristic admittance of the high impedance line and the rectangular patch respectively. The high impedance transmission line of length  $l_4$  represents the inductance.  $C_i$  represents the capacitance of the interdigital structure embedded between the dual rectangular patches and  $C$  is the capacitance of the rectangular patch and the ground plane. This symmetric circuit has its transmission characteristics derived using even and odd mode analysis as described by Li and Li, (2008),

$$S_{21} = \frac{Y_0 - Y_e}{(1 + Y_0)(1 + Y_e)} \quad (4.1)$$

$$Y_o = \frac{1}{Z_o} = -jY_{01} \tan(\beta_{01}l_2) + 2jY_{01} \frac{\omega(C + 2C_i) + Y_{01} \tan(\beta_{01}l_4)}{Y_{01} - \omega(C + 2C_i) \tan(\beta_{01}l_4)} \quad (4.2)$$

$$Y_e = \frac{1}{Z_e} = jY_{01} \tan(\beta_{01}l_2) + 2jY_{01} \frac{\omega C + Y_{01} \tan(\beta_{01}l_4)}{Y_{01} - \omega C \tan(\beta_{01}l_4)} \quad (4.3)$$

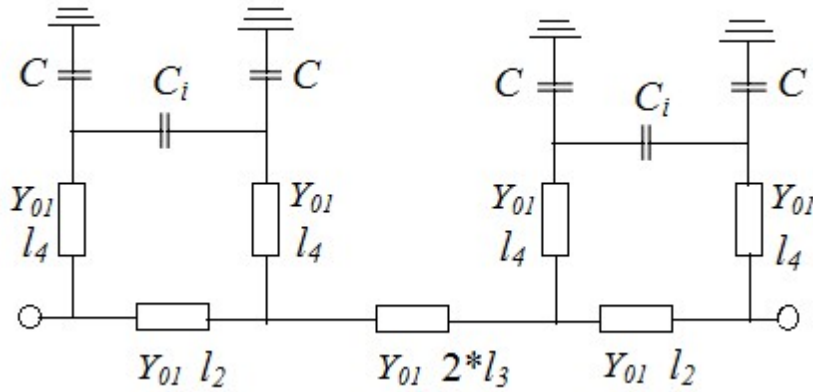


Fig. 4.6 LC equivalent circuit of the basic lowpass filter

The capacitance  $C$  is calculated using the Equation (4.4) as,

$$C = \frac{Y_{02} \tan(\beta_{02}l_5)}{2\pi f} \quad (4.4)$$

The inductance values of the thin lines are calculated using the Equation (4.5) for the corresponding values of  $l$  as,

$$L_{2,3,4} = \frac{l_{2,3,4}\beta_{01}}{2\pi f Y_{01}} \quad (4.5)$$

where  $f$  is the cutoff frequency of the basic lowpass filter.  $\beta_{01}$  and  $\beta_{02}$  are the propagation constant of high impedance transmission line and the low impedance rectangular patch respectively.  $C_i$  is the interdigital capacitance and its value depends not only on the interdigital finger dimension but also on the gap between each fingers.



The gap capacitance is calculated using the Equations (3.10)-(3.17). From the Equation (4.1), when odd mode admittance becomes equal to the even mode admittance, a finite transmission zero of the basic lowpass filter occurs.

The calculated  $LC$  values of the equivalent circuit of the basic lowpass filter are  $L_2 = 2.2879$  nH,  $L_3 = 2.8426$  nH,  $L_4 = 1.5946$  nH,  $C = 0.2789$  pF and  $C_i = 0.1835$  pF. The stopband bandwidth of the basic lowpass filter is improved as compared to the primary SI lowpass filter and its value is from 4.0 GHz to 8.1 GHz at 20 dB suppression level. As compared to the primary SI lowpass filter, the cutoff frequency of the basic lowpass filter comes down to 3.86 GHz, which reduces the normalized circuit size of the filter. The physical size of the basic lowpass filter is 16.8 mm x 7.55 mm.

#### 4.2.4 Parametric Analysis

A detailed parametric analysis has been conducted on the basic lowpass filter for different values of interdigital capacitance  $C_i$  as shown in Fig. 4.7. When  $C_i = 0$  pF, no interdigital capacitance appears between the dual branch resonators and thus only single transmission zero occurs at frequency 6.5 GHz. This transmission zero is generated due to the series resonance of the symmetric dual stepped impedance resonators positioned on the high impedance transmission line. Once the interdigital structure is introduced, another coupling route is created between the dual patch resonators. Thus an additional transmission zero occurs, which is very near to the cutoff frequency and thus the roll-off rate of the filter increases. It is seen in the Figure that as the value of  $C_i$  increases, the first transmission zero moves towards the lower frequency end, the second one towards the higher frequency end and thus the stopband bandwidth of the filter increases.

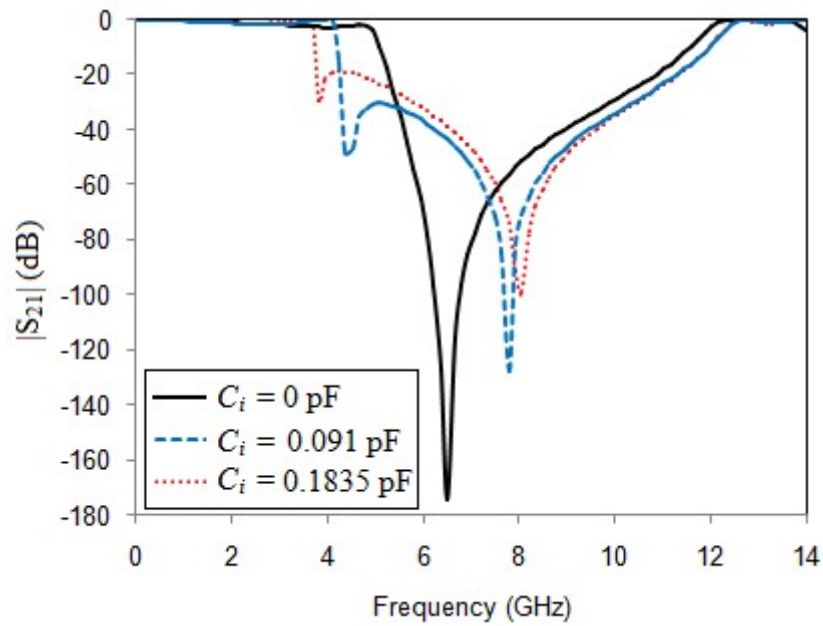


Fig. 4.7 The transmission characteristics of the Basic lowpass filter for different values of  $C_i$

The variation of transmission zero values for increasing values of interdigital capacitance,  $C_i$  is depicted in Fig. 4.8. When  $C_i = 0$ , there is only one transmission zero as seen in the Figure. As the value of  $C_i$  increases, the separation between the transmission zero also increases, and thus the stopband bandwidth increases. In the Figure, two transmission zeros  $TZ_1'$  and  $TZ_2$  occur when the value of  $C_i = 0.1835$  pF.

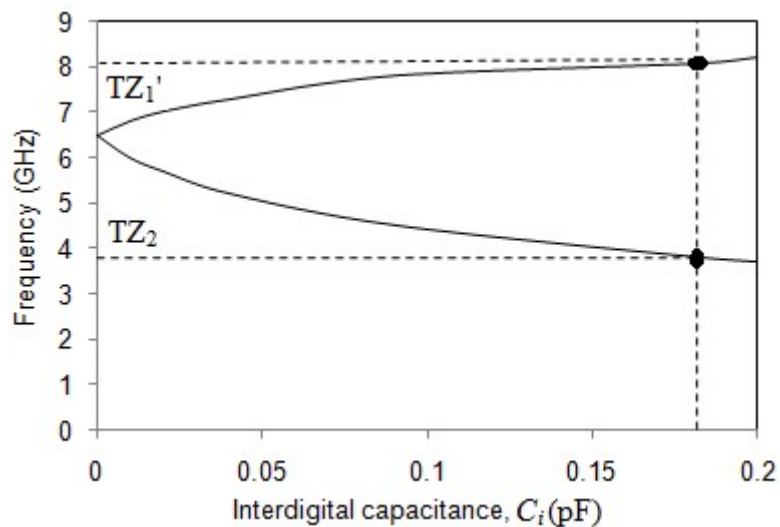


Fig. 4.8 The variation in transmission zero values for increasing values of  $C_i$

The parametric study is also conducted by varying the stub length  $l_4$  of the basic lowpass filter. Fig. 4.9 shows the transmission characteristics of the basic lowpass filter for different values of high impedance stub length,  $l_4$ . As the stub length increases from 2.3 mm to 3.7 mm, in steps of 0.7 mm, the stopband bandwidth of the filter decreases. Thus from the Fig. 4.7 and Fig. 4.9, it is understood that the stopband bandwidth of the basic lowpass filter depends on the equivalent capacitance and inductance value of the resonator.

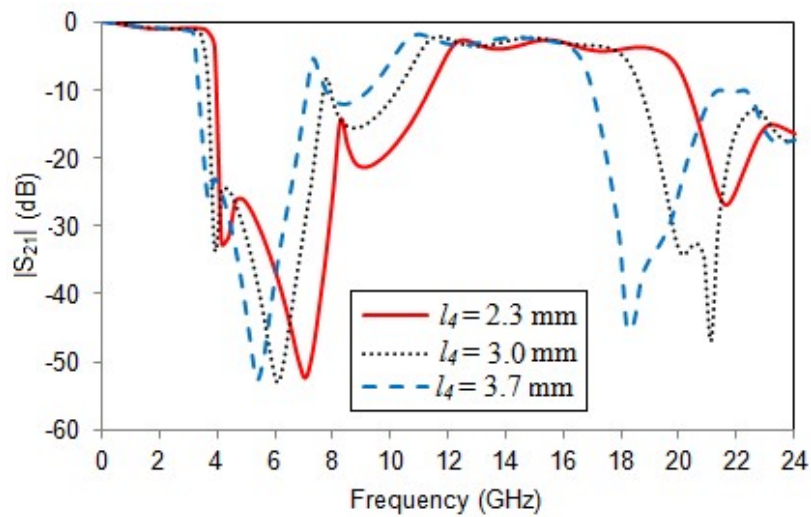


Fig. 4.9 Transmission characteristics of the basic lowpass filter for various values of  $l_4$

#### 4.2.5 Design of Improved Basic lowpass filter

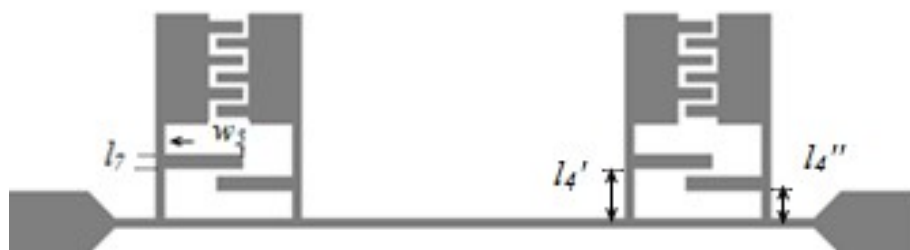


Fig. 4.10 Geometry of the improved basic lowpass filter

To improve the frequency response characteristics of the basic microstrip lowpass filter, finite attenuation poles have to be generated at high frequency. To obtain transmission zeros at high frequency, symmetrically paired interdigital structures are added at a distance  $l_4'$  and  $l_4''$  from the main high impedance transmission line as shown in Fig. 4.10 and thus the effective capacitance value of the filter increases. The frequency response characteristics of the improved basic lowpass filter is shown in Fig. 4.11. With the addition of interdigital stubs, the roll-off rate of the filter increases and two transmission zeros at frequency 14.4 GHz and 19.6 GHz are also generated.

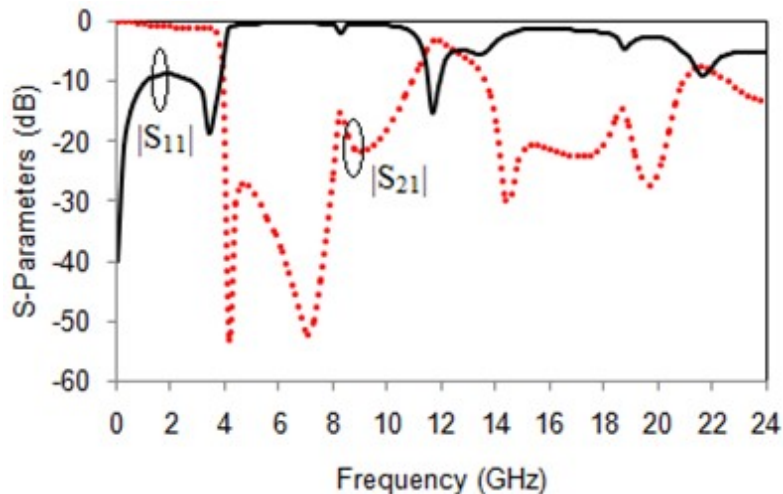


Fig. 4.11 The frequency response characteristics of the improved basic lowpass filter

#### 4.2.6 Design of Coupled Inductive Stub Resonator

To suppress the spurious passband and thus to extend the stopband bandwidth of the proposed filter, multiple transmission zeros have to be generated at high frequency. For this purpose, symmetrical series connected coupled inductive stubs and rectangular patch capacitors are introduced between the improved basic microstrip lowpass filter. The introduction of this branch resonance circuit does not increase the physical size of the filter. The structure of the coupled inductive stub resonator is

shown in Fig. 4.12. The resonators are placed at a distance  $l$  from the end of the main transmission line. The structure consists of the coupled inductive stub, each of length  $l_8$  and width  $w_6$ , separated by a gap,  $g'$  connected in series with a rectangular patch capacitor. The length and width of the rectangular patch capacitor are  $l_9$  and  $w_7$  respectively. These symmetrical resonators are embedded between the improved basic lowpass filter and thus the addition of these resonators does not increase the physical size of the filter.

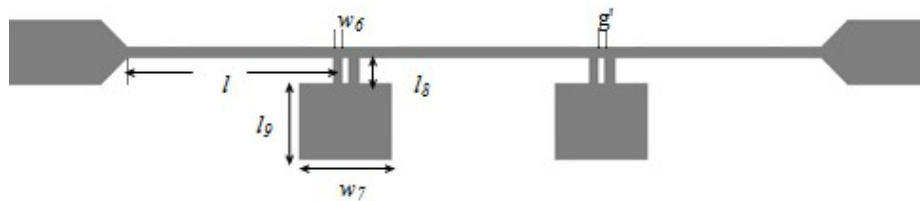


Fig. 4.12 Layout of the coupled inductive stub resonator

Fig. 4.13 shows the transmission response characteristics of the resonator with coupled inductive stub and the single stub. In the Figure, coupled inductive stub resonator generates wide stopband bandwidth when compared to the resonator designed using single stub with rectangular patch. For very low value of  $g'$ , the coupling between the inductive stubs increases, which results wide stopband bandwidth at high suppression level. The stopband bandwidth at 20 dB suppression level is from 7.60 GHz to 20.12 GHz. These two inductive stubs are connected in parallel, which is in series with the rectangular patch capacitor to obtain transmission zero at 12.18 GHz at 56 dB suppression level. Thus the effective inductance of the resonator decreases, which results in the shift of transmission zero towards the high frequency end.

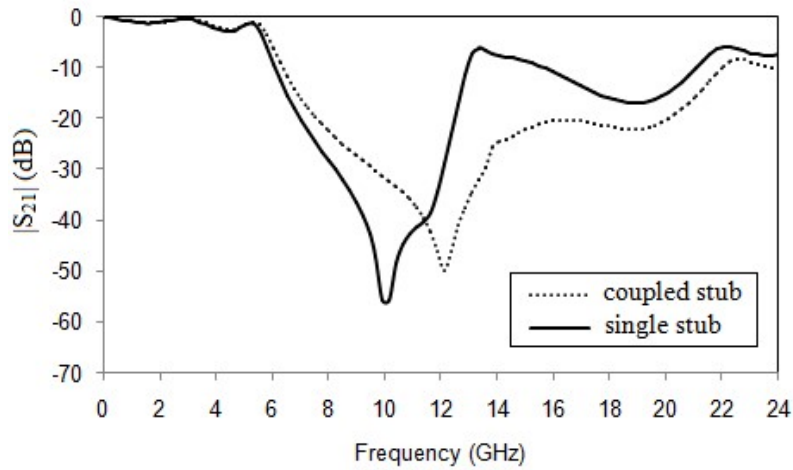


Fig. 4.13 Comparison of the frequency response characteristics of the single stub and coupled stub resonator

#### 4.2.7 The Lowpass Filter Design

Fig. 4.14 shows the structure of Filter-1 designed using FR4 substrate. The high roll-off rate of the proposed filter is mainly contributed by the improved basic lowpass filter structure and ultra-wide stopband bandwidth at high suppression level is achieved using the mirrored coupled inductive stub resonators embedded in the improved basic lowpass filter structure. The parameters of the proposed design are  $l = 5.0$ ,  $l_4' = 1.25$ ,  $l_4'' = 0.7$ ,  $l_7 = 0.3$ ,  $l_8 = 0.65$ ,  $l_9 = 1.8$ ,  $w_5 = 1.85$ ,  $w_6 = 0.2$ ,  $w_7 = 2.2$  and  $g' = 0.2$  (all in mm).

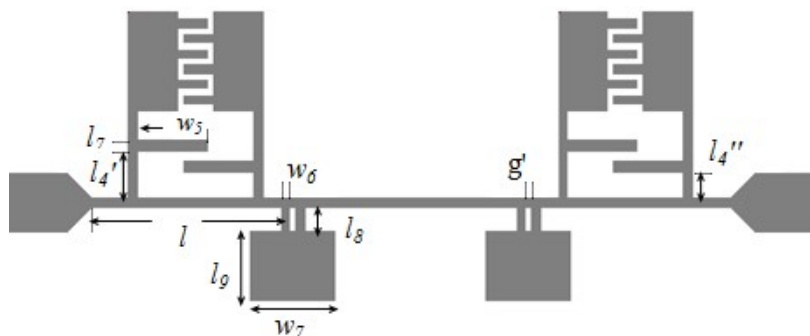


Fig. 4.14 The structure of the proposed lowpass filter (Filter-1)

The simulated S-parameters of the Filter-1 are depicted in Fig. 4.15. The 3 dB cutoff frequency of the lowpass filter is 3.675 GHz. The passband insertion loss is less than 0.6 dB up to frequency of 2.6 GHz and the return loss is better than 14 dB in the entire passband. The frequency corresponding to 40 dB attenuation point is 4.003 GHz and thus the transition band frequency between the 3 dB and 40 dB attenuation point is 0.328 GHz. The roll-off rate of the designed filter calculated using Equation (2.15) is 112.8 dB/GHz. The proposed structure has a wide stopband bandwidth from 3.92 GHz to 21 GHz at 20 dB suppression level and, it is from 3.895 GHz to 24 GHz at 14.8 dB suppression level.

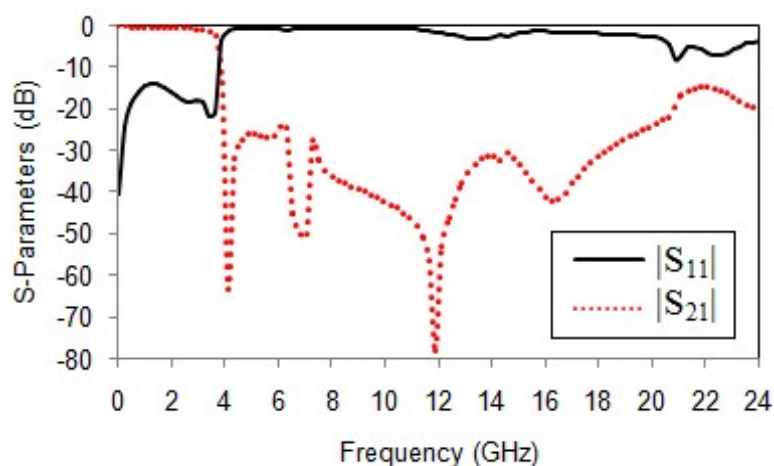


Fig. 4.15 Simulated frequency response characteristics of Filter-1

#### 4.2.8 EM Field Distribution Along the Proposed Filter

The EM field simulation demonstrates the rationality of the equivalent circuit of the proposed filter and is helpful to study the behavior of the filter in its passband and stopband frequencies. The field distribution of the filter is analyzed at two different frequencies, at the passband frequency of 1 GHz and at the first attenuation pole frequency of 4.1 GHz. Fig. 4.16(a) shows the field distribution at the passband frequency of 1 GHz. Here the desired range of RF energy is distributed from input

port to output port freely through the main high impedance transmission line. Only negligible amount of energy is appearing around the rectangular capacitive patch and the interdigital capacitor structure, which proves the passband characteristics of the filter. Here, the transmitted power between input port and output port is magnetic. At the first attenuation pole frequency of 4.1 GHz, most of the RF energy is concentrated around the first branch structure and the ground and no transmission occurs to the output, which indicates the stopband characteristics of the filter as shown in Fig. 4.16(b).

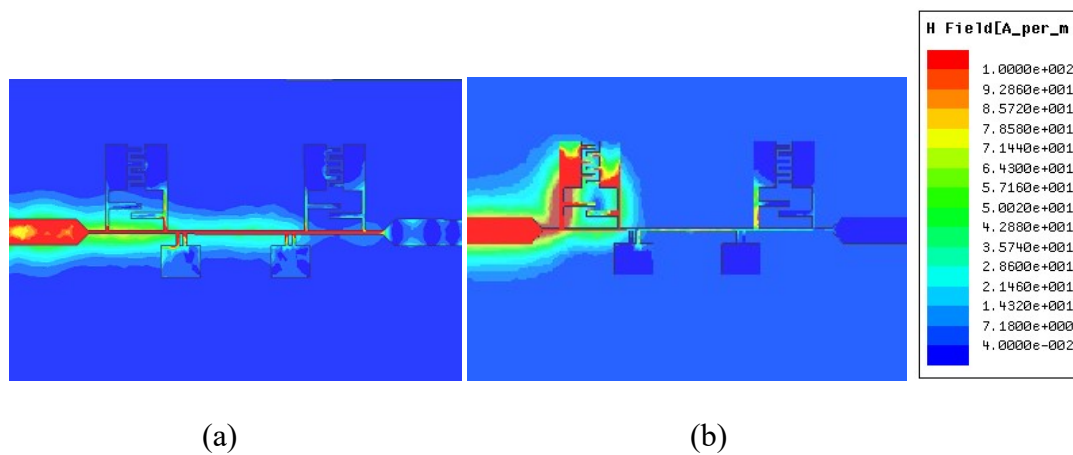


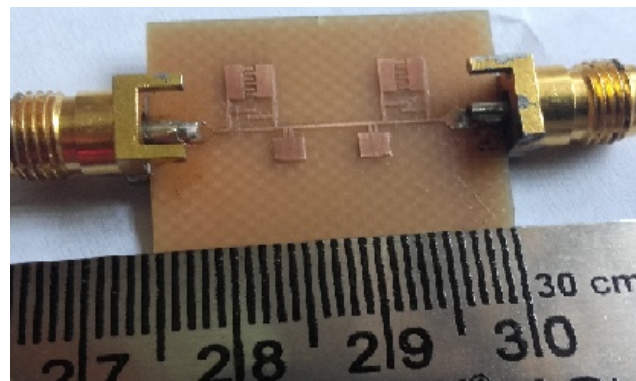
Fig. 4.16 The field distribution of Filter-1 (a) In the passband frequency of 1 GHz (b) In the stopband frequency of 4.1 GHz

#### 4.2.9 Measured and Simulated Results

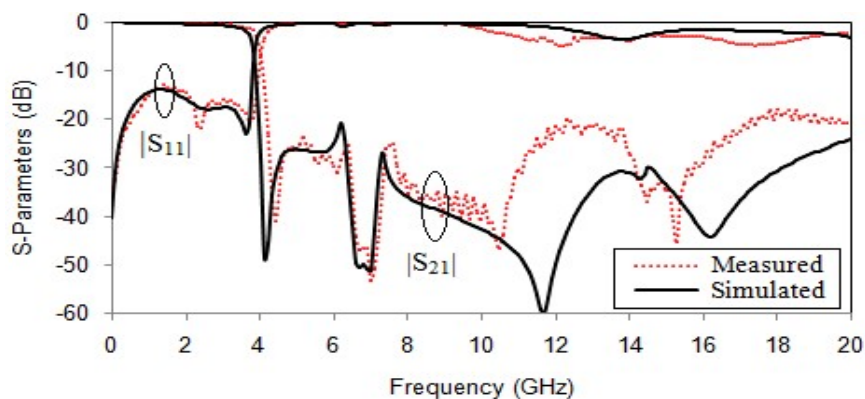
The designed filter is fabricated and the characteristics of the filter is measured using the available R & S ZVB 20 Vector Network Analyzer. The prototype of the proposed structure and its measured and simulated results up to the frequency of 20 GHz are shown in Fig. 4.17. The 3 dB cutoff frequency of the proposed structure is 3.9 GHz. The passband insertion loss is less than -0.5 dB up to 3 GHz and the return loss is better than -13 dB in the entire band. The measured frequency at 40 dB suppression level is 4.365 GHz. The transition band between passband and stopband at 3 dB and 40 dB is



0.465 GHz and thus the calculated roll-off rate is 79.5 dB/GHz. The decrease in the value of measured roll-off rate is due to the fabrication tolerance of the filter. The stopband return loss value is negligible up to 9 GHz and increases up to 4 dB at frequencies above 9 GHz. This increase in return loss at high frequency values is due to the inherent dielectric losses associated with the FR4 substrate. The filter has wide stopband bandwidth and its value is from 4.175 GHz to 18 GHz at 20 dB rejection level and from 4.155 GHz to 20 GHz at suppression level of 18 dB. The RSB, calculated using Equation (2.16) of the proposed filter at 18 dB suppression level is 131.2 %.



(a)



(b)

Fig. 4.17 (a) The prototype of the proposed lowpass filter (b) Simulated and measured results

Group delay is the true signal delay and for the filter, it represents the time required for an RF signal to propagate from input to output. The measured group delay of the proposed filter is shown in Fig. 4.18. The flat group delay in the passband represents the minimum distortion or no distortion of signals. For the proposed filter, the passband group delay is almost flat and the peak to peak group delay variation is less than 0.6 ns.

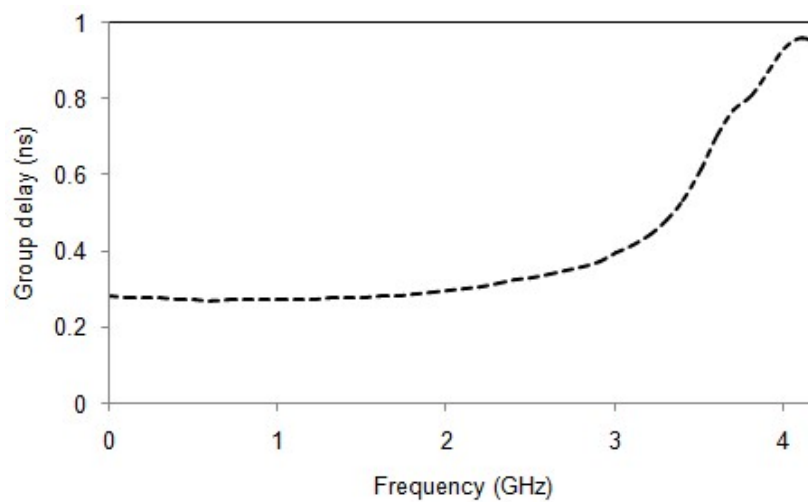


Fig. 4.18 The measured group delay of the proposed lowpass filter

For a lossless transmission line, when all the RF signal from the source is delivered to the load, there will not be any reflected power and the return loss will be infinite. Fig. 4.19 shows the VSWR of the proposed filter and its value is almost unity in the entire passband which proves there is only negligible radiation loss.

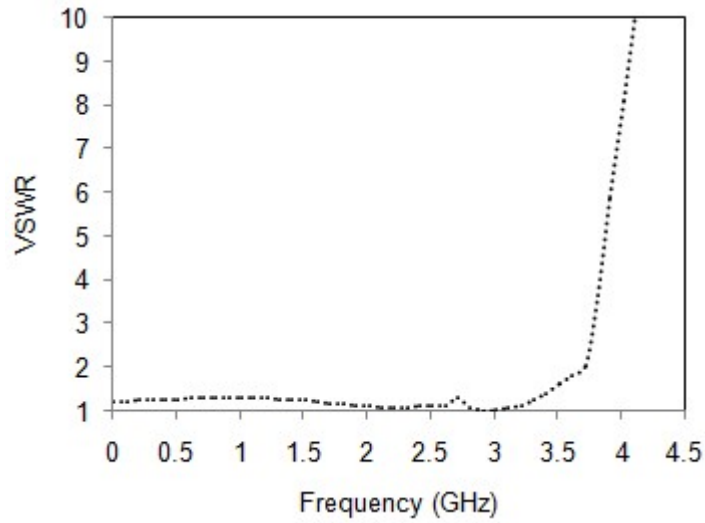


Fig. 4.19 The measured VSWR of the proposed lowpass filter

#### 4.2.10 Performance Comparison of Filter-1

The proposed Filter-1 is compared with other related works from the literature as shown in Table 4.1. From the table, it is observed that the proposed filter has good characteristics of high roll-off rate,  $\xi$  and wide stopband bandwidth.

Table 4.1 Comparison between proposed work and related works from the literature

Ref	$\xi$ (dB/GHz)	Stopband (GHz @ dB)	Substrate
Xu and Duan, (2017)	61.7	1.44 - 12.35 @ 17	FR4
Zhang <i>et al.</i> (2015)	57.8	1.65 - 19 @ 35	Taconic TLY-8
Li and Li (2008)	25.75	2.8 - 9.35 @ 20	F4B
Wei <i>et al.</i> (2012)	43.9	2.0 - 20 @ 10	RT/Duroid
Filter-1	79.5	4.175 - 20 @ 18	FR4

### 4.3 COMPACT LOWPASS FILTER WITH SHARP ROLL-OFF USING FOLDED STEPPED IMPEDANCE RESONATOR (FILTER-2)

A novel microstrip lowpass filter with sharp transition band and wide stopband using symmetric folded stepped impedance resonator (FSIR) and mirrored modified hexagonal shaped resonator (MMHSR) is presented in Filter-2. By folding the high impedance stub of FSIR, the overall physical size of the filter is reduced. The FSIRs are symmetrically connected on both ends of the high impedance main transmission line together with MMHSR are used to obtain a lowpass filter with sharp roll-off and wide stopband characteristics. The 3 dB cutoff frequency of the filter is 1.97 GHz. The stopband bandwidth at 20 dB suppression level is from 2.1 GHz to 10.12 GHz. The fabricated filter achieves the relative stopband bandwidth of 131.2% at 20 dB rejection level and sharp transition band from 1.97 GHz to 2.215 GHz for the attenuation level of -3 dB and -40 dB respectively. The normalized circuit size of the filter is only  $0.0344 \lambda_g^2$ , where  $\lambda_g$  is the guided wavelength at 3 dB cutoff frequency.

The design procedure of resonators is described below.

#### 4.3.1 Design Procedure of Mirrored Modified Hexagonal Shaped Resonator

The design procedure of Mirrored Modified Hexagonal Shaped Resonator (MMHSR) is shown in Fig. 4.20. Fig. 4.20(a) shows the design of a three pole microstrip lowpass filter with open-circuited stub. The high impedance line having length  $L_0$  and width  $W_1$  acts as inductor and the low impedance open-circuited stub of length  $L_5'$  and width  $L_4$  as capacitor. As in Fig. 4.20(e), the filter using open-circuited stub has very low suppression level in the stopband. To obtain sharper rate of cutoff with wide stopband characteristics, a length  $L_0'$  and width  $W_1$  is added to the main high impedance transmission line and the open stub is replaced with a series resonant

branch as shown in Fig. 4.20(b). The series resonant branch has a high impedance stub of length  $L_3$  and width  $W_2$  is in series with a tapered patch of length  $L_5''$  and width  $L_4'$  and  $L_4$  respectively. From the transmission characteristics of Fig. 4.20(e), this filter has sharp cutoff and wide stopband characteristics with an attenuation peak at 7.5 GHz. The cutoff frequency of the filter can be made sharper when the open stub of length  $L_5'$  and width  $L_4$  is added with the series resonant branch so as to form a modified hexagonal shaped resonator as shown in Fig. 4.20(c). This filter exhibits a high suppression level of nearly 44 dB at 5 GHz. By using mirrored modified hexagonal shaped resonator, the filter achieves lower cutoff frequency as well as wide stopband bandwidth with transmission zero at 6.7 GHz as shown in Fig. 4.20(e). The cutoff frequency of the filter is 1.57 GHz and a wide stopband bandwidth with suppression level of 15 dB is achieved from 2.9 GHz to 10.79 GHz.

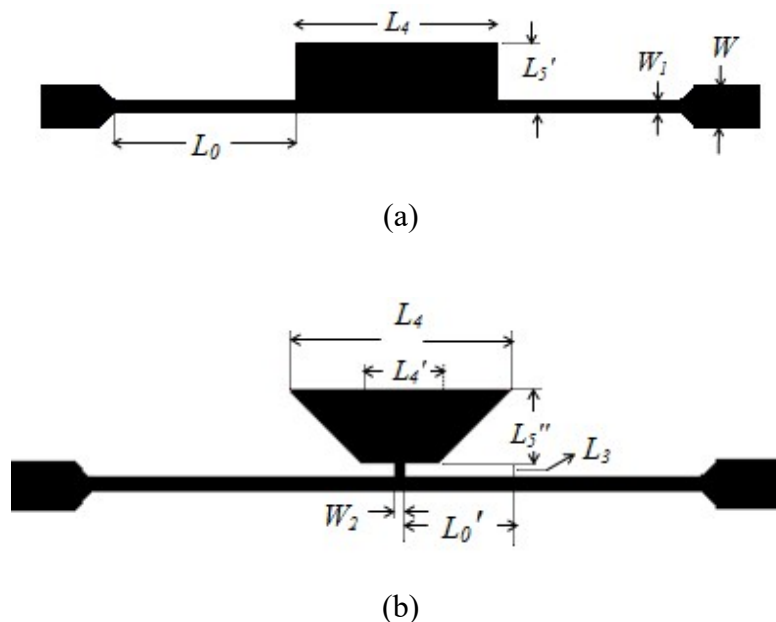
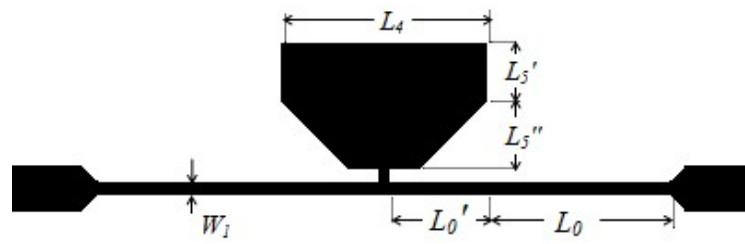
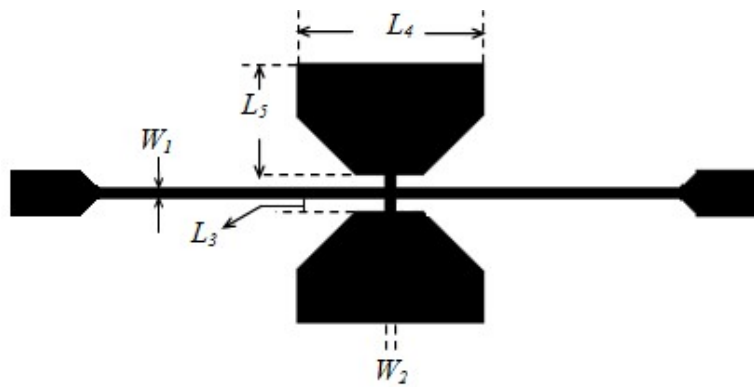


Fig. 4.20 Step by step design process of MMHSR and its simulation result  
 (a) A 3-pole lowpass filter (b) A high impedance stub loaded with tapered structure  
 (c) Modified hexagonal shaped resonator (d) Mirrored modified hexagonal shaped resonator  
 (e) Transmission characteristics of Fig.4.20a,b,c,d

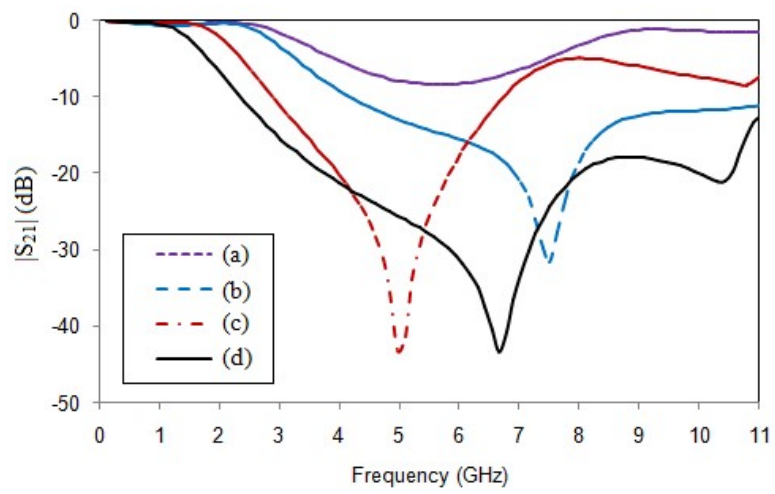
Fig. 4.20 (Contd.)



(c)



(d)



(e)

### 4.3.2 Design of folded stepped impedance resonator

Even though the filter using MMHSR has wide stopband bandwidth with high suppression level, the selectivity of the filter is very low and needs improvement. To improve the roll-off rate of the filter, a folded stepped impedance resonator (FSIR) is used in the design. FSIR is a high impedance stub connected in series with a low impedance patch. To make the structure compact, the high impedance stub of FSIR is folded and its vertical and horizontal length is represented as  $L_6$  and  $L_7$  respectively and the square shaped microstrip bend, A-A' of dimension 0.2 mm x 0.2mm. The width of the high impedance stub is represented as  $W_3$ . The folded high impedance stub is in series with a rectangular patch of length  $L_8$  and width  $L_9$  and this combination form a folded stepped impedance resonator. Fig. 4.21 shows the structure of FSIR in which the high impedance stub acts as inductor and the low impedance patch as capacitor.

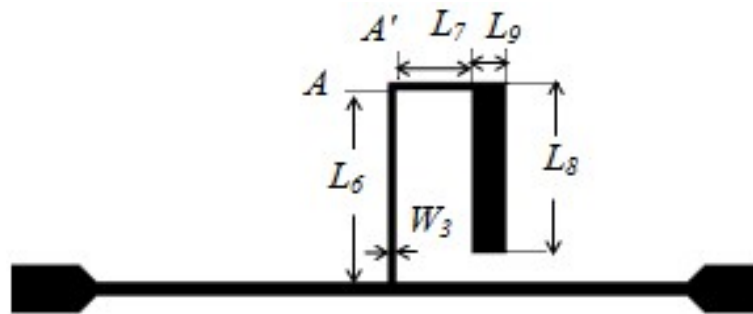


Fig. 4.21 Structure of folded stepped impedance resonator

Fig. 4.22 shows the frequency response of FSIR. It creates two deep transmission zeros at 2.18 GHz and 8.59 GHz with suppression level at 25.9 dB and 15 dB respectively. The 3 dB cutoff frequency of the filter is 1.78 GHz and the passband to stopband transition slope from 3 dB and 20 dB is only 0.34 GHz . Thus the roll-off rate of the filter is improved with low insertion loss and high return loss in the passband.

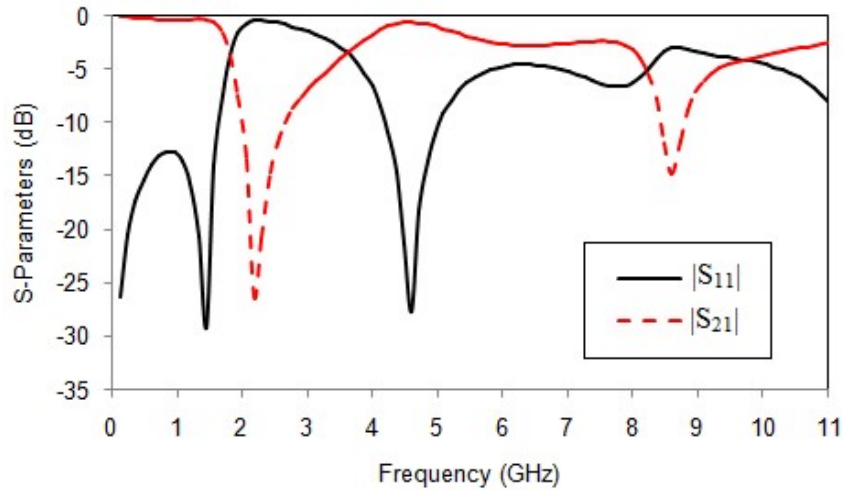
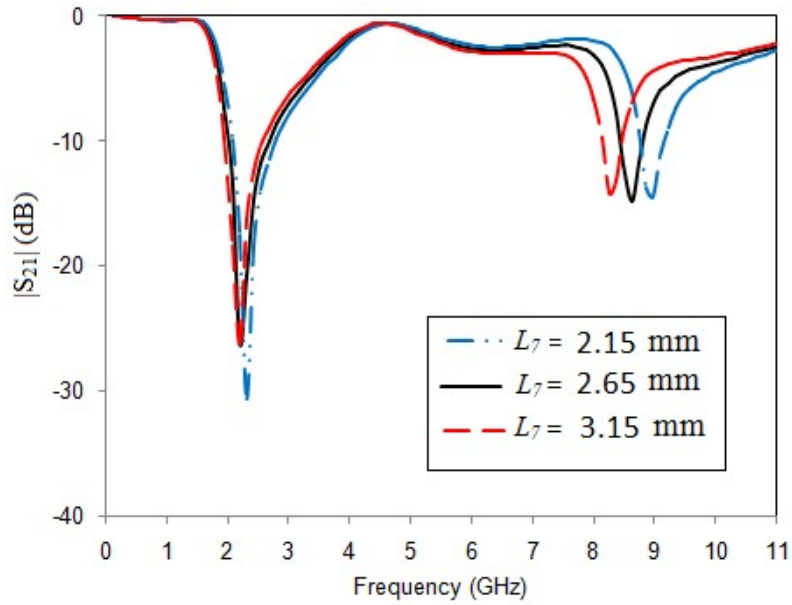


Fig. 4.22 Frequency response characteristics of the folded stepped impedance resonator

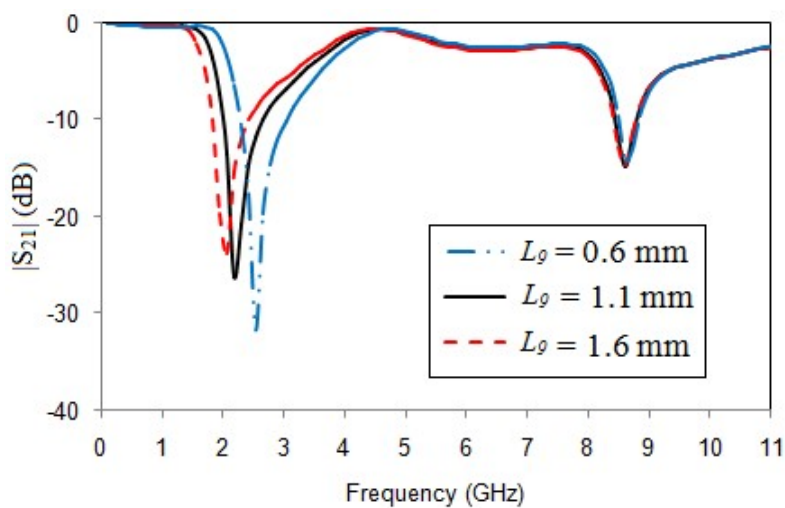
### 4.3.3 Parametric Analysis of FSIR

The filter performance is found to be varying with changes in values of  $L_7$  and  $L_9$ . Fig. 4.23(a) shows the frequency response of FSIR for different values of  $L_7$ . As horizontal length of the folded stub  $L_7$  varies from 2.15 mm to 3.15 mm in steps of 0.5 mm, the upper transmission zero moves towards the cutoff frequency whereas the position of lower transmission zero remains almost unchanged. However, as the width  $L_9$  of rectangular patch increases from 0.6 mm to 1.6 mm as shown in Fig. 4.23(b), the upper transmission zero remains constant but the lower transmission zero is shifted towards the lower frequency end. Thus by changing the parameters  $L_7$  and  $L_9$ , the location of transmission zero can be varied.





(a)



(b)

Fig. 4.23 Transmission characteristics of FSIR (a) For various values of horizontal stub length,  $L_7$  (b) Different values of rectangular patch width,  $L_g$

#### 4.3.4 Design of Lowpass Filter (Filter-2)

Wide stopband and sharp roll-off can be obtained by cascading MMHSR and FSIR. The transition band from passband to stopband can be improved by placing two units of FSIR at distance  $L_{10}'$  from both ends of high impedance main transmission line. Thus by cascading one unit of MMHSR and two units of FSIR the filter performance is

greatly improved. A tapered stub of length  $L_{11}'$  is placed for providing the impedance matching between  $50 \Omega$  input/output port and high impedance main transmission line.

Fig. 4.24 shows the structural geometry of the proposed lowpass filter.

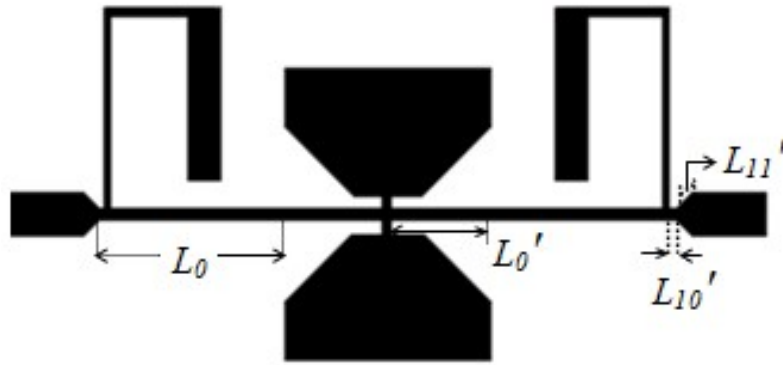


Fig. 4.24 Structural geometry of the proposed lowpass filter

The dimensions of the proposed filter are  $L_0 = 6.45$ ,  $L_0' = 3.4$ ,  $L_3 = 0.5$ ,  $L_4 = 7.1$ ,  $L_4' = 2.5$ ,  $L_5' = 2$ ,  $L_5'' = 2.3$ ,  $L_6 = 6.7$ ,  $L_7 = 2.65$ ,  $L_8 = 5.85$ ,  $L_9 = 1.1$ ,  $L_{10}' = 0.2$ ,  $L_{11}' = 0.55$ ,  $W = 1.5$ ,  $W_1 = 0.4$ ,  $W_2 = 0.3$  and  $W_3 = 0.2$  (all dimensions in mm).

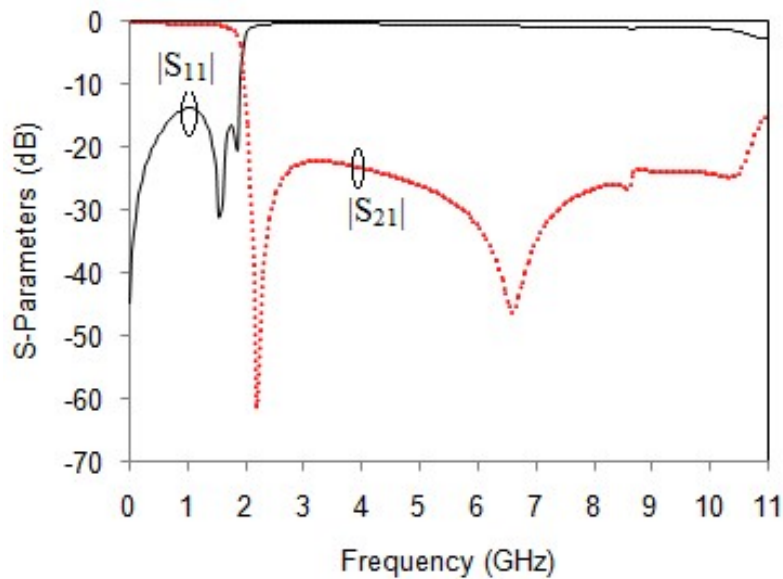
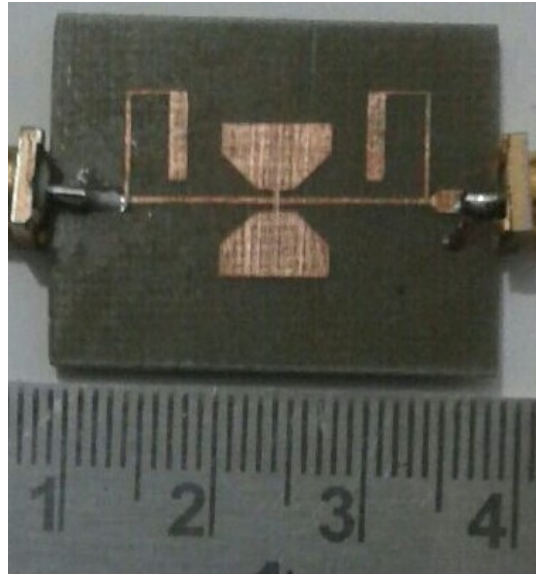


Fig. 4.25 The simulated characteristics of the Filter-2

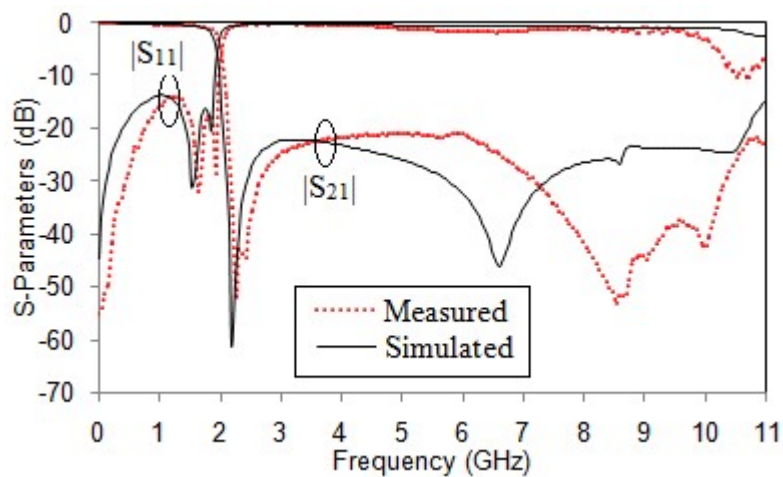
The simulated frequency response characteristic of the Filter-2 is in Fig. 4.25. The cutoff frequency of the proposed filter is 1.9 GHz. The roll off rate of the filter is 148 dB/GHz and a wide stopband bandwidth of 2.05 GHz to 10.7 GHz is achieved at 20 dB suppression level. The physical size of the filter is only 20 mm x 12.1 mm. The passband insertion loss of the filter is less than 0.6 dB from DC to 1.5 GHz and the minimum return loss is less than 13.8 dB.

#### 4.3.5 Fabrication and Measurement Results

The proposed lowpass filter is fabricated and the prototype is shown in Fig. 4.26(a). Fig. 4.26(b) shows the comparison of measured and simulated results. The measurements are carried out using R & S ZVL 13 Vector Network Analyzer and the measurement results are in good approximation with the simulated results. The measured 3 dB cutoff frequency of the proposed filter is 1.97 GHz. The physical size of the filter is 20 mm x 12.1 mm and  $\lambda_g$  is the guided wavelength at the cutoff frequency and its value is 83.68 mm. By substituting these values in Equation (2.17), the calculated NCS of the proposed filter is found to be  $0.239 \lambda_g \times 0.144 \lambda_g$ . The roll-off rate of the filter is calculated using the Equation (2.15), where  $\alpha_{\max}$  is the 40 dB attenuation point and  $\alpha_{\min}$  is the 3 dB cutoff point and the  $f_s$  and  $f_c$  are the corresponding frequencies at the 40 dB attenuation point and 3 dB cutoff point respectively. The transmission frequency at 40 dB attenuation point is 2.215 GHz and the calculated value of roll-off rate is 151 dB/GHz. The structure has a wide stopband from 2.1 GHz to 10.12 GHz at 20 dB suppression level. The minimum passband return loss is better than 14.32 dB and the insertion loss is less than 0.5 dB from dc to 1.3 GHz. The proposed lowpass filter is fabricated using low cost FR4 substrate of same specifications mentioned above.



(a)



(b)

Fig. 4.26 The fabricated lowpass filter (a) Photograph (b) Measured and simulated results

#### 4.3.6 Performance Comparison of Filter-2

The comparison between the proposed work and other related works is shown in Table 4.2. From the table it is clear that the proposed filter, Filter-2, has achieved high roll-off rate compared with all other filters fabricated using FR4 substrate. The stopband bandwidth of the filter is also wide with high suppression level.

Table 4.2 Comparison of the proposed filter with other related works

Ref	$\xi$ (dB/GHz)	Size (mm <sup>2</sup> )	SB (GHz)	SSL (dB)	Substrate
Velidi <i>et al.</i> (2011)	95	34.62 x 70.95	0.8 - 4.6	20	FR4
Karthikeyan <i>et al.</i> (2011)	46	32.6 x 26	1.45 - 6.0	30	FR4
Xu <i>et al.</i> (2017)	61.7	11 x 13.9	1.44 - 2.35	17	FR4
Sen <i>et al.</i> (2018)	36	42.29 x 13.8	2.4 - 6.0	20	FR4
Filter-2	151	20 x 12.1	2.05 - 10.7	20	FR4

$\xi$  - roll-off rate, SB - Stopband, SSL - Stopband Suppression Level

#### 4.4 HIGH SELECTIVITY AND ULTRA-WIDE STOPBAND MICROSTRIP LOWPASS FILTER (FILTER-3)

In order to block harmonic emissions that can potentially cause interference, high performance planar microstrip lowpass filters with compact size and sharp roll-off with wide stopband bandwidth are necessary in the wireless communication systems. To obtain sharp roll-off rate, symmetrical folded stepped impedance resonators are used in Filter-2. Here, modified mirrored hexagonal shaped resonators are used to obtain stopband bandwidth up to 10.7 GHz. In order to extend the stopband bandwidth of the Filter-2 so as to achieve higher order harmonics suppression, symmetrical open stubs are added to the design and named as Filter-3. Each open stub acts as a shunt capacitor to the ground plane. At high frequencies, these open stubs behave as short circuit to the ground, which causes high attenuation level in the stopband of the filter. The proposed filter is simple and of compact structure with very low insertion loss in the passband. The dimensions of the filter are optimized so as to obtain the desired performance.

#### 4.4.1 Design of Filter-3

The structure consists of Resonator-1, Resonator-2 and two identical units of open stubs. The width  $W_2$  of the high impedance stub of MMHSR used in Filter-2 is changed to  $W_1$  and thus named as Resonator-1, which is used to obtain wide stopband in the lower frequencies of stopband. Resonator-2 is two units of FSIR, loaded on the main transmission line, placed at opposite side of the Resonator-1 and it is positioned at a distance  $L_1$  from the end of the main high impedance transmission line. The high selectivity of the proposed filter is achieved using the Resonator-2. Two identical units of open stubs at both ends of the main high impedance transmission line act as the suppressing cells. These open stubs are able to suppress high frequencies in the stopband. By cascading Resonator-1, Resonator-2 and open stubs, a lowpass filter, Filter-3 is designed with sharp selectivity, ultra-wide stopband bandwidth extending from 2.04 GHz to 20 GHz at 20 dB suppression level. The LC equivalent circuit of the individual resonators is analyzed and developed the final equivalent circuit of the Filter-3 and compared with the EM simulation results.

#### 4.4.2 Analysis of Resonator-1

Resonator-1 is a symmetrical arrangement of short straight stub having a characteristic impedance  $Z_{L1}$  as 95.41  $\Omega$  loaded by a modified hexagonal patch having an impedance  $Z_{C1}$ , 24.46  $\Omega$ . This is connected to the centre of the main transmission line having an impedance  $Z_{L1}$  of 95.41  $\Omega$ . The lower value of characteristic impedance results in better approximation of lumped element capacitor and higher characteristic impedance leads to the better approximation of lumped element inductor. Fig. 4.27(a) shows the structure of Resonator-1 and the simulated frequency response is shown in Fig. 4.27(b).

Resonator-1 creates a wide stopband bandwidth from 2.89 GHz to 10.88 GHz with suppression level of 15 dB. The cutoff frequency of the filter is 1.533 GHz. The filter achieves low insertion loss and high return loss in the passband. The roll-off rate of the filter is very low and the stopband attenuation is achieved only at low frequencies of the stopband. The dimensions of Resonator-1 are  $L_{12} = 10$  mm,  $L_3 = 0.5$  mm,  $L_4 = 7.1$  mm,  $L_5 = 4.3$  mm,  $W = 1.5$  mm and  $W_1 = 0.4$  mm.

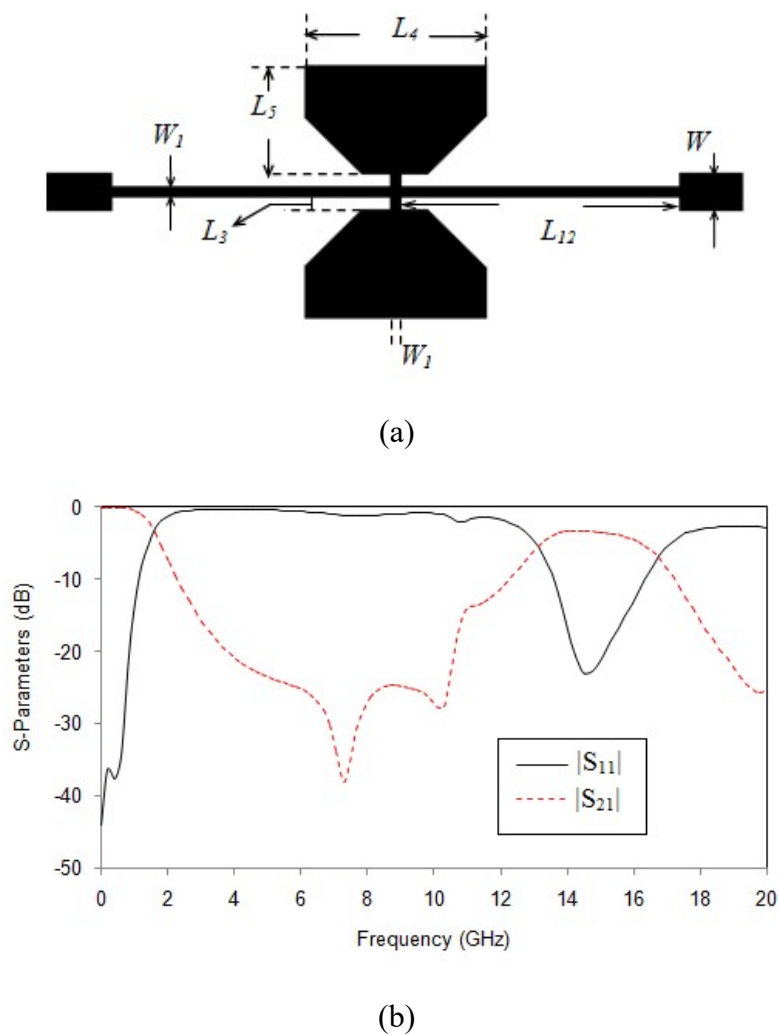


Fig. 4.27 (a) The structure of Resonator-1 (b) The frequency response

Fig. 4.28 shows the LC equivalent circuit of Resonator-1. The values of L and C are calculated using Equations (4.6)-(4.7) as,

$$L_i' = \frac{L_i * Z_{L1}}{c / \sqrt{\epsilon_{re}}} \quad (4.6)$$

$$C_1' = \frac{L_4}{Z_{C1} * c / \sqrt{\epsilon_{re}}} \quad (4.7)$$

where  $c$  is the velocity of light and  $\epsilon_{re}$  is the effective dielectric constant of FR4 substrate having relative dielectric constant 4.4 and thickness 0.8 mm. The lumped element values of Fig. 4.28 are  $L_{12}' = 6.1152$  nH,  $L_3' = 0.278$  nH and  $C_1' = 1.847$  pF. Even though the filter with Resonator-1 creates a wide stopband bandwidth up to 10.88 GHz at 15 dB suppression level, the selectivity of the filter needs improvement and to suppress the unwanted high frequency harmonics, the stopband bandwidth of the filter has to be extended.

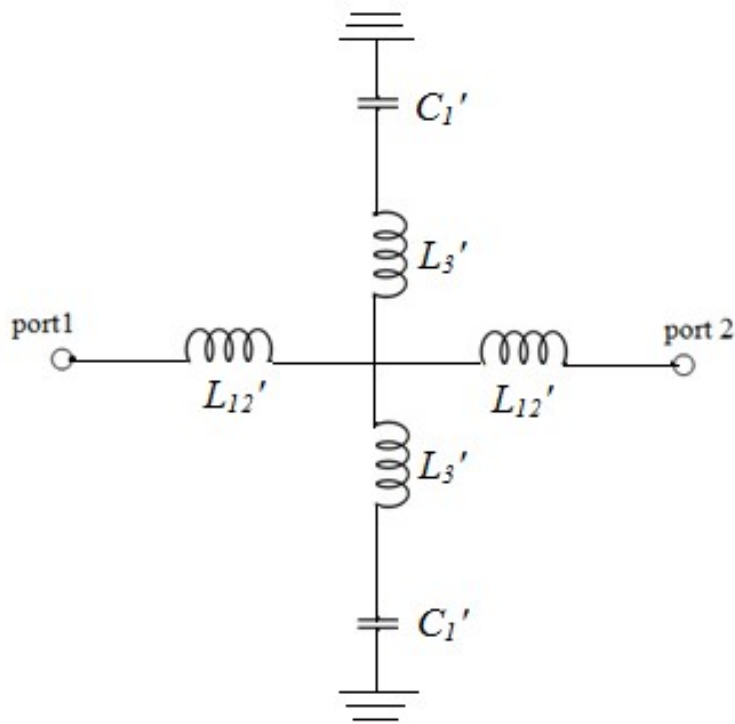


Fig. 4.28 The LC equivalent circuit of Resonator-1



### 4.4.3 Analysis of Resonator-2

To improve the selectivity of the filter, a pair of folded stepped impedance resonators (FSIR) is used in the design. Resonator-2 is the symmetrical arrangement of folded stepped impedance resonators. The folded stepped impedance resonator is a high impedance stub of  $Z_{L2}$  as  $120.5 \Omega$  loaded by a low impedance rectangular patch. In order to make the structure compact, the high impedance stub of FSIR is folded in the form of an inverted L-shaped structure. Fig. 4.29(a) shows the structure of Resonator-2 and Fig. 4.29(b) shows its simulated characteristics.

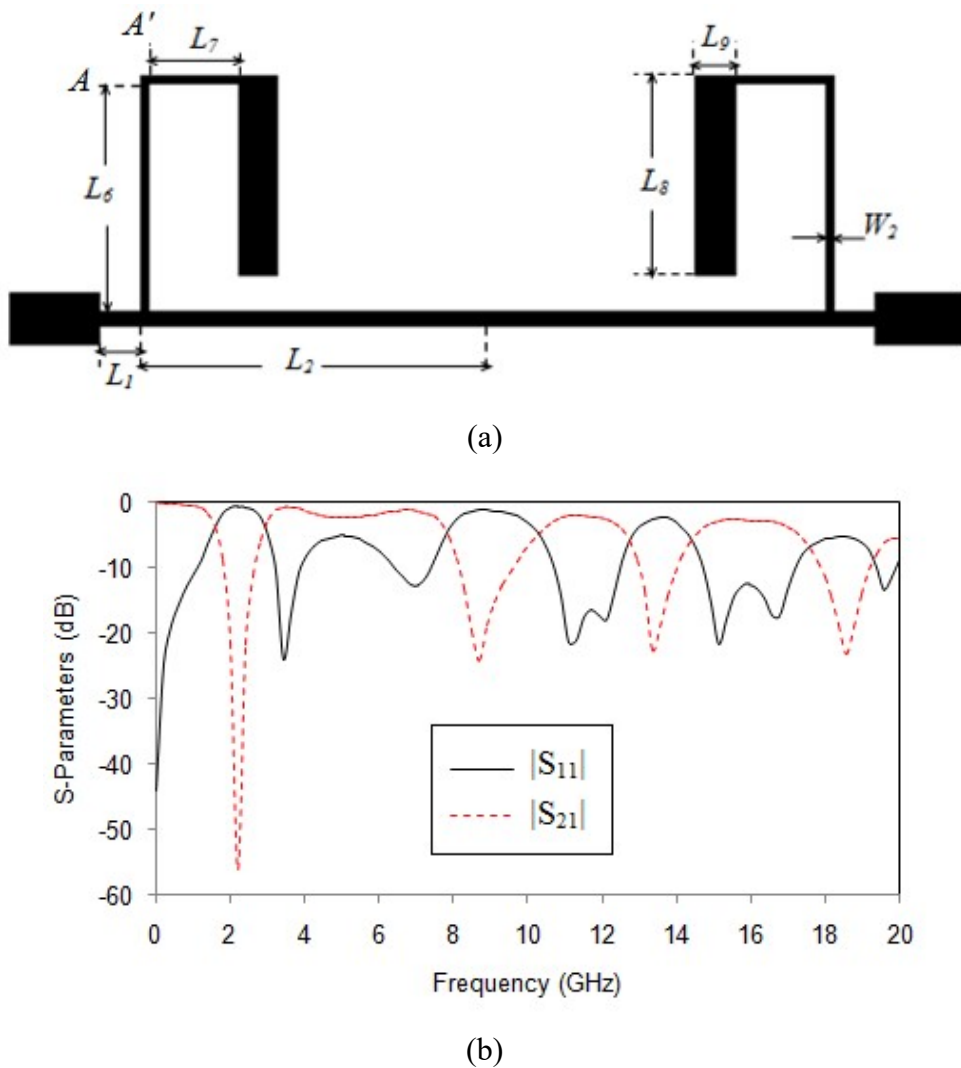


Fig. 4.29 (a) Layout of Resonator-2 (b) Frequency response

The main high impedance line having length  $L_{12}$  is divided into  $L_1$  and  $L_2$  and each FSIR is placed at a distance  $L_1$  from the end of main transmission line. The inverted L-shaped stub has a vertical and horizontal length represented as  $L_6$  and  $L_7$  respectively and the microstrip bend A-A' is the square shaped structure having dimension  $0.2 \times 0.2 \text{ mm}^2$ . From the simulated frequency response of Resonator-2, the roll-off rate of the filter is seen to be greatly improved. The cutoff frequency of the filter is 1.55 GHz. The filter creates four transmission zeros at 2.22 GHz, 8.68 GHz, 13.35 GHz and 18.57 GHz with suppression level of 55.55 dB, 24.09 dB, 22.21 dB and 23.04 dB respectively. A deep transmission zero occurs near the cutoff frequency with very low transition band from passband to stopband resulting in sharp roll-off rate of the filter. The filter offers very low insertion loss and high return loss values in the passband. Fig. 4.30 shows the LC equivalent circuit of Resonator-2. The equivalent lumped element values are calculated as,  $L_1' = 0.6672 \text{ nH}$ ,  $L_2' = 5.448 \text{ nH}$ ,  $L_4' = 4.645 \text{ nH}$ ,  $L = 0.176 \text{ nH}$ ,  $L_5' = 1.837 \text{ nH}$ ,  $C = 0.005159 \text{ pF}$  and  $C_2' = 0.6009 \text{ pF}$ .

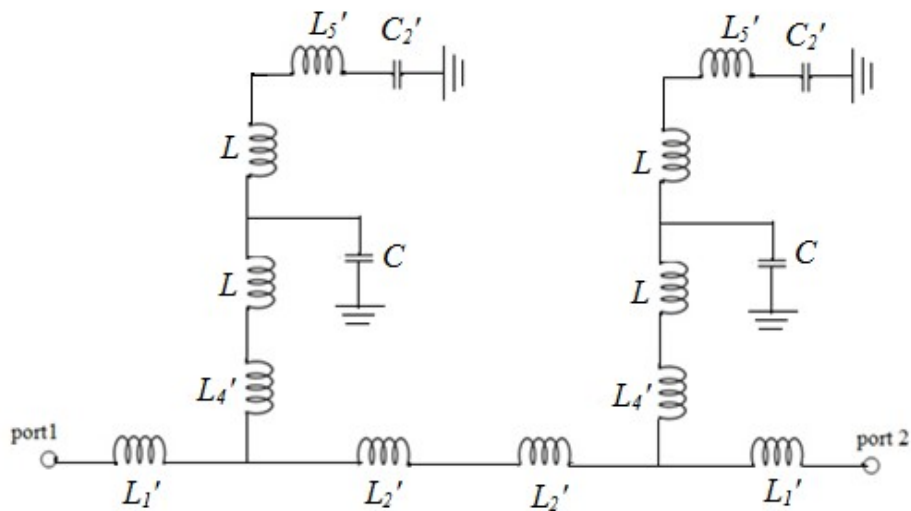


Fig. 4.30 LC equivalent circuit of Resonator-2

#### 4.4.4 Cascaded Arrangement of Resonator-1 and Resonator-2

By cascading Resonator-1 and Resonator-2, sharp roll-off is achieved for the filter. Fig. 4.31(a) shows the cascaded structure of Resonator-1 and Resonator-2 and (b) its simulated characteristics. The cutoff frequency of the combined filter is 1.85 GHz. As seen in Fig. 4.31(b), the roll-off rate of the filter is greatly improved and the stopband bandwidth is from 2.03 GHz to 10.78 GHz at 20 dB suppression level. The filter has very low insertion loss of 0.63 dB till 1.5 GHz and the minimum return loss achieved is better than 13.317 dB.

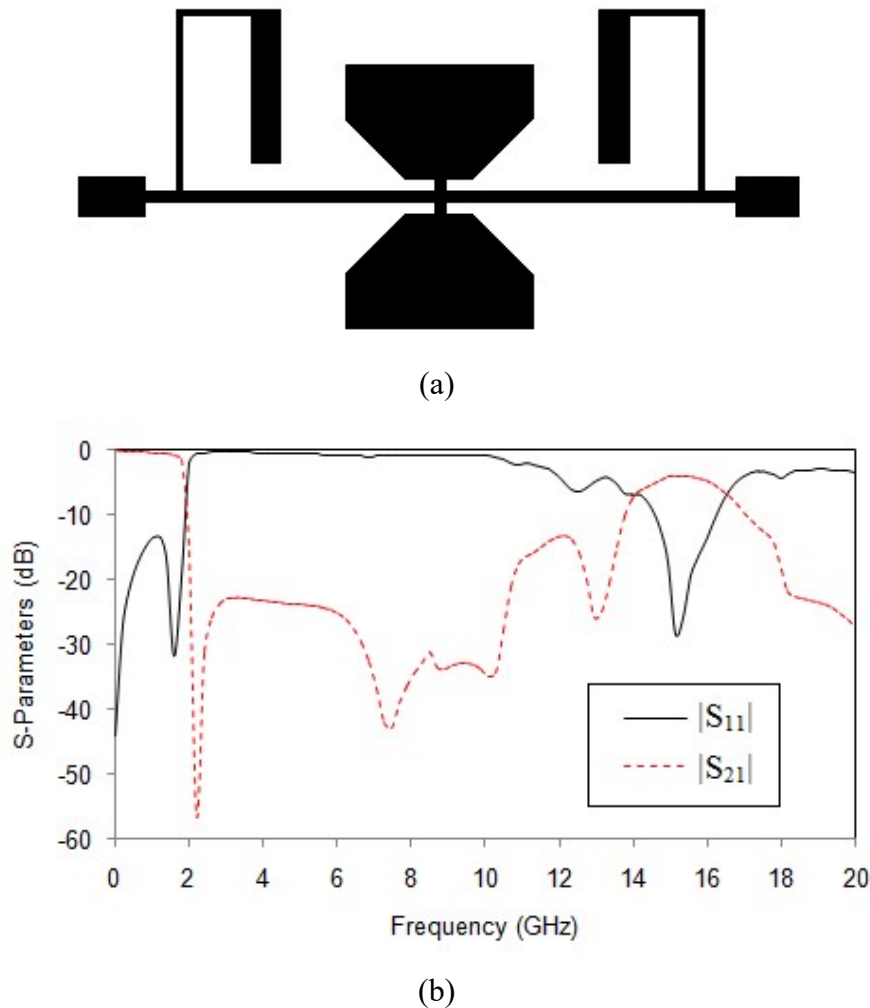


Fig. 4.31 (a) Cascaded structure of Resonator-1 and Resonator-2 (b) Frequency response

#### 4.4.5 Final Layout of Filter-3

To suppress the high frequency harmonics, the stopband bandwidth of the proposed filter has to be improved. To increase the attenuation level at high frequencies, a pair of open stubs is used in the proposed design. Each open stub of width  $L_{10}$  and length  $L_{11}$  are placed at the end of the main high impedance transmission line for the suppression of signals at high frequencies. Two microstrip lines of width  $W$  are utilized for effective impedance matching between the input and output ports. Fig. 4.32 shows the cascaded structure of Resonator-1, Resonator-2 and open stubs.

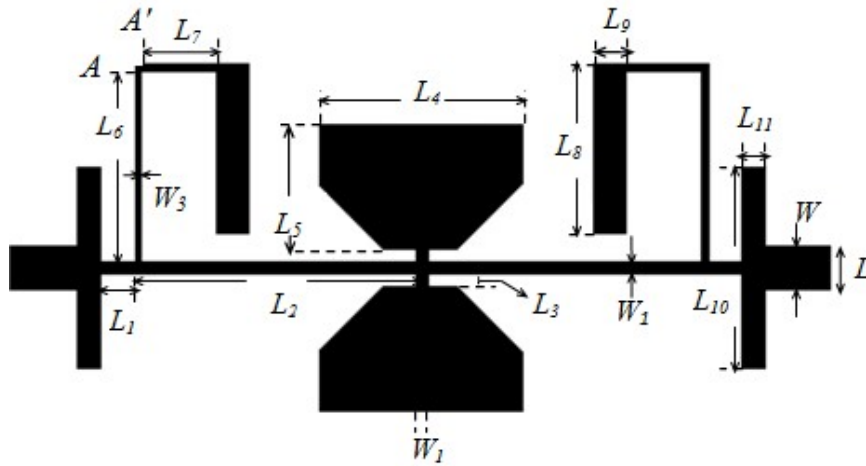


Fig. 4.32 Layout of the proposed Filter-3

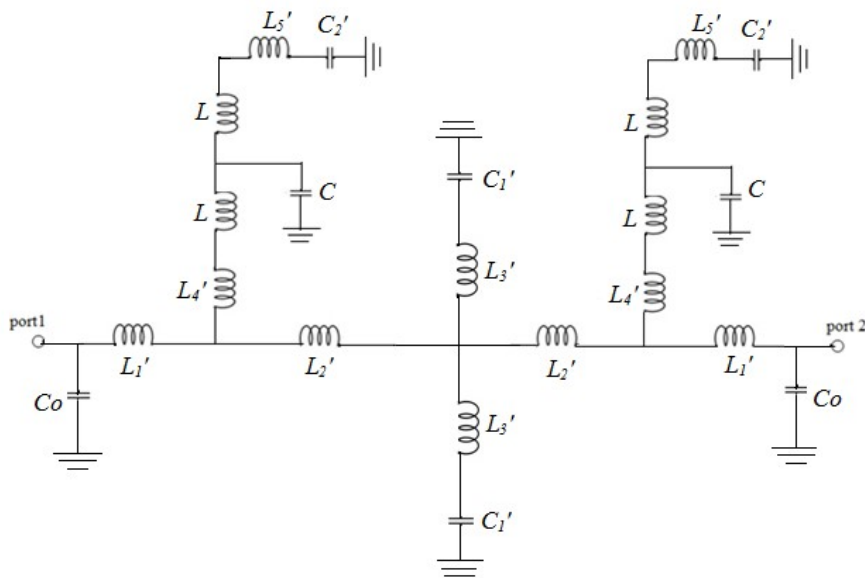
The dimensions of the proposed structure shown in Fig. 4.32 are listed in Table 4.3.

Table 4.3 The physical dimensions of the proposed lowpass filter layout

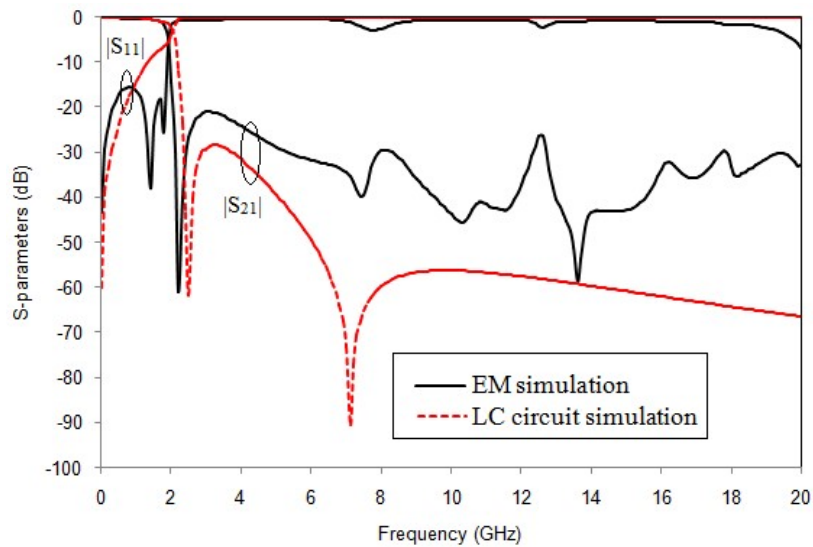
Elements	Value (mm)	Elements	Value (mm)
$L_1$	1.2	$L_8$	5.85
$L_2$	10.0	$L_9$	1.1
$L_3$	0.5	$L_{10}$	7.0
$L_4$	7.1	$L_{11}$	0.8
$L_5$	4.3	$W_1$	0.4
$L_6$	6.9	$W_2$	0.2
$L_7$	2.65	$W$	1.5

#### 4.4.6 Equivalent Circuit of Filter-3

The LC equivalent circuit of the Filter-3 is shown in Fig. 4.33(a) and the comparison of EM and LC circuit simulation results is shown in Fig. 4.33(b). The equivalent lumped element values of the proposed lowpass filter are  $L_1' = 0.6672$  nH,  $L_2' = 5.448$  nH,  $L_3' = 0.278$  nH,  $L_4' = 4.645$  nH,  $L_5' = 1.837$  nH,  $L = 0.176$  nH,  $C = 0.005159$  pF,  $C_1' = 1.847$  pF,  $C_2' = 0.6009$  pF and  $C_0 = 0.3154$  pF.



(a)



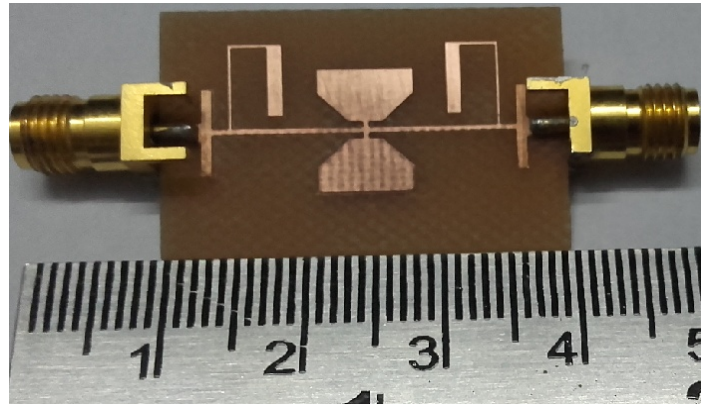
(b)

Fig. 4.33 (a) The LC equivalent circuit of Filter-3 (b) Frequency response of EM and LC circuit simulation

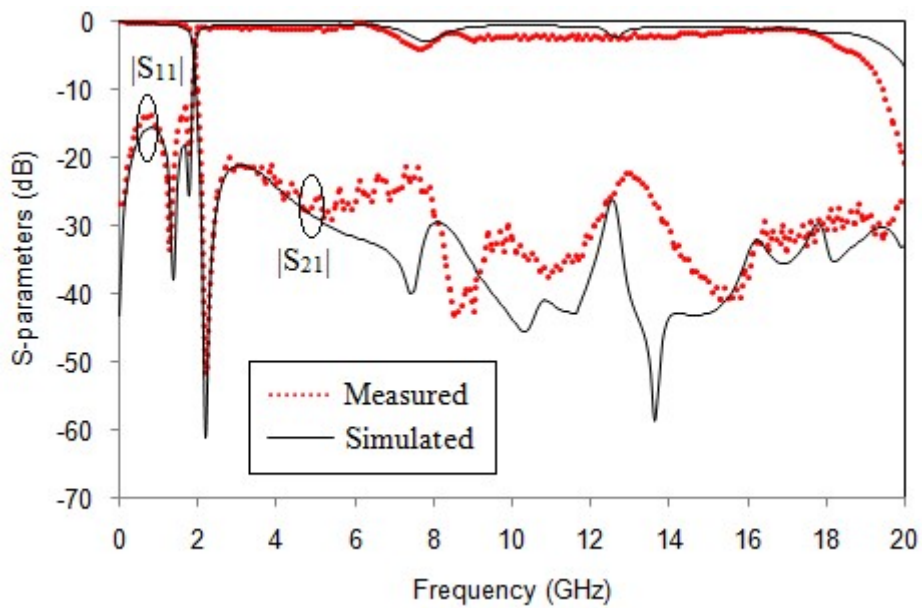
The frequency response of Filter-3 is shown in Fig. 4.33(b). The 3 dB cutoff frequency is 1.85 GHz. The passband insertion loss is better than 0.47 dB till 1.3 GHz and the minimum return loss is better than 14.9 dB. The transition from -3 dB to -40 dB is only 0.275 GHz, which indicates the sharp roll-off rate of the filter. The filter has wide stopband bandwidth from 2.04 GHz to 20 GHz with the rejection level of 20 dB. From the simulation result we can see that both results agree well only in the low frequency range of the lowpass filter. At high frequency range, the transmission characteristics of LC simulation result remains almost flat due to the non-periodic nature of electrical signals in the circuit. The simulations are performed by Electromagnetic simulation software IE3D.

#### 4.4.7 Measured and Simulated Results

The raw material used to fabricate the designed filter is FR4 substrate with  $\epsilon_r = 4.4$ , thickness,  $h = 0.8$  mm and loss tangent 0.02. The measurement is carried out using the Vector Network Analyzer R & S ZVB 20. Fig. 4.34 shows the fabricated prototype and the comparison between the simulated and measured results of Filter-3, which are in good agreement to each other. The measured cutoff frequency of Filter-3 is 1.912 GHz. The frequency at 40 dB attenuation point is 2.161 GHz and thus the calculated value of roll-off rate is 148.6 dB/GHz. The proposed filter has wide stopband bandwidth from 2.09 GHz to 20 GHz at 20 dB suppression level and thus the relative stopband bandwidth of the filter calculated using the Equation (2.16) is 162.15 % at 20 dB rejection level. Wide stopband bandwidth of the proposed filter is utilized to suppress up to 10<sup>th</sup> order harmonics. The measured passband insertion loss of the Filter-3 is very low and its value is less than 0.2 dB in the entire passband. The passband return loss is better than 12.5 dB in the entire band. The physical size of the proposed filter is 24 mm x 12.1 mm, thereby the normalized circuit size of the filter is only  $0.0391 \lambda_g^2$ , where the guided wavelength at cutoff frequency,  $\lambda_g = 86.232$  mm.



(a)



(b)

Fig. 4.34 (a) The fabricated prototype of Filter-3 (b) Comparison between the measured and simulated results

The group delay of the Filter-3 in the passband region is shown in Fig. 4.35. The group delay variation, only in the passband region of the filter characteristics is considered here. If the group delay variation in the passband region is large, more losses occur. ie. More swings occur in the signal amplitude and current swinging occurring between the resonators is also more. In the proposed filter, the group delay is almost flat in the lower frequencies of the passband and it increases near the cutoff frequency of the filter.

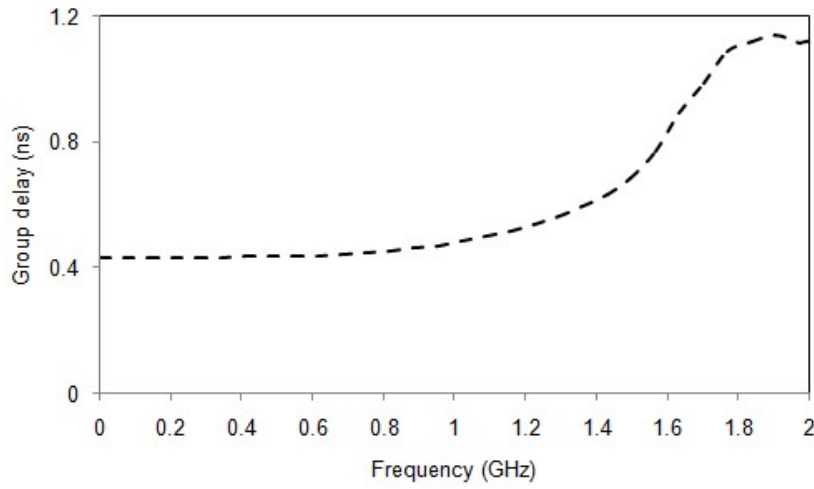


Fig. 4.35 The measured group delay of Filter-3

The group delay in 63 % of the passband region is shown in Fig. 4.36. The group delay is almost flat in this region and the maximum group delay variation is less than 0.1 ns only.

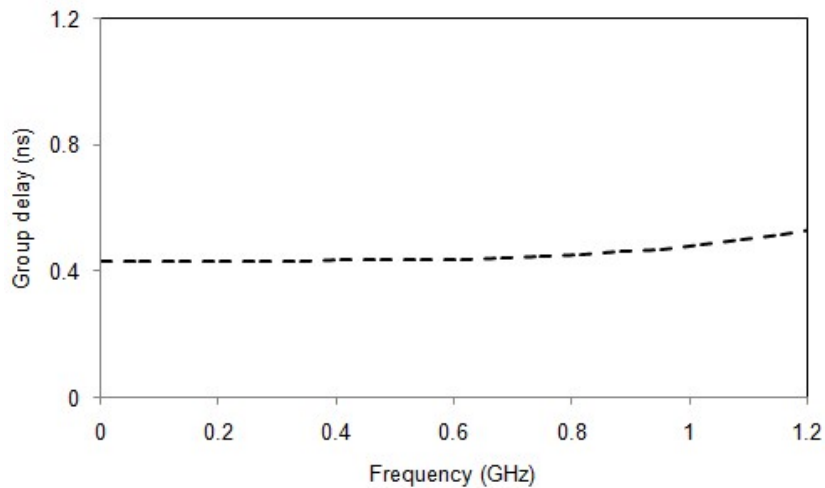


Fig. 4.36 The measured group delay of Filter-3 for 63 % of the passband

The VSWR of Filter-3 in the passband region is represented in Fig. 4.37. Its value is almost equal to one, which represents that only negligible loss occurs in the passband due to radiation.



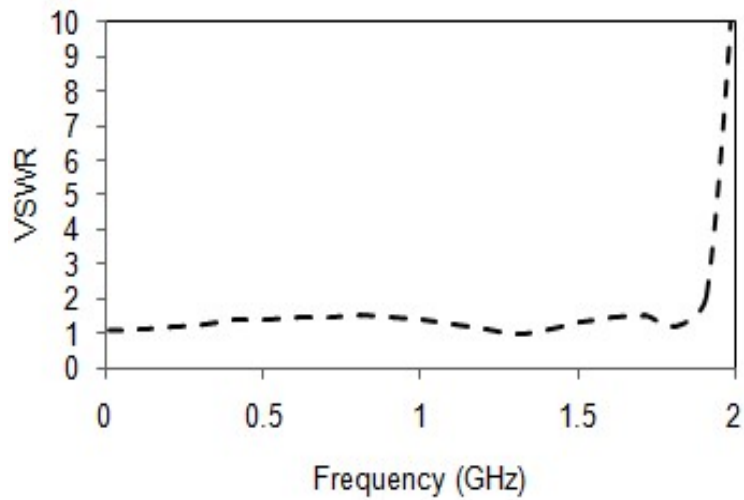


Fig. 4.37 The measured VSWR of Filter-3

The sharpness factor (SF) of the filter is calculated as in Verma and Kumar (2011),

$$\text{sharpness factor} = \frac{f_0}{f_c} \quad (4.8)$$

where  $f_c$  is the 3 dB cutoff frequency of the proposed filter and  $f_0$  is the attenuation pole frequency and its value is 2.22 GHz. The sharpness factor of Filter-3 is 1.16, which indicates that the Filter-3 has sharp selectivity with narrow transition from passband to stopband.

#### 4.4.8 Performance Comparison of Filter-3

In Table 4.4 the Filter-3 is compared to the recent works mentioned in the literature making use of same FR4 substrate. It is seen that the proposed structure has high roll-off rate with very low insertion loss in the passband and wide stopband bandwidth among all the compared works. By making use of this filter with high RSB, rejection of spurious passband frequencies up to 10<sup>th</sup> order is possible.

Table 4.4 The comparison of the Filter-3 with other works from the literature

Ref	$\xi$ (dB/GHz)	IL-PB (dB)	SB (GHz)	SSL (dB)	RSB (%)	Substrate, $h$ (mm)
Wang and Hsu, (2018)	44.73	0.25	1.25 - 12	20	162.27	FR4, 0.8
Vala <i>et al.</i> (2017)	15.45	0.8	3.5 - 10	14	96.2	FR4, 1.2
Xu and Duan, (2017)	61.7	0.4	1.44 - 12.4	17	158.2	FR4, 0.6
Raphika <i>et al.</i> (2016)	60	0.7	2.65 - 13.6	31	134	FR4, 0.8
Kumar and Parihar, (2016)	100	0.85	2.62 - 20	20	153.6	FR4, 1.6
Karthikeyan <i>et al.</i> (2011)	46	0.66	1.45 - 6.0	30	122	FR4, 1.6
Validi and Sanyal, (2010)	117.3	0.3	0.99 - 4.63	20	129.5	FR4, 1.6
Filter-3	148.6	0.2	2.09 - 20	20	162.15	FR4, 0.8

$\xi$  - Roll-off rate, IL-PB - Insertion loss-Passband, SB - Stopband, SSL - Stopband Suppression Level, RSB - Relative Stopband Bandwidth.

#### 4.5 CHAPTER SUMMARY

This chapter presents the design technique of three microstrip lowpass filters, Filter-1, Filter-2 and filter-3. All the designed filters have sharp selectivity, wide stopband and compact size and thus suitable for various wireless communication applications. The performance characteristics of the proposed filters are compared in Table 4.5.

Table 4.5 Comparing the performance characteristics of the proposed filters

Filter	$f_c$ GHz	$\xi$ dB/GHz	Size mm <sup>2</sup>	NCS $\lambda_g^2$	RSB %	SL	IL-PB dB	harmonic suppression
Filter-1	3.9	79.5	16.8 x 7.55	0.071	131.2	18	0.5	5 <sup>th</sup> order
Filter-2	1.97	151	20 x 12.1	0.034	131.2	20	0.5	5 <sup>th</sup> order
Filter-3	1.91	148.6	24 x 12.1	0.039	162.15	20	0.2	10 <sup>th</sup> order

In Filter-1, a lowpass filter is designed using interdigital structure and coupled inductive stub resonator to obtain sharp roll-off and wide stopband characteristics. The cutoff frequency of the filter is 3.9 GHz. The physical size of the filter is only 16.8 mm x 7.55 mm. The passband insertion loss is very low and its value is only 0.5 dB. The filter is used to suppress up to 5<sup>th</sup> order harmonics. Due to wide passband up to 3.9 GHz, the proposed filter can be used widely in applications such as Bluetooth, WLAN, RFID, Wi-Max, UMTS etc.

A sharp roll-off lowpass filter designed using folded stepped impedance resonator and mirrored modified hexagonal shaped resonator is presented in Filter-2. The cutoff frequency of the filter is 1.97 GHz. The roll-off rate of the proposed filter is 151 dB/GHz with wide stopband and thus up to 5<sup>th</sup> order harmonic rejection is possible. With these desirable features the proposed filter is suitable for modern communication system especially in GSM and PCS applications.

A lowpass filter with sharp roll-off and wide stopband up to 10th harmonic suppression is presented in Filter-3. The LC equivalent circuit of the proposed filter is developed and validated with EM simulation result and found both the results are in good agreement. As seen in the Table 4.5, the filter is very compact with its circuit size of only  $0.039 \lambda_g^2$ . The insertion loss of the filter in the entire passband frequency range is only 0.2 dB. These advantages make the filter suitable for various wireless communication applications, especially in the L-band applications.

All the three filters have improved characteristics than the structures described in chapter-3. Lowpass filters with wide stopband and sharp roll-off based on dual plane structure is presented in chapter-5. To design high performance lowpass filters while maintaining compact size, defected ground structure technique is proposed.

## CHAPTER 5

### COMPACT MICROSTRIP LOWPASS FILTERS USING DEFECTED GROUND STRUCTURES

#### 5.1 INTRODUCTION

Lowpass filters are vital components in microwave and wireless communication devices. Compactness, unity voltage standing wave ratio, low insertion loss, high degree of harmonic rejection and good selectivity are the most desirable parameters in the design of lowpass filters. Recently, defected ground structures (DGSs), which are realized by etching a few defects in the ground plane, have been a subject of increasing interest in analyzing the microstrip line characteristics and the size, shape and orientation of the slot have significant influence on the performance of the lowpass filter (Park *et al.*, 1999; Ahn *et al.*, 2001; Abdel-Rahman *et al.*, 2004). Different simple and complex shaped DGS geometries used so far include dumbbell (Kim *et al.*, 2000), U and V slot (Woo *et al.*, 2006), split ring resonator (SRR) (Xiao *et al.*, 2015), quasi yagi slot (Boutejdar and Ellatif, 2016) etc.

Cascades of inductively coupled fractal defected ground resonators are utilized in Kurgan and Kitlinski (2009) to design a microstrip lowpass filter with high stopband suppression level. To improve the roll-off rate of the filter, the DGS cells combined with stepped impedance resonators are presented by Xi *et al.* (2010); Xiao *et al.*(2015). A high performance lowpass filter suitable for microwave mixer application introduced by Belbachir (2016), has good characteristics such as sharp selectivity and wide stopband. Wang and Lin (2011) designed a meandered slot resonator to develop a compact lowpass filter with a uniform transmission line. A

lowpass filter designed with stepped impedance type resonators and circular shaped slots to obtain sharp selectivity and high harmonic rejection is introduced by Kumar and Parihar, 2018.

The design of DGS based Bessel and elliptic lowpass filter is reported in Kumar and Verma (2016). Flat group delay and good selectivity make the filter useful for wide band communication applications. The stopband bandwidth of the lowpass filter is improved using a multilayer structure with open stubs and DGS by Mohra (2011). However, the filter suffers from large physical size and wider transition band from passband to stopband.

Miniaturized size lowpass filters fabricated using half circle DGS and compensated capacitors (Boutejdar, 2017), combination of compact microstrip resonant cell and uniquely shaped DGS (Yang *et al.*, 2012), open complementary split ring resonator (OCSRR) and tapered dumbbell DGS (Karthikeyan and Kshetrimayum, 2015) provide good selectivity and wide stopband bandwidth.

However, most of these filters suffer from one or more drawbacks like large physical size, low roll-off rate, low impedance matching and limited harmonic rejection. The primary aim of the proposed lowpass filter designs are to satisfy the desired characteristics such as wide stopband bandwidth, sharp roll-off rate, good impedance matching in both passband and stopband, high harmonic suppression with less complexity and physical size.

The performance characteristics of basic lowpass filter, designed using stepped impedance resonators and open circuited stubs (SIR-UIS) improved using defected ground structures are discussed in the first section (Filter-I). The designed filter has stopband bandwidth up to 9.874 GHz at 20 dB suppression level. The frequency response characteristic of the basic filter is improved using H-shaped DGS resonators etched on the surface of the metallic ground plane. The performance of the basic filter improved using 2-H shaped DGS etched from the ground plane is illustrated first and it is named as Filter-1. The stopband bandwidth up to 20 GHz at 18 dB suppression level is achieved in Filter-1 with high passband return loss of 21 dB and its normalized circuit size is  $0.0338 \lambda g^2$ . The characteristics of Filter-1 is again improved by maintaining same circuit size with low insertion loss and high return loss of 27 dB in the passband by etching 3-H shaped DGS on the ground plane of the basic filter as explained in the next section and named as Filter-2. These DGS resonators improved the selectivity of the filter together with a wide stopband up to 20 GHz at 20 dB rejection level. Due to the defects etched from the ground plane of the basic filter, harmonic suppression is improved from 5<sup>th</sup> order to 10<sup>th</sup> order. The proposed DGS filters have better performance than most of the previously mentioned DGS lowpass filters, as far as the frequency response and size reduction are concerned.

A microstrip lowpass filter designed with good selectivity and ultra wide stopband bandwidth at a rejection level of 20 dB is presented in Filter-II. The sharp roll-off is achieved using one pair of stair shaped resonators and wide stopband with high suppression level is obtained using an open stub, defected ground structures and suppressing cells. The experimental results show that the roll-off rate of the proposed filter is 88.5 dB/GHz with a wide stopband from 2.342 GHz to 20 GHz at 20 dB suppression level. The cutoff frequency of the filter is 2.072 GHz and the return loss is better than 24.5 dB throughout the passband.

The lowpass filters designed using novel DGS are presented in this chapter. The H-shaped and modified dumbbell shaped DGS are designed to develop lowpass filter with cutoff frequency near 2 GHz with low insertion loss, wide stopband with high suppression level. The designed filters are able to suppress higher order harmonics up to 9<sup>th</sup> and 10<sup>th</sup> order and thus the unwanted spurious signals are effectively eliminated and hence any possibility of interference with nearby circuits. Both filters are designed using FR4 substrate with relative dielectric constant 4.4, thickness  $h = 0.8$  mm and dielectric loss tangent 0.02

## **5.2 IMPROVED FREQUENCY RESPONSE OF MICROSTRIP LOWPASS FILTER USING DEFECTED GROUND STRUCTURES (FILTER-I)**

The performance characteristics of the basic lowpass filter improved using defected ground structures are presented.

### **5.2.1 Basic Microstrip Lowpass Filter Design**

Conventional lowpass filter design using SIR-UIS has the capability to generate transmission zeros at their resonant frequencies. To obtain a wider stopband, more elements have to be added which will naturally increase the physical size of the filter. Here, a basic microstrip lowpass filter is designed using SIR-UIS to achieve the desired characteristics.

Before going into the basic filter design, a primary resonator is analyzed. A series resonant branch having a high impedance stub and a low impedance patch, modelled as inductor and capacitor respectively, is connected in shunt with a high impedance main transmission line as shown in Fig. 5.1(a). The dimensions are  $l_1' = 6.4$  mm,  $l_2' = 4$  mm,  $l_3' = 3.6$  mm,  $w' = 0.2$  mm and  $w_l' = 3.6$  mm. The high impedance main

transmission line of length  $l_1'$  is represented as  $Z_{L1}$  and the impedances of the series resonant branch are  $Z_{L2}$  and  $Z_{C1}$  respectively. The width,  $w_o'$  of the microstrip line is chosen to be 1.5 mm which corresponds to the characteristic impedance of 50  $\Omega$ . All simulations are carried out using full wave EM simulator IE3D. The  $LC$  equivalent circuit of the primary resonator is shown in Fig. 5.1(b). The values of  $L$  and  $C$  are calculated using equations in Hong and Lancaster (2001).  $L_1' = 4.437$  nH,  $L_2' = 3.273$  nH and  $C_1' = 0.9108$  pF. The ABCD parameters of the symmetrical two port T-network (Pozar *et al.* 1998), shown in Fig. 5.1(a) are,

$$A = D = 1 + \frac{Z_{L1}}{Z_{L2} + Z_{C1}} \quad (5.1)$$

$$B = 2(Z_{L1}) + \frac{Z_{L1}^2}{Z_{L2} + Z_{C1}} \quad (5.2)$$

$$C = \frac{1}{Z_{L2} + Z_{C1}} \quad (5.3)$$

Substituting the impedance of the inductors and capacitor,

$$A = D = 1 + \frac{\omega^2 L_1' C_1'}{\omega^2 L_2' C_1' - 1} \quad (5.4)$$

$$B = \frac{2j\omega L_1' - 2j\omega^3 L_1' L_2' C_1' - j\omega^3 (L_1')^2 C_1'}{1 - \omega^2 L_2' C_1'} \quad (5.5)$$

$$C = \frac{j\omega C_1'}{1 - \omega^2 L_2' C_1'} \quad (5.6)$$



The S-parameters of the primary resonator (Pozar *et al.* 1998) are,

$$S_{11} = \frac{A + \frac{B}{Z_0} - CZ_0 - D}{A + \frac{B}{Z_0} + CZ_0 + D} \quad S_{21} = \frac{2}{A + \frac{B}{Z_0} + CZ_0 + D} \quad (5.7)$$

Substituting (5.4)-(5.6) in Equation (5.7),

$$S_{11} = \frac{2j\omega L_1'(1 - \omega^2 L_2' C_1') - j\omega C_1'(\omega^2 (L_1')^2 + Z_0^2)}{2Z_0(1 - \omega^2 L_2' C_1' - \omega^2 L_1' C_1') + 2j\omega L_1'(1 - \omega^2 L_2' C_1') - j\omega C_1'(\omega^2 (L_1')^2 - Z_0^2)} \quad (5.8)$$

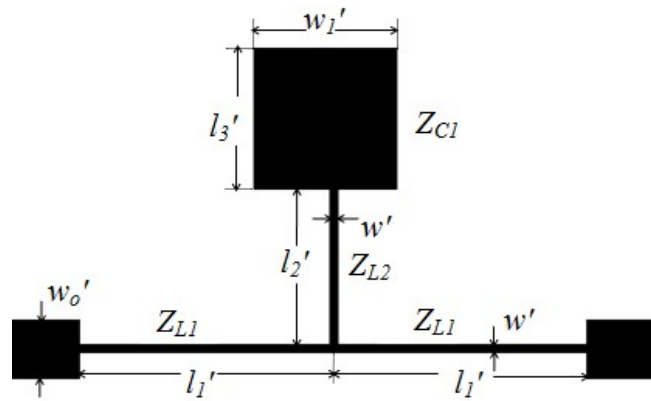
$$S_{21} = \frac{2Z_0(1 - \omega^2 L_2' C_1')}{2Z_0(1 - \omega^2 L_2' C_1' - \omega^2 L_1' C_1') + 2j\omega L_1'(1 - \omega^2 L_2' C_1') - j\omega C_1'(\omega^2 (L_1')^2 - Z_0^2)} \quad (5.9)$$

From Equations (5.8)-(5.9) it is clear that the transmission and reflection characteristics are controlled by varying the values of  $L_1'$ ,  $L_2'$  and  $C_1'$ . By setting  $|S_{21}| = 0$ , a single finite frequency attenuation pole occurs at  $f_0$  and is given in Equation (5.10).

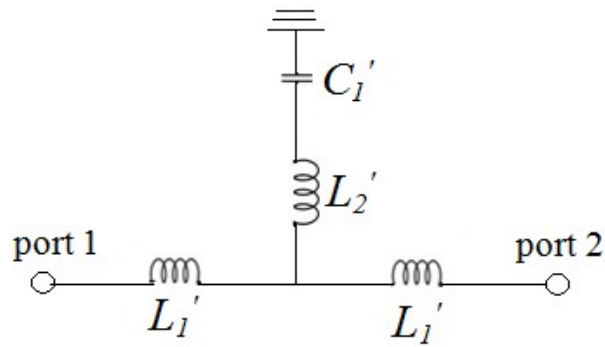
$$f_0 = \frac{1}{2\pi\sqrt{L_2' C_1'}} \quad (5.10)$$

The calculated value of resonant frequency,  $f_0$  is 2.914 GHz.

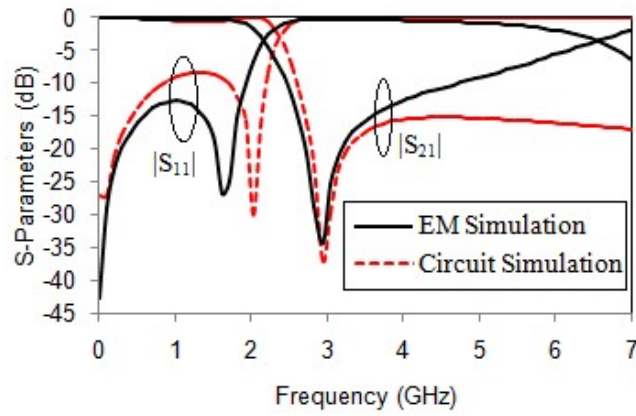
Fig. 5.1(c) shows the simulated frequency response of the EM and LC circuit of the primary resonator and both results are in good agreement with theory. The cutoff frequency of the microstrip implementation of the structure is 2.13 GHz and the single transmission zero occurs at 2.916 GHz.



(a)



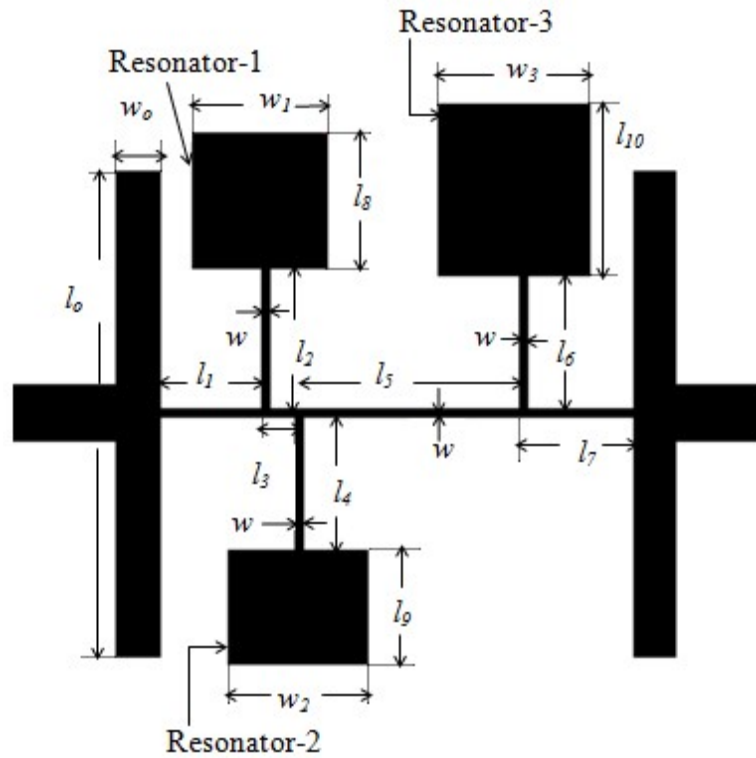
(b)



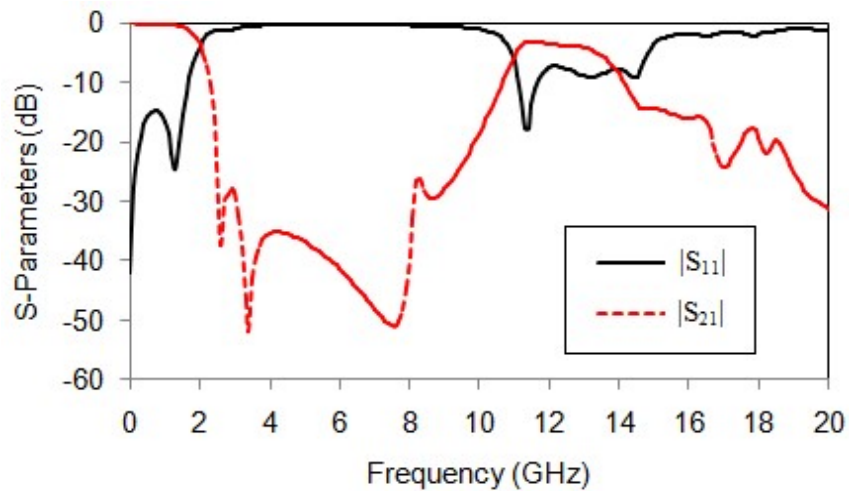
(c)

Fig. 5.1 The primary resonator (a) Structure (b) LC equivalent circuit (c) Frequency response characteristics

By using the same idea, the primary resonator is extended to the basic microstrip lowpass filter design using SIR-UIS to obtain a wide stopband up to 9.874 GHz at 20 dB suppression level as shown in Fig. 5.2(a).



(a)



(b)

Fig. 5.2 (a) Layout of the basic lowpass filter (b) Simulated frequency response

The structure consists of two uniformly shaped low impedance stubs and three stepped impedance resonators, Resonator-1, Resonator-2 and Resonator-3 loaded on the high impedance main transmission line. The uniformly shaped low impedance stubs can be modelled as a capacitor, having width and length  $l_0$  and  $w_0$  respectively.

The three stepped impedance resonators have a high impedance line loaded by low impedance square and rectangular patches as represented in the Fig. 5.2(a). The dimensions of the layout are  $w = 0.2$ ,  $w_1 = 3.6$ ,  $w_2 = 3.7$ ,  $w_3 = 4.05$ ,  $w_o = 1.15$ ,  $l_1 = 2.8$ ,  $l_2 = 3.8$ ,  $l_3 = 0.9$ ,  $l_4 = 3.6$ ,  $l_5 = 6.05$ ,  $l_6 = 3.6$ ,  $l_7 = 3.05$ ,  $l_8 = 3.6$ ,  $l_9 = 3.0$ ,  $l_{10} = 4.55$  and  $l_o = 13.0$  (all in mm). The frequency response of the basic lowpass filter is shown in Fig. 5.2(b). The cutoff frequency of the filter is 1.95 GHz and the frequency at 20 dB suppression level is 2.464 GHz. The selectivity of the filter is 33.36 dB/GHz. The insertion loss is less than 0.35 dB up to 1.1 GHz of the passband and the return loss in the passband is better than 14.7 dB. The stopband bandwidth at 20 dB suppression level is from 2.464 GHz to 9.874 GHz and the relative stopband bandwidth calculated as a percentage (the ratio of stopband bandwidth to stopband centre frequency) is 120.1%. The physical size of the filter is only 15.1 mm x 14.95 mm.

The main drawback of this filter is the presence of out of band spurious frequencies. To improve the performance, these components have to be suppressed, without increasing the physical size. DGS is the appropriate choice due to its attractive features such as like simplicity, wide and deeper stopband characteristics.

To improve the performance of the basic lowpass filter without compromising the size, the defected ground structures are used to design the proposed filter, Filter-1. It is the same SIR-UIS structure with two symmetrical H-shaped slots etched on the ground plane. The size and shape of DGS is selected such that it should resonate at a higher frequency so as to extend the stopband bandwidth of the basic structure.

### 5.2.2 Characteristics of H-Shaped DGS

A one pole microstrip lowpass filter with an H-shaped slot etched on the metallic ground plane is analyzed and its structure is shown in Fig. 5.3(a). In order to analyze the frequency characteristics of the DGS section, the structure is simulated with IE3D software. The dimensions of the DGS unit shown in Fig. 5.3(a) are  $a = 7.1$  mm,  $b = 1.6$  mm,  $c = 1.8$  mm,  $d = 2.2$  mm and  $w_o' = 1.5$  mm. The EM simulated transmission characteristics of Fig. 5.3(a) is in Fig. 5.3(b), and this unit DGS section can provide the desired cutoff and attenuation pole frequency values. The cutoff frequency of the filter is 10.26 GHz and the transmission zero occurs at 14.85 GHz. As seen in the Fig. 5.3(b), wide stopband bandwidth is achieved by using the H-shaped DGS. The equivalent circuit of the H-shaped DGS can be modeled as a parallel LC circuit as shown in Fig. 5.3(c). Depending on the size and shape of the etched lattice, an attenuation pole can be generated by the combination of inductance and capacitance elements. By employing the proposed etched lattice, the effective permittivity and thereby the reactance of the microstrip line is increased. The values of  $L$  and  $C$  can be derived by using the EM simulation result. The reactance value of the proposed DGS section can be expressed using Equation (5.11) (Ahn *et al.* 2001) as,

$$X_{LC} = \frac{1}{\omega_o C_H \left( \frac{\omega_o}{\omega} - \frac{\omega}{\omega_o} \right)} \quad (5.11)$$

where  $\omega_o$  is the angular resonance frequency at 14.85 GHz. The series inductance  $X_L$  of Butterworth lowpass filter can be derived as,

$$X_L = \omega L = \frac{\omega}{\omega_c} (Z_0 g_1) \quad (5.12)$$

where  $\omega_c$  is the angular 3 dB cutoff frequency,  $Z_0$  is the source impedance and  $g_1$  is the prototype element value of Butterworth lowpass filter. The circuit parameters of Fig. 5.3(c) are calculated by equating the reactance values of the DGS structure and one pole Butterworth lowpass filter at the cutoff frequency and thus the capacitance  $C_H$  and the inductance  $L_H$  can be calculated by using Equations (5.13)-(5.15).

$$\frac{1}{\omega_o C_H \left( \frac{\omega_o - \omega_c}{\omega_c \omega_o} \right)} = Z_0 g_1 \quad (5.13)$$

$$C_H = \frac{\omega_c}{Z_0 g_1 (\omega_o^2 - \omega_c^2)} \quad (5.14)$$

$$L_H = \frac{1}{4\pi^2 f_o^2 C_H} \quad (5.15)$$

The discontinuity of the DGS structure in the ground plane results in large fringing fields and it can be represented by the capacitance  $C_p$ . The capacitance  $C_p$  changes the value of characteristic impedance and its value is calculated as described by Park *et al.* (2002). The calculated values of equivalent lumped elements of Fig. 5.3(c) are  $L_H = 0.8089$  nH,  $C_H = 0.142$  pF, and  $C_p = 0.28$  pF. The simulated EM and LC equivalent circuit results are shown in Fig. 5.3(b). The current distribution of one pole H-shaped DGS at the resonant frequency is shown in Fig. 5.3(d). The transmitted energy is reflected back to the source and thus the transmission zero occurs at the resonant frequency of 14.85 GHz.

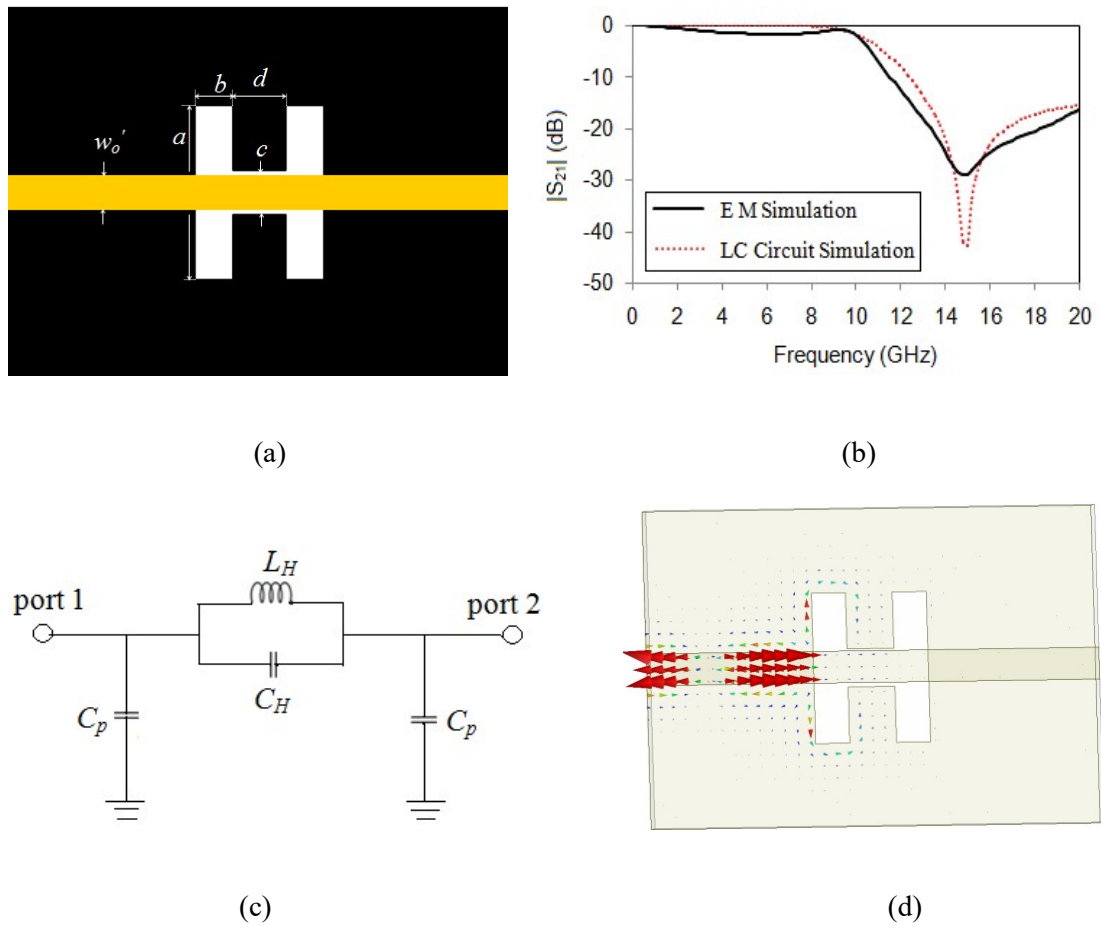
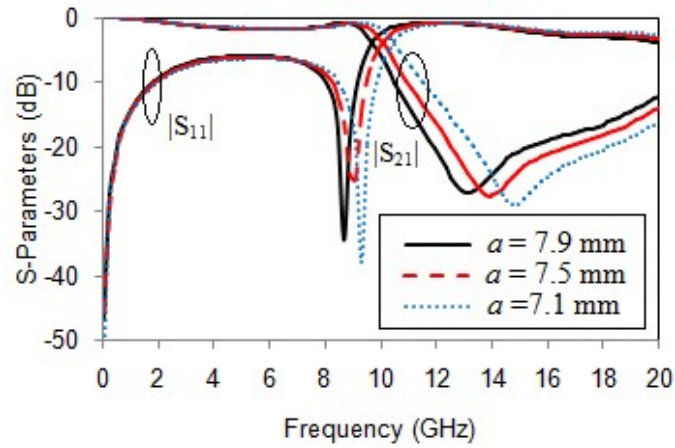
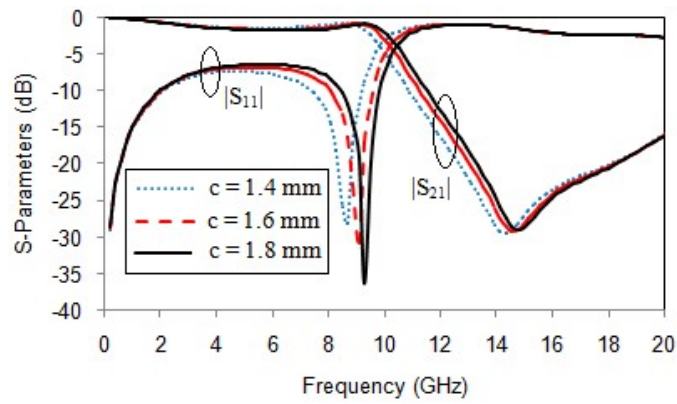


Fig. 5.3 One pole H-shaped DGS lowpass filter (a) Schematic Diagram (b) Transmission response of EM and LC circuit simulation (c) LC equivalent circuit (d) Current distribution at resonant frequency

The increase in parameter  $a$  causes a corresponding increase in effective inductance of the etched structure, which results in lowering the cutoff frequency as depicted in Fig. 5.4(a). For the selected value of  $a = 7.1$  mm, the suppression level is found to increase. As the value of  $c$  increases from 1.4 mm to 1.8 mm the effective capacitance of the etched lattice decreases and the resonance frequency is found to increase as shown in Fig. 5.4(b).



(a)



(b)

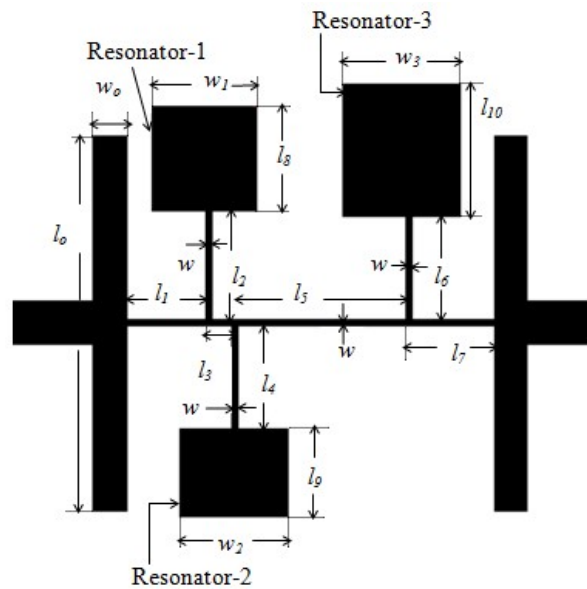
Fig. 5.4 Frequency response of H-shaped DGS (a) For various values of  $a$  (b) For various values of  $c$

### 5.2.3 Compact Stepped Impedance Filter with Wide Stopband (Filter-1)

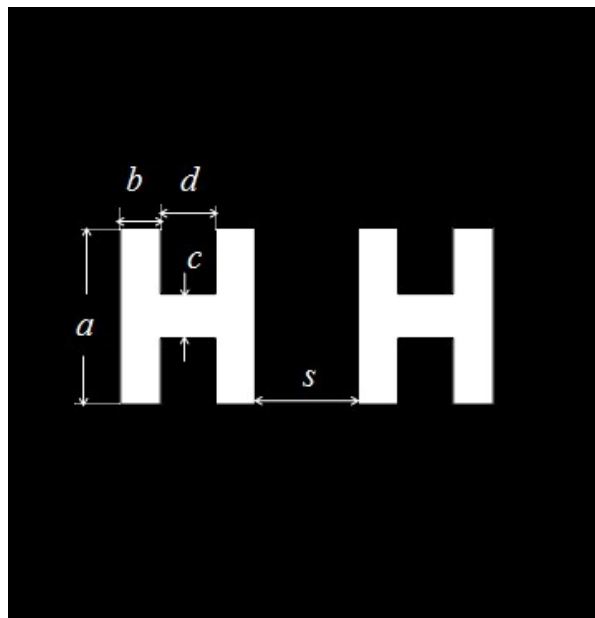
Fig. 5.5(a) and 5.5(b) show the top and bottom view of the proposed lowpass filter, named as Filter-1, which consists of two symmetric H-shaped DGSs etched on the ground metallic plane of the basic lowpass filter structure. Two H-shaped units in the ground plane are separated by the spacing,  $s = 4.1$  mm. The stopband bandwidth of the filter is improved by the use of etched units in the ground plane without increasing the physical size. The introduced H-shaped DGS units allow good selectivity and wide stopband bandwidth up to 20 GHz at 18 dB suppression level. The simulated 3 dB cutoff frequency of Filter-1 is 1.945 GHz and wide stopband bandwidth from 2.315



GHz to 20 GHz with rejection level of 18 dB is achieved. The selectivity of the filter is 42.71 dB/GHz at 20 dB suppression level. The insertion loss is lower than 0.3 dB up to 1.1 GHz of the passband and the return loss is higher than 30.4 dB.



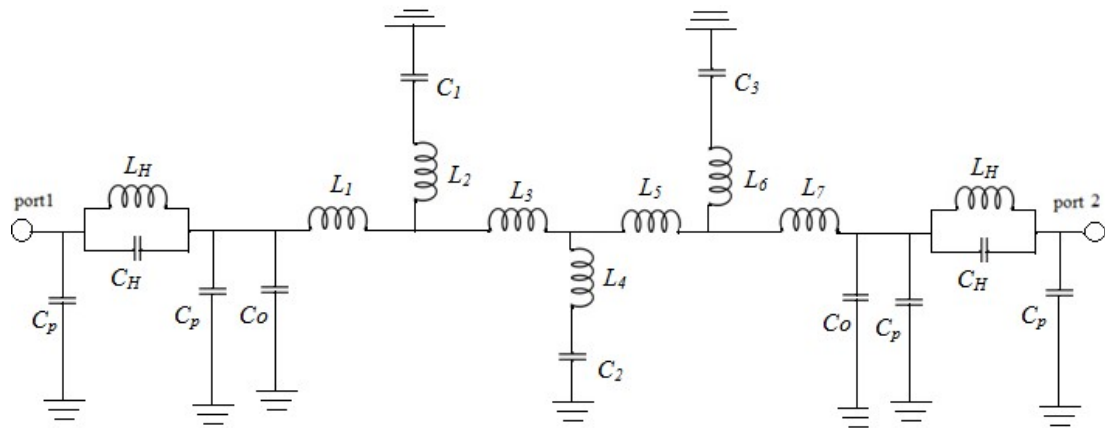
(a)



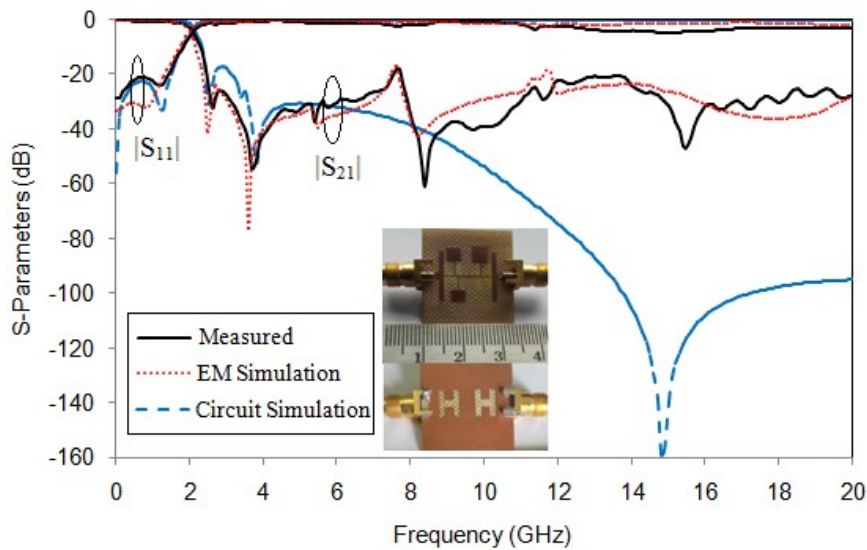
(b)

Fig. 5.5 Layout of the proposed Filter-1 (a) Top view (b) Bottom view

The LC equivalent circuit of Filter-1 is depicted in Fig. 5.6(a). The lumped element values of the basic lowpass filter are calculated using equations of Hong and Lancaster, (2001). The values  $L_1, L_3, L_5$  and  $L_7$  represent the inductance of the main high impedance transmission line of length  $l_1, l_3, l_5$  and  $l_7$  respectively.  $L_2, L_4$  and  $L_6$  are the inductance values and  $C_1, C_2$  and  $C_3$  are the capacitance values of Resonators 1, 2 and 3 respectively and  $C_0$  is the capacitance value of the uniform impedance stub. Component values of equivalent circuit are  $L_1 = 1.941$  nH,  $L_2 = 2.634$  nH,  $L_3 = 0.6239$  nH,  $L_4 = 2.495$  nH,  $L_5 = 4.194$  nH,  $L_6 = 3.4959$  nH,  $L_7 = 2.114$  nH,  $L_H = 0.8089$  nH,  $C_1 = 0.8108$  pF,  $C_2 = 0.69048$  pF,  $C_3 = 1.1275$  pF,  $C_0 = 0.793$  pF,  $C_H = 0.142$  pF, and  $C_p = 0.28$  pF. The proposed Filter-1 is fabricated on an FR4 substrate with same specifications as mentioned earlier. The physical size of the filter is 15.1mm x 14.95 mm. The measurements are carried out on an R & S ZVB 20 Vector Network Analyzer. The measured insertion loss is found to be lower than 0.59 dB up to 1.1 GHz and return loss in the passband is higher than 21 dB. The cutoff frequency of the filter is 2.02 GHz and the selectivity obtained is 37.117 dB/GHz at 20 dB suppression level. The stopband bandwidth of Filter-1 at 18 dB suppression level is from 2.45 GHz to 20 GHz. The relative stopband bandwidth of the filter is 156.3% and the normalized circuit size is  $0.0338 \lambda_g^2$  where  $\lambda_g = 81.61$  mm. Fig. 5.6(b) shows the comparison between measured, EM and LC circuit simulation of Filter-1. It is clear that there is a good agreement between the transmission characteristics of all the results up to 9 GHz and after that the stopband rejection level of LC circuit simulation result increases rapidly. In the LC equivalent circuit, due to the effect of H-shaped slots in the ground plane, the stopband suppression level increases and the values of L and C are the only dependent parameters for the analysis of transmission characteristics whereas in EM simulation and measurement results, substrate losses also play a vital role.



(a)



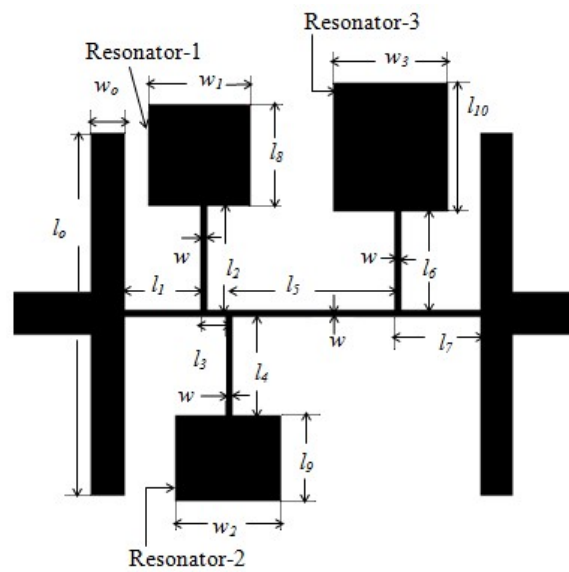
(b)

Fig. 5.6 (a) LC equivalent circuit of Filter-1 (b) Frequency response of measured, EM and LC circuit simulation of Filter-1

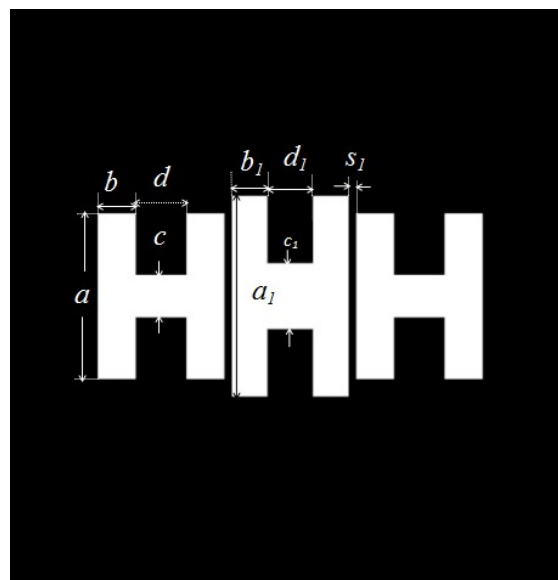
### 5.2.4 Improved Lowpass Filter Design (Filter-2)

To improve the characteristics of Filter-1, one more H-shaped slot is added to the ground plane and the coupling between the DGS resonators is increased. The new filter, Filter-2 is designed using the same FR4 substrate, which is used in Filter-1. Filter-2 offers improved passband and stopband characteristics as compared to that of Filter-1 without changing its normalized circuit size. Fig. 5.7(a) and 5.7(b) show the

top and bottom view of Filter-2. Due to the addition of one more H-shaped slot of different dimension, the effective permittivity and coupling between DGS resonators are increased. The proposed Filter-2 is designed, fabricated and measured. The dimensions of the newly added H-shaped slot are  $a_1 = 8.6$  mm,  $b_1 = 1.5$  mm,  $c_1 = 2.8$  mm,  $d_1 = 2$  mm and  $s_1 = 0.35$  mm.



(a)



(b)

Fig. 5.7 The structure of Filter-2 (a) Top view (b) Bottom view

### 5.2.5 Field Distribution of Filter-2

The detailed analysis of the field distribution has been done to study the performance of Filter-2. The surface current distribution is simulated at two different frequencies, in the passband of 1 GHz and at the stopband of 11 GHz. At 1 GHz, almost all RF power is transferred from input to output and around the DGS which indicates that the filter is in the passband state as shown in Fig. 5.8(a). In the stopband frequency of 11 GHz, energy is concentrated only at the input and around the first DGS resonator. The total RF energy is blocked around the input as shown in Fig. 5.8(b), which represents that the filter is in the stopband state.

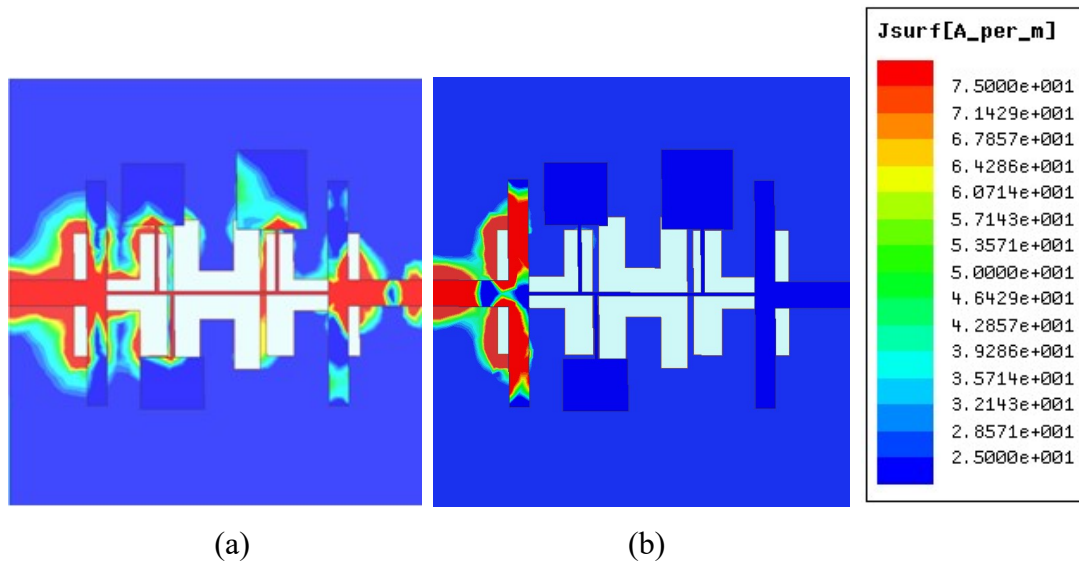


Fig. 5.8 EM field distribution of Filter-2 (a) In the passband frequency of 1 GHz (b) In the stopband frequency of 11 GHz

### 5.2.6 Simulation and Measurement Results of Filter-2

The passband and stopband characteristics of the basic lowpass filter are improved using the DGSs. Due to increased etched area in the ground plane, the simulated 3 dB cutoff frequency of the proposed Filter-2 is reduced to 1.88 GHz. The frequency at 40 dB suppression level is 2.535 GHz and the selectivity of the filter is 56.48 dB/GHz. The designed Filter-2 has low insertion loss and high return loss values in the

passband together with a wide stopband up to 20 GHz at 21 dB suppression level. Fig. 5.9(a) shows the top and bottom photographic view of the fabricated Filter-2. The comparison between measured and simulated results which are in good agreement is shown in Fig. 5.9(b).

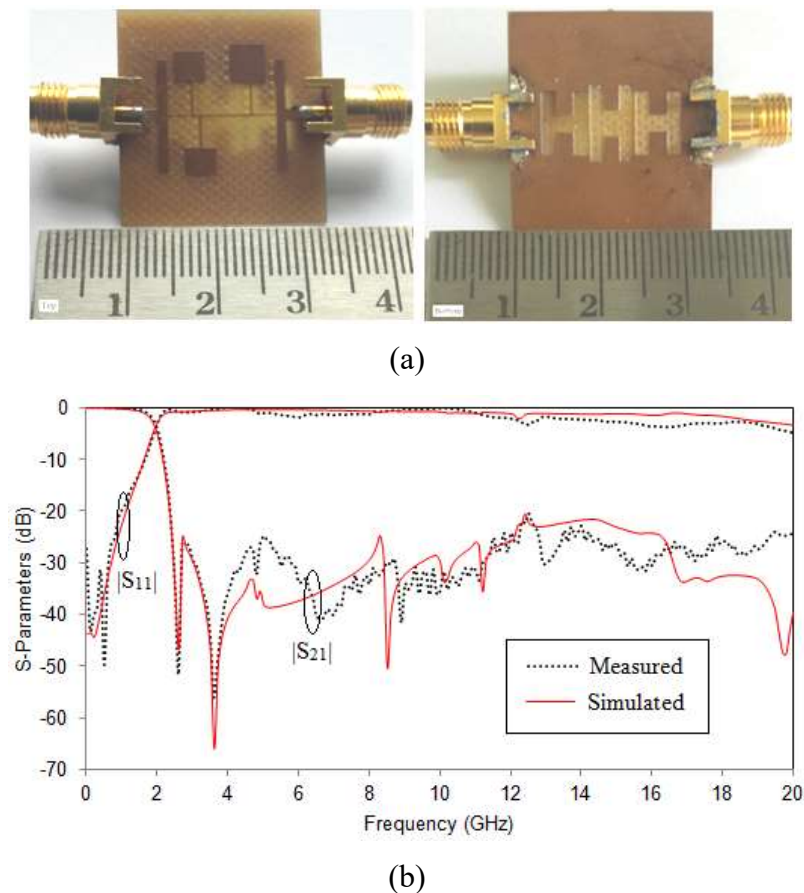


Fig.5.9 (a) Top and bottom view of the Filter-2 (b) Measured and simulated frequency response

The measured 3 dB cutoff frequency of the proposed filter is 1.935 GHz. The transition from passband to stopband frequency at 3 dB and 40 dB is 1.935 GHz to 2.536 GHz and therefore the selectivity of the proposed filter is 61.56 dB/GHz. The insertion loss in the passband is less than 0.22 dB up to 1.1 GHz and high return loss of 27 dB is achieved in Filter-2. The stopband bandwidth is from 2.37 GHz to 20 GHz at 20 dB suppression level and the relative stopband bandwidth achieved is 157.6%. The RSB is

increased from 120.1% of the basic lowpass filter to 157.6% by the use of DGSs and suppression up to 10th harmonics is achieved in Filter-2. The group delay of Filter-2 is shown in Fig. 5.10. The group delay is almost flat till 1.6 GHz of the passband frequency and the peak to peak group delay variation is only 0.4 ns.

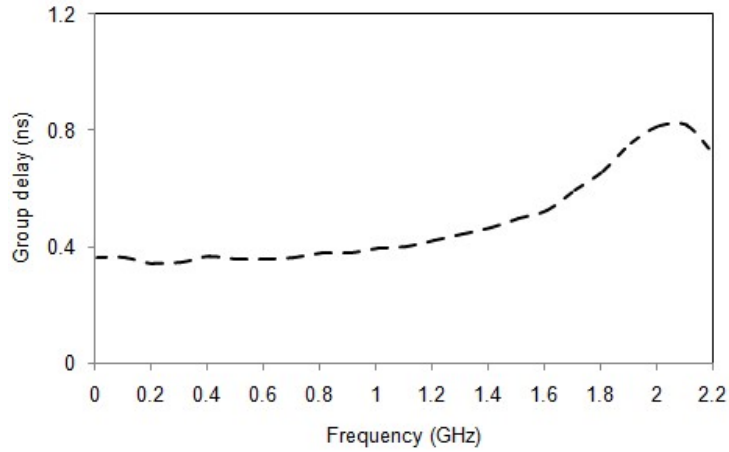


Fig. 5.10 The measured group delay of Filter-2

The voltage standing wave ratio (VSWR) of the fabricated Filter-2 is shown in Fig. 5.11. The SWR value of the proposed filter is almost equal to one in the entire passband and increases near the cutoff frequency. The value of SWR = 1 implies good impedance matching between the i/p-o/p ports ie. the load is perfectly matched.

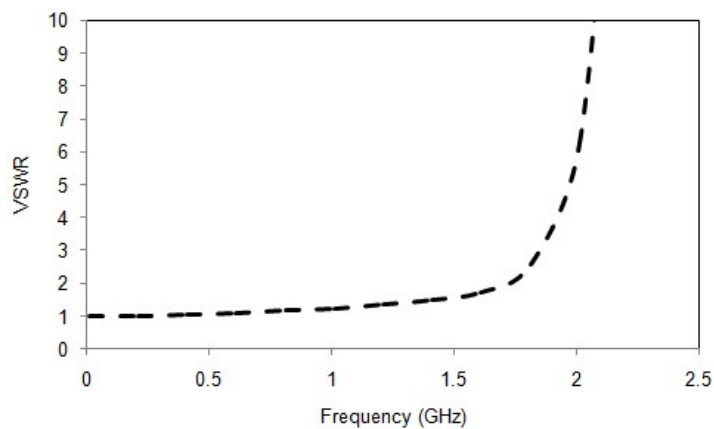


Fig. 5.11 The measured VSWR of Filter-2

### 5.2.7 Performance Comparison of Filter-I

Table 5.1 shows the performance characteristics of the proposed filters, Filter-1 and Filter-2 are compared with other related works. It is seen that the designed filters have good characteristics such as high return loss in the passband and wide stopband bandwidth at high suppression level. As compared to other works in the related fields, the proposed filters have compact circuit size, high value of RSB with higher order harmonic rejection.

Table 5.1 Performance comparison of the proposed work with related works

Ref	CF (GHz)	PB-RL (dB)	SB (GHz @dB)	RSB %	Harmonic suppression	NCS
Boutejdar <i>et al.</i> (2016)	1.8	16	2.8 - 10 @ 20	112.5	5 <sup>th</sup> order	$0.1575 \lambda_g^2$
Xi <i>et al.</i> (2010)	2.5	18.5	2.58 - 7.5 @ 20	97.6	3 <sup>rd</sup> order	$0.0756 \lambda_{\text{re}}^2$
Xiao <i>et al.</i> (2015)	3.37	10	3.46 - 9.2 @ 20	90.6	2 <sup>nd</sup> order	$0.036 \lambda_g^2$
Zhang <i>et al.</i> (2016)	3.38	12.5	4.07 - 15 @20	114.6	4 <sup>th</sup> order	$0.2016 \lambda_{\text{re}}^2$
Kumar and Parihar (2018)	1.95	12	2.0 - 16 @ 15	155.5	8 <sup>th</sup> order	$0.0336 \lambda_g^2$
Wang <i>et al.</i> (2011)	2.5	11	2.9 - 12 @ 20	122.1	4 <sup>th</sup> order	$0.0646 \lambda_{\text{re}}^2$
Filter-1	2.02	21	2.45 - 20 @ 18	156.3	9 <sup>th</sup> order	$0.0338 \lambda_g^2$
Filter-2	1.935	27	2.37 - 20 @ 20	157.6	10 <sup>th</sup> order	$0.0338 \lambda_{\text{re}}^2$

CF - 3 dB Cutoff frequency, PB-RL - Passband return loss, SB - Stopband, RSB - Relative stopband bandwidth, NCS - Normalized circuit size.



### **5.3 COMPACT MULTILAYER MICROSTRIP LOWPASS FILTER WITH WIDE STOPBAND (FILTER-II)**

High frequency harmonics are generated at different stages of digital switching circuits and cause severe interference with other devices and systems. It is necessary to block all unwanted frequency components and permit only the required band of signals. Lowpass filters with high performance and compact size are in great demand nowadays. It finds wide applications in modern wireless communication systems.

A microstrip lowpass filter with good selectivity and ultra wide stopband bandwidth at a rejection level of 20 dB is presented in Filter-II. The sharp roll-off is achieved using one pair of stair shaped resonators (SSRs) and wide stopband with high suppression level is obtained using an open stub (OS), modified dumbbell shaped DGS and suppressing cells. The experimental results show that the roll-off rate of the proposed filter is 88.5 dB/GHz with a wide stopband from 2.342 GHz to 20 GHz at 20 dB suppression level. The cutoff frequency of the filter is 2.072 GHz and the return loss is better than 24.5 dB throughout the passband. The proposed filter is compact in size and its normalized circuit size is only  $0.04719 \lambda_g^2$ , where  $\lambda_g$  is the guided wavelength at cutoff frequency and its value is 80.32 mm. The experimental results are in par with the simulated results.

The first step of the Filter-II is the design of main resonator.

#### **5.3.1 The Design of Main Resonator**

A lowpass filter with sharp roll-off rate can be designed by using filter structures of infinite attenuation obtained at finite frequency components (Hong and Lancaster, 2001). The design of the main resonator starts with the analysis of a 3-pole lumped

element circuit of a basic T-shaped resonator as shown in Fig. 5.12(a). The filter is designed with the cutoff frequency,  $f_c$  of 1.9 GHz and the input/output ports having the characteristic impedance  $Z_0$  of 50  $\Omega$ .

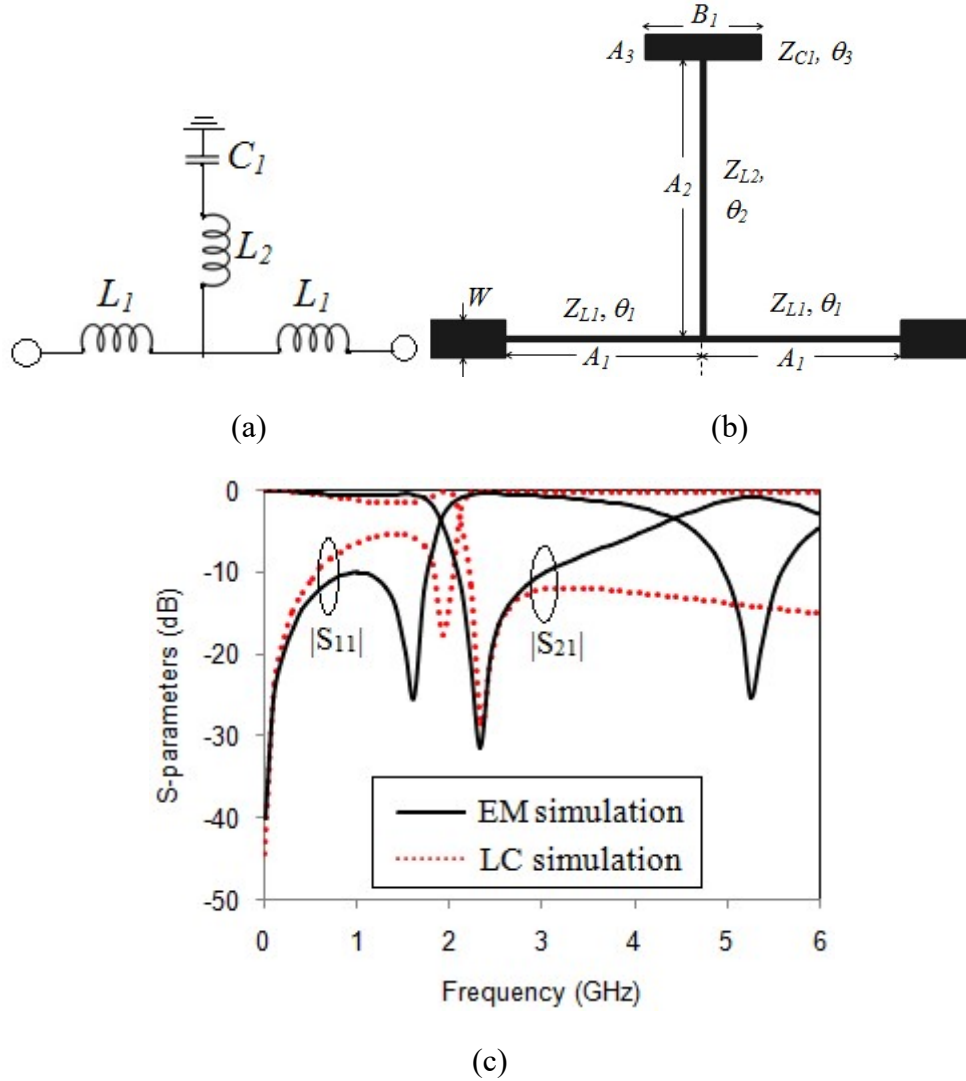


Fig. 5.12 The T-shaped resonator (a) LC equivalent circuit (b) Layout (c) The comparison of EM and LC circuit simulation

The L and C values scaled at  $f_c$  and  $Z_0$  are calculated using the Equations (5.16)-(5.17) as,

$$L_i = \frac{Z_0 g_{Li}}{\omega_c} \quad (5.16)$$

$$C_i = \frac{g_{Ci}}{\omega_c Z_0} \quad (5.17)$$

where  $g_{Li}$  and  $g_{Ci}$  are the element values of 3-pole lowpass filter having Chebyshev response. The values of the T-shaped resonator are,  $L_1 = 5.44$  nH,  $L_2 = 9.62$  nH, and  $C_1 = 0.474$  pF.

The corresponding microstrip implimentation of the T-shaped filter developed on an FR4 substrate of dielectric constant 4.4, thickness 0.8 mm and dielectric loss tangent 0.02 is shown in Fig. 5.12(b). The inductors are realized with the characteristic impedance,  $Z_{Li}$  as  $120.5 \Omega$  and the capacitor, with the impedance,  $Z_{Ci}$  of  $23.3 \Omega$ . The physical length of the inductor and capacitor are realized by using the equations,

$$l_{Li} = \frac{\lambda_{gL}(f_c)}{2\pi} \sin^{-1} \left( \frac{\omega_c L_i}{Z_{Li}} \right) \quad (5.18)$$

$$l_{Ci} = \frac{\lambda_{gc}(f_c)}{2\pi} \sin^{-1} (\omega_c Z_{ci} C_i) \quad (5.19)$$

where  $\lambda_{gL}(f_c)$  and  $\lambda_{gc}(f_c)$  are the guided wavelengths of the inductor and capacitor at the cutoff frequency respectively. The calculated values of corresponding microstrip implimentation is  $A_1 = 7.85$  mm,  $A_2 = 11$  mm,  $A_3 = 1$  mm and  $B_1 = 4.6$  mm.

From the ABCD parameters, S-parameters of the T-shaped resonator are calculated and derived the equation for the resonant frequency  $f_0$  as in Equation (5.20) as,

$$f_0 = \frac{1}{2\pi \sqrt{L_2 C_1}} \quad (5.20)$$

The calculated value of the resonant frequency  $f_0$  is 2.35 GHz. Thus the resonant and cutoff frequency of the filter varies with the values of  $L_2$  and  $C_1$ . Fig. 5.12(c) shows the comparison of the EM and LC simulated frequency response characteristics of the T-shaped lowpass filter. As seen in the Figure, the simulated resonant frequency occurs at 2.32 GHz, which is in good agreement with the calculated value of the resonant frequency.

The microstrip implementation of inductance  $L_2$  is  $A_2$ . Fig. 5.13 shows the simulated frequency response of the T-shaped filter for different values of  $A_2$ . From the Figure it is noted that as the values of  $A_2$  increases from 11 mm to 12.2 mm in steps of 0.6 mm, the cutoff frequency and resonant frequency move towards the lower frequency end and the roll-off rate of the filter also increases. Thus to improve the roll-off rate and to reduce the physical size of the filter, the high impedance stub of the resonator is modified as stair shaped and this symmetric modified T-shaped structure and its frequency response characteristics is shown in the Fig. 5.14. As seen in the Figure, the roll-off rate of the filter is greatly improved together with the generation of two transmission zeros at 2.4 GHz and 8.69 GHz respectively. The dimensions of modified T-shaped resonator are:  $A_1' = 4.4$ ,  $A_1'' = 3.45$ ,  $A_2' = 12.2$ ,  $A_3' = 4.5$  and  $B_1' = 1$  (all dimensions in mm).

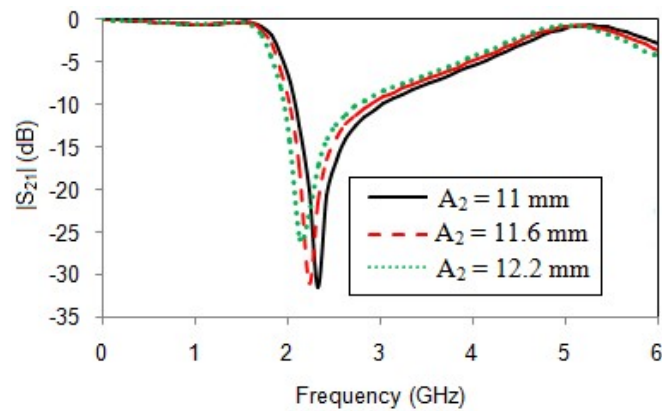


Fig. 5.13  $S_{21}$  characteristics of the filter for different values of  $A_2$

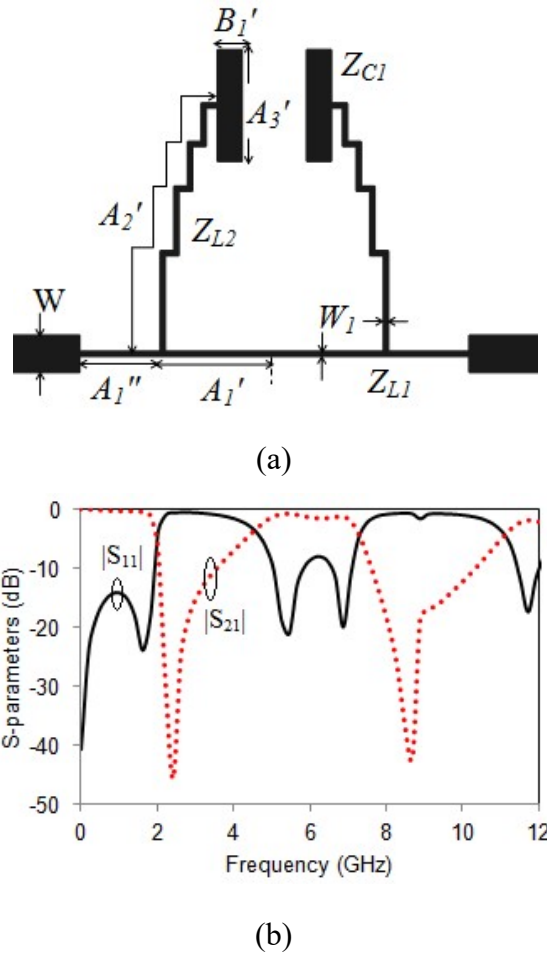


Fig. 5.14 Modified T-shaped structure (a) Layout (b) Frequency response characteristics

In the modified T-shaped structure, the roll-off rate is improved but the presence of passband harmonics is observed. To extend the stopband bandwidth of the filter, an open stub and a pair of suppressing cells is used in the design. The open stub is placed in the middle of the high impedance main transmission line and one pair of suppressing cell is placed at distance  $l_1$  from the end of the main transmission line, which suppresses the high frequency harmonics. Although high frequency harmonics can be removed by using this structure, one spurious transmission pole occurs at 2.83 GHz and this also has to be eliminated to obtain wide stopband bandwidth. The suppression of this spurious frequency does not cause any increase in the physical size, so a novel defected ground structure is thus developed.

### 5.3.2 The Characteristics of Modified Dumbbell DGS

Fig. 5.15(a) shows the one pole microstrip lowpass filter with the proposed modified dumbbell DGS etched on the metallic ground plane. A  $50\ \Omega$  microstrip line having width  $w$  is placed on the top of the substrate. The modified dumbbell DGS has two rectangular blocks having length and width  $a$  and  $b$  respectively. These two rectangular blocks are separated by two narrow strips having length  $c$  and width  $d$ . The narrow strips are joined at the centre through a channel having width and length  $e$  and  $f$  respectively. The EM simulated frequency response of proposed DGS is shown in Fig. 5.15(b). It is well known that an attenuation pole is generated by the combination of inductance and capacitance. Thus the frequency response characteristics of the modified dumbbell DGS depend on the dimension of the etched rectangular blocks and the H-shaped structure between the blocks. The dimensions of the DGS are:  $a = 3.55$ ,  $b = 3.1$ ,  $c = 7.0$ ,  $d = 0.25$ ,  $e = 0.3$  and  $f = 0.4$  (all in mm). The cutoff frequency of the filter is 3.6 GHz and the resonant frequency occurs at 5.88 GHz.

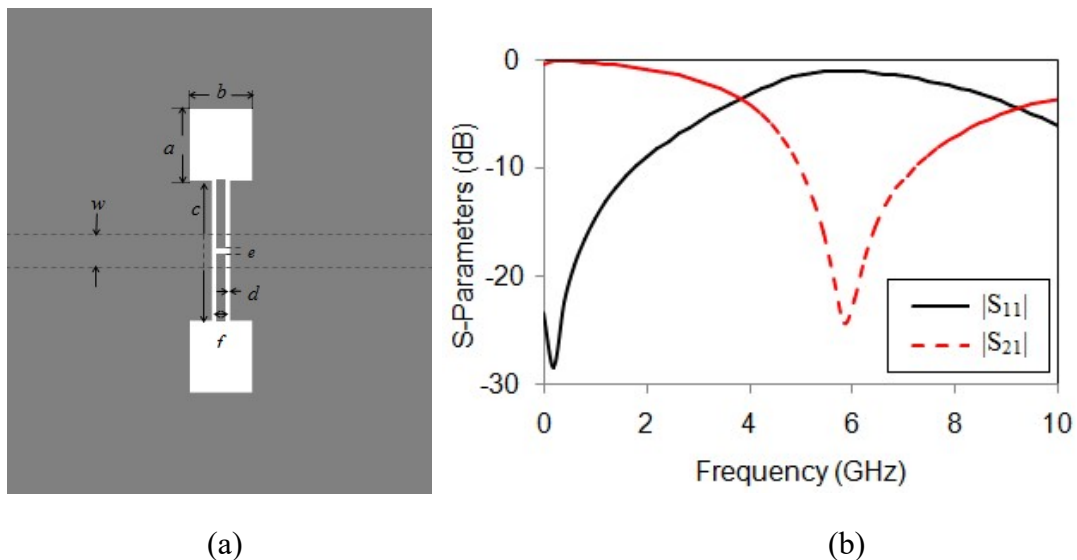


Fig. 5.15 One pole lowpass filter with modified dumbbell DGS (a) Structure (b) Frequency response characteristics

Here the equivalent circuit of the DGS is realized through field distribution method. The surface current and electric field distribution of one pole lowpass filter with modified dumbbell DGS at the resonant frequency is shown in Fig. 5.16(a) and (b) respectively.

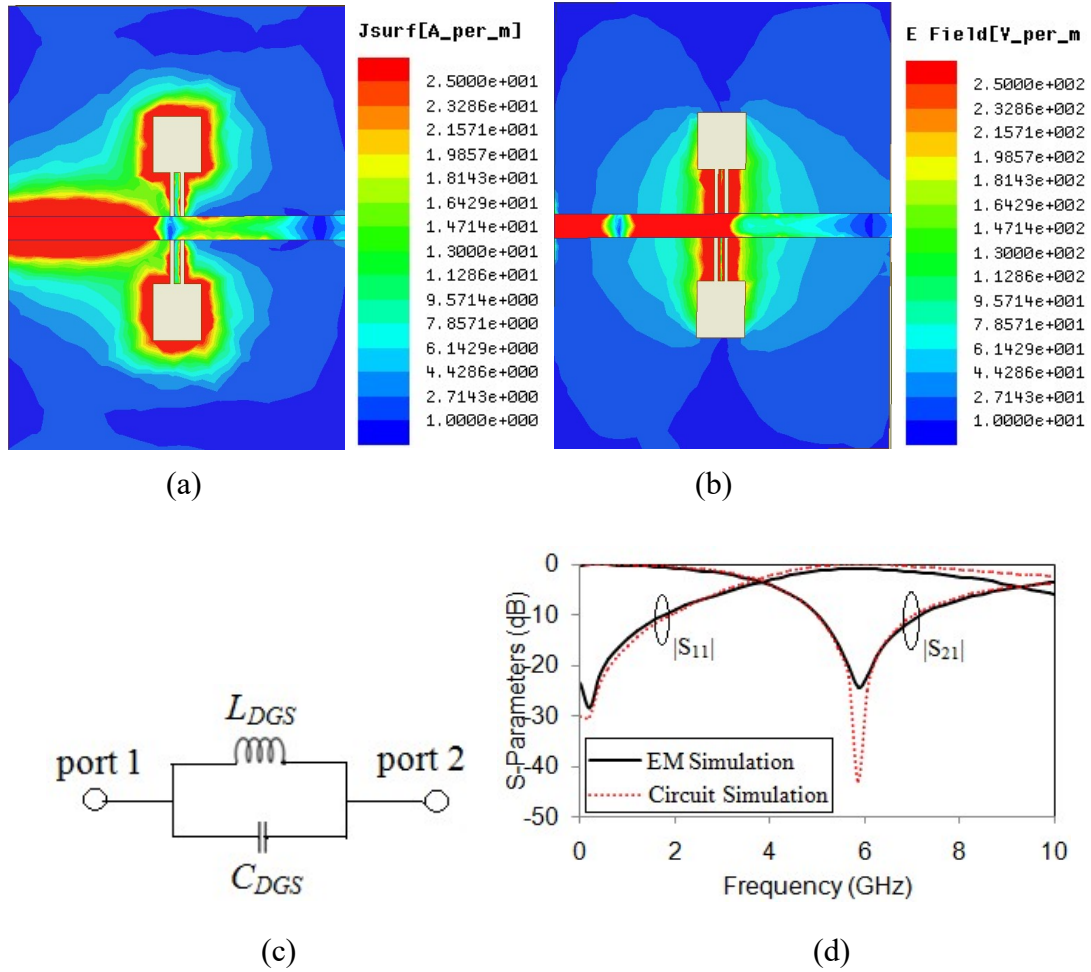


Fig. 5.16 One pole lowpass filter with modified dumbbell DGS (a) Surface current at resonant frequency (b) Electric field at resonant frequency (c) LC equivalent circuit (d) Comparison between EM simulation and circuit simulation

As seen in the Fig. 5.16, at resonant frequency all transmitted energy is reflected back to the source. The surface current distribution shows that the charge crowding occurs in the rectangular area of the DGS, proving its inductive behavior. The electric field

distributed at the H-shaped narrow strips placed between the rectangular blocks shows the capacitive nature of the DGS. Fig. 5.16(c) shows the equivalent circuit of the proposed DGS which consists of parallel combination of inductance,  $L_{DGS}$  and capacitance,  $C_{DGS}$ . The circuit parameters are extracted using Equations (5.21)- (5.22).

$$C_{DGS} = \frac{\omega_c}{2Z_0(\omega_o^2 - \omega_c^2)} \quad (5.21)$$

$$L_{DGS} = \frac{1}{4\pi^2 f_o^2 C_{DGS}} \quad (5.22)$$

where  $\omega_o$  and  $\omega_c$  are the angular resonance frequency and angular cutoff frequency respectively and  $Z_0$  is the characteristic impedance of the microstrip line. The parasitic capacitance generated as a result of the discontinuity of the modified dumbbell DGS is of very low value and therefore neglected. The calculated values are  $L_{DGS} = 2.7639$  nH and  $C_{DGS} = 0.26507$  pF. The frequency response characteristics of the EM and LC circuit simulation are in good agreement as depicted in Fig. 5.16(d). The proposed DGS has wide 10 dB bandwidth and thus the stopband bandwidth of the proposed filter is extended.

### 5.3.3 The Filter-II Structure

Fig. 5.17 shows the 3D view of the proposed lowpass filter, Filter-II. The top surface consists of an open stub (OS) placed in the middle of the high impedance transmission line. The SSRs of decreasing step size placed symmetrically on both sides of the open stub result in the generation of multiple transmission zeros in the frequency region. The SSR consists of stair shaped high impedance stub connected to the centre of a low impedance rectangular patch. One pair of suppressing cells (SCs)



placed at a distance  $l_1$  from both ends of the main transmission line suppresses the high frequency harmonics. The SC consists of a high impedance line of length  $l_5$  connected with a low impedance rectangular patch. The microstrip line of width  $w$  on both ends of the high impedance transmission line is chosen so as to get the characteristic impedance of  $50 \Omega$ . In the bottom layer, two units of modified dumbbell DGS etched from the ground metallic plane are used to improve the passband and stopband characteristics of the filter. The DGS units spaced at distance  $s'$  and placed below the SSRs enhance the stopband bandwidth, which offers higher order harmonics rejection. By properly placing the resonators and the open stub, a sharp roll-off and wide stopband lowpass filter is designed with only  $15.7 \text{ mm} \times 19.5 \text{ mm}$  physical size. The dimensions of the proposed lowpass filter are  $l_1 = 1.5$ ,  $l_2 = 1.55$ ,  $l_3 = 4.05$ ,  $l_4 = 14.5$ ,  $l_5 = 0.95$ ,  $l_6 = 1.75$ ,  $l_7 = 4.05$ ,  $l_8 = 2.6$ ,  $l_9 = 1.8$ ,  $l_{10} = 1.55$ ,  $l_{11} = 4.5$ ,  $w = 1.5$ ,  $w_1 = 0.2$ ,  $w_2 = 0.2$ ,  $w_3 = 2.0$ ,  $w_4 = 1.1$ ,  $w_5 = 1.0$ ,  $w_6 = 0.2$ ,  $s = 0.55$ ,  $a = 3.55$ ,  $b = 3.1$ ,  $c = 7.0$ ,  $d = 0.25$ ,  $e = 0.3$ ,  $f = 0.4$ ,  $g = 1.1$  and  $s' = 5.6$  (all dimensions are in mm). Fig. 5.18 shows the top and bottom view of Filter-II.

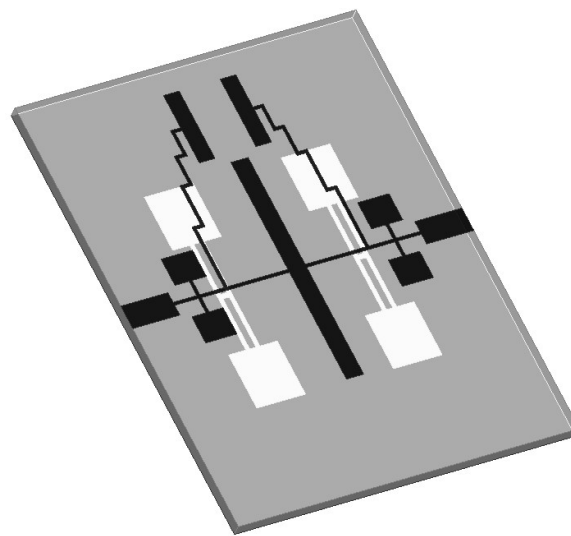


Fig. 5.17 3 D view of the Filter-II

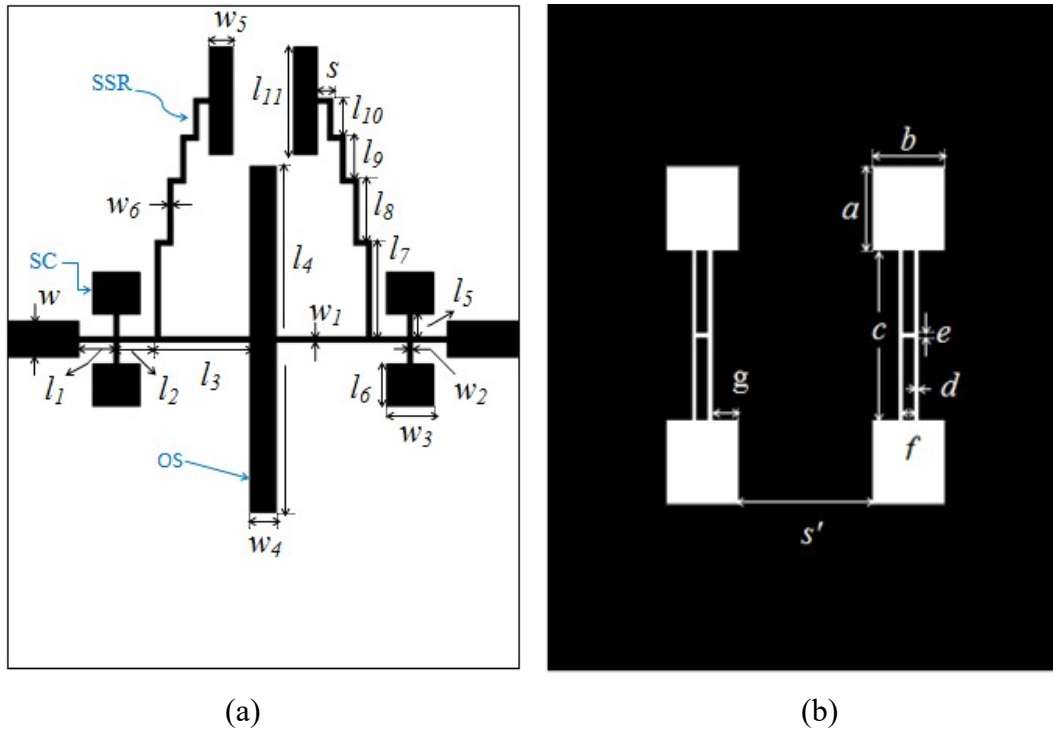


Fig. 5.18 Layout of the proposed filter (a) Top view (b) Bottom view

### 5.3.4 Filter Analysis and Discussion

Detailed analysis has been performed to sequence the design process of Filter-II. The performance characteristics of the proposed filter are studied by analyzing the frequency response characteristics of all resonators used in the process. Fig. 5.19(a) shows the frequency response characteristics of the filter with only OS placed in the middle of the high impedance main transmission line. The OS acts as a capacitor and generates two transmission zeros  $TZ_1$  and  $TZ_2$  at 6.66 GHz and 18.396 GHz with suppression levels 48.03 dB and 36.07 dB respectively. As seen in the Figure, the roll-off rate of the filter is very low and it is to be improved. Fig. 5.19(b) shows the frequency response characteristics of the filter with OS and SSRs. The symmetrical SSRs placed on either side of OS, create four transmission zeros. These additional transmission zeros,  $TZ_3$  to  $TZ_6$  are generated at frequencies 2.40 GHz, 8.67 GHz, 15.53 GHz and 15.91 GHz with rejection levels at 34.5 dB, 47.42 dB, 51.23 dB and 43.66 dB

respectively. The transmission zero  $TZ_3$  occurs very near to the cutoff frequency and thus the roll-off rate of the filter is greatly improved. The stair shaped stub improves the impedance matching of the filter and thus return loss is greater than 30 dB in the low frequency region of the passband. By adding SCs to the design, the characteristic of the lowpass filter is varied as shown in Fig. 5.19(c). The addition of SCs to the OS and SSRs generates five more transmission zeros ( $TZ_7 - TZ_{11}$ ) at frequencies 9.77 GHz, 11.30 GHz, 13.35 GHz, 14.61 GHz and 17.59 GHz with suppression level 50.19 dB, 65.50 dB, 28.80 dB, 40.42 dB and 49.25 dB respectively. Here all transmission zeros are generated at frequencies above 9 GHz, which increases the high frequency stopband rejection level of the filter. Although, high frequency stopband suppression level of the filter increases, spurious passband occurs, which results in the generation of lower order harmonics. This unwanted pole is neutralized by the use of modified dumbbell DGS. The simulated frequency response of the proposed lowpass filter after etching two units of the DGS to the ground metallic plane of the structure is shown in Fig. 5.19(d). The modified dumbbell DGS units produce two transmission zeros  $TZ_{12}$  and  $TZ_{13}$  at frequencies 5.01 GHz and 7.44 GHz with rejection levels 35.07 dB and 44.75 dB respectively, which increases the stopband bandwidth of the filter. The attenuation levels of three transmission zeros  $TZ_3$ ,  $TZ_7$  and  $TZ_9$  which are generated by the SSRs and SCs are enhanced in Fig. 5.19(d). Thus the roll-off rate of the Filter-II is improved by increasing the attenuation level of  $TZ_3$  from 34.5 dB to 46.5 dB. The return loss of the filter is also improved, which is better than 20.7 dB in the entire passband. Using the proposed lowpass filter design a wide stopband bandwidth is achieved from 2.24 GHz to 20 GHz at 20 dB suppression level except a small peak appearing at 2.64 GHz. The simulated 3 dB cutoff frequency of the filter is 2 GHz and the passband insertion

loss is less than 0.45 dB up to 1.5 GHz. The transition band from passband to stopband at 3 dB and 40 dB is 0.37 GHz. The roll-off rate is calculated as the ratio of the difference in 40 dB and 3 dB attenuation point to the transition band and its value is 100 dB/GHz. All simulations are carried out using EM simulation software IE3D.

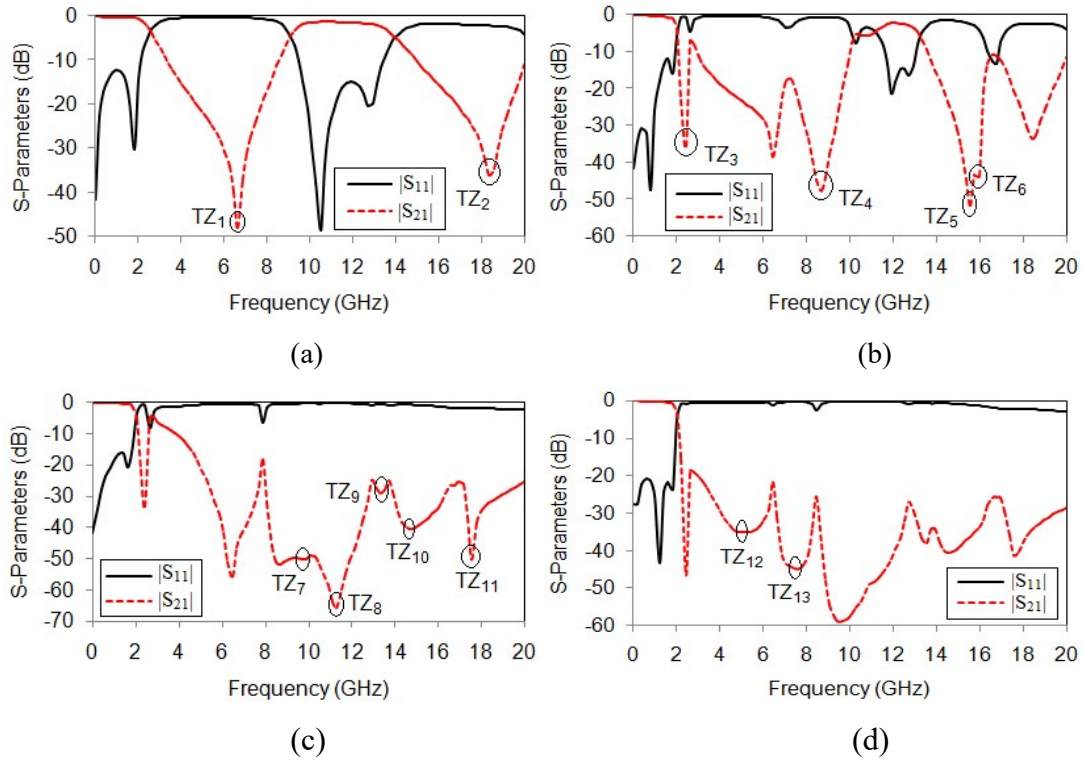


Fig. 5.19 Simulated S-parameters of the Filter-II (a) Filter with OS only (b) Filter with OS and SSRs (c) Filter with OS, SSRs and SCs (d) The proposed Filter-II

### 5.3.5 The Equivalent Circuit of Filter-II

The LC equivalent circuit of Filter-II is shown in Fig. 5.20. The top structure consists of open stub and a pair of SSRs and SCs. The calculated value of the impedance of the main transmission line and the stubs of SSRs and SCs are  $120.5 \Omega$ . The high impedance transmission lines act as inductors and the low impedance patch as capacitors. The low impedance values corresponding to the capacitors are calculated using Equation (2.23). The  $L$  and  $C$  values of the top structure are calculated using the

Equations of Hong and Lancaster (2001). The calculated values of  $L$  and  $C$  are  $L_1 = 1.109$  nH,  $L_2 = 1.143$  nH,  $L_3 = 2.807$  nH,  $L_4 = 8.458$  nH,  $L_5 = 0.6586$  nH,  $L_{DGS} = 2.7639$  nH,  $C_1 = 0.4249$  pF,  $C_2 = 0.2543$  pF and  $C_{DGS} = 0.26507$  pF.

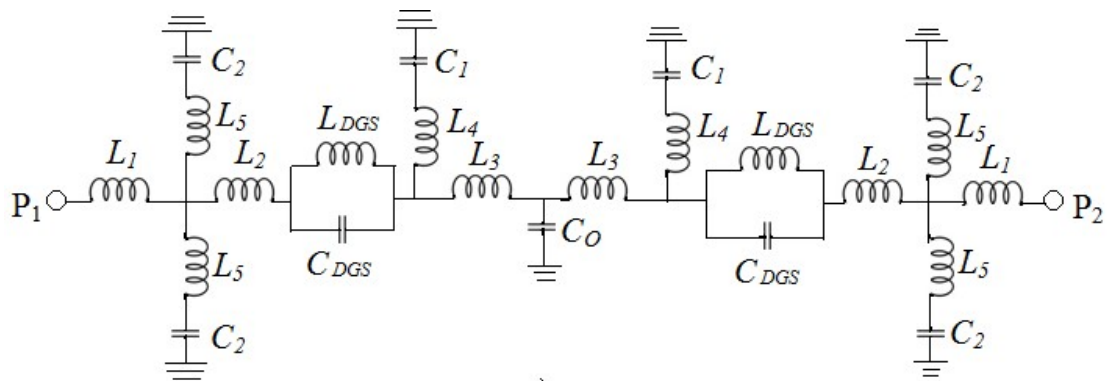


Fig. 5.20 The LC equivalent circuit of Filter-II

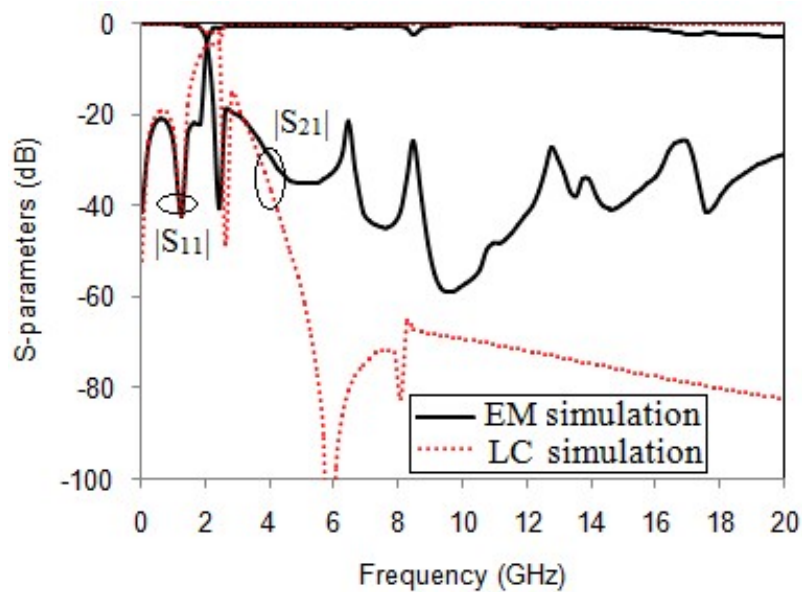


Fig. 5.21 The EM and LC circuit simulation result of Filter-II

Fig. 5.21 shows the comparison between the EM and LC circuit simulation results. In the passband frequency range, both the results are at par as shown in the Figure. The stopband suppression level of LC simulated results is high as compared with the EM

simulated results. This is due to the fact that in LC simulation, the lumped element components are used in the design, which are not affected by the substrate dielectric loss whereas in EM simulation the high value of dielectric losses of FR4 substrate play a vital role in the reduction of stopband attenuation level.

### **5.3.6 Fabrication and Results**

The proposed filter is fabricated using very low cost FR4 substrate. Fig. 5.22 shows the photograph of the top and bottom view of Filter-II. The fabricated filter is measured using R & S ZVB 20 Vector Network Analyzer. The comparison between the EM simulated and measurement results are depicted in Fig. 5.22(c).

The measured 3 dB cutoff frequency of the filter is 2.072 GHz. The return loss of the filter is better than 24.5 dB in the entire passband frequency range. The impedance matching bandwidth (IMBW) calculated by the frequency range in the passband having return loss better than 24.5 dB is 1.853 GHz (Kumar and Verma, 2016). The passband insertion loss of the proposed filter is only 0.21 dB up to 1.5 GHz. The transition from passband to stopband at 3 dB and 40 dB attenuation level is 2.072 GHz and 2.49 GHz. The roll-off rate of the filter is 88.5 dB/GHz. The stopband bandwidth at 20 dB suppression level is from 2.342 GHz to 20 GHz and thus the Filter-II has the ability to suppress up to 9<sup>th</sup> order harmonics. The relative stopband bandwidth calculated as the ratio of stopband bandwidth to stopband centre frequency of the filter is 158.07%.

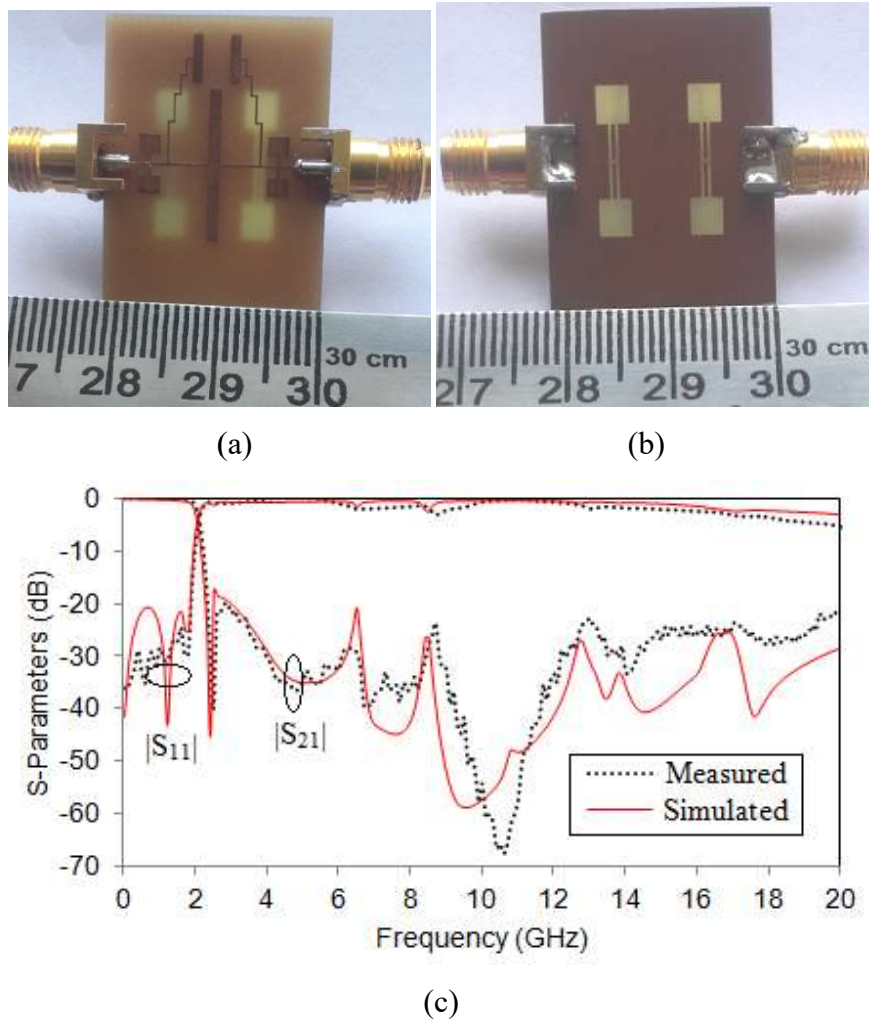


Fig. 5.22 The proposed Filter-II (a) Top view (b) Bottom view (c) Measured and simulated results

One of the important parameters that determine the quality of any lowpass filter is the group delay. The group delay of the proposed filter within the passband frequency range is reasonably flat which ensures minimum distortion to the signal. The comparison between measured and simulated results is shown in Fig. 5.23. It is observed in the Figure that the maximum group delay variation is only 0.33 ns within the 24.5 dB IMBW.

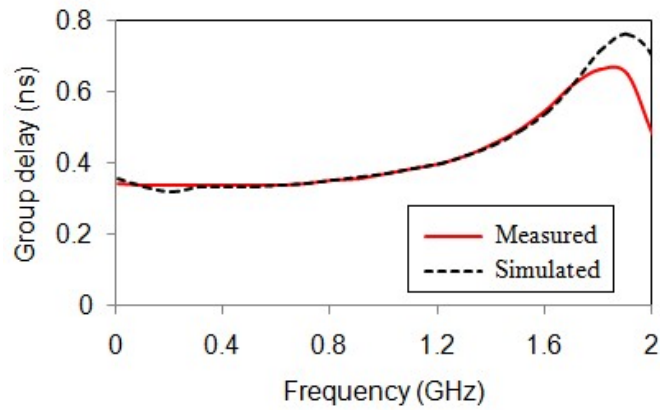


Fig. 5.23 Measured and simulated group delay

The VSWR of Filter-II is shown in Fig. 5.24. The measured VSWR value is one in the entire passband frequency range of the proposed filter, which indicates matched load.

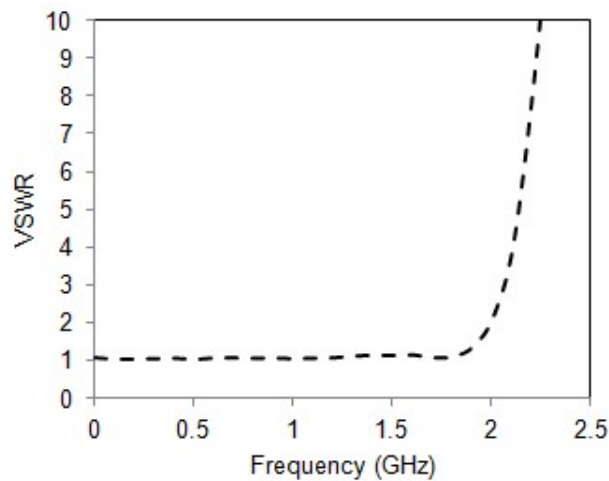


Fig. 5.24 The measured VSWR of Filter-II

### 5.3.7 Performance Comparison of Filter-II

Comparison between the Filter-II and some other works in the literature is shown in Table 5.2. The proposed filter has high value of relative stopband bandwidth when the considered suppression factor is 2. The passband return loss of the filter is also very high with sharp roll-off rate. Compared to most of the other filters, the proposed filter is very cost effective also. The wide stopband with high rejection level of the filter is useful to suppress the harmonics up to 9<sup>th</sup> order.



Table 5.2 Comparison between the proposed Filter-II and similar works in the literature

Ref	$f_c$ GHz	RL dB	$\xi$ dB/GHz	RSB %	SF	Harmonic suppression	Substrate, $h$ (mm)
Kumar and Verma (2016)	2.5	10	39	105.69	2	4 <sup>th</sup> order	Neltec-NX 9320, 0.762
Mohra, (2011)	2.62	25	30.66	122.39	2.6	5 <sup>th</sup> order	RT/Duroid 5880, 0.787
Karthikeyan <i>et al.</i> (2015)	1.09	15	48.57	149.9	2	10 <sup>th</sup> order	Rogers 5880, 0.381
Boutejdar, (2017)	3.7	27	17	91.6	2	3 <sup>rd</sup> order	Roger, 0.813
Yang <i>et al.</i> (2012)	2.76	18	53.4	126.73	2	4 <sup>th</sup> order	Taconic TLX-0, 0.79
Filter-2	1.935	27	61.56	157.6	2	10 <sup>th</sup> order	FR4, 0.8
Filter-II	2.072	24.5	88.5	158.07	2	9 <sup>th</sup> order	FR4, 0.8

$f_c$  - Cutoff frequency, RL - return loss,  $\xi$  - roll-off rate, RSB - Relative stopband bandwidth, SF - suppression factor.

#### 5.4 CHAPTER SUMMARY

The occurrence of the spurious frequency bands is a fundamental limitation of microstrip filters. To remove these spurious frequency bands, another design approach using defected structures etched from the metallic ground plane is proposed in this chapter.

This chapter discusses two novel DGS, which are used to suppress the harmonics and extend the stopband bandwidth to meet today's emerging applications. Both filters are designed with cutoff frequency near 2 GHz and thus useful for L-band applications.

The performance characteristics of the proposed filters are compared in Table 5.3.

Table 5.3 Comparing the performance characteristics of the proposed filters

Filter	$f_c$ GHz	$\xi$ dB/GHz	NCS $\lambda g^2$	RSB %	SL	IL- PB in dB	RL-PB in dB	Harmonic suppression
Basic filter	2.03	33.36	0.0342	120.1	20	1.2	11	5 <sup>th</sup> order
Filter-1	2.02	37.12	0.0338	156.3	18	0.59	21	9 <sup>th</sup> order
Filter-2	1.935	61.56	0.0338	157.6	20	0.22	27	10 <sup>th</sup> order
Filter-II	2.072	88.5	0.0471	158.1	20	0.21	24.5	9 <sup>th</sup> order

By using a multilayer structure, the performance characteristics of the basic lowpass filter are greatly improved in Filter-I. For validation of the structure, the proposed lowpass filters are fabricated and their frequency response is analyzed. The designed filters, Filter-1 and Filter-2 have very low insertion loss and high return loss in the passband as compared to the performance of the basic filter structure. It also has good selectivity and high rejection in the stopband up to 20 GHz at 20 dB suppression level. Suppression up to the 10<sup>th</sup> order harmonics is achieved as compared to the basic filter capable of suppressing only up to 5<sup>th</sup> order. The proposed filter is very compact and offers good performance characteristics in both passband and stopband, thus making it a good choice for mobile and wireless communication applications.

A microstrip lowpass filter designed based on dual plane structure to achieve ultra wide stopband characteristics is presented in Filter-II. The proposed filter is able to suppress up to 9<sup>th</sup> order harmonics. The roll-off rate and RSB of Filter-II is improved as compared with Filter-I. The filter exhibits very good characteristics like minimum group delay variation, low insertion loss and high return loss in the passband. The structure is very compact and thus ideal for wide band communication applications.

The proposed filters have achieved sharp roll-off rate along with wide stopband bandwidth by maintaining compact size. To further improve the roll-off rate and to obtain wide stopband with miniaturized circuit size, a new lowpass filter designed using DGS and defected microstrip resonator is discussed in the next chapter.

## CHAPTER 6

### COMPACT, SHARP ROLL-OFF LOWPASS FILTER WITH WIDE STOPBAND USING DEFECTED STRUCTURES

#### 6.1 INTRODUCTION

The concept of filtering is very important in the field of modern wireless communication applications. Lowpass filters are commonly used to suppress the unwanted high frequency harmonics. The important factors to be considered during efficient filter design are: compact size, low insertion loss, high roll-off rate and wide stopband with higher order harmonics suppression. To meet these requirements, several lowpass filters are designed by adopting different techniques.

The commonly adopted lowpass filter design is based on loading stepped impedance resonators/open circuited stubs in the high impedance transmission line (Hong and Lancaster, 2001). However, higher the characteristic impedance of the microstrip line, larger the fabrication difficulties and lower the power handling capability. Cascading hexangular shaped resonators with open circuited stubs, a wide stopband lowpass filter with good roll-off rate is designed by Hayati *et al.* (2015). Cascaded arrangement of square shaped open loop resonators (Hammed *et al.*, 2018) are used to develop a lowpass filter with stopband up to 6 GHz. But these filters suffer from low roll-off rate.

Defected ground structures are used to improve the roll-off rate and stopband bandwidth of the conventional filter by introducing defects etched from its ground plane. DGS with inherent bandgap in certain frequency bands are used in the lowpass filter design to achieve wide stopband characteristics (Ahn *et al.*, 2001). Several techniques are used in the literature to improve the performance of DGS based filters.

Fractal shaped DGSs are utilized to miniaturize the circuit size of the conventional filter developed with open stubs (Kufa and Raida, 2013). A lowpass filter designed using slotted ground plane resonator to generate multiple transmission zeros in the stopband, so as to obtain wide stopband rejection characteristics is presented by Wang and Hsu, (2018). A lowpass filter designed to achieve wide stopband up to 10 GHz using DGS is presented by Vala *et al.* (2017). A compact lowpass filter with wide stopband designed using microstrip line loaded by folded patches on the top of the substrate and hybrid slot in the ground plane is presented by Jiang and Xu, (2017). However, the structure complexity is high in most of these filters and hence difficult to fabricate. Chen *et al.* (2015) presented a lowpass filter with wide stopband by introducing DGS along with open stubs and stepped impedance stubs (SIS). Open complementary type split ring resonator designed on the top side of the substrate and dumbbell DGS etched from the ground plane are used to design compact lowpass filter with low roll-off rate by Karthikeyan and Kshetrimayum, (2015). Song *et al.* (2010) introduced a lowpass filter with wide stopband response by adding coupled slots along with the dumbbell shaped DGS.

Combinations of octagonal shaped resonators along with DGS and DMS are used to design lowpass filter with wide stopband up to 12 GHz is presented by Boutejdar *et al.* (2019). However, the achieved filter selectivity is very low. Lowpass filter designed using modified split ring resonator is presented by Sen *et al.* (2018). Here, the selectivity and stopband bandwidth of the filter is improved by incorporating DGS and DMS in the filter structure. The filters described above are used to generate wide stopband bandwidth only. However, along with wide stopband, sharp transition skirt with miniaturized circuit size is also essential for an ideal lowpass filter used in modern communication systems.

In this article, the unit cell model of basic DGS, which consists of mirrored symmetrical square head slot connected with rectangular gap  $g$  is used to design one pole lowpass filter with cutoff frequency 3.715 GHz. Then the geometrical shape of basic DGS is modified without changing its overall physical size to improve the performance characteristics of the filter. Comparing the characteristics of basic DGS and the modified DGS, the proposed modified structure reduces the passband to stopband transition band with reduced cutoff frequency of 2.075 GHz. The phase characteristics of modified DGS prove its slow wave characteristics. Detailed analysis has been conducted to study the influence of structure parameters on the resonant and cutoff frequency of the filter. The proposed lowpass filter is designed with symmetrical open stubs on the top surface and modified DGS in the ground plane to achieve wide stopband up to 20 GHz with cutoff frequency 2.11 GHz. The LC equivalent circuit is developed and compared with the EM simulated results and found that both results are in good agreement. To improve the stopband suppression level at a certain band of frequencies, spurline resonator is incorporated in the top surface of the filter. The improvement in rejection band is achieved without any compromise in the passband characteristics of designed 2.11 GHz filter. Excluding the dimension of I/P-O/P ports, the physical size of the filter is only 15.5 mm x 12.7 mm. The filters are fabricated using very low cost, easily available FR4 substrate having thickness 0.8 mm, dielectric constant 4.4 and loss tangent 0.02.

## 6.2 DESIGN OF THE PROPOSED DGS

The procedure used for designing the proposed DGS is discussed in detail.

### 6.2.1 Comparison of the Basic DGS with the Modified DGS

Fig. 6.1(a) shows the basic defected ground structure, which consists of a pair of symmetric square head slots of dimension  $a' \times b'$ , connected with a narrow rectangular gap,  $g$  which is etched on the metallic ground plane. The top layer consists of a microstrip line of width  $w = 1.5$  mm, which ensures the characteristic impedance of  $50 \Omega$ . The square head slot corresponds to the inductance value, and the rectangular gap,  $g$  exactly below the microstrip line represents the capacitance of the filter (Kim *et al.* 2000). The effective series inductance introduces 3 dB cutoff frequency at 3.715 GHz and as the frequency increases, the reactance also increases and starts the rejection of higher frequency bands. A transmission zero  $T_Z$  occurs at 5.958 GHz, depending on the parallel capacitance with the series inductance, at the resonance frequency and as frequency increases the reactance decreases and causes a band gap. From Fig. 6.1(c), it is noted that the transition band from passband to stopband is very wide and its value is 2.243 GHz and thus the attenuation rate of the filter is very low. The overall physical size of basic DGS is  $a \times b$  mm<sup>2</sup>.

The geometrical shape of DGS slots has great influence on the filter characteristics such as transition steepness and stopband bandwidth (Abdel-Rahman *et al.* 2004). Thus to improve the roll-off rate of the filter, the basic DGS is modified by placing interdigital slots between the square head slots and the proposed modified DGS is shown in Fig. 6.1(b). The addition of interdigital slot does not make any change in the

overall physical size of the structure. Each finger of the interdigital structure has length  $l_f$ , width  $w_f$  and spacing between the fingers  $s$ .

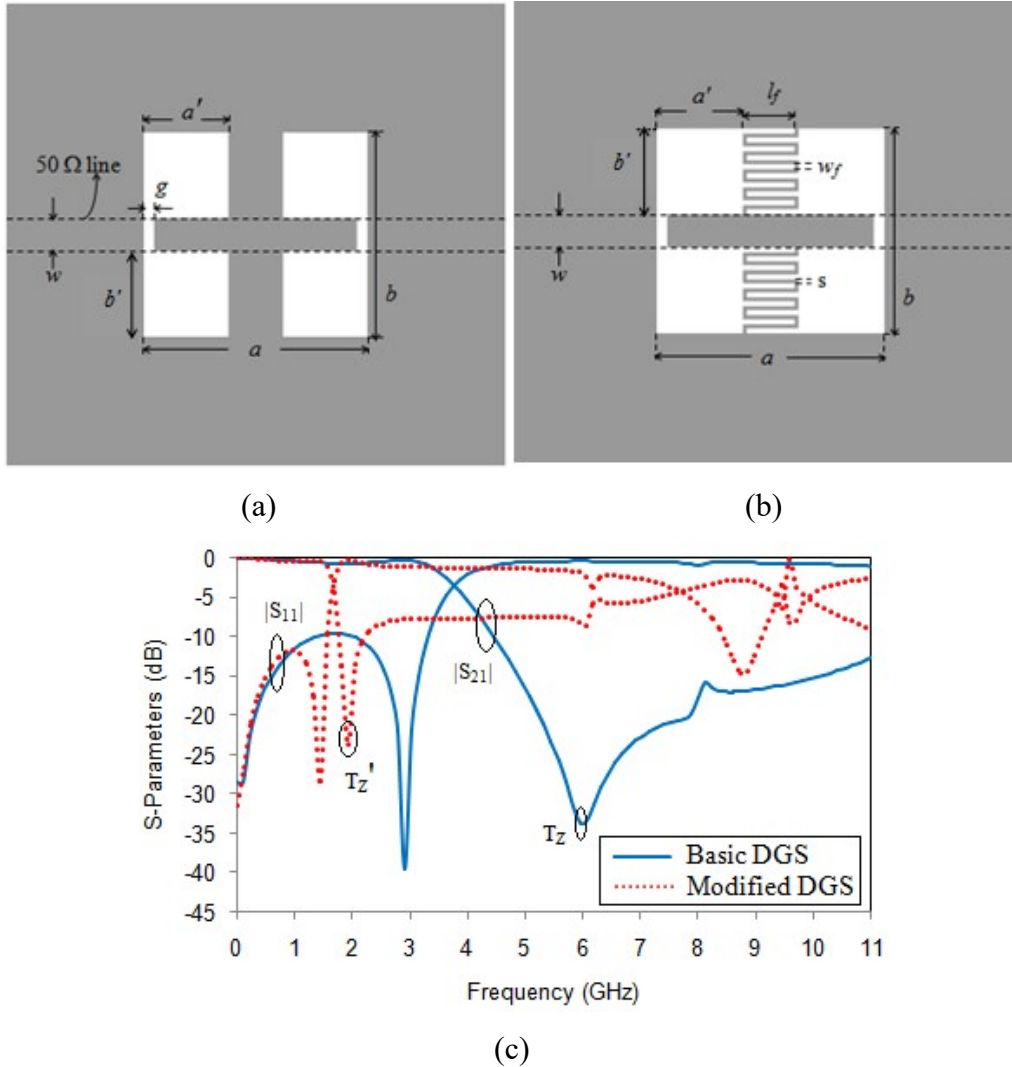


Fig. 6.1 Layout of one pole basic DGS filter (b) Structure of the proposed one pole modified DGS filter (c) Comparison of frequency response characteristics

The S-parameters of the filter designed using basic DGS and the modified DGS are compared in Fig. 6.1(c). The cutoff frequency of the proposed modified DGS is 2.075 GHz and the transmission zero,  $T_Z'$  occurs at 2.42 GHz. With the addition of interdigital structure between the square head slots, the transmission zero frequency is shifted from  $T_Z$  to  $T_Z'$ , without increasing the overall physical size, of the structure.



Thus the modified DGS reduces the circuit size by 68.8 %. Depending on the size and shape of defects etched from the ground plane, the shield current distribution is modified, which results controlled excitation of EM waves through the substrate.

The basic DGS shows characteristics such as single resonance and gradual transition from passband to stopband. With the addition of interdigital slots between the square head slots, both electric and magnetic coupling occurs between the resonators and thus resonant and cutoff frequency moves towards the lower frequency end. As the spacing  $s$  between the interdigital fingers increases, the coupling effect reduces. The dimensions of the proposed modified DGS are  $a' = 3.8$ ,  $b' = 3.8$ ,  $g = 0.45$ ,  $l_f = 2.4$ ,  $w_f = 0.2$ ,  $s = 0.2$ ,  $a = 10.1$ ,  $b = 9.1$  and  $w = 1.5$  (all dimensions in mm).

The comparison between the characteristics of the basic DGS and the modified DGS in a  $50 \Omega$  microstrip shown in Table 6.1, is simulated using IE3D EM simulation software. The cutoff frequency, the resonant frequency, the transition band ( $f_{20\text{dB}} - f_{3\text{dB}}$ ), the normalized circuit size (NCS) and the sharpness factor are compared in the table. The NCS and sharpness factor of the filter are calculated using the Equations (2.17) and (2.19).

From the table, it is seen that the NCS of the modified DGS is only  $0.0145 \lambda_g^2$  as compared to the circuit size of the basic DGS. By maintaining constant physical size of both DGS slots, the circuit size of modified DGS is improved by the reduction in cutoff frequency of the modified DGS based filter. Thus it is proved that by reforming the basic DGS to the modified DGS, the circuit size of the filter is reduced. The sharpness factor of the modified DGS is of low value, *i.e.* 1.16; whereas for the

basic DGS, it is 1.603. The lower value of sharpness factor indicates the sharp transition from passband to stopband and thus the selectivity of the modified DGS filter is improved.

Table 6.1 Comparing the characteristics of basic DGS and the modified DGS

One pole filter with	CF GHz	RF GHz	Transition band ( $f_{20dB} - f_{3dB}$ ) GHz	NCS $\lambda_g^2$	Sharpness factor
Basic DGS	3.715	5.958	1.485	0.0465	1.603
Modified DGS	2.075	2.42	0.3	0.0145	1.16

CF- cutoff frequency, RF- Resonant frequency

### 6.2.2 LC Equivalent Circuit of the Modified DGS

The equivalent circuit model of the one pole filter with modified DGS is shown in Fig. 6.2(a).  $L_0$  and  $C_0$  represent the inductance and capacitance values of the modified DGS and the series combination of  $L_1$  and  $C_1$  is due to the relatively large values of the fringing field. These fringing fields occur due to the step discontinuities of the interdigital slots in the ground plane and this discontinuity effect may change the overall characteristic impedance of the circuit. The capacitance  $C_0$  and inductance  $L_0$  are calculated using the Equations (6.1)-(6.2) (Ahn *et al.* 2001) as,

$$C_0 = \frac{\omega_c}{Z_0 g_1 (\omega_0^2 - \omega_c^2)} \quad (6.1)$$

$$L_0 = \frac{1}{\omega_0^2 C_0} \quad (6.2)$$

where  $\omega_0$  is the angular frequency corresponding to the transmission zero location  $T_Z'$  and  $\omega_c$  is the angular cutoff frequency of the one pole filter with modified DGS. The fringe field effect, which represents the series  $L_1$  and  $C_1$  in the  $\pi$ -network is calculated

according to Park *et al.* (2002). The calculated values of the LC circuit are,  $L_0 = 2.13$  nH,  $C_0 = 2.03$  pF,  $L_1 = 0.1$  nH and  $C_1 = 0.5$  pF. The frequency response characteristics of the EM and LC circuit simulation shown in Fig. 6.2(b) are having good approximation, which validates the circuit design.

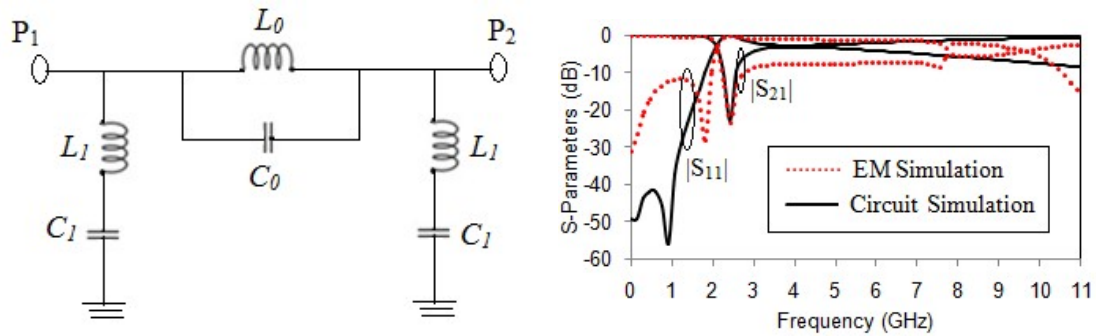


Fig. 6.2 (a) The LC equivalent circuit of one pole filter with modified DGS  
(b) Comparison between EM and LC circuit simulation results

### 6.2.3 Phase Characteristics of Modified DGS and SWF

Fig. 6.3 shows the comparison between the phase characteristics of transmission coefficient ( $S_{21}$ ) of microstrip line, microstrip line with basic DGS and microstrip line with modified DGS. In DGS based filters, a phase difference occurs to the signal frequency, which is due to the resonant characteristics of the structure. The phase of modified DGS changes rapidly as compared to the phase change of basic DGS and the uniform microstrip line and accordingly, the phase velocity of the modified DGS is slow as compared with the other two structures. The reduction in phase velocity results in the slow wave effect and it is analyzed by defining the slow wave factor (SWF).

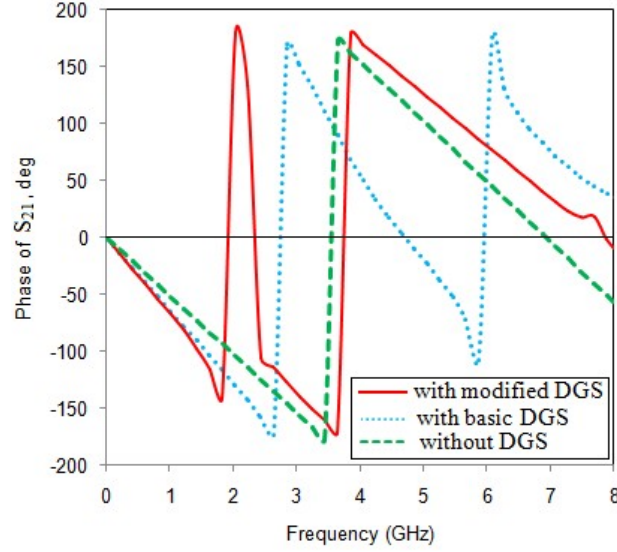


Fig. 6.3 Phase characteristics of microstrip line with modified DGS, microstrip line with basic DGS and the microstrip line without DGS

For a microstrip line without DGS, the relation for slow wave factor (SWF) is  $\sqrt{\epsilon_{\text{eff}}}$ , where  $\epsilon_{\text{eff}}$  is the effective permittivity of the microstrip line and is calculated using the Equation (2.20). For the FR4 substrate the calculated value of SWF is 1.823.

The SWF of the microstrip line loaded with modified DGS is calculated using Equation (6.3) as,

$$SWF = \frac{\lambda_0 \Delta\theta}{360L} + \sqrt{\epsilon_{\text{eff}}} \quad (6.3)$$

where  $\lambda_0$  is the free space wavelength at the cutoff frequency of microstrip line with modified DGS,  $\Delta\theta$  is the phase difference between the microstrip line with and without modified DGS and  $L$  is the physical length of the line. For the microstrip with modified DGS, the SWF increases and its value is 4.626 at the cutoff frequency. This increase in the SWF shows that the proposed modified DGS is a good slow wave transmission line and this validates its size reduction capability. The Fig. 6.4 compares the characteristics of SWF with modified DGS and without DGS.

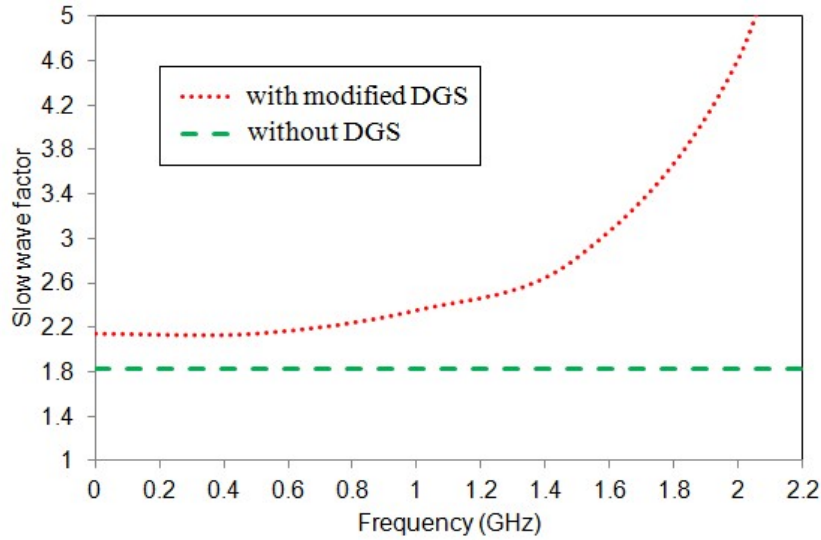


Fig. 6.4 Slow wave factor of modified DGS

When the modified DGS is etched from the ground metallic plane, the current path in the ground plane is fully disturbed and it is then confined along its periphery. This results in the increase of current path length and thus propagation delay occurs. Hence for the modified DGS filter, the reduction in phase velocity occurs and this results the slow wave effect of microstrip line.

#### 6.2.4 Parametric Analysis of Modified DGS

The influence of various modified DGS parameters ( $a'$ ,  $g$  and  $l_f$ ) on the frequency response characteristics is analyzed in detail using IE3D simulations.

##### Effect of slot head $a'$

First, only the length  $a'$  of the slot head is varied by keeping the rectangular gap,  $g$  and the dimension of interdigital slot as constant. Simulation result of the resonant frequency,  $f_0$  and cutoff frequency,  $f_c$  with the length  $a'$  is shown in Fig. 6.5(a). As the length  $a'$  increases, the etched area of the slot head increases, and this results in increase in the series inductance. This increase in series inductance results in lowering the cutoff

frequency as shown in Figure. Also, from the Fig. 6.1(c), attenuation poles are present in the simulation results on etched modified DGS. Thus as the length  $a'$  increases, the resonant frequency  $f_0$  corresponding to the attenuation pole (transmission zero) location decreases. This transmission zero location corresponds to the parallel combination of  $L$  and  $C$  circuit. Thus, although all other dimensions are kept constant, the increase in the value of  $a'$  results in the increase in effective inductance and thus the resonant and cutoff frequency shift towards the lower frequency end.

### **Influence of gap width, $g$**

The influence of  $g$ , ie, the etched gap width is analyzed in the next step. Here, except  $g$ , all other dimensions are kept constant. As the value of  $g$  increases in steps of 0.1 mm, the resulting decrease in the effective capacitance value leads to shifting of transmission zero location towards higher frequency. The value of  $g$  does not have much effect on the series inductance value of the microstrip line and hence the change in the value of cutoff frequency is marginal as shown in Fig. 6.5(b).

### **Influence of the interdigital slot length, $l_f$**

A parametric study has been conducted to analyze the effect of the length of the interdigital slot,  $l_f$  on the resonant and cutoff frequency, which is depicted in Fig. 6.5(c). The increase in the value of finger length results in the shifting of resonant frequency,  $f_0$  and cutoff frequency,  $f_c$  towards the lower end and also it is noted from the Figure that as  $l_f$  increases, the transition band from passband to stopband decreases and thus the roll-off rate of the filter increases. This means that as the length,  $l_f$  increases, by keeping all other dimensions of the modified DGS constant, the equivalent inductance and capacitance of the microstrip line increases and thus the resonant and cutoff frequency decreases towards the lower frequency end.

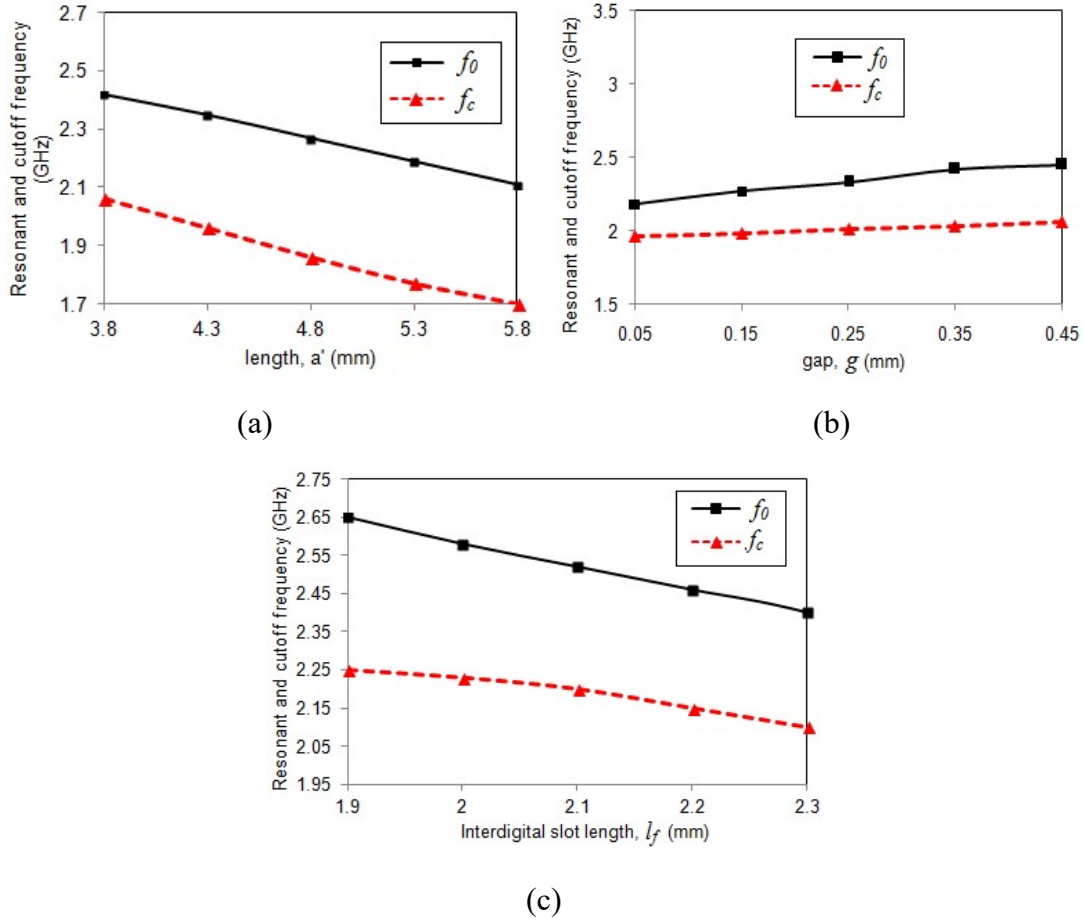


Fig. 6.5 The frequency response characteristics of modified DGS based filter for different values of  $a'$ ,  $g$  and  $l_f$

Based on the above parametric studies, proper optimization of the proposed structure is done to design a compact and wide stopband lowpass filter with good roll-off rate.

### 6.3 THE LOWPASS FILTER DESIGN USING MODIFIED DGS

The modified DGS improves the roll-off rate of the filter, but the stopband bandwidth has to be extended to suppress the unwanted harmonics. To extend the stopband bandwidth, multiple transmission zeros has to be generated at high frequency. For that, two different pairs of symmetrical uniform impedance stubs (UIS) are designed in the top surface of the filter. The UIS should have length less than the quarter guided wavelength,  $\lambda_g/4$  for generation of multiple transmission zeros. The proposed lowpass filter shown in Fig. 6.6 has three layers: the top layer consists of two UIS,

which are symmetrically arranged and this mirrored symmetrical stubs are loaded on the transmission line  $TL_3$  and the middle layer is the dielectric substrate and the bottom layer is the modified DGS slots etched from the ground plane.

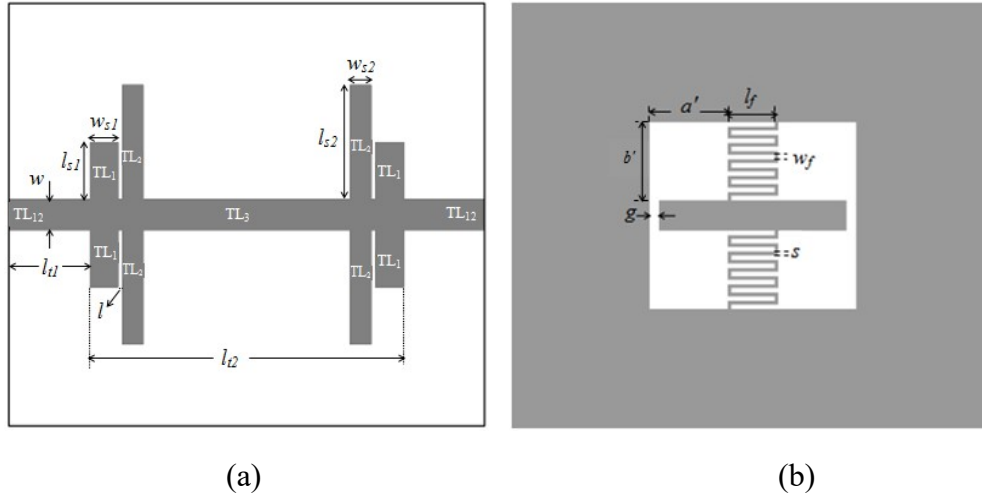


Fig. 6.6 Layout of the proposed filter (a) Top view (b) Bottom view

### 6.3.1 Characteristics of Symmetrical UIS

The top layer of the designed filter consists of two different pairs of symmetrical UIS, which act as compensated capacitors loaded on the transmission line, each of length and width represented as  $l_{s1}$ ,  $w_{s1}$  and  $l_{s2}$ ,  $w_{s2}$  respectively.  $l$  is the optimized distance between symmetrical  $TL_1$  and  $TL_2$ . The equivalent circuit of the top surface of the designed filter is shown in Fig. 6.7. The ABCD matrix of lossless transmission lines  $TL_{12}$  and  $TL_3$  having characteristic impedance  $Z_{t1}$  and  $Z_{t2}$  of length and phase constant  $l_{t1}$ ,  $l_{t2}$ ,  $\beta_{t1}$  and  $\beta_{t2}$  respectively is expressed in Equation (6.4) as,

$$M_x = \begin{bmatrix} \cos \beta_x l_x & jZ_x \sin \beta_x l_x \\ \frac{j \sin \beta_x l_x}{Z_x} & \cos \beta_x l_x \end{bmatrix} \quad (x = t1, t2) \quad (6.4)$$

The ABCD matrix of the UIS,  $TL_1$  and  $TL_2$  of characteristic impedance  $Z_{s1}$  and  $Z_{s2}$  having length and phase constant  $l_{s1}$ ,  $l_{s2}$ ,  $\beta_{s1}$  and  $\beta_{s2}$  respectively in Equation (6.5) is,



$$M_y = \begin{bmatrix} 1 & 0 \\ \frac{j \tan \beta_y l_y}{Z_y} & 1 \end{bmatrix} \quad (y = s1, s2) \quad (6.5)$$

For the main transmission line  $TL_3$ , ABCD matrix is represented as  $M_{t2}$ . ABCD matrix of the two different pairs of UIS is represented in Equation (6.6) as,

$$M_{UIS} = M_{s1}M_{s2}M_{s2}M_{s1} \quad (6.6)$$

The total ABCD matrix of two pairs of symmetrical UIS loaded on the transmission line  $TL_3$  is expressed in Equation (6.7),

$$M_{Total} = M_{UIS} + M_{t2} + M_{UIS}. \quad (6.7)$$

The overall ABCD matrix of the equivalent circuit shown in Fig. 6.7 is derived as,

$$M_{EC} = M_{t1}.M_{Total}.M_{t1} \quad (6.8)$$

For matched load, the S - parameters of the equivalent circuit is calculated using the overall ABCD matrices.

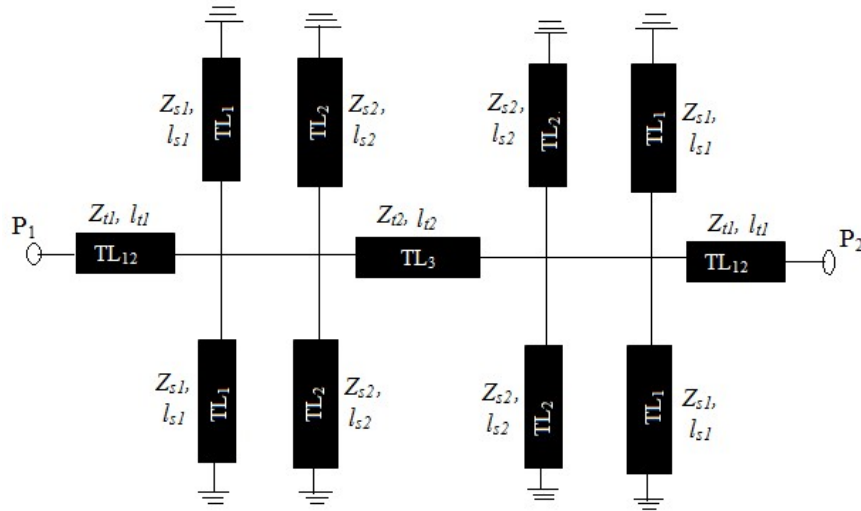


Fig. 6.7 The equivalent circuit of the top surface of the proposed structure

The low impedance transmission lines  $TL_1$  and  $TL_2$  are modelled as shunt capacitor and at high frequencies it acts as short circuit to ground and generates transmission zeros. The two pairs of symmetrical UIS produces two transmission zeros at

frequencies 8.08 GHz and 14.5 GHz with the suppression level of 42.84 dB and 55.75 dB respectively. Thus by etching the proposed modified DGS on the ground plane of the compensated capacitors a wide stopband and sharp roll-off lowpass filter is designed with compact circuit size. The dimensions of the structure in mm are,  $l_{t1} = 3$ ,  $l_{t2} = 9.5$ ,  $l = 0.2$ ,  $l_{s1} = 5.6$ ,  $l_{s2} = 2.8$ ,  $w_{s1} = 1.05$ ,  $w_{s2} = 1.4$ .

### 6.3.2 Equivalent Circuit of the Proposed Filter

The equivalent circuit of the proposed lowpass filter is shown in Fig. 6.8(a), which is the combination of the mirrored symmetrical two pairs of UIS present in the top surface of the filter and the modified DGS structure in the ground plane. The capacitors  $C_{s1}$  and  $C_{s2}$  represent the capacitance of the symmetric  $TL_1$  and  $TL_2$  respectively are calculated using Equation (6.9)

$$C_{si} = \frac{W_{si}}{v_p Z_{si}} \text{ for } i = 1, 2 \quad (6.9)$$

The component values of the equivalent circuit of the proposed filter are  $C_{s1} = 0.5516$  pF,  $C_{s2} = 0.7118$  pF,  $L_0 = 2.13$  nH,  $L_1 = 0.1$  nH,  $C_0 = 2.03$  pF and  $C_1 = 0.5$  pF.

The frequency response characteristics of the EM and LC circuit simulation are shown in Fig. 6.8(b). From the Figure we can see that both the results are in very good agreement with each other which validates the equivalent circuit of the proposed filter. From the simulated characteristics of the proposed filter, we can see that the transition band from passband to stopband is reduced and its value is only 0.19 GHz between 3 dB and 40 dB attenuation point. Thus the roll-off rate of the filter is improved and its EM simulated value is 194.7 dB/GHz at 40 dB suppression level. The 3 dB cutoff frequency of the proposed filter is 2.22 GHz. The passband return loss of the filter is better than 12 dB and the insertion loss is less than 0.7 dB in the entire passband.

Stopband return loss is almost zero up to 16.5 GHz except in the frequency range 7.7 GHz to 9 GHz and at high frequencies the inherent dielectric losses associated with FR4 material causes a rise in return loss. It is seen that multiple transmission poles occur in the above mentioned frequency range of 7.7 GHz to 9 GHz. The stopband bandwidth of the filter is 2.32 GHz to 22 GHz at 15 dB suppression level.

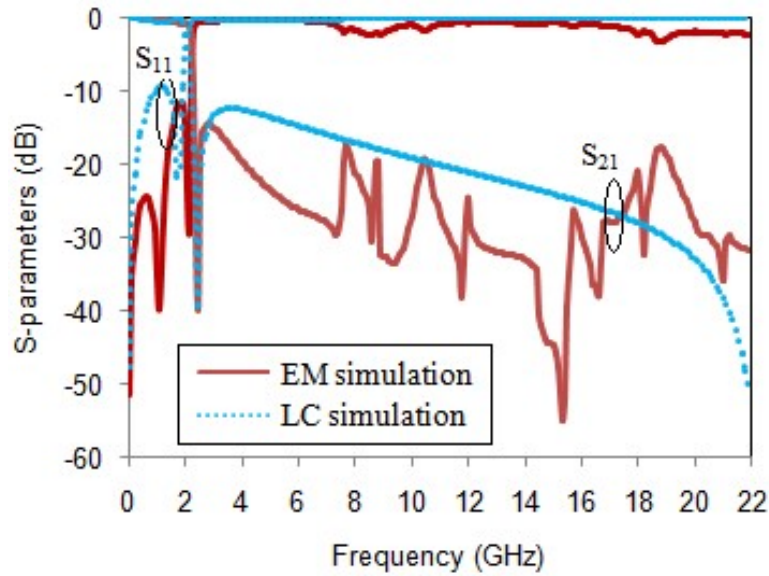
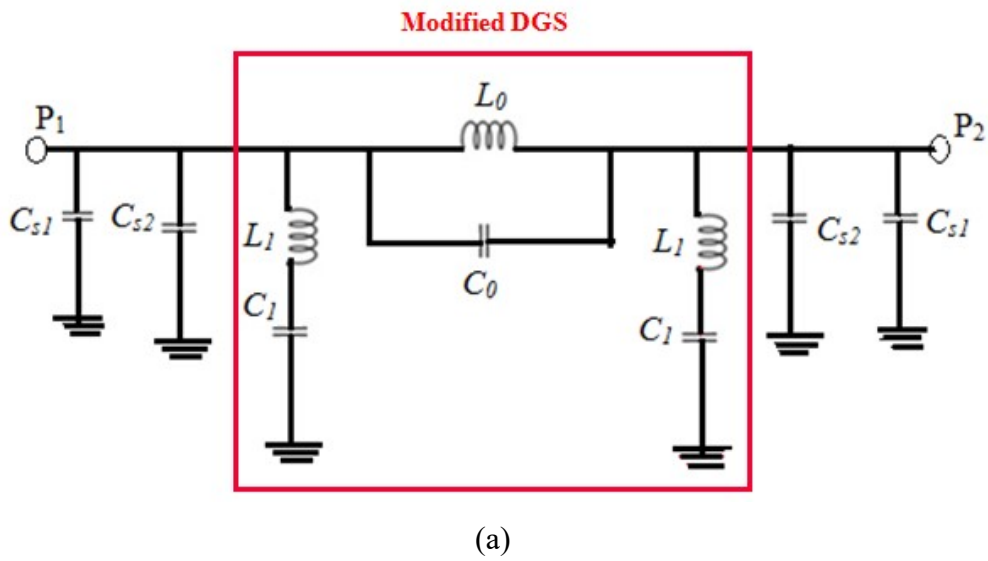


Fig. 6.8 (a) LC equivalent circuit of the proposed filter (b) EM and LC circuit simulation comparison

### 6.3.3 Comparison Between Filters with Basic DGS and Modified DGS

Fig.6.9 shows the comparison between the proposed filter designed using modified DGS and the one developed using basic DGS. The paired symmetric UIS are present in the top side of both the filters. We can see that multiple transmission zeros are generated at high frequencies in both type of filters. The filter with basic DGS has 3 dB cutoff frequency of 3.85 GHz and the transition band from passband to stopband is 2.55 GHz and thus the roll-off rate obtained is 13.21 dB/GHz. From the figure it is clear that, the proposed filter offers sharp cutoff frequency which greatly improves the roll-off rate. Thus by placing interdigital slots between the square head slots of basic DGS filter, we can improve the steepness of the roll-off slope with reduced circuit size.

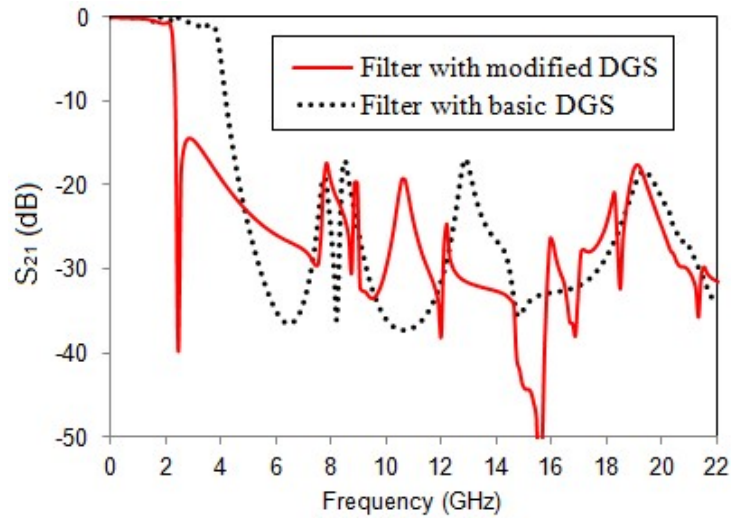
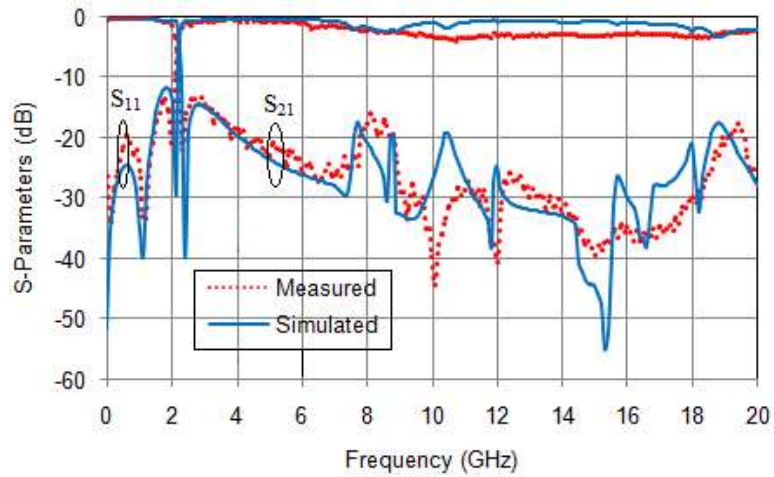


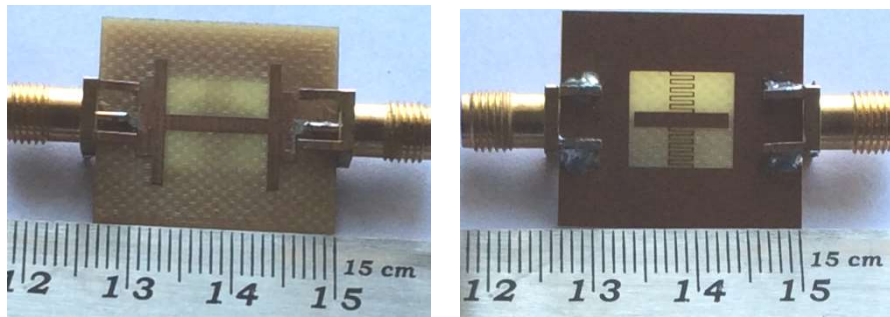
Fig. 6.9 Comparing the frequency response characteristics of filter with basic DGS and modified DGS

### 6.3.4 Experimental Results

The proposed filter is fabricated and the S-parameters are measured, which is compared with the simulated results as shown in Fig. 6.10(a). The photograph of the fabricated structure with its top and bottom view is in Fig. 6.10(b).



(a)



(b)

Fig. 6.10 (a) Measured and simulated results of the proposed filter (b) The top and bottom prototype

Although EM simulation studies were done up to 22 GHz, the experimental result is only up to 20 GHz as the available R & S ZVB 20 Vector Network Analyzer in our laboratory has the upper frequency limit of 20 GHz. The measured cutoff frequency of the proposed filter is 2.11 GHz. The insertion loss is less than 0.3 dB till 1.4 GHz of the passband. In the low frequencies of the passband the return loss is less than 19.5 dB and in the entire passband it is less than 13.5 dB. The roll-off rate at only 20 dB attenuation level is obtained due to the fabrication inaccuracy of the filter. The transition band between 3 dB and 20 dB is 0.17 GHz and the calculated roll-off rate of the proposed filter using Equation (2.14) is 100 dB/GHz. The stopband bandwidth of the fabricated filter is from 2.25 GHz to 20 GHz at 15 dB suppression level.

The measured results of the fabricated structure is shown in Fig. 6.11. As seen in the result, two transmission poles occur in the frequency range 7.7 GHz to 9 GHz (at frequencies 8.1 GHz and 8.4 GHz). The occurrence of these transmission poles causes only 16 dB stopband suppression level of the filter in this range. To improve this, a bandstop filter is designed using a spurline filter, which can resonate at this frequency range.

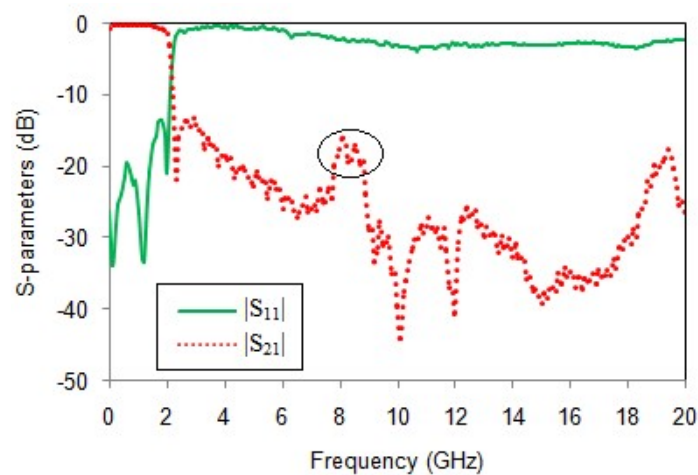


Fig. 6.11 Measured results of the proposed filter

#### 6.4 THE SPURLINE RESONATOR

Microstrip spurline was first reported by (Bates, 1977), which is used as a bandstop filter to generate moderate bandwidth and thus suitable to suppress the harmonics present in the stopband. Asymmetric two line filters designed in an inhomogeneous medium provides wider stopband by choosing appropriate dimensions of coupled lines (Nguyen and Chang, 1985). Thus to increase the suppression level between 7.7 GHz to 9 GHz frequency range, an asymmetric spurline resonator is designed, which acts as defected microstrip structure (DMS). It is designed using slots etched from the top microstrip line of the substrate, which provides resonant characteristics in the above said frequency range. Similar to DGS, the resonant characteristics of DMS depends on

the size and shape of the slot ( La *et al.* 2010). The radiation due to spurline filters is small compared with the conventional methods of bandstop filter design such as the shunt stubs or by using parallel coupled lines. The configuration of the spurline resonator shown in Fig. 6.12, has length  $d$ , which is equal to the quarter guided wavelength calculated at the resonant frequency. The width of the slot is represented as  $c$  and the slot height is  $h$  as shown in the Figure. The spurline filter is etched from the top microstrip line of the substrate having width 1.5 mm. The dimensions of the structure are  $w = 1.5$ ,  $c = 0.25$ ,  $d = 5.1$  and  $e = 0.5$  (all units of dimension in mm). The slot spacing provides the capacitance of the circuit and the narrow line provides the inductance. The increase in effective inductance and capacitance results in the increase of the value of effective permittivity of the substrate.

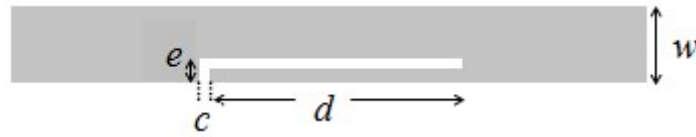


Fig. 6.12 Configuration of spurline resonator

The frequency response characteristics of the spurline filter is analyzed using EM simulation software IE3D as shown in Fig. 6.13(b). The resonant frequency ( $f'_0$ ) of the proposed spurline filter is 8 GHz at 19.2 dB suppression level and the -3 dB frequency is from 7.23 GHz to 8.88 GHz. The cutoff frequency,  $f'_c$  of the filter is 7.23 GHz. Thus by etching spurline filter in the top of the proposed lowpass filter, the spurious harmonics are reduced and a wide stopband with high suppression level is achieved.

The  $LC$  equivalent circuit of the spurline filter shown in Fig. 6.13(a), acts as a parallel  $RLC$  resonator and its  $R_s$ ,  $L_s$  and  $C_s$  values are derived using the Equations (6.10) - (6.12) (Boutejdar *et al.* 2015) as,

$$C_s = \frac{\omega_c'}{2Z_0((\omega_0')^2 - (\omega_c')^2)} \quad (6.10)$$

$$L_s = \frac{1}{(\omega_0')^2 C_s} \quad (6.11)$$

$$R_s = \frac{2Z_0}{\sqrt{1/|S_{11}(\omega_0')|^2 - (2Z_0(\omega_0' C - 1/\omega_0' L))^2 - 1}} \quad (6.12)$$

The calculated values of  $C_s$ ,  $L_s$  and  $R_s$  is 1.085 pF, 0.3647 nH and 1000  $\Omega$  respectively. The EM and LC circuit simulation results shown in Fig. 6.13(b) are having very good similarity.

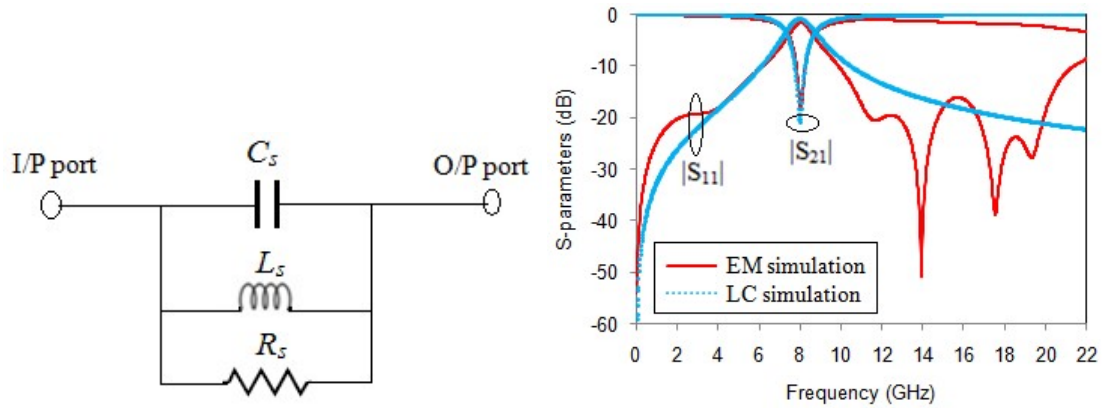


Fig. 6.13 (a) LC equivalent circuit of the spurline filter (b) Comparing EM and LC circuit simulation

## 6.5 IMPROVED LOWPASS FILTER USING DGS-DMS TECHNIQUE

With the introduction of a spurline in the proposed lowpass filter, the stopband suppression level of the filter is improved without increasing the physical size. The improved final filter structure with the spurline etched from the top surface is shown in Fig. 6.14(a) and the modified DGS etched from the metallic ground plane of the bottom side of the substrate is shown in Fig. 6.14(b).



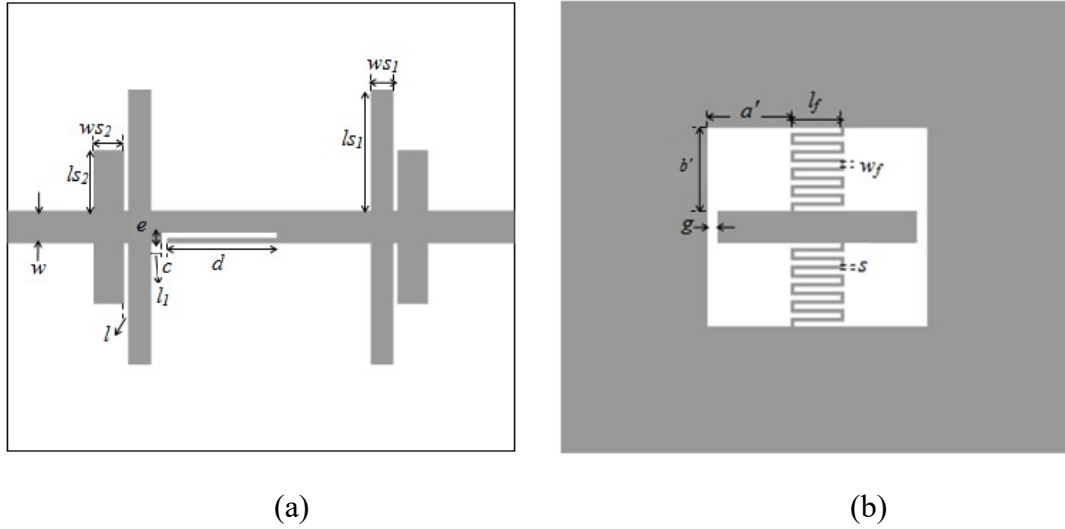


Fig. 6.14 Geomaty of the DGS-DMS lowpass filter (a) Top view (b) Bottom view

### 6.5.1 Experimental Results

The photograph of the fabricated filter is shown in Fig. 6.15 and its frequency response characteristics in Fig. 6.16. From the measured and simulated results we can see that the stopband suppression level of the final filter is improved from 16 dB to 20 dB in the frequency range between 7.7 GHz to 9 GHz. Here, the performance of the filter is improved without affecting the passband characteristics of the proposed filter without spurline. The cutoff frequency of the improved filter is 2.11 GHz. Wide stopband bandwidth up to 20 GHz at 20 dB rejection level is achieved except a small peak near 2.6 GHz, ie. about 95 % of the overall stopband bandwidth, the stopband suppression level is 20 dB. The measured results of the proposed filter exhibit wide stopband up to 20 GHz ( $9.47 f_c$ ) with a physical size of 15.5 mm x 12.7 mm. The relative stopband bandwidth of the final filter calculated using Equation (2.16) is 1.592 at 18 dB suppression level. The normalized circuit size of the filter is of  $0.198 \lambda_g \times 0.162 \lambda_g$  ( $\lambda_g$  is guided wavelength at 2.11 GHz). The wide passband frequency range of the proposed filter covers the GSM, GPS, Wi-Fi communications and various L-band applications such as aircraft surveillance, telecommunication systems etc.

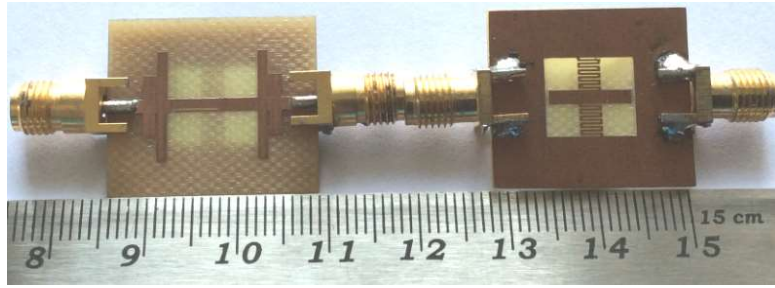


Fig. 6.15 Proto type of the DGS-DMS lowpass filter

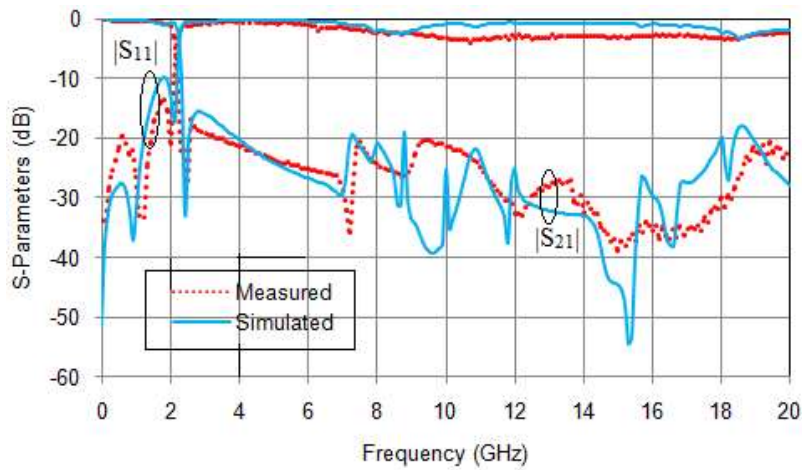


Fig. 6.16 Frequency response characteristics of DGS-DMS lowpass filter

The measured group delay of the DGS-DMS filter in the passband region is shown in Fig. 6.17. The maximum peak to peak group delay variation is only 0.28 ns which indicates that only minimum distortion occurs to the signal while passing from input to the output.

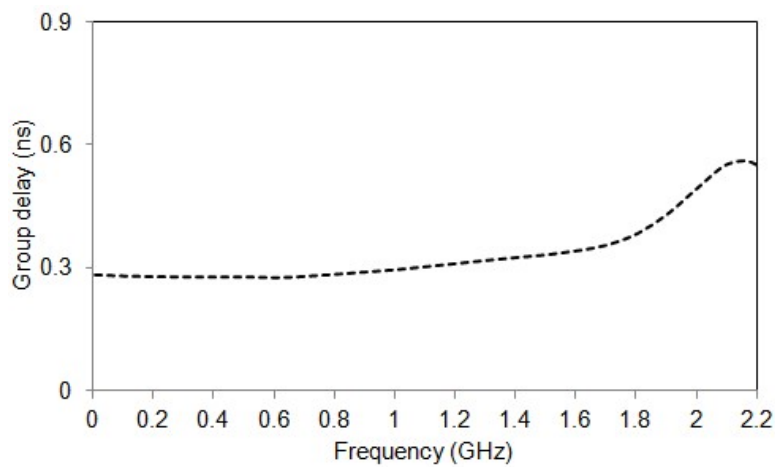


Fig. 6.17 Measured passband group delay

### 6.5.2 Performance Evaluation

Table 6.2 summarizes the comparison of the proposed work with the filters so far described in the literature. The filters with FR4 substrate as well as the low loss tangent substrates are analyzed in the table. It is seen that the designed filter has high roll-off rate  $\xi$ , high value of RSB and wide stopband up to 9.5 times the cutoff frequency,  $f_c$  when compared to all other works. SF represents the suppression factor and its value is calculated as the stopband suppression level divided by 10.

Table 6.2 Comparing the performance characteristics of the proposed work with other related works

Ref.	$f_c$ (GHz)	$\xi$ (dB/GHz)	RSB %	SF	SB up to	Substrate
Boutejdar, (2019)	2.4	19	111.2	2	$5f_c$	Roger
Sen <i>et al.</i> (2018)	2.4	36	85.7	2	$2.5f_c$	FR4
Vala <i>et al.</i> (2017)	3.5	15.45	96.2	1.4	$2.8f_c$	FR4
Kufa and Raida, (2013)	3.195	43.206	95.6	2	$3.2f_c$	Arlon 25 N
Song <i>et al.</i> (2010)	3.0	18.8	128.7	2	$6f_c$	Roger
This Work	2.11	100	159.2	1.8	$9.5f_c$	FR4

### 6.6 CHAPTER SUMMARY

A compact microstrip lowpass filter with sharp selectivity and wide stopband designed on the basis of dual-plane, is presented. In comparison with the basic DGS based filter of same overall physical size, an improvement in roll-off rate and a reduction in circuit size by 68.8 % are achieved in the modified DGS. To suppress higher order harmonics, mirrored symmetrical uniform impedance stubs are placed on the  $50 \Omega$  microstrip line and a spurline acting as DMS are incorporated in the top surface of the substrate, thereby

wide stopband up to 20 GHz is achieved. The designed filter has 3 dB cutoff frequency of 2.11 GHz. The results indicate that a relative stopband bandwidth of 159.2 % within the rejection band of 18 dB is achieved together with small circuit size of  $0.198 \lambda_g \times 0.162 \lambda_g$  ( $\lambda_g$  is guided wavelength at 2.11 GHz). The transition band between -3 dB and -20 dB attenuation point is only 0.17 GHz. The measured results are at par with the simulated results. The proposed filter covers the GSM, GPS, Wi-Fi communications and various L-band applications.

## **CHAPTER 7**

### **CONCLUSION AND FUTURE SCOPE OF THE WORK**

This chapter describes briefly the summary of the proposed filters and discusses the distinct features of the developed filters. Some suggestion on the future scope is also mentioned.

#### **7.1 SUMMARY OF THE WORK AND CONCLUSION**

The motivation behind the work presented in this thesis is the need to design a lowpass filter with high performance characteristics developed using very low cost, easily available material for various applications in modern wireless communication. Different methodologies such as design using a variety of resonators and dual plane structure based approach are followed to achieve these requirements. Multilayer design techniques such as filter design using defected ground resonators and implementation of defected ground and defected microstrip resonators are followed to develop compact lowpass filters with good frequency response characteristics with a low cost material.

Parametric analyses of the filters are conducted using the assigned simulation tool and its current distributions are analyzed to study the filter characteristics in the passband and the stopband. The LC equivalent circuits of the optimized structures are developed and validated with the EM simulation result. Accordingly, the final optimized structures are fabricated. Then the measurement results are compared to the simulation results. The characteristics of each of the designed filter are summarised below.

**Filter design using cascaded patch resonators-** In this method polygonal patch resonators are cascaded to develop a lowpass filter (Filter-I) with good selectivity. To extend the stopband, symmetrical open circuited stubs are introduced in the design and thereby the filter is able to reject up to 6<sup>th</sup> order harmonics. The detailed analysis of the filter is presented in chapter 3 and this work has been reported in *Publication 1*. To increase the order of harmonics rejection, the open stubs of the filter are replaced by suppressing cells. The selectivity as well as the stopband bandwidth of this filter (Filter-II) is improved with very low insertion loss and this improved structure is reported in *Publication 6*. Both the designed filters are suitable for use in wireless LAN, L-band applications, Bluetooth networking etc.

**Developments with interdigital structures and folded stepped impedance resonators-**To improve the roll-off rate and stopband characteristics with high suppression level, an interdigital structure embedded between the dual rectangular patches along with the coupled inductive stub resonators are designed and named as Filter-1. Wide passband up to 3.9 GHz is achieved and thus the filter finds its application in various high frequency networks such as Wi-Max, WLAN, UMTS, Bluetooth, etc and harmonic rejection up to 5<sup>th</sup> order is possible. Result of this work is narrated in *Publication 5*. To obtain sharp selectivity along with good passband and stopband characteristics, Filter-2 is designed using folded stepped impedance resonators and modified hexagonal shaped resonators. The outcome of this work is presented in *Publication 3*. Generally, both sharp selectivity and ultra wide stopband are difficult to achieve in a low cost, lossy substrate such as FR4. Filter-3 is designed so as to have sharp roll-off and wide stopband up to 20 GHz using folded stepped impedance resonators, modified hexagonal shaped resonators and open stubs. The

insertion loss of the filter is very low and has constant passband group delay characteristics. This design is reported in *Publication 4*. The proposed Filter-2 and Filter-3 are designed near the cutoff frequency of 2 GHz and are thus suitable for various L-band applications. These three works are discussed in chapter 4.

**Filter development using defected ground structures-** The frequency response characteristics of a basic lowpass filter improved using defected ground structures is presented in Filter-I. Filter-I describes three structures, the basic lowpass filter, Filter-1 and Filter-2. A basic lowpass filter designed for the cutoff frequency of 2 GHz is improved without compromising on its physical size by using H-shaped defected ground structures is discussed in Filter-1. The structure is further improved with same circuit size of Filter-1 and named it as Filter-2. It is able to suppress up to 10<sup>th</sup> order harmonics as compared to 5<sup>th</sup> order in the case of basic lowpass filter. The in-band characteristics such as the very low value of insertion loss, high return loss with good selectivity and out-of-band responses of wide stopband with high rejection level are obtained in Filter-2 and the results of this work is narrated in *Publication 2*. To improve the roll-off rate along with ultra wide stopband bandwidth, a modified dumbbell defected ground resonator is designed in Filter-II. The filter is designed with the cutoff frequency,  $f_c$  of 2.07 GHz using stair shaped resonators, open stub and suppressing cells along with defected ground structures. The stopband up to  $9.7f_c$  is achieved using this filter and thus higher order harmonics are effectively suppressed. This work is reported in *Publication 7*. The detailed analysis of Filter-I and Filter-II are discussed in chapter 5.

**Filter developed using defected ground and defected microstrip resonators-** A lowpass filter designed for the cutoff frequency of 2.11 GHz using defected structures to improve the roll-off rate and stopband bandwidth with miniaturized circuit size is discussed in chapter 6. Here, the basic defected ground structure is modified by incorporating interdigital slots and thus the roll-off rate as well as the circuit miniaturization are achieved. Results show that the proposed defected ground structure improves the roll-off rate and 68.8% circuit miniaturization as compared to the basic defected structure. An inverted L-shaped slot acting as spurline resonator is introduced in the top 50  $\Omega$  microstrip line to increase the stopband suppression level at a certain band of frequencies and symmetrical open stubs are loaded on the microstrip line. Simulation results indicated sharp selectivity of 194.7 dB/GHz and wide stopband up to 22 GHz. Measurement could be done up to 20 GHz only and 9.5  $f_c$  stopband width is achieved along with selectivity of 100 dB/GHz due to the fabrication tolerance of the structure. This paper is communicated to an international publication and waiting for their response.

Even though FR4 is a lossy material, it has advantages like low cost, easy availability, light weight and good mechanical strength. By adopting appropriate design methodology, high performance lowpass filters suitable for modern wireless communication applications are designed and fabricated. The performance is comparable to those filters realized based on high cost materials.



## 7.2 SCOPE OF FUTURE DEVELOPMENTS IN THE WORK

For the overall improvement of lowpass filter characteristics, the following possibilities are suggested based on the study conducted in the field.

1. In this work, only three variety of defected ground structures are utilized to develop compact, sharp roll-off and wide stopband filters. By suitably designing defected ground structures of different shape, the frequency response characteristics of the lowpass filter can be improved.
2. As mentioned in the thesis, as the thickness of the substrate decreases, the cutoff frequency of the filter also reduces and thus size miniaturization can be achieved. Similarly, as relative permittivity of the substrate increases, the cutoff frequency reduces. Thus a filter fabricated using low substrate thickness with high permittivity, compact, wide stopband and good selectivity can be achieved.
3. As we know, the electromagnetic spectrum is valuable and very limited and the spectrum is utilized for a variety of applications. The spectrum utilization can be done more efficiently by using tunable or reconfigurable microstrip lowpass filters. Reconfigurable planar filters are highly desirable nowadays to use in modern wireless communications. Using simple resonator structures, tunable lowpass filters can be designed for modern efficient use of the spectrum.

4. The most important characteristics of a lowpass filter is its passband insertion loss. It should be of very low value so as to transfer maximum energy from the source to the load. To generate a filter with very low passband insertion loss as well as wide stopband bandwidth, High Temperature Superconducting (HTS) technique can be used. But this method is very expensive to be implemented.
  
5. Miniaturized lowpass filters can be fabricated using modern technology such as the Integrated Passive Device (IPD) or Through-Silicon-Via (TSV) based method. This type of filters may take only 1 mm x 1 mm size, which indicates that these methods of filter fabrication is very effective for realizing compact structures.

## REFERENCES

1. **Abdel-Rahman, A. B., A. K. Verma, A. Boutejdar, and A. S. Omar** (2004) Control of bandstop response of Hi-Lo microstrip low-pass filter using slot in ground plane. *IEEE Transactions on Microwave Theory and Techniques*, **52**, 1008-1013.
2. **Abdipour, A., A. Abdipour, and S. Lotfi** (2015) A lowpass filter with sharp roll-off and high relative stopband bandwidth using asymmetric high-low impedance patches. *Radio Engineering*, **24**, 712-716.
3. **Abdipour, A., A. Nouritabar, A. Abdipour, H. Shamsi and S. A. Ahmadi** (2017) A miniaturized microstrip lowpass filter with sharp skirt performance and wide stopband utilizing modified hairpin resonator with long straight slots. *Progress in Electromagnetics Research C*, **78**, 83-92.
4. **Abid, A. and H. Zhirun** (2007) Sharp cut-off, miniaturized metamaterial binomial microstrip low-pass filter. *Microwave and Optical Technology Letters*, **49**, 2406-2409.
5. **Ahn, D., J.-S. Park, C.-S. Kim, J. Kim, Y. Qian, and T. Itoh** (2001) A design of the low-pass filter using the novel microstrip defected ground structure. *IEEE Transactions on Microwave Theory and Techniques*, **49**, 86-93.
6. **Aznar, F., A. Velez, J. Bonache, J. menes, and F. Martin** (2009) Compact lowpass filters with very sharp transition bands based on open complementary split ring resonators. *Electronics Letters*, **45**, 316-317.
7. **Baena, J. D., J. Bonache, F. Martín, R. M. Sillero, F. Falcone, T. Lopetegi, M. A. G. Laso, J. García-García, I. Gil, M. F. Portillo, and M. Sorolla** (2005) Equivalent-circuit models for split-ring resonators and complementary split-ring resonators coupled to planar transmission lines. *IEEE Transactions on Microwave Theory and Techniques*, **53**, 1451-1461.
8. **Balalem, A., A. R. Ali, J. Machac, and A. Omar** (2007) Quasi-elliptic microstrip low-pass filters using an interdigital DGS slot. *IEEE Microwave and Wireless Components Letters*, **17**, 586-588.
9. **Bates, R. N.** (1977) Design of microstrip spur-line band-stop filters. *IEE Journal on Microwaves, Optics and Acoustics*, **1**, 209-214.
10. **Belbachir, A. K., M. Boussouis, and N. A. Touhami** (2016) High-performance LPF using coupled C-shape DGS and radial stub resonators for microwave mixer. *Progress In Electromagnetics Research Letters*, **58**, 97-103.

11. **Boutejdar, A., A. Elsherbini, and A. S. Omar** (2008) Method for widening the reject-band in low-pass/band-pass filters by employing coupled C-shaped defected ground structure. *IET Microwaves, Antennas and Propagation*, **2**, 759-765.
12. **Boutejdar, A.** (2014) Design of broad-stop band lowpass filter using a novel quasi-yagi-DGS-resonators and metal box-technique. *Microwave and Optical Technology letters*, **56**, 523–528.
13. **Boutejdar, A., A. A. Ibrahim, and E. P. Burte** (2015) Design of a novel ultrawide stopband lowpass filter using a DMS-DGS technique for Radar applications. *International Journal of Microwave Science and Technology*, 1-7.
14. **Boutejdar, A., and W. A. Ellatif** (2016) Improvement of compactness of low pass filters using new quasi-yagi-DGS-resonator and multilayer-technique. *Progress In Electromagnetics Research C*, **69**, 115-124.
15. **Boutejdar, A.** (2017) Design of compact reconfigurable broadband band-Stop Filter based on a low-pass Filter using Half Circle DGS resonator and multi-layer technique. *Progress In Electromagnetics Research C*, **71**, 91-100.
16. **Boutejdar, A., M. Challal, S. Das, and S. El Hani** (2019) Design and manufacturing of a novel compact 2.4 GHz LPF using a DGS-DMS combination and quasi octagonal resonators for radar and GPS applications. *Progress In Electromagnetics Research C*, **90**, 15-28.
17. **Burokur, S. N., M. Latrach, and S. Toutain** (2005) A novel type of microstrip coupler utilizing a slot split ring resonators defected ground plane. *Microwave and Optical Technology letters*, **48**, 138–141.
18. **Cao, H., W. Guan, S. He, and L. Yang** (2012) Compact lowpass filter with high selectivity using G-shaped defected microstrip structure. *Progress In Electromagnetics Research Letters*, **33**, 55-62.
19. **Cauer, W.** *Synthesis of Linear Communications Networks*, McGraw-Hill, New York, 1958.
20. **Chen, F., H. Hu, J. Qiu, and Q. Chu** (2015) High-selectivity low-pass filters with ultrawide stopband based on defected ground structures. *IEEE Transactions on Components, Packaging and Manufacturing Technology*, **5**, 1313-1319.

21. **Chen, H.-J., T.-H. Huang, C.-S. Chang, L.-S. Chen, N.-F. Wang, Y.-H. Wang, and M.-P. Houng** (2006) A novel cross-shape DGS applied to design ultra-wide stopband low-pass filters. *IEEE Microwave and Wireless Components Letters*, **16**, 252-254.
22. **Chen, W.-L., G.- M. Wang, and Y.-N. Qi** (2007) Fractal-shaped hi-lo microstrip low-pass filters with high passband performance. *Microwave and Optical Technology letters*, **49**, 2577-2579.
23. **Chen, X., L. Zhang, Y. Peng, Y. Leng, H. Lu, and Z. Zhang** (2015) Compact lowpass filter with wide stopband bandwidth. *Microwave and Optical Technology letters*, **57**, 367-371.
24. **Chen, X. Q., R. Li, S. J. Shi, Q. Wang, L. Xu, and X. W. Shi** (2008) A novel low pass filter using elliptic shape defected ground structure. *Progress In Electromagnetics Research B*, **9**, 117-126.
25. **Chu, A., W. E. Courtney, L. J. Mahoney, M. J. Manfra, and A. R. Calawa** (1985) Dual function mixer circuit for millimeter wave transceiver applications. *Microwave and Millimeter-Wave Monolithic Circuits*, Dallas, TX, USA, 78-81.
26. **Cui, H., J. Wang, and G. Zhang** (2012) Design of microstrip lowpass filter with compact size and ultra-wide stopband. *Electronics Letters*, **48**, 854-856.
27. **Darlington S.** (1939) Synthesis of reactance 4-poles which produce prescribed insertion loss characteristics: including special applications to filter design. *Journal of Mathematics and Physics*, **30**, 257-353.
28. **Deng, k., Q. Xue, and W. Che** (2007) Improved compact microstrip resonance cell lowpass filter with wide stopband characteristics. *Electronics Letters*, **43**, 463-464.
29. **Dingsheng, La., Yinghua Lu, Siyang Sun, Ning Liu, and Jingling Zhang** (2011) A novel compact bandstop filter using defected microstrip structure. *Microwave and Optical Technology letters*, **53**, 433-435.
30. **Ellis, T. J. and G. M. Rebeiz** (1996) MM-wave tapered slot antennas on micromachined photonic bandgap dielectrics. *IEEE MTT-S International Microwave Symposium Digest*, San Francisco, USA, June, 1157-1160.
31. **García-García, J., F. Martín, F. Falcone, J. Bonache, I. Gil, T. Lopetegi, M. A. G. Laso, M. Sorolla, and R. Marques** (2004) Spurious passband suppression in microstrip coupled line band pass filters by means of split ring resonators. *IEEE Microwave and Wireless Components Letters*, **14**, 416-418.

32. **García-García, J., F. Martín, F. Falcone, J. Bonache, J. D. Baena, I. Gil, E. Amat, T. Lopetegui, A. G. Laso, J. A. M. Iturmendi, M. Sorolla, and R. Marques** (2005) Microwave filters with improved stopband based on sub-wavelength resonators. *IEEE Microwave and Wireless Components Letters*, **53**, 1997-2006.
33. **Giannini, F., R. Sorrentino, and J. Vrba** (1984) Planar circuit analysis of microstrip radial stub. *IEEE Transactions on Microwave Theory and Techniques*, **32**, 1652-1655.
34. **Gu, J. and X. Sun** (2005) Compact lowpass filter using spiral compact microstrip resonant cells. *Electronics Letters*, **41**, 1065-1066.
35. **Guha, D., S. Biswas, M. Biswas, J. Y. Siddiqui, and Y. M. M. Antar** (2006) Concentric ring-shaped defected ground structures for microstrip applications. *IEEE Antennas and Wireless Propagation Letters*, **5**, 402-405.
36. **Gupta, K. C., R. Garg, I. Bahl, and P. Bhartis** *Microstrip Lines and Slotlines*, Second Edition, Artech House, Boston, 1996.
37. **Hameed, R. T., S. H. Hassan, and S. L. Ajeel** (2018) New compact low-pass filter (LPF) using cascaded square open loop resonator. *International Journal of Electronic Communication (AEU)*, **92**, 93-97.
38. **Hayati, M. and A. Lotfi** (2010a) Elliptic-function lowpass filter with sharp cutoff frequency using slit-loaded tapered compact microstrip resonator cell. *Electronics Letters*, **46**, 143-144.
39. **Hayati, M. and A. Lotfi** (2010b) Compact lowpass filter with high and wide rejection in stopband using front coupled tapered CMRC. *Electronics Letters*, **46**, 846-848.
40. **Hayati, M., A. Sheikhi, and A. Lotfi** (2010c) Compact lowpass filter with wide stopband using modified semi-elliptic and semi-circular microstrip patch resonator. *Electronics Letters*, **46**, 1507-1509.
41. **Hayati, M., A. Sheikhi, and A. A. Vand** (2012a) Wide-stopband microstrip low-pass filter using modified semi-circle patch resonator. *International Journal of Electronics*, **99**, 1575-1580.
42. **Hayati, M., H. A.-D. Memari, and H. Abbasi** (2012b) Compact microstrip lowpass filter with sharp roll-off and wide stopband using semicircle ended stub resonator. *Progress In Electromagnetics Research Letters*, **35**, 73-81.

43. **Hayati, M., A. Abdipour, and A. Abdipour** (2013) Compact microstrip lowpass filter with sharp roll-off and ultra-wide stop-band. *Electronics Letters*, **49**, 1159-1160.
44. **Hayati, M., S. Naderi, and F. Jafari** (2014) Compact microstrip lowpass filter with sharp roll-off using radial resonator. *Electronics Letters*, **50**, 761-762.
45. **Hayati, M., M. Gholami, H. S. Vaziri, and T. Zaree** (2015) Design of microstrip lowpass filter with wide stopband and sharp roll-off using hexangular shaped resonator. *Electronics Letters*, **51**, 69-71.
46. **Hayati, M., S. Zarghami, and A. H. Kazemi** (2018) Very sharp roll-off ultrawide stopband low-pass filter using modified flag resonator. *IEEE Transactions on Components, Packaging and Manufacturing Technology*, **8**, 2163-2170.
47. **Hong, J.-S. and M. J. Lancaster** (1996) Couplings of microstrip square open-loop resonators for cross-coupled planar microwave filters. *IEEE Transactions on Microwave Theory and Techniques*, **44**, 2099-2109.
48. **Hong, J.-S. and M. J. Lancaster** (2000) Microstrip triangular patch resonator filters. *IEEE MTT-S International Microwave Symposium Digest*, Boston, USA, 331-334.
49. **Hong, J. S. and M. J. Lancaster** *Microstrip Filters for RF/Microwave Applications*, John Wiley & Sons, New York, 2001.
50. **Hsiao, C., Y. Huang, and T. Wu** (2015) An ultra-compact common-mode bandstop filter with modified-T circuits in integrated passive device (IPD) process. *IEEE Transactions on Microwave Theory and Techniques*, **63**, 3624-3631.
51. **Hsieh, L. H. and K. Chang** (2001) Compact lowpass filter using stepped impedance hairpin resonator. *Electronics Letters*, **37**, 899-900.
52. **Hsieh, L. H. and K. Chang** (2003) Compact elliptic-function low-pass filters using microstrip stepped impedance hairpin resonators. *IEEE Transactions on Microwave Theory and Techniques*, **51**, 193-199.
53. **Hou, Z. Z.** (2008) Novel wideband filter with a transmission zero based on split-ring resonator DGS. *Microwave and Optical Technology letters*, **50**, 1691-1693.

54. **Jiang, S. and J. Xu** (2017) Compact microstrip lowpass filter with ultra-wide stopband based on dual-plane structure. *Electronics Letters*, **53**, 607-609.
55. **Karimi, G., F. Khamin-Hamedani, and H. Siahkamari** (2013) Miniaturised microstrip lowpass filter with sharp roll-off and ultra-wide stopband. *Electronics Letters*, **49**, 1343-1345.
56. **Karimi, G., F. K. Hamedani, and H. Siahkamari** (2014) Ultra-wide stopband low-pass filter using symmetrical cascaded modified hairpin resonators. *International Journal of RF and Microwave Computer-Aided Engineering*, **24**, 314-321.
57. **Karthikeyan, S. S. and R. S. Kshetrimayum** (2011) Compact, deep and wide rejection bandwidth low-pass filter using open complementary split ring resonator. *Microwave and Optical Technology letters*, **53**, 845-848.
58. **Karthikeyan, S. S. and R. S. Kshetrimayum** (2015) Compact and wide stopband lowpass filter using open complementary split ring resonator and defected ground structure. *Radio Engineering*, **24**, 708-711.
59. **Ke, L., M. Zhao, Y. Fan, Z. Zhu, and W. Cui** (2013) Compact lowpass filter with wide stopband using novel double-folded SCMRC structure with parallel open-ended stub. *Progress in Electromagnetics Research Letters*, **36**, 77-86.
60. **Kesler, M. P., J. G. Maloney, and B. L. Shirley** (1996) Antenna design with the use of photonic bandgap material as all dielectric planar reflectors. *Microwave and Optical Technology letters*, **11**, 169-174.
61. **Kim, C. S., J-S. Park, D. Ahn, and J-B. Lim** (2000) A novel 1-D periodic defected ground structure for planar circuits. *IEEE Microwave and Guided Wave Letters*, **10**, 131-133.
62. **Kim, C. S., J-S Lim, S. Nam, K.-Y. Kang, and D. Ahn** (2002) Equivalent circuit modeling of spiral defected ground structure for microstrip line. *Electronics Letters*, **38**, 1109-1110.
63. **Kufa, M. and Z. Raida** (2013) Lowpass filter with reduced fractal defected ground structure. *Electronics Letters*, **49**, 199-201.
64. **Kumar, A. and A. K. Verma** (2016) Design of Bessel low-pass filter using DGS for RF/Microwave Applications. *International Journal of Electronics*, **09**, 1460-1474.



65. **Kumar, A. and K. Machavaram** (2013) Microstrip filter with defected ground structure: A close perspective. *International Journal of Microwave and Wireless Technologies*, **5**, 589-602.
66. **Kumar, L. and M. S. Parihar** (2016) Compact hexagonal shape elliptical low pass filter with wide stop band. *IEEE Microwave and Wireless Components Letters*, **26**, 978-980.
67. **Kumar, L. and M. S. Parihar** (2018) A wide stopband low-pass filter with high roll-off using stepped impedance resonators. *IEEE Microwave and Wireless Components Letters*, **28**, 404-406.
68. **Kurgan, P. and M. Kitlinski** (2009) Novel microstrip low-pass filters with fractal defected ground structures. *Microwave and Optical Technology letters*, **51**, 2473-2477.
69. **La, D., Y. Lu, S. Sun, N. Liu, and J. Zhang** (2011) A novel compact bandstop filter using defected microstrip structure. *Microwave and Optical Technology letters*, **53**, 433-435.
70. **Li, J.-L., S.-W. Qu, and Q. Xue** (2009) Compact microstrip lowpass filter with sharp roll-off and wide stop-band. *Electronics Letters*, **45**, 110-111.
71. **Li, L. and Z.-F., Li** (2008) Compact quasi-elliptic lowpass filter using symmetric rectangular coupled capacitors. *Electronics Letters*, **44**, 1384-1385.
72. **Li, L., Z.-F. Li, and Q.-F. Wei** (2009) Compact and selective lowpass filter with very wide stopband using tapered compact microstrip resonant cells. *Electronics Letters*, **45**, 267-268.
73. **Li, L., Z.-F. Li, and J.-F. Mao** (2010) Compact lowpass filters with sharp and expanded stopband using stepped impedance hairpin units. *IEEE Microwave and Wireless Components Letters*, **20**, 310-312.
74. **Li, Y., H.-C. Yang, and S.-Q. Xiao** (2013) Lowpass filter with wide stopband and sharp skirt using novel defected ground structure. *Progress In Electromagnetics Research Letters*, **41**, 185-191.
75. **Liu, H. W., Z. F. Li, and X. W. Sun** (2003) A novel fractal defected ground structure and its application to the low-pass filter. *Microwave and Optical Technology letters*, **39**, 453-456.
76. **Liu, S., J. Xu, and Z. Xu** (2015) Sharp roll-off lowpass filter using interdigital DGS slot. *Electronics Letters*, **51**, 1343-1345.

77. **Ma, K. and K. S. Yeo** (2010) Novel low cost compact size planar lowpass filter with deep skirt selectivity and wide stopband rejection. *IEEE MTT-S International, Microwave Symposium Digest*, Anaheim, USA, May, 233-236.
78. **Ma, K. and K. S. Yeo** (2011) New ultra-wide stopband low-pass filter using transformed radial stubs. *IEEE Transactions on Microwave Theory and Techniques*, **59**, 604-611.
79. **Ma, K., K. S. Yeo, and W. M. Lim** (2012) Ultra-wide rejection band lowpass cell. *Electronics Letters*, **48**, 99-100.
80. **Mandal, M. K. and S. Sanyal** (2006a) A novel defected ground structure for planar circuits. *IEEE Microwave and Wireless Components Letters*, **16**, 93-95.
81. **Mandal, M. K., P. Mondal, S. Sanyal, and A. Chakrabarty** (2006b ) Low insertion loss, sharp-rejection and compact microstrip low-pass filters. *IEEE Microwave and Wireless Components Letters*, **16**, 600-602.
82. **Mansour, R. R., B. Jolley, Shen Ye, F. S. Thomson, and V. Dokas** (1996) On the power handling capability of high temperature superconductive filters. *IEEE Transactions on Microwave Theory and Techniques*, **44**, 1322-1338.
83. **Mattaei, G., L. Young, and E. M. T. Jones** *Microwave Filters, Impedance-Matching Networks, and Coupling Structures*, Artech House, Norwood, MA, 1980.
84. **Mirzaee, M. and B. S. Virdee** (2013) Realisation of highly compact planar lowpass filter for UWB RFID applications. *Electronics Letters*, **49**, 1396-1398.
85. **Mohra, A. S.** (2011) Microstrip lowpass filter with wideband rejection using opened circuit stubs and Z-slots defected ground structures. *Microwave and Optical Technology letters*, **53**, 811-815.
86. **Mousavi, S. M. H., S. V. A. Makki, H. Siahkamari, S. Alirezaee, and M. Ahmadi** (2016) Performance improvement of microstrip LPF based on transfer function analysis. *IEEE Microwave and Wireless Components Letters*, **26**, 322-324.
87. **Nguyen, C. and K. Chang** (1985) On the analysis and design of spurline bandstop filters. *IEEE Transactions on Microwave Theory and Techniques*, **33**, 1416-1421.

88. **Papoulis, A.** *The Fourier Integral and Its Applications*, McGraw-Hill, New York, 1962.
89. **Park, J., J. Kim, and S. Nam** (2007) Design of a novel harmonic-suppressed microstrip low-pass filter. *IEEE Microwave and Wireless Components Letters*, **17**, 424-426.
90. **Park, J. L., C. S. Kim, J. Kim, J. S. Park, Y. Qian, D. Ahn, and T. Itoh** (1999) Modeling of a photonic bandgap and its application for the low-pass filter design. Proceedings of *Asia Pacific Microwave Conference*, Singapore, November-December 331-334.
91. **Park, J.-S., J.-H. Kim, J.-H. Lee, S.-H. Kim, and S.-H. Myung** (2002) A novel equivalent circuit and modeling method for defected ground structure and its application to optimization of a DGS lowpass filter. *IEEE MTT-S International Microwave Symposium Digest*, Seattle, WA, USA, 417-420.
92. **Pozar, D. M.** *Microwave Engineering*, Second Edition, Wiley, New York, 1998.
93. **Raaed, T. H., S. H. Hassan, and S. L. Ajeel** (2018) New compact low-pass filter (LPF) using cascaded square open loop resonator. *International Journal of Electronics Communication (AEU)*, **92**, 93-97.
94. **Radisic, V., Y. Qian, and T. Itoh** (1998) Broadband power amplifier using dielectric photonic bandgap structure. *IEEE Microwave and Guided Wave Letters*, **8**, 13-14.
95. **Raphika, P. M., P. Abdulla, and P. M. Jasmine** (2014) Compact lowpass filter with a sharp roll-off using patch resonators. *Microwave and Optical Technology letters*, **56**, 2534-2536.
96. **Raphika, P. M., P. Abdulla, and P. M. Jasmine** (2015) Compact wide stopband lowpass filter with high suppression using corrugated transmission line. *IOP Conference Series: Material and Engineering*, **120**, 1-4.
97. **Raphika, P. M., P. Abdulla, and P. M. Jasmine** (2016) Planar elliptic function lowpass filter with sharp roll-off and wide stopband. *Microwave and Optical Technology letters*, **58**, 133-136.
98. **Rhodes, J. D.** *Theory of Electrical Filters*, Wiley, New York, 1976.
99. **Saal, R. and E. Ulbrich** (1958) On the design of filters by synthesis. *IRE Transactions on Circuit Theory*, **5**, 284-327.

100. **Sen, S., T. Moyra, and D. Sarkar** (2018) Modelling and validation of microwave LPF using modified rectangular split ring resonators (SRR) and defected structures. *AEU - International Journal of Electronics and Communications*, **88**, 1-10.
101. **Shama, F., M. Hayati, and M. Ekhteraei** (2018) Compact microstrip lowpass filter using meandered unequal T-shaped resonator with ultra-wide rejection band. *AEU - International Journal of Electronics and Communications*, **85**, 78-83.
102. **Shaman, H., S. Almorgi, and A. Alamoudi** (2015) Composite microstrip lowpass filter with ultra wide stopband and low insertion loss. *Microwave and Optical Technology letters*, **57**, 871-874.
103. **Sheikhi, A., A. Alipour, and H. Hemesi** (2017a) Design of microstrip wide stopband lowpass filter with lumped equivalent circuit. *Electronics Letters*, **53**, 1416-1418.
104. **Sheikhi, A., A. Alipour, and A. Abdipour** (2017b) Design of compact wide stopband microstrip low-pass filter using T-shaped resonator. *IEEE Microwave and Wireless Components Letters*, **27**, 111-113.
105. **Song, K., Y.-Z. Yin, X. Yang, J.-Y. Deng, and H.-H. Xie** (2010) Compact LPF with pair of coupling slots for wide stopband suppression. *Electronics Letters*, **46**, 922-924.
106. **Sorrentino, R. and L. Roselli** (1992) A new simple and accurate formula for microstrip radial stub. *IEEE Microwave and Guided Wave Letters*, **2**, 480-482.
107. **Temes, G. C. and S. K. Mitra** *Modern Filter Theory and Design*, Wiley, New York, 1973.
108. **Ting, S.-W., K.-W. Tam, and R. P. Martins** (2006) Miniaturized microstrip lowpass filter with wide stopband using double equilateral U-shaped defected ground structure. *IEEE Microwave and Wireless Components Letters*, **16**, 240-242.
109. **Tu, W. H. and K. chang** (2005) Compact microstrip lowpass filter with sharp rejection. *IEEE Microwave and Wireless Components Letters*, **15**, 404-406.
110. **Vala, A., A. Patel, R. Goswami, and K. Mahant** (2017) Defected ground structure based wideband microstrip low-pass filter for wireless communication. *Microwave and Optical Technology letters*, **59**, 993-996.

111. **Velez, A., F. Aznar, J. Bonache, M. C. Velazquez-Ahumada, J. Martel, and F. Martin** (2009) Open complementary split ring resonators (OCSRRs) and their application to wideband CPW band pass filters. *IEEE Microwave and Wireless Components Letters*, **19**, 197-199.
112. **Velidi, V. K. and Sanyal, S.** (2010) High-rejection wide-stopband lowpass filters using signal interference technique. *International Journal of RF and Microwave Computer-Aided Engineering*, **20**, 253-258.
113. **Velidi, V. K. and S. Sanyal** (2011) Sharp roll-off lowpass filter with wide stopband using stub-loaded coupled-line hairpin unit. *IEEE Microwave and Wireless Components Letters*, **21**, 301-303.
114. **Wang, C. J. and T. H. Lin** (2011) A multi-band meandered slotted-ground plane resonator and its application of lowpass filter. *Progress In Electromagnetics Research*, **120**, 249-262.
115. **Wang, C.-J. and L.-J. Hsu** (2018) Design and analysis of a low-pass filter utilizing a slotted-ground-plane resonator. *Microwave and Optical Technology letters*, **60**, 905-915.
116. **Wang, J., L.-J. Xu, S. Zhao, Y.-X. Guo, and W. Wu** (2010) Compact quasi-elliptic microstrip lowpass filter with wide stopband. *Electronics Letters*, **46**, 1384-1385.
117. **Wang, J., H. Cui, and G. Zhang** (2012) Design of compact microstrip lowpass filter with ultra-wide stopband. *Electronics Letters*, **48**, 854-856.
118. **Wang, L., H. C. Yang, and Y. Li** (2010) Design of compact microstrip low-pass filter with ultra-wide stopband using SIRs. *Progress in Electromagnetics Research Letters*, **18**, 179-186.
119. **Wang, J. P., L. Ge, Y.-X. Guo, and W. Wu** (2010) Miniaturised microstrip lowpass filter with broad stopband and sharp roll-off. *Electronics Letters*, **46**, 573-575.
120. **Wei, F., L. Chen, and X.-W. Shi** (2012) Compact lowpass filter based on coupled-line hairpin unit. *Electronics Letters*, **48**, 379-381.
121. **Wei, X. B., P. Wang, M. Q. Liu, and Y. Shi** (2011) Compact wide-stopband lowpass filter using stepped impedance hairpin resonator with radial stubs. *Electronics Letters*, **47**, 862-863.
122. **Weinberg, L.** *Network Analysis and Synthesis*. McGraw-Hill, New York, 1962.

123. **Woo, D.-J., T.-K. Lee, J.-W. Lee, C.-S. Pyo, and W.-K. Choi** (2006) Novel U-slot and V-slot DGSs for bandstop filter with improved Q factor. *IEEE Transactions on Microwave Theory and Techniques*, **54**, 2840-2847.
124. **Xi, D., Y.-Z. Yin, L.-H. Wen, Y. N. Mo, and Y. Wang** (2010) A compact low-pass filter with sharp cutoff and low insertion loss characteristic using novel defected ground structure. *Progress In Electromagnetics Research Letters*, **17**, 133-143.
125. **Xiao, M., G. Sun, and X. Li** (2015) A lowpass filter with compact size and sharp roll-off. *IEEE Microwave and Wireless Components Letters*, **25**, 790-792.
126. **Xu, L.-J. and Z. Duan** (2017) Miniaturized lowpass filter with wide band rejection using modified stepped-impedance hairpin resonator. *Microwave and Optical Technology letters*, **59**, 1313-1317.
127. **Xue, Q., K. M. Shum, and C. H. Chan** (2000) Novel 1-D microstrip PBG cells. *IEEE Microwave and Guided Wave Letters*, **10**, 403-405.
128. **Xue, Q., Y. F. Liu, K. M. Shum, and C. H. Chan** (2003) A study of compact microstrip resonant cells with applications in active circuits. *Microwave and Optical Technology letters*, **37**, 158-162.
129. **Yablonovitch, E.** (1987) Inhibited spontaneous emission in solid-state physics and electronics. *Physical Review Letters*, **58**, 2059-2062.
130. **Yang, M. H., J. Xu, Q. Zhao, L. Peng, and G. P. Li** (2010) Compact, broad stopband lowpass filters using SIRs-loaded circular hairpin resonators. *Progress in Electromagnetics Research*, **102**, 95-106.
131. **Yang, Y., Xi Zhu, and N. C. Karmakar** (2012) A novel microstrip lowpass filter using compact microstrip resonant cells and uniquely shaped defected ground structures. *Microwave and Optical Technology letters*, **54**, 2462-2464.
132. **Yasuzumi, T., S. Hasegawa, T. Uwano, and O. Hashimoto** (2010) A microstrip LPF with attenuation poles using hairpin structural and interdigital capacitor. *Proceedings of Asia Pacific Microwave Conference*, Yokohama, March, 1166-1169.
133. **Yin, X., Z. Zhu, Y. Liu, Q. Lu, X. Liu, and Y. Yang** (2019) Ultra-compact TSV-based L-C low-pass filter with stopband up to 40 GHz for microwave application. *IEEE Transactions on Microwave Theory and Techniques*, **67**, 738-745.

134. **Yum, T. Y., Q. Xue, and C. H. Chan** (2003) Novel subharmonically pumped mixer incorporating dual-band stub and in-line SCMRC. *IEEE Transactions on Microwave Theory and Techniques*, **51**, 2538 -2547.
135. **Zhang, B., S. Li, and J. Huang** (2015) Compact lowpass filter with wide stopband using coupled rhombic stubs. *Electronics Letters*, **51**, 264-266.
136. **Zhang, F., J. Z. Gu, C. Y. Gu, L. N. Shi, C. F. Li, and X. W. Sun** (2006) Lowpass filter with in-line beeline CMRC. *Electronics Letters*, **42**, 472-474.
137. **Zhang, P. and M. Li** (2016) A novel sharp roll-off microstrip lowpass filter with improved stopband and compact size using dual-plane structure. *Microwave and Optical Technology letters*, **58**, 1085–1088.
138. **Zhou, W., C. Liu, G.-L. Huang, W. Xia, J. Zhang, D. He, and Z. Wu** (2019) Design and manufacture of lowpass microstrip filter with high conductivity graphene films. *Microwave and Optical Technology letters*, **61**, 972– 978.

# LIST OF PUBLICATIONS

## INTERNATIONAL JOURNALS

---

1. **T. K. Rekha, P. Abdulla, P. M. Raphika, and P. M. Jasmine** (2017) Compact microstrip lowpass filter with ultra-wide stopband using patch resonators and open stubs. *Progress In Electromagnetics Research C*, **72**, 15-28. doi:10.2528/PIERC16110202.
2. **T. K. Rekha, P. Abdulla, P. M. Jasmine, and P. M. Raphika** (2018) Improved frequency response of microstrip low pass filter using defected ground structures. *Progress In Electromagnetics Research C*, **81**, 31-40. doi:10.2528/PIERC17112002

## INTERNATIONAL CONFERENCES

---

3. **T. K. Rekha, P. Abdulla, A. R. Anu and Ami Iqubal.** Compact microstrip low pass filter with sharp roll off using folded stepped impedance resonator. *International Symposium on Antennas & Propagation (APSYM)*, Cochin, December, 2016.
4. **T. K. Rekha, P. Abdulla, A. R. Anu, P. M. Jasmine and P. M. Raphika.** High selectivity and ultra-wide stopband microstrip lowpass filter using high-low impedance resonators. *International Conference on Information, Communication, Instrumentation and Control (ICICIC)*, Indore, August, 2017. doi: 10.1109/ICOMICON.2017.8279042.
5. **T. K. Rekha, P. Abdulla and T. A. Nisamol** Compact microstrip lowpass filter with ultra-wide stopband. *Asia-Pacific Microwave Conference (APMC)*, Kyoto, Japan, November, 2018. doi: 10.23919/APMC.2018.8617485
6. **T. K. Rekha, P. Abdulla and T. A. Nisamol.** Compact microstrip lowpass filter with high harmonic suppression. *IEEE MTT-S International Microwave & RF Conference (IMaRC)*, Kolkata , November, 2018.
7. **T. K. Rekha, P. Abdulla, A. R. Anu, Ami Iqubal, U. Sam Kollannore and T. A. Nisamol.** Compact multilayer microstrip lowpass filter with ultra wide stopband for L-band applications. *International Symposium on Antennas & Propagation (APSYM)* Cochin, December, 2018.
8. **A. R. Anu, P. Abdulla, T. K. Rekha and Ami Iqubal.** Rectangular and semicircular shaped aperture coupled HDRA. *International Symposium on Antennas & Propagation (APSYM)* Cochin, December, 2016.



9. **Ami Iqubal, P. Abdulla, T. K. Rekha, A. R. Anu, P. M. Jasmine and P. M. Raphika.** A novel band pass filter using dual mode chamfered square patch resonator with diamond shaped slots. *International Symposium on Antennas & Propagation (APSYM) Cochin, December, 2016.*
10. **P. M. Jasmine, P. Abdulla, P. M. Raphika and T. K. Rekha.** Double step junction for coupling enhancement of rectangular wave guide fed cylindrical DRA. *Eighth International Joint Conference on Advances in Engineering and Technology (AET) 2017.*
11. **P. M. Raphika, P. Abdulla, P. M. Jasmine and T. K. Rekha.** Wide stop band low pass filter with sharp roll off using multiple resonators. *Eighth International Joint Conference on Advances in Engineering and Technology (AET) 2017.*
12. **Jyothishree Pillai, P. Abdulla and Rekha T. K.** Compact microstrip lowpass filter with ultra-wide stopband bandwidth. *International Symposium on Antennas & Propagation (APSYM) Cochin, December, 2018.*
13. **T. A. Nisamol, P. Abdulla, T. K. Rekha, C. K. Aanandan, P. M. Raphika and P. M. Jasmine.** Highly compact microstrip S-band hairpin resonator lowpass filter with ultra wide stopband. *International Symposium on Antennas & Propagation (APSYM) Cochin, December, 2018.*
14. **Ami Iqubal, P. Abdulla, A. R. Anu, T. K. Rekha, U. Sam Kollannore, P. M. Jasmine and P. M. Raphika.** A novel hextuple-mode wideband bandpass filter with sharp roll-off and ultra-wide upper stopband. *International Symposium on Antennas & Propagation (APSYM), Cochin, December, 2018.*
15. **A. R. Anu, P. Abdulla, P. M. Jasmine, T. K. Rekha, Ami Iqubal and U. Sam Kollannore.** Frequency tuning of cylindrical dielectric resonator antenna using varactor diode. *International Symposium on Antennas & Propagation (APSYM) Cochin, December, 2018.*
16. **U. Sam Kollannore, P. Abdulla, Sheeba Varghese, A. R. Anu, T. K. Rekha and Ami Iqubal.** Simple and compact single feed circularly polarized microstrip antenna for ultra wideband applications. *International Symposium on Antennas & Propagation (APSYM) Cochin, December, 2018.*

# CURRICULUM VITAE

## EDUCATION

### Doctoral Degree

Registration date 10.10.2013, Div. of Electronics Engineering, School of Engineering, Cochin University of Science and Technology, Cochin, Kerala.

Registered as full time research scholar w.e.f (14.10.2015 to 11.10.2018) under the Faculty Development Programme of UGC.

### M Tech Degree in Electronics

2002-2004, Department of Electronics, CUSAT, Kerala

CGPA: 7.99

### BE Degree in Electronics and Communication

1992-1996, Jawaharlal Nehru National College of Engineering, Kuvempu University, Karnataka

Percentage: 75.5

## EXPERIENCE

Assistant Professor

Department of Electronics

N S S College Rajakumari, Idukki (From 1997 - till date)

## PERSONAL DETAILS

Nationality : Indian  
Date of Birth : 30.05.1975  
Place of Residence : Alappuzha, Kerala  
Email Id : rekhamuralitk@gmail.com  
Phone No : 9447438642